Geologic Map of the Socorro 30 x 60-Minute Quadrangle, Socorro, Torrance, and Valencia Counties, New Mexico

By

Daniel J. Koning[1], Andrew P. Jochems[1], Jon M. Krupnick[1], Virginia T. McLemore[1], Christina M. Neudorf[2], Julia Ricci[1], and Snir Attia[1]

[1]New Mexico Bureau of Geology and Mineral Resources, 801 Leroy Place, Socorro, NM 87801
[2]Division of Earth and Ecosystem Sciences, Desert Research Institute, 2215 Raggio Parkway, Reno, NV 89512

January 2025

New Mexico Bureau of Geology and Mineral Resources
Open-File Geologic Map OF-GM 317

Scale 1:100,000

https://doi.org/10.58799/OF-GM-317

This geologic map was funded in part by the USGS National Cooperative Geologic Mapping Program under STATEMAP award number G22AC00601, 2022. Additional support was made possible by the 2023 Technology Enhancement Fund provided by the New Mexico Higher Education Department. Funding is administered by the New Mexico Bureau of Geology and Mineral Resources (Dr. Nelia W. Dunbar, *Director and State Geologist [2023]*; Dr. J. Michael Timmons, *Director and State Geologist [2024]*; Dr. Matthew J. Zimmerer, *Geologic Mapping Program Manager*).

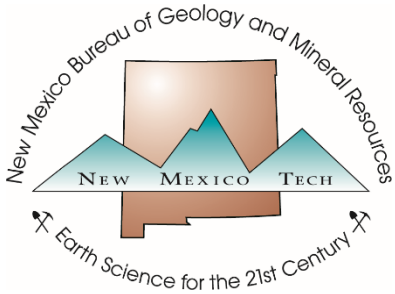

New Mexico Bureau of Geology and Mineral Resources
801 Leroy Place, Socorro, New Mexico, 87801-4796

TABLE OF CONTENTS

TABLE OF FIGURES

TABLE OF TABLES

EXECUTIVE SUMMARY

The Socorro 30 x 60-minute quadrangle (1:100,000 scale) covers an area with a wide variety of rock types that have undergone deformation in three tectonic events: Ancestral Rocky Mountains (ARM) tectonism, Laramide orogeny, and Rio Grande rifting. An important geographic feature on the west side of the quadrangle is the Rio Grande valley. In the northwest corner of the map area, the southeast-flowing Rio Puerco joins the Rio Grande near Bernardo. The Socorro valley is flanked to the west by the Socorro and Lemitar Mountains and to the east by the Los Pinos Mountains and the hilly terrain of the Quebradas highlands. Near the center of the quadrangle lies the northern Jornada del Muerto Basin, rimmed by the Quebradas to the west, Rayo Hills to the northwest, and Chupadera Mesa to the northeast and east. Chupadera Mesa and the Claunch uplands are topographic features found in the eastern third of the quadrangle and are underlain by relatively flat to gently dipping, erosionally resistant limestone intervals of the San Andres Formation. The north-trending Monte Prieto-Liberty Hill structural zone separates the Chupadera Mesa (west) from the lower, slightly hilly terrain of the Claunch uplands to the east. The Claunch uplands feature many small, topographically closed basins as well as the Ancestral Puebloan site of Gran Quivira. The community of Claunch lies a few kilometers east of the eastern boundary of the quadrangle and Mountainair is located a few kilometers to the north of the eastern part of the northern boundary.

The oldest rocks exposed in the Socorro 30 x 60-minute quadrangle are Paleoproterozoic to Mesoproterozoic metasediments, metarhyolites, a variety of granites, and minor diorites to gabbros. These rocks form the cores of the Lemitar Mountains and Los Pinos Mountains. The Manzano group comprises metasediments and metarhyolites emplaced between 1,700 and 1,580 Ma in an arc setting, where both back-arc extension and contraction occurred (Holland et al., 2020). The Manzano group was intruded by non- to weakly foliated granitic rocks during 1,650–1,660 Ma. Northwest-directed contraction during 1,580–1,550 Ma, probably related to the early Picuris orogeny (Holland et al., 2020), formed the Manzano Mountains synclinorium. The axial plane of this synclinorium was intruded by the 1,459- to 1,430-Ma Priest Mountain granite (Luther et al., 2005; Holland et al., 2020). Unconformably overlying these crystalline basement rocks is the Sandia Formation (Pennsylvanian) or, as observed in the Lemitar Mountains; Mississippian-age sedimentary rocks of the Kelly Formation (limestones, shales, and minor sandstones).

Phanerozoic sedimentary rocks in the quadrangle are interpreted to reflect deposition in a range of environments that include coastal margins, shallow seas, and uplifted continental interiors. The Pennsylvanian and Permian formations contain about 1,600 m of terrestrial and marine sedimentary strata. The Sandia Formation constitutes the lower part of the extensive Pennsylvanian–Permian stratigraphic section. The Pennsylvanian strata (200–740 m thick) are composed of shale, limestone, siltstone, and sandstone that are relatively gray or drab-colored compared to the overlying, vividly colored Permian section. The lower part of the Pennsylvanian—the Sandia Formation—contains much less limestone than the overlying Madera

Group, which is differentiated into the Gray Mesa and Atrasado Formations. Thinning or absence of upper Atrasado strata over the Joyita Hills indicates concomitant uplift related to ARM tectonism. The purplish-red, arkosic Bursum Formation serves as a transitional unit between the Pennsylvanian and Permian strata. Pebbly sandstones in this formation were derived from local ARM uplifts, and an unconformity at its base is tied to ARM uplift. The Permian strata (700 m thick) are noteworthy for the colorful red-bed sequence of the Abo Formation and the Yeso Group (Meseta Blanca and Los Vallos Formations), which are composed of siltstone, very fine- to medium-grained sandstone, mudstone, and minor dolomite and gypsum. The Yeso Group is overlain by the Glorieta Sandstone and limestone-dominated San Andres Formation, which are commonly depicted as a single map unit in this publication; these two formations often cap mesas and ridges. Reddish siltstone and very fine- to fine-grained sandstone of the upper Permian-age Artesia Formation are only locally preserved overlying the San Andres Formation.

A ≈800-m-thick sequence of Mesozoic clastic sedimentary rocks is mapped east of the Rio Grande. The Triassic section is ≈200 m thick and is a reddish-brown to chocolate-brown sequence of mudstones, sandstones, and minor conglomerates. It is unconformably overlain by the pastel-colored Morrison Formation, which pinches out to the southwest. The yellowish-tan Cretaceous section, which includes the Dakota Sandstone, Mancos Shale, Tres Hermanos Formation, Gallup Sandstone, and Crevasse Canyon Formation, offers important evidence of three major marine transgression-regression cycles of the Western Interior Seaway (WIS), with the last transgression represented by a 30-m-thick tongue of the Mancos Shale (Mulatto Tongue) interbedded in the lower Crevasse Canyon Formation.

The fact that Permian and Mesozoic strata are only preserved east of the Rio Grande is a testament to notable Laramide tectonism that occurred in the latter part of the Late Cretaceous and the Paleogene. During this time, what is now the Rio Grande rift was a paleotopographic high called the Sierra uplift (Cather, 1983). The Laramide uplift resulted in 1,500–1,900 m of exhumation of the entire Mesozoic and Permian sequence in addition to variable erosion of the Madera Group. This is well-illustrated in the Lemitar Mountains, where the eroded top of the Madera Group is unconformably overlain by middle to late Eocene strata. The Baca Formation, which is mainly of middle Eocene age, was deposited during the latter part of the Laramide orogeny. Uplift may have been most intense in the early–middle Eocene and waned near the middle–late Eocene boundary; this is inferred because the Baca Formation onlaps the Sierra uplift.

A thick succession of late Eocene to late Oligocene volcanic and volcaniclastic strata, up to several hundred meters thick, is present in the Socorro 30 x 60-minute quadrangle. The lowest stratum is the Eocene Spears Group, which is 120–330 m thick west of the Rio Grande but 70–800 m thick to the east. The base of the Spears Group is gradational with the Baca Formation. Above the gradational zone, the Spears Group is composed mainly of sandstone and conglomerate derived from erosion of intermediate volcanic rocks and, in its upper part, from erosion of basaltic andesites and plagioclase- and pyroxene-phyric andesites.

The upper Spears Group intertongues with the ignimbrites, basaltic andesites, and minor andesites and dacites of the Datil Group. Ignimbrites in the Datil Group include the Datil Well and Rockhouse Tuffs and the tuff of Veranito Arroyo. A particularly widespread ignimbrite sheet is the 90- to 150-m-thick Hells Mesa Tuff. This outflow tuff came from the 32.35-Ma Socorro caldera, the northeast part of which is located in the southwest corner of the map area. The Socorro caldera was backfilled by sedimentary rocks and volcanic flows of the Luis Lopez Formation between 31 and 29 Ma. Very little sediment deposition, and perhaps possible widespread erosion, occurred outside of the Socorro caldera during 32.35–29 Ma.

Outside of source calderas, the upper volcanic succession (0.3–0.5 km thick) is characterized by regional felsic ignimbrites interbedded with flows of the La Jara Peak Basaltic Andesite. At 29 Ma, the Sawmill caldera overprinted the earlier Socorro caldera and ejected the La Jencia Tuff (whose outflow sheet is up to 120 m thick). Subsequent local ignimbrites erupted between 29 and 27.5 Ma, resulting in the emplacement of the Vicks Peak, Lemitar, and South Canyon Tuffs. These tuffs are interbedded with the pyroxene-phyric (and plagioclase-aphyric) La Jara Peak Basaltic Andesite. The wedge-shaped geometry of the basaltic andesites between tuff strata in fault-bounded grabens indicates early extension at 29–27 Ma. In the southern Joyita Hills, there is evidence that extension occurred as early as 34 Ma (Chamberlin et al., 2022a). The ages of the northeast- and east-northeast-trending dikes tend to fall into two population groups; 33–30 Ma and 28.0–27.0 Ma, suggesting that their formation may be related to voluminous magmatism associated with the Socorro (32.35 Ma) and Mount Withington (27.6 Ma) calderas; these magmas may have traveled up to 150 km from their postulated source calderas via dikes propagating along crustal weaknesses of the Morenci lineament. We speculate that magmatism associated with the first population may have produced topographic uplift, creating the relative gap in the stratigraphic record during 32–29 Ma (i.e., little deposition or possible erosion) outside of the Socorro caldera.

The Santa Fe Group records deposition during Rio Grande rifting. The lower and middle part of the Santa Fe Group, the Popotosa Formation, was deposited in a closed-basin setting before the integration of the axial river. The basal Santa Fe Group is a coarse-grained deposit eroded from local uplifts and deposited mainly via debris flows, which is indicated by the clast compositions in these basal strata being correlative to the upper part of the underlying volcanic sequence. The medial strata of the Popotosa Formation are spectacularly exposed in the San Lorenzo Canyon area, adjoining the central part of the map border. There, a fine-grained basin-floor facies, containing playa deposits, interfingers southwestward and southeastward with piedmont-slope sediments that were being shed from volcanic-cored highlands to the southwest and southeast. Stratigraphic relations show that the playa moved progressively southward through the Socorro Basin in the late Miocene until it was replaced by a throughgoing axial river (the ancestral Rio Grande) at 7.4–7.0 Ma (Koning et al., 2024). The upper part of the Santa Fe Group, the Sierra Ladrones Formation, was deposited after this axial river integration. The Sierra Ladrones Formation has an eastern piedmont facies and a western piedmont facies that interfinger with a

centralized, axial-fluvial depositional belt. In contrast to the volcanic-dominated western piedmont facies of the Popotosa Formation, the eastern piedmont facies of the Sierra Ladrones Formation contains gravel composed predominately of Pennsylvanian–Permian sedimentary clasts. This indicates notable exhumation was occurring in the Quebradas highlands during the late Miocene through Pliocene, which likely began even earlier in the early to middle Miocene.

The Rio Grande valley and adjoining highlands are topographic expressions of Rio Grande rifting, a tectonic feature that mainly formed from ≈25–20 Ma to the Quaternary. Tectonic extension began as early as 34 Ma, but workers continue to debate whether this extension was truly rift-related. Rio Grande rift-related normal faulting is pervasive throughout the western part of the Socorro 30 x 60-minute quadrangle, decreasing eastwards from the Quebradas region. Major normal faults bounding the western rift exhibit down-to-the-east throw and include the Socorro Canyon, Loma Blanca, and Loma Peleda faults. Noteworthy west-down normal faults bounding the eastern margin of the rift include the Coyote and Veranito faults to the south, with more distributed faulting occurring to the north (Contreras Cemetery, Abo-Maes, and Military Road faults). A gap in Quaternary faulting and a right-stepping relay of extensional strain at the north end of the Socorro Canyon fault coincide with a structural high between the Socorro Basin to the south and the Albuquerque Basin to the north.

Rift-related extensional strain is characterized by fault-bounded, domino-block tilting (particularly in the Lemitar Mountains) and a late Miocene concentration of strain onto faults bounding the Socorro Basin. Faults near the Lemitar Mountains illustrate fault-bounded, domino-block tilting (Chamberlin, 1983). Three such generations of faults have been recognized in the Polvadera Mountains (Chamberlin, 1983; Chamberlin et al., 2022b). Geologic mapping, paleocurrent data, and gravel-clast observations in middle Miocene strata of the Popotosa Formation, west of the modern Rio Grande, suggest northwestward to northeastward paleoflow (Chamberlin, 1999; Chamberlin et al., 2001) into a playa lake that lay north of San Lorenzo Canyon and possibly a paleo playa in the La Jencia Basin. In the early late Miocene (12–8 Ma), what is now the Socorro Mountain block was being buried by playa sedimentation, indicating relatively low vertical displacement rates along the Socorro Canyon fault. By the early late Miocene, the Quebradas region was a notable paleotopographic high, shedding voluminous, relatively large-caliper gravel westward into the Socorro Basin. The concentration of extensional strain onto Socorro Basin-bounding faults occurred ca. 8 Ma (Koning et al., 2022a). Subsequently, relatively higher slip rates occurred on the Socorro Canyon fault system and other faults bounding the Socorro Basin. This change in strain distribution played an important role in the integration of the axial river ca. 8–6 Ma (Koning et al., 2024). It also provided a sink to store sediment that continued to be eroded from the Quebradas region during the latest Miocene into the Pliocene. This denudation eventually removed most of the volcanic and volcaniclastic cover that existed earlier in the Miocene, exposing the Mesozoic to upper Paleozoic rocks observed in the Quebradas region today.

The Quaternary deposits in the western Socorro 30 x 60-minute quadrangle have received renewed attention recently (e.g., Sion et al., 2020; Phillips and Sion, 2022). After the culmination of Santa Fe Group deposition at ≈800 ka, which is marked by the Las Cañas geomorphic surface, the Rio Grande has progressively incised about 100 m. During the middle to late Pleistocene, notable periods of aggradation followed by Rio Grande incision resulted in four major allostratigraphic terrace-fan units in the Rio Grande inner valley. A major highlight of this compilation is showing, for the first time, the correlation of these allostratigraphic units from the middle Socorro Basin northward into the southern Albuquerque Basin. Several optically stimulated luminescence (OSL) ages from the Matanza formation (Qt2) in the study area indicate four allostratigraphic units and at least two cut-and-fill events during Marine Isotope Stage 5 (130–71 ka), plus another cut-and-fill event at the start of Marine Isotope Stage 4 (71–62 ka).

INTRODUCTION

This report accompanies the geologic map of the Socorro 30 x 60-minute quadrangle. Its purpose is to describe the topographic and geologic features of the area, summarize the stratigraphic units and related rock and sediment types, elaborate on major structural features, summarize mineral and hydrocarbon resources, and discuss the geologic history. Appendix A presents detailed descriptions of the stratigraphic units, and appendix B shows plots of argon-40/argon-39 ($^{40}Ar/^{39}Ar$) analyses related to geochronologic data given in Table 1.

TOPOGRAPHY AND GEOGRAPHY

Topographic and geographic features are shown in Figure 1 for the Socorro 30 x 60-minute quadrangle and Figure 2 for the larger region around the quadrangle. The main geographic features near the western border are the Socorro and Albuquerque Basins and flanking mountains, which are a consequence of the tectonic processes of the Rio Grande rift. In the northwest corner of the map area, the southeast-flowing Rio Puerco flows into the Rio Grande near Bernardo. West of the Rio Grande valley are the aligned Lemitar and Socorro Mountains (north to south), reaching elevations of 3,419 m and 2,220 m at their highest peaks (Polvadera Mountain and Socorro Peak, respectively). Both mountains contain a sequence of Proterozoic rocks overlain by Mississippian–Pennsylvanian strata, which are in turn overlain by late Paleogene to early Neogene volcanic and volcaniclastic rocks. In the southwest corner of the Socorro 30 x 60-minute quadrangle lies the northernmost Chupadera Hills, separated from the Socorro Mountains by Socorro Canyon (Fig. 2). The mountains support grasses and low-density juniper woodlands.

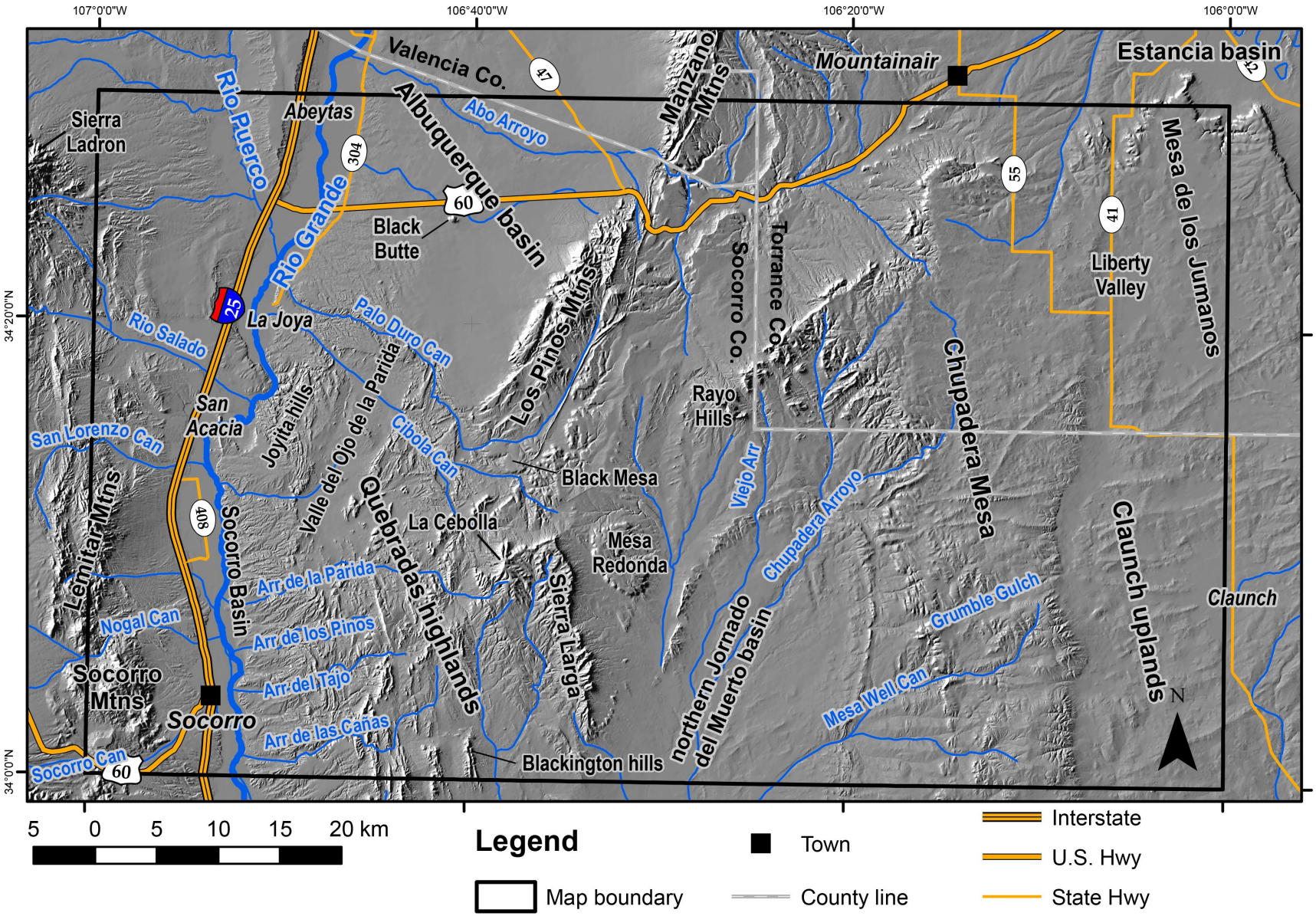

Figure 1—Topographic and drainage features of the Socorro 30 x 60-minute quadrangle. Shaded relief map background created from a 30-m digital elevation model (DEM).

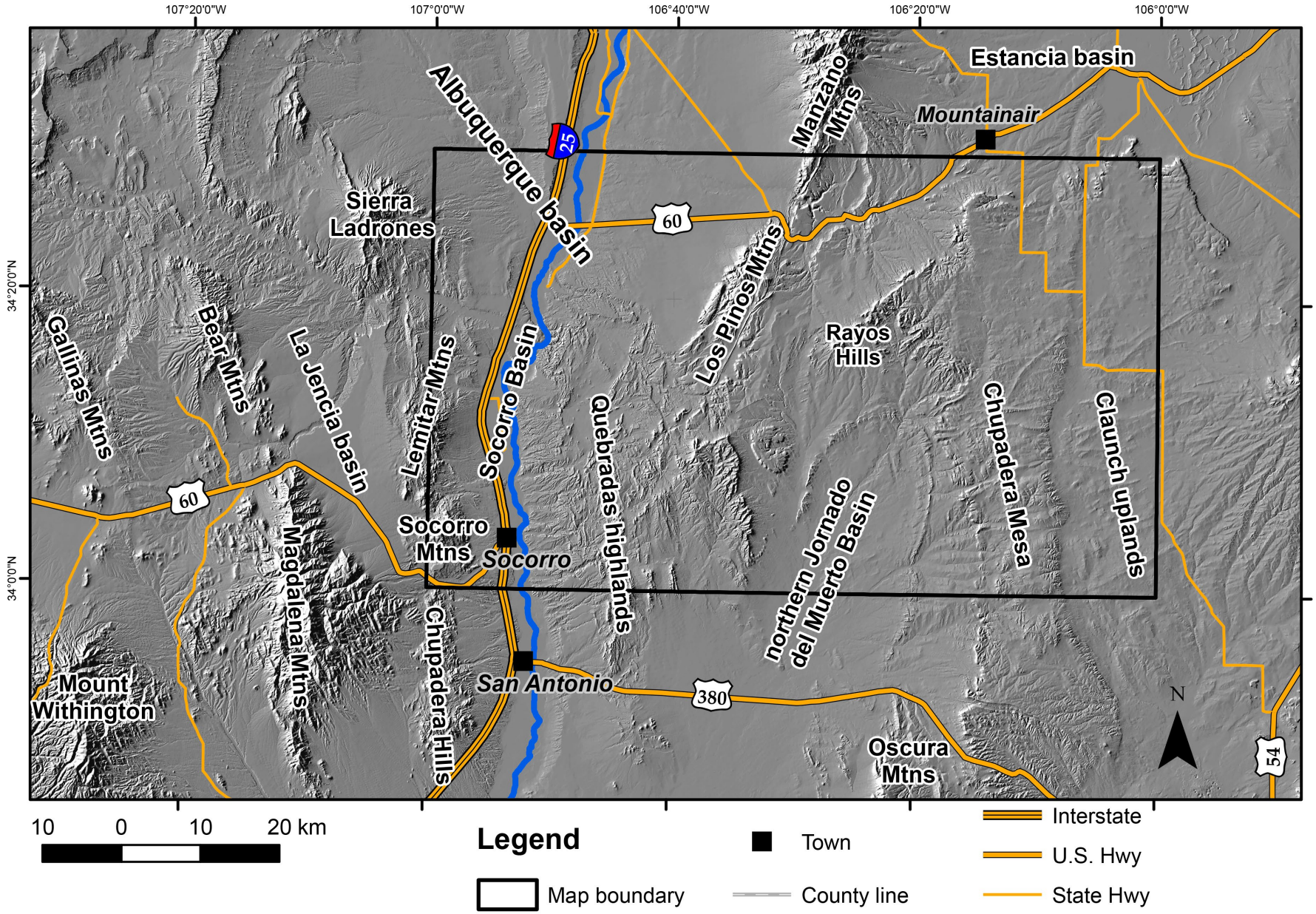

Figure 2—Major topographic and geographic features in the Socorro 30 x 60-minute quadrangle and surrounding areas. Shaded relief map background created from a 30-m DEM.

The Rio Grande flows southward across the Albuquerque and Socorro Basins, supporting many communities and farms. The town of Socorro (population of ≈8,400; U.S. Census Bureau, 2023) lies in the Socorro Basin, due east of Socorro Peak. To the north of Socorro are the smaller communities of Lemitar, Polvadera, and San Acacia (only the northernmost of these, San Acacia, is shown in Fig. 1). The Rio Grande makes a pronounced westward bend east of San Acacia. North of this bend, the valley widens and includes the communities of La Joya and Abeytas (Fig. 1). The Sevilleta Wildlife Refuge encompasses about 930 km^2 on either side of the westward bend. Riparian forest occupies the entire Rio Grande valley in the refuge. To the north and south, however, this forest is restricted to immediately adjacent to the Rio Grande, and most of the valley bottom is occupied by farms producing hay, alfalfa, chile, and various vegetable crops.

Highlands east of the Rio Grande valley include the Quebradas and, to the northeast, the Los Pinos Mountains (Fig. 2). The Quebradas highlands lie at 1,500–1,800 m elevation and have moderate relief. There, sinuous canyons and ridges are underlain by a picturesque sequence of faulted Pennsylvanian–Permian sedimentary rocks. The 350° trending ridge known as Sierra Larga (1,900–2,100 m elevation) bounds the eastern side of the Quebradas highlands. The Los Pinos Mountains trend 025°, expose Proterozoic rocks on their west side and are capped by shallowly dipping Pennsylvanian strata. On the north end of the Los Pinos Mountains, the 1,200-km^2 Abo Arroyo drainage flows westward and reaches the Rio Grande three kilometers north of the northern boundary of the quadrangle. Relatively low-relief terrain (1,900–1,950 m elevation) extends ten kilometers eastward from the Los Pinos Mountains to the Rayo Hills and northern Chupadera Mesa (Fig. 1). These highlands support a creosote scrubland grading upward into a grassland supporting a low density of junipers, although relatively dense juniper-piñon woodlands are found at the crest of the Los Pinos Mountains.

The 17-km-wide northern Jornada del Muerto Basin extends into the south-central part of the Socorro 30 x 60-minute quadrangle (Figs. 1 and 2). On its relatively low surface (1,585–1,768 m elevation) grows a yucca-grassland interspersed with stands of juniper-piñon, with the woodlands being more common on the margins. The basin is flanked by the Sierra Larga on the west, Rayo Hills on the north, and Chupadera Mesa on the east (Fig. 1). Weakly consolidated sediment in the Jornada del Muerto Basin in the quadrangle is thin (typically less than 20 m). The northern Jornada del Muerto Basin spatially corresponds to a large geologic structure called the Torres syncline.

Chupadera Mesa lies south-southwest of the community of Mountainair, which is a town of ≈900 residents located 2 km north of the eastern part of the northern boundary of the quadrangle (Figs. 1 and 2). Chupadera Mesa is 70 km long (extending off the quadrangle to the south) and 10–20 km wide. This highland is underlain by relatively flat to gently dipping, erosionally resistant limestones of the San Andres Formation. It has a general elevation of 1,950–2,200 m and supports juniper-piñon woodlands interspersed with patches of grassland.

East of Chupadera Mesa lies lower, slightly hilly terrain at 1,860–2,010 m elevation that we informally call the Claunch uplands. The lower, eastern terrain features many small, topographically closed basins as well as the Ancestral Puebloan site of Gran Quivira. The community of Claunch lies 1 km east of the eastern boundary of the quadrangle.

Outside of the Rio Grande valley, the main land use is grazing. Grassland appears to be more productive in and east of the Quebradas highlands. Springs are sparse, and scattered wells provide water for livestock. Potential land uses are mining (especially aggregate and perlite, and possibly metals and uranium) and oil drilling, as discussed below. Mining and oil extraction are dormant except for the Dicaperl Minerals perlite mine on the southeastern end of the Socorro Mountains.

METHODS

There were two phases of work in producing the Socorro 30 x 60-minute quadrangle (1:100,000 scale). The western half of the quadrangle was mostly covered by preexisting 1:24,000-scale mapping, except for the Sierra Larga North and Sierra Larga South 7.5-minute quadrangles. Work in the western half mainly consisted of compiling preexisting 1:24,000-scale mapping into a product suitable for depiction at 1:100,000 scale. A ArcGIS file geodatabase compliant with the U.S. Geological Survey Geologic Map Schema (GeMS) was constructed for the 1:100,000-scale product. We iteratively developed a lithologic unit scheme consistent with a 1:100,000-scale map. Then we systematically went through each 1:24,000 quadrangle and drew generalized contacts or copied and pasted contacts (from the 1:24,000-scale maps) relevant to 1:100,000-scale lithologic units. Mapping for the Sierra Larga North and Sierra Larga South 7.5-minute quadrangle was conducted by photogrammetric techniques on National Agriculture Imagery Program (NAIP) aerial photography; contacts and units were spot-checked in the field.

The second phase of the map mainly entailed new mapping in the eastern half of the Socorro 30 x 60-minute quadrangle. Only three quadrangles were previously mapped in this area: the Scholle, Abo, and Gran Quivira 7.5-minute quadrangles (Scott et al., 2005; Oviatt, 2010, 2013). For this work, two additional quadrangles were mapped at 1:24,000 scale and published by the New Mexico Bureau of Geology and Mineral Resources (NMBGMR): the Rayo Hills and Chupadera 7.5-minute quadrangles (Aby and Jochems, 2022; Jochems and Aby, 2024). The remaining area of the eastern half (equivalent to 11 new quadrangles) was mapped using photogrammetry software and limited field checks. Photogrammetry software acquired by NMBGMR (i.e., Stereo Analyst for ArcGIS 10.4, an ERDAS extension, version 11.0.6) allows for accurate placement of geologic contacts and point data directly into a GIS geodatabase.

Once the mapping was completed, additional simplification of the line work and consolidation of the lithologic units was required. A description of map units (DMU) was completed by compiling previous 7.5-minute quadrangle descriptions and new observations. Lastly, we constructed a geologic cross section and correlation of map units.

STRATIGRAPHY

The Socorro 30 x 60-minute quadrangle covers an area with an impressive variety of rock types. Aside from Quaternary surficial deposits, there are five basic rock packages separated by major unconformities, with tens to hundreds of millions of years incorporated in their respective lacunas. The oldest rock package is Proterozoic in age and comprises mainly granites, gneisses, schists, and quartzites. The second-oldest package is late Paleozoic (mainly Pennsylvanian and Permian) and consists of sedimentary rocks such as limestone, sandstone, siltstone, shale, and gypsum/anhydrite. The third-oldest rock package is reddish-brown to brown Triassic strata (sandstones, mudstones, and minor conglomeratic sandstones) unconformably overlain by thin Jurassic strata (Morrison Formation) that pinches out to the south. The fourth-oldest package includes yellow, gray, and brown shale, siltstone, and sandstone of Late Cretaceous age. The fifth (youngest) stratigraphic package reflects episodic deposition since ca. 55 Ma (middle to late Cenozoic). Although several lacunas are present in the middle-late Cenozoic strata, they are typically less than 10 Ma. Brief lithologic descriptions are presented below with detailed descriptions available in appendix A. Carbonate morphology stages in soils and paleosols follow modifications of Gile et al. (1966) by Birkeland (1984) and Birkeland et al. (1991). Formal stratigraphic units are noted by having the full name capitalized (e.g., Gallup Sandstone, Mancos Shale), whereas the last part of the name of an informal unit is not capitalized (e.g., Sevilleta metarhyolite).

Proterozoic

Proterozoic rocks are mainly exposed in the western Los Pinos Mountains and eastern Lemitar Mountains (Fig. 3). Limited outcrops occur at the eastern base of Socorro Peak and on the western edge of the Quebradas highlands, 11–12 km east of Socorro. The informal Manzano group (proposed by Holland et al., 2020) comprises the majority of the Proterozoic rocks in the Los Pinos Mountains, where it records deposition and metamorphism that occurred between 1,700 and 1,580 Ma. The sequence of map units that make up the Manzano group includes the following (listed in ascending stratigraphic order): the local and informal Bootleg Canyon sequence (interbedded amphibolite, pelitic schists, quartzites, and "layered" schists), the Sevilleta metarhyolite (which contains quartz and feldspar phenocrysts and exhibits flow- to shear-banding; interlayered with olive- to dark-green, gneissic metavolcanic rocks), the Abajo metasedimentary rocks (informal name that includes schists, meta-arkosic sandstones, and impure quartzites), the White Ridge and Sais Quartzites (separated by the Estadio schist informal marker unit) and the Blue Springs Formation (interlayered metarhyolites, schists, and quartzites). The Abajo metasedimentary rocks are tentatively correlated in this work to meta-arkoses, quartzites, greenschist, and pelitic schists on the eastern side of Polvadera Peak.

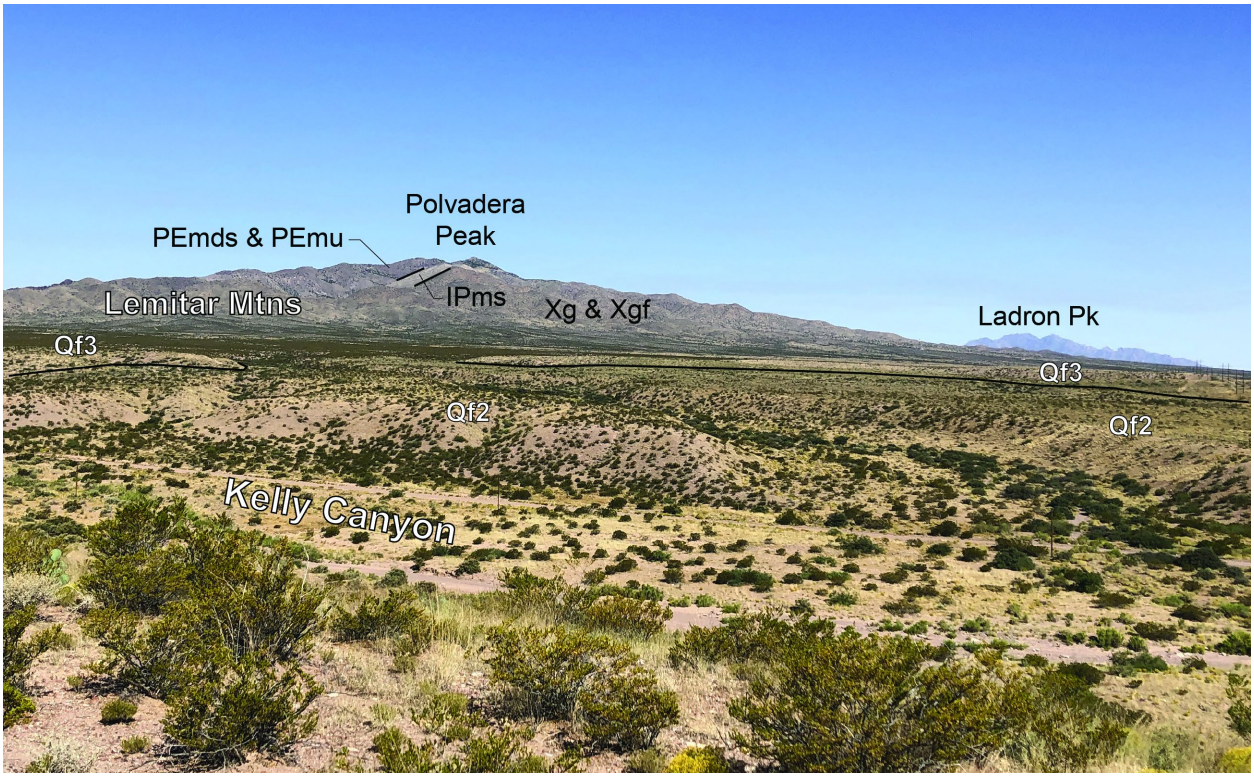

Figure 3—Photograph looking north-northwest across Kelly Canyon toward Polvadera Peak, the high point of the Lemitar Mountains. Ladron Peak is to the right. On the east side of Polvadera Peak is a mapped granite that is weakly to nonfoliated (**Xg**) or strongly foliated (**Xgf**). A cliff-forming band of the Madera Group overlies the Sandia Sandstone and is tilted 55°–60° to the west. Most of the Madera Group here consists of the Gray Mesa Formation. The Madera Group is unconformably overlain by volcanic ignimbrites and volcaniclastic sediment of the Spears, Datil, and Mogollon Groups (**PEmds** and **PEmu**). In the foreground are two alluvial fan allostratigraphic units. **Qf2** correlates to the Matanza formation of Sion et al. (2020). It has less than Stage III+ calcic horizon development in its topsoil, and its strath is close to modern grade. **Qf3** correlates to the Bowling Green formation of Sion et al. (2020), which commonly has Stage III to Stage IV calcic horizon development in its topsoil. Here, the tread (top surface of **Qf3**) is 6–15 m above that of **Qf2**. Figure modified from Koning et al., (2022a, fig. 1.20).

Intrusive Proterozoic rocks are excluded from the Manzano group and include non- to weakly foliated granites, strongly foliated granites, and mafic intrusives. Non- to weakly foliated granites (map unit Xg) include the Los Pinos Granite (1,668–1,655 Ma; Shastri, 1993; Holland et al., 2020) on the west side of the Los Pinos Mountains and the Polvadera granite on the east flank of Polvadera Peak (Lemitar Mountains). Both contain quartz, albite, and potassium feldspar. The Los Pinos Granite locally has a distinctive myrmekite texture. The Polvadera granite contains minor amounts of biotite + hornblende + magnetite. Strongly foliated granites (map unit Xgf) are found both in the Los Pinos Mountains (granite of Sepulveda Canyon) and on the west side of Polvadera Peak. The foliated granite at Polvadera Peak, which intrudes Abajo(?) metasediments, yielded a uranium-lead (U-Pb) age from zircon of 1,648 ± 6 Ma (Bowring et al., 1983). The granite of Sepulveda Canyon predates major deformation events that affect the Manzano group (Allen et al., 2014), so it is likely older than 1,660 Ma (see geologic history section below). Both of these foliated granites are composed of potassium feldspar + quartz + plagioclase ± biotite. Mafic

intrusives are mapped east of Polvadera Peak, where they are generally not foliated and range from diorite and gabbro to quartz diorite and quartz gabbro. Minerals in these mafic rocks include hornblende, plagioclase feldspar, and quartz.

The Priest Granite is a nonfoliated granite present north of Abo Canyon, where it appears to postdate most Proterozoic tectonism. It is a porphyritic to megacrystic, coarse-grained quartz monzonite. The mineral assemblage includes plagioclase, potassium-feldspar, and quartz ± muscovite ± chlorite ± epidote granite. Microline phenocrysts are up to 4 cm long and plagioclase is 0.5–1.0 cm. Its age is 1,458 ± 13 Ma (Holland et al., 2020) to ca. 1,430 Ma (Bauer et al., 1993).

Upper Paleozoic

In the Pennsylvanian and Permian periods, up to 1,600 m of sedimentary rocks were deposited on a low-relief coastal plain or in the adjoining shallow ocean. These rocks lie nonconformably over the aforementioned Proterozoic rocks. The basal formation of this sequence is typically the Sandia Formation, which is overlain by Pennsylvanian strata of the Madera Group. However, up to 30 m of Mississippian strata (i.e., Kelly Limestone) are preserved in the Lemitar Mountains. The Caloso Member of the Kelly Limestone consists of micritic limestones, shales, and a basal conglomeratic sandstone. It is conformably overlain by gray to buff, fine- to coarse-grained, bioclastic limestones of the Ladron Member. Succeeding Pennsylvanian–Permian strata cover most of the region east of the Rio Grande valley and have been the subject of numerous detailed investigations. For the descriptions summarized below, in appendix A, and on the geologic map, we primarily use summaries of recent and earlier stratigraphic studies compiled by Lucas et al. (2022a, 2022b) and Cather and Koning (2024).

Pennsylvanian strata (200–740 m thick) are composed of shale, limestone, siltstone, and sandstone that are relatively dull-colored compared to the overlying, vividly colored Permian section. The lowest unit of the Pennsylvanian—the Sandia Formation (140–180 m thick)—contains much less limestone than the overlying Gray Mesa Formation. It is composed of intercalated shale, siltstone, quartzose sandstone, and minor quartz-conglomeratic sandstone and limestone. The proportion of limestone in this formation is mostly 5%–25% (Cather and Koning, 2024), and these are typically coarse-grained, bioclastic wackestones/packstones (Lucas et al., 2022a). Shale and siltstone are drab brown to gray to dark-gray and locally contain plant fossils. The lower two-thirds of the Sandia Formation consists of shale, siltstone, and very fine- to fine-grained sandstone intercalated with ledge-forming, fine- to coarse-grained sandstone. The upper third of the formation contains shales interbedded with several (but still proportionally minor) fossiliferous limestones and fine-grained quartz-arenite sandstones. The Sandia Formation was deposited in the Atokan primarily on a coastal plain, with periodic sedimentation in shallow oceans.

In most of the Madera Group in the Socorro 30 x 60-minute quadrangle, one can differentiate the Gray Mesa and Atrasado Formations. The Madera Group is applied to Pennsylvanian strata with notable limestones in New Mexico (Kues, 2001, and references therein). Lucas et al. (2009 and 2022a) do not apply the Madera Group to the study area, but we retain the term because of

abundant past usage, especially west of the Rio Grande, and because of difficulties in differentiating the Gray Mesa versus the Atrasado Formations in well data. Both formations were deposited in shallow marine to nearshore environments during the Desmoinesian to Virgilian, with periodic fluvial deposition (the latter more common in the Atrasado Formation). The Gray Mesa Formation is the most limestone-rich part of the Madera Group (e.g., Fig. 3), and its basal contact is placed at the base of the first thick, chert-bearing limestone above the siliciclastic-dominated Sandia Formation. The Gray Mesa is 130–220 m thick and consists of intercalated grayish limestone and poorly exposed shale deposited during the Desmoinesian. This formation is composed of three members (Lucas et al., 2009, 2022a, and references therein) that are not mapped (listed in ascending order): the Elephant Butte Member (40–93 m), which consists of limestone and shale beds and has a 10-m-thick sandstone near its base; the Whiskey Canyon Member (25–42 m), which is composed mainly of very cherty limestone; and the Garcia Member (61–103 m), which is composed of diverse shales, limestone, sandstone, and conglomerate (Fig. 4A). The Madera Group mapped by past workers in the Socorro and Lemitar Mountains likely consists only of the Gray Mesa Formation. Any overlying Pennsylvanian–Permian strata have been removed during Laramide uplift and erosion.

The Atrasado Formation (Fig. 4B) consists of intercalated shales and limestones, with minor arkosic sandstones. Fusulinids and conodonts indicate a Virgilian to Desmoinesian age. Past workers have divided the Atrasado Formation into the following ascending members (not mapped): Bartolo, Amado, Tinajas, Council Spring, Burrego, Story, Del Cuerto, and Moya (Lucas et al., 2009, 2022a, and references therein). The dominant presence of limestone in the Amado, Council Spring, Story, and Moya Members is a useful criterion in this subdivision. Fossils include fusulinids, brachiopods, crinoids, and corals. Discrepancies in age (using fusulinids) of the Council Spring and higher strata between stratotypes in the Oscura Mountains and the Quebradas highlands may lead to stratigraphic revision; an upcoming report by W.J. Nelson et al. (in preparation) will likely not use member-rank terms for strata above the Tinajas Member, but rather just refer to the interval as “upper Atrasado Formation” (Fig. 4B).

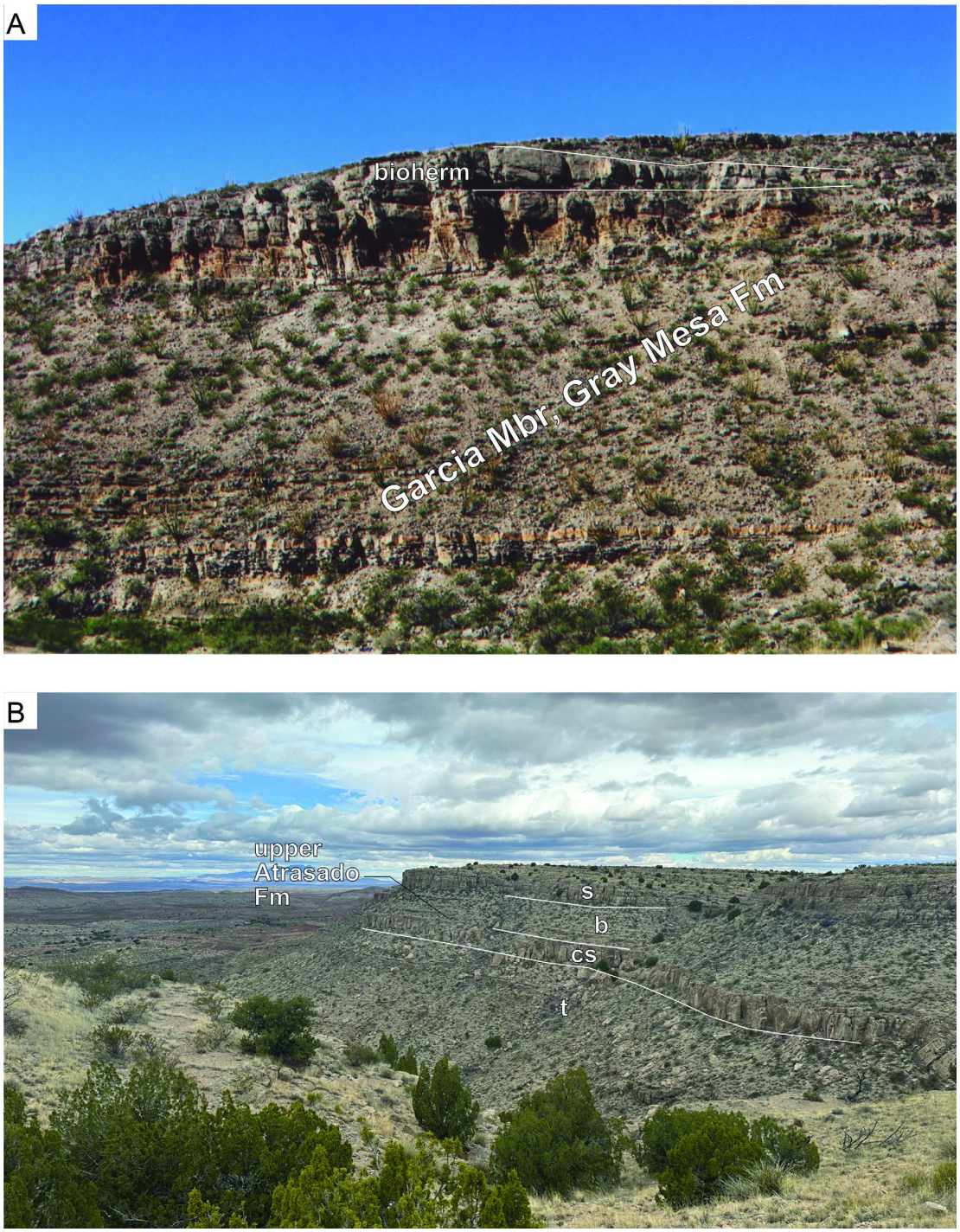

Figure 4—(**A**) Garcia Member of the Gray Mesa Formation with a bioherm at the top of the exposure. The locality is SW1/4NW1/4NW1/4 sec. 35, T. 2 S., R. 1 E., New Mexico Meridian in the Loma de las Cañas quadrangle (approx. UTM 13S 332422m E, 3774459m N, NAD83). The view is looking north, and the height of the bluff is about 40 m. Photograph courtesy of W. John Nelson. (**B**) Photograph of Atrasado Formation. The view is to the north along a west-facing escarpment north of the Arroyo Tinajas (NE1/4NE1/4 sec. 33, T. 2 S., R. 2 E., New Mexico Meridian in the Bustos Well quadrangle (approx. UTM 13S 340057m E, 3774422m N, NAD83). Member-rank terms include the Tinajas (t), Council Spring (cs), Burrego (b), and Story (s). Photograph courtesy of Scott Elrick and W. John Nelson.

The Bursum Formation (25–120 m thick) is early Wolfcampian in age and serves as a transitional unit. The Wolfcampian spans the Pennsylvanian–Permian contact according to Davydov et al. (1998), but others consider the Wolfcampian to be all Permian (e.g., Lucas et al., 2022a, 2022b; S. Lucas, in preparation). The Bursum Formation consists of purplish-red to variegated greenish-gray mudstone, sandstone, and conglomerates that are interbedded with marine limestones (Fig. 5, unit **Pb**). There are also local calcic pedogenic horizons. Limestones are micritic and most common in the lower part. The upper part of the formation contains local conglomeratic sandstones, where clasts are composed of quartz, granite, and sedimentary (e.g., siltstone, limestone) clasts eroded from underlying Pennsylvanian strata (Cather, 2018). Its lower contact is unconformable and locally angular due to ARM tectonism. Cather (2018) interprets the upper contact as disconformable or conformable, depending on location, although Krainer and Lucas (2009) interpret that the entire upper contact is disconformable in the Quebradas highlands. The Bursum Formation was deposited by fluvial, nearshore, and marine processes.

Permian strata (700 m thick) are noteworthy for the colorful red-bed and gypsiferous rocks of the Abo Formation and Yeso Group. The Abo Formation is a brick-red-colored unit composed of mudstones and siltstones with subordinate sandstones (Fig. 5). Channel-fill sandstone is typically arkosic to subarkosic, but sheet-like beds of fine sandstone and siltstone are relatively quartzose (Cappa, 1975; Colpitts, 1986; Lucas and Krainer, 2017). The lower contact is mapped at a color change from purplish to brick-red colors (Fig. 5), which locally may be stratigraphically close to the uppermost limestone bed in the Bursum Formation. The Abo is divided into two members (not mapped) separated by a conformable contact (Fig. 5; Tonking, 1957; Lucas et al., 2005). The lower Scholle Member (37–69 m thick) consists of mudstone (some containing numerous calcrete nodules) with interbedded, relatively lenticular paleochannels (as much as 5 m thick) backfilled by cross-bedded sandstone and conglomerate. Clasts in the conglomerate are commonly composed of intraformational limestone (ripped-up calcrete nodules) with only sparse extraformational clasts. The overlying Cañon de Espinoso Member (≈50–175 m thick) has lower mudstone content and consists of mudstone, siltstone, and several laterally extensive, sheet-like, thin (<10 m) beds of very fine- to medium-grained sandstone exhibiting ripple laminations (Fig. 6A). The Abo Formation was deposited during the Wolfcampian to early Leonardian ages by south- to southwest-flowing rivers that were sourced from relict ARM uplifts (Kues and Giles, 2004). It is conformably overlain by the Yeso Group.

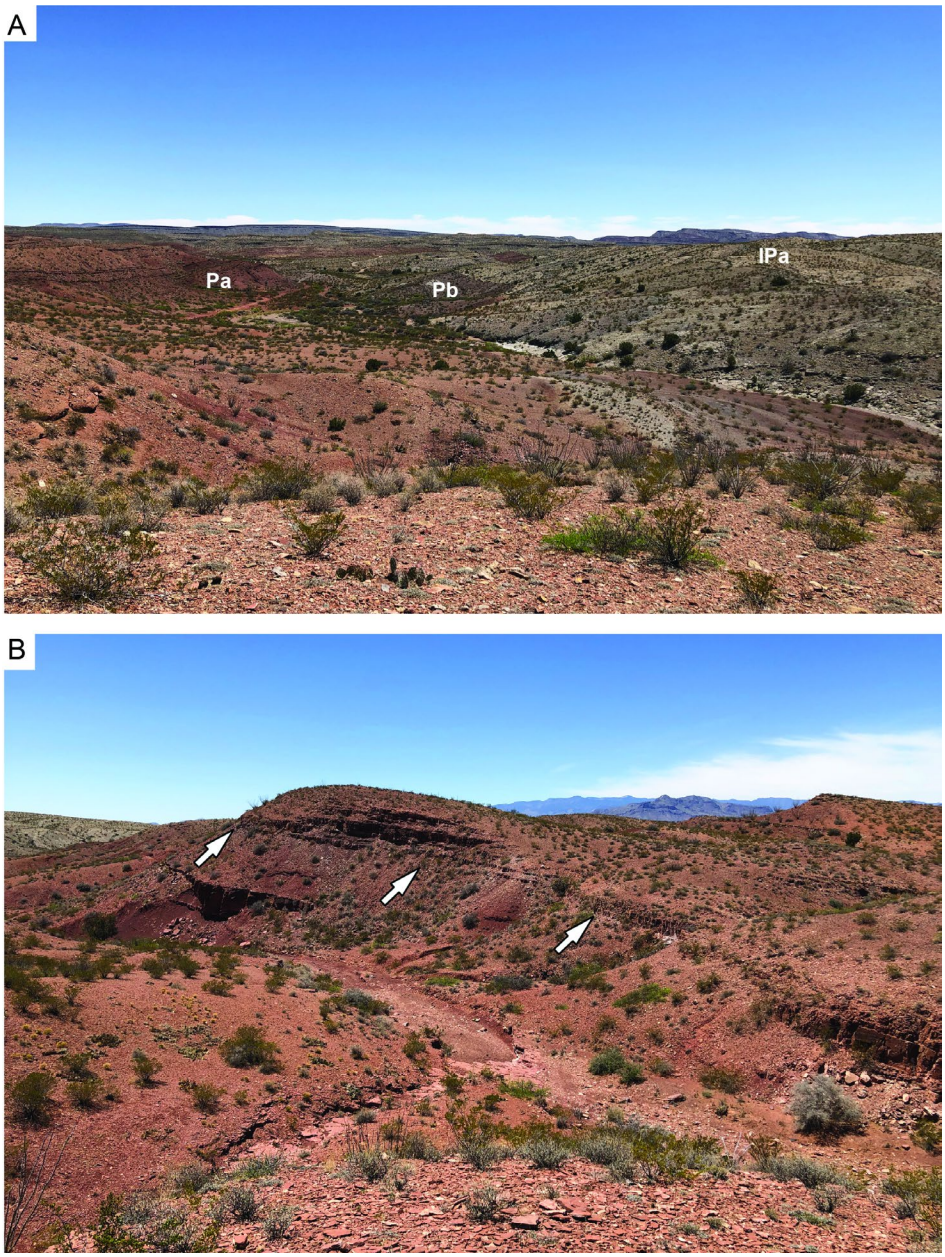

Figure 5—Photographs of lower Permian strata in the middle reach of Arroyo de los Pinos. **(A)** Photograph of upper Pennsylvanian and lower Permian strata exposed 1.5 km east of Ojo de Amado Spring. View to the east-southeast. The upper Atrasado Formation (**IPa**) is overlain by dark-purplish-red, mudstone- and sandstone-dominated strata of the Bursum Formation (**Pb**). The brick-red Abo Formation (**Pa**) is observed on the left (north) slopes of the canyon. **(B)** The Abo Formation at Stop 2 of the Quebradas Backcountry Byway (4.0 mi from the northwestern end of the dirt road (approx. UTM 13S 333040m E, 3776380m N, NAD83). The contact between the upper Cañon de Espinoso Member and the lower Scholle Member of Lucas et al. (2005) is denoted by the white arrows. The upper member contains more sandstone beds than the lower member (mostly very fine- to fine-grained), and the siltstone to sandstone beds are notably tabular and laterally extensive. Both photographs used with permission from the New Mexico Geological Society (Koning et al., 2022a, figs. 1.28 and 1.30).

The Yeso Group consists of the Meseta Blanca Formation conformably overlain by the Los Vallos Formation, whose collective ages span the early to middle Leonardian. With one exception, we use Yeso Group as defined by Lucas et al. (2005) and utilized by Cather and Koning (2024). However, we follow Cather et al. (2013) in retaining the Meseta Blanca Formation in the study area rather than using the Arroyo de Alamillo Formation of Lucas et al. (2005).

The Meseta Blanca Formation (synonymous with the Arroyo de Alamillo Formation of Lucas et al., 2005) is 70–110 m thick and consists of red to reddish-orange and pastel-colored, tabular-bedded strata composed of sandstone, siltstone, and minor silty mudstone (Fig. 6B). Sandstone is very fine- to fine-grained (minor medium-grained), quartzose, and horizontal-planar laminated with subordinate ripple laminations (including climbing ripples). Ripple marks (symmetric and asymmetric), halite pseudomorphs, and mud cracks are locally seen on bedding planes. The conformable lower contact is placed at an upward color change from brick-red and reddish-brown (Abo Formation) to more orangish and grayish colors. The inferred depositional environment is eolian sheet sands and loessic silts that were reworked to varying degrees by floods and marine inundations (Cather and Koning, 2024).

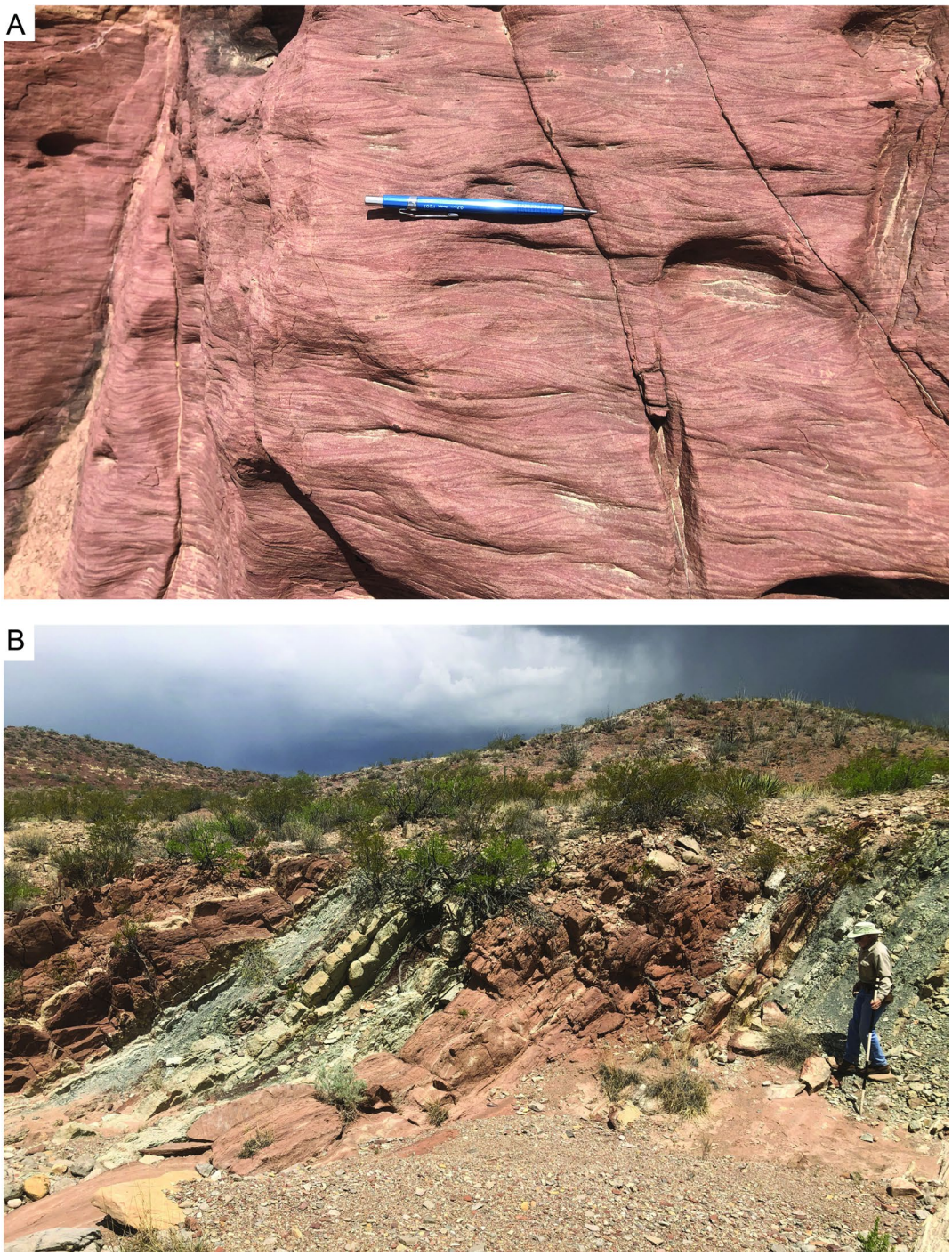

Figure 6—(**A**): Photograph of ripple-laminations near the top of the Abo Formation (UTM 13S 336030m E, 3769640m N, NAD83). Pencil for scale. (**B**): Reddish to pastel-colored Meseta Blanca Formation of the Yeso Group. It is composed of very fine- to fine-grained, relatively quartzose sandstone and siltstone with minor mudstones. "Up direction" indicators using crossbedding indicate these strata are overturned, consistent with the Abo Formation being located to the left (west) of the image. View to the north (UTM 13S 336169m E, 3769750m N, NAD83).

The Los Vallos Formation is characterized by grayish-red, grayish-yellow, or grayish-orange sandstone, siltstone, claystone, gypsiferous sandstone and siltstone, and muddy sandstone interbedded with gypsum and ledge-forming dolomite (Fig. 7A). Sandstones are very fine- to fine-grained and quartzose. The Los Vallos Formation is 230–240 m thick and consists of three members. The lowest, the Torres Member (≈145–160 m thick in the Quebradas highlands), contains sporadic ledge-forming dolomite and limestone intervals; representing marine incursions, these are up to a few meters thick and range from a micrite to wackestone (Fig. 7B). The basal contact of the Torres Member is placed at the base of the lowest bed of limestone or dolomite that is >1 m thick (typically 2–3 m thick). The overlying Cañas Member is gypsum-dominated and variably thick (10–20 m, locally up to 100 m). The Cañas Member includes subordinate buff to greenish-gray siltstone to very fine-grained sandstone and gray dolomite and limestone. The uppermost member of the Los Vallos Formation is the Joyita Member, which is ≈12–20 m thick and composed of orangish- to light-reddish-brown (locally gray and yellowish-gray), well-sorted siltstone and very fine- to fine-grained, quartz-rich sand and silty sand with <10% mudstone (Fig. 7B). There is locally a 5- to 6-m-thick vertical gradation between the Joyita Member and the Glorieta Sandstone, but in other places the contact is sharp. The Los Vallos Formation reflects deposition in a shallow-marine to coastal-sabkha environment (Cather and Koning, 2024). The uppermost strata (the Cañas and Joyita Members) are commonly excised due to low-angle faulting associated with the Quebradas detachment fault system (see structure section below).

Figure 7—Photographs of the upper Yeso Group, Glorieta Sandstone, and the San Andres Formation as viewed from the middle part of the Quebradas Backcountry Byway. The Los Vallos Formation is mapped as **Pyv**, but split into members for this figure. **(A):** View to the southeast from Stop 2 of the 2022 NMGS Fall Field Conference (photograph taken from approx. UTM 13S 337280m E, 3761760m N, NAD83), with the Torres Member of the Los Vallos Formation occupying the foreground. A dolomite or limestone caps the ledge-capped knoll in the center-right of the photograph. Note the absence of the Joyita Member, which was probably excised by a low-angle detachment fault at the base of the Glorieta Sandstone. **Psa** = San Andres Formation, **Pg** = Glorieta Sandstone, **Pyvc** = Cañas Member of the Los Vallos Formation (mapped as **Pyv**). **(B):** Stratigraphic succession that typically caps the upper part of ridges in the Loma de las Cañas. Gray, limestone-rich strata of the San Andres Formation (**Psa**) overlie tan, tabular-bedded sandstones of the Glorieta Sandstone (**Pg**). The top and bottom of the Glorieta Sandstone may be bounded by fault flats of the Quebradas detachment fault system. Reddish sandstones, siltstones, and mudstones of the Joyita Member (**Pyvj**) of the Los Vallos Formation lie between the Glorieta Sandstone and whitish, crusty outcrops of the Cañas Member (**Pyvc)** of the Los Vallos Formation. Photograph looks southeast at outcrops located ≈0.5 km south of Arroyo de las Cañas (UTM 13S 337120m E, 3766700m N, NAD83). Both photographs used with permission from the New Mexico Geological Society (Koning et al., 2022a, figs. 1.42 and 1.43).

The Glorieta Sandstone and overlying limestone-dominated San Andres Formation were deposited in the late Leonardian (Lucas et al., 2022b) and are commonly depicted as a single map unit (**Psag**). Due to their relative hardness, they typically underlie mesas and the tops of ridges. Intertonguing of limestone and sandstone typifies their contact near Chupadera Mesa, and these tongues are locally mapped. In most places on the map, the lower contact of the San Andres Formation is placed at the base of the first thick (≥30 cm) bed of limestone above the Glorieta Sandstone. However, on Mesa Jumanos the lower limestone occurs as a relatively thin (meter-scale) tongue overlain by a thicker tongue of Glorieta Sandstone. There, the base of the San Andres Formation is placed at the top contact of the upper Glorieta tongue.

The Glorieta Sandstone is a 70- to 90-m-thick, light-gray to white to yellow, ledge-forming sandstone (Fig. 8). Its medium to thick, tabular beds exhibit internal horizontal-planar laminations and a variable amount of cross-stratification, whose foresets dip mainly to the southwest (Fig. 8). In the eastern map area, the Glorieta consists of two tongues (each of comparable thickness) separated by ≈10 m of slope-forming gypsum, silt, and very fine-grained sandstone; igneous sills locally intrude into this ≈10 m of relatively soft sediment. The Glorieta records eolian sand sheets and local dune deposition on an arid sabkha or coastal plain (Mack, 2003; Lucas et al., 2013).

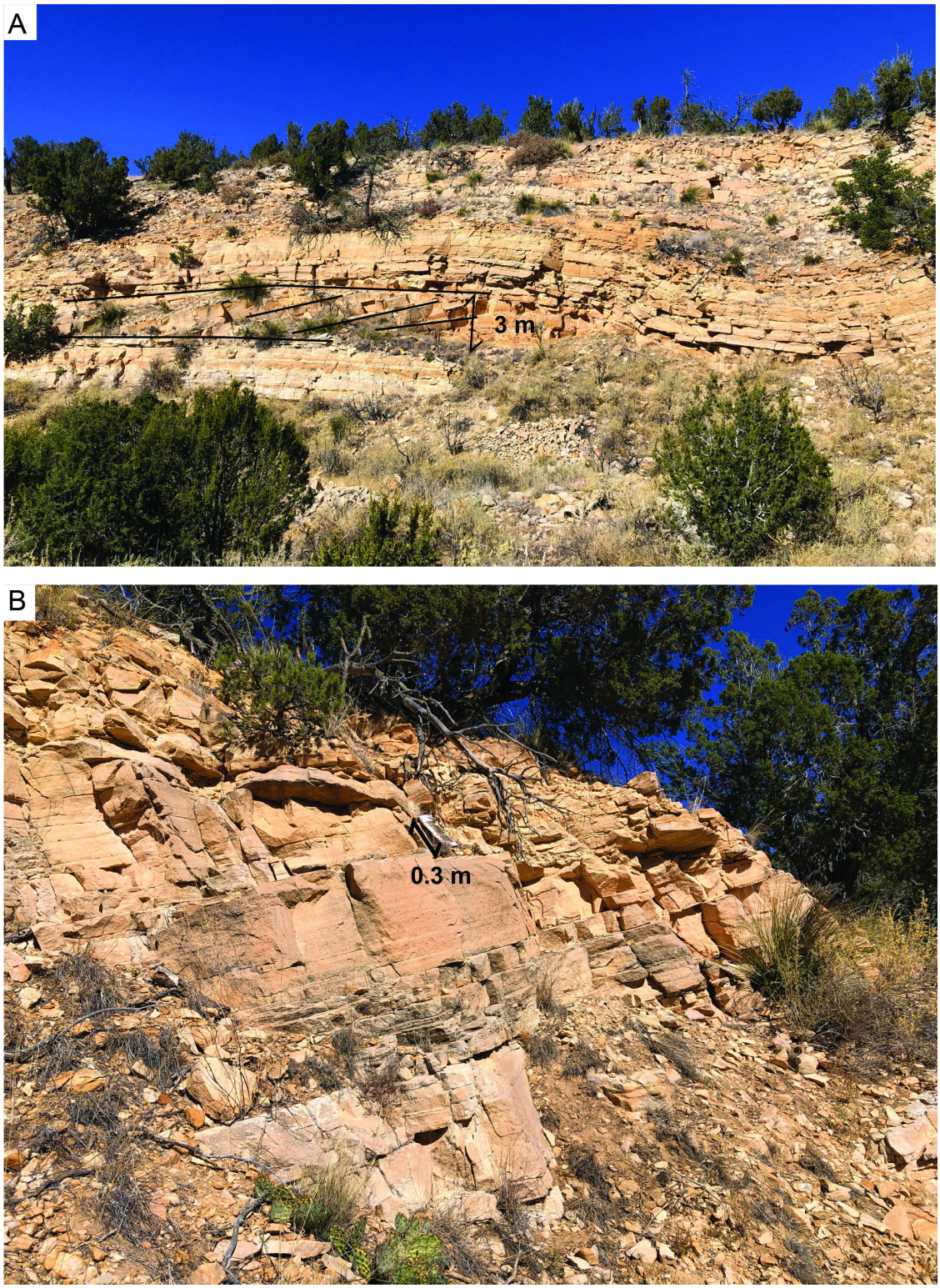

Figure 8—Photographs of the Glorieta Sandstone exposed on the north end of Chupadera Mesa, 7.7 km south of Mountainair. **(A)** Medium-thick, tabular beds of fine- to medium-grained sandstone. Note planar foresets of a paleo-dune; these are 3 m in height and face south-southwest. View to the north. **(B)** Close-up of cross-stratified Glorieta Sandstone (≈1 m thick), where foresets dip gently to the southwest. Sand is fine-grained and quartzose.

The 140- to 150-m-thick San Andres Formation includes gray to tannish-brownish-gray, tabular-bedded, ledge-forming carbonates (limestone and minor dolomite) interbedded with intervals composed of gypsum and variable siltstone-mudstone (Figs. 9 and 10). Limestone dominates in the lower 60 m of the unit, forming steep slopes. Gypsum, dolomite beds, and gypsiferous grayish-purple to reddish-brown siltstone-mudstone are more abundant in the upper 80–90 m of the formation (Fig. 10), resulting in subdued topography. Gypsum intervals may be associated with dolomite beds. Sinkholes develop where dissolution has occurred in gypsiferous intervals that underlie the land surface. Limestone is mostly thin- to thick-bedded and typically micritic (subordinate wackestone, floatstone, and rudstone; Fig. 9). Locally there are bivalves (brachiopods, pelecypods) and rare gastropods, bryozoans, scaphopods, rugose corals, crinoids, and phylloid algae (Fig. 9). The San Andres Formation was deposited in various shallow-marine environments, including open-shelf, intertidal, and hypersaline lagoon settings, the latter particularly conducive for gypsum precipitation (Cather and Koning, 2024). The top contact is rarely preserved due to Neogene erosion.

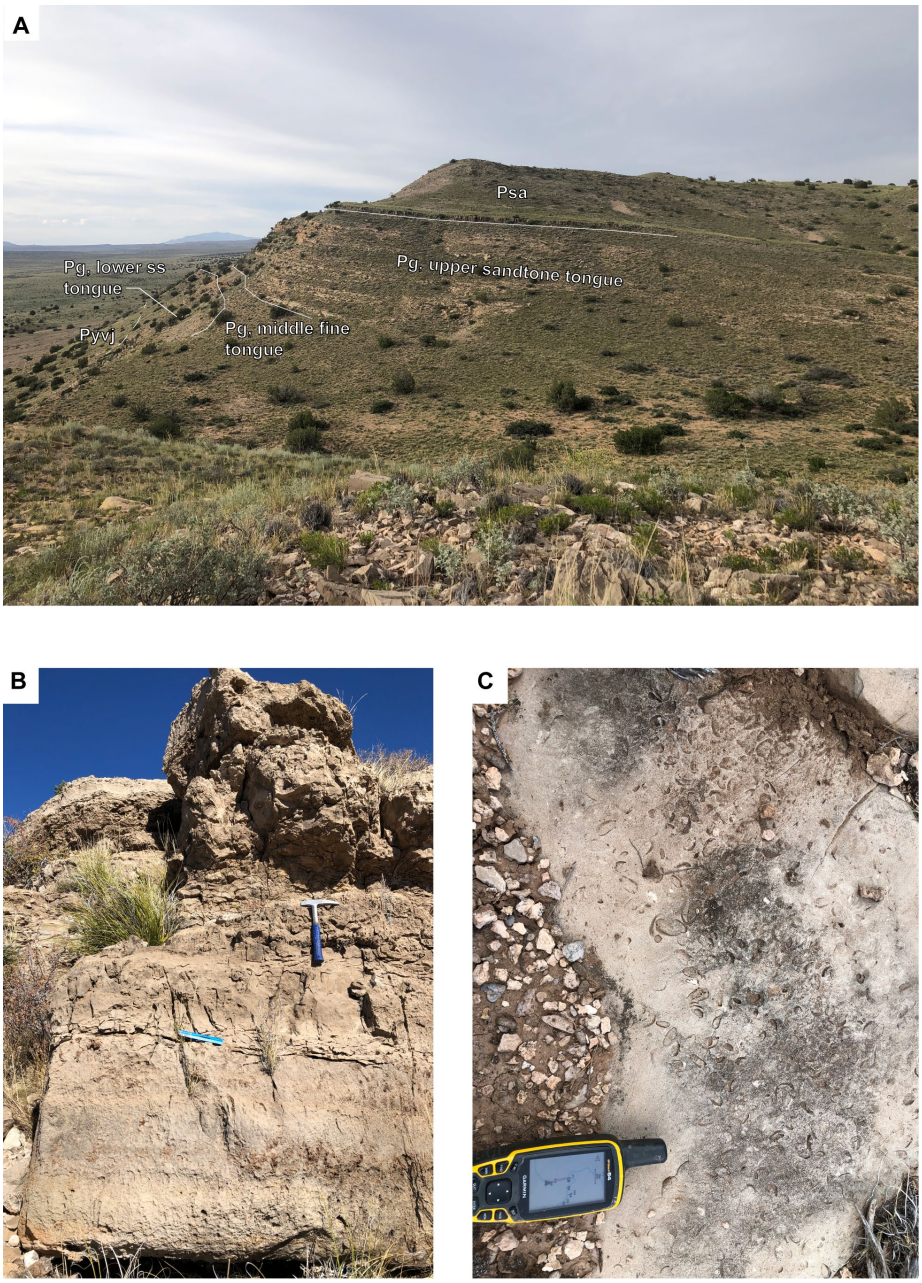

Figure 9—(A): Lowest San Andres Formation (**Psa**) underlain by the Glorieta Sandstone (**Pg**). The planar contact between the two formations is placed at the base of the lowest, relatively continuous ledge of dolomite. No sandstone tongues were noted above this contact at this location (west limb of the Torres syncline), but on the north and northeast side of the syncline there is a notable tongue of cemented sandstone above the lowest dolomite. The Glorieta Sandstone in the eastern half of the quadrangle has a lower and upper sandstone tongue separated by a middle, fine-grained interval that is several meters thick (labeled here as **Pg**, middle fine tongue). North and east of the Torres syncline, the middle fine-grained interval locally hosts intermediate-composition sills. The Joyita Member (**Pyvj**) of the Los Vallos Formation lies below the lower Glorieta Sandstone tongue. The Los Vallos Formation is split into members for this figure, but is mapped as **Pyv**. **(B):** Micritic limestones at the base of the main body of the San Andres Formation. The base of the San Andres here is gradational with the underlying Glorieta Sandstone. Below the blue ruler is calcareous sandstone (sand content decreasing upsection) and above the ruler is a micritic limestone. Rock hammer for scale. The Glorieta Sandstone lies just below the view of the photograph. Outcrop at UTM 13S 399854m E, 3813666m N, NAD83. **(C)**: Bivalve shells in the lower San Andres Formation (UTM 13S 389458 E, 3811566 N, NAD83).

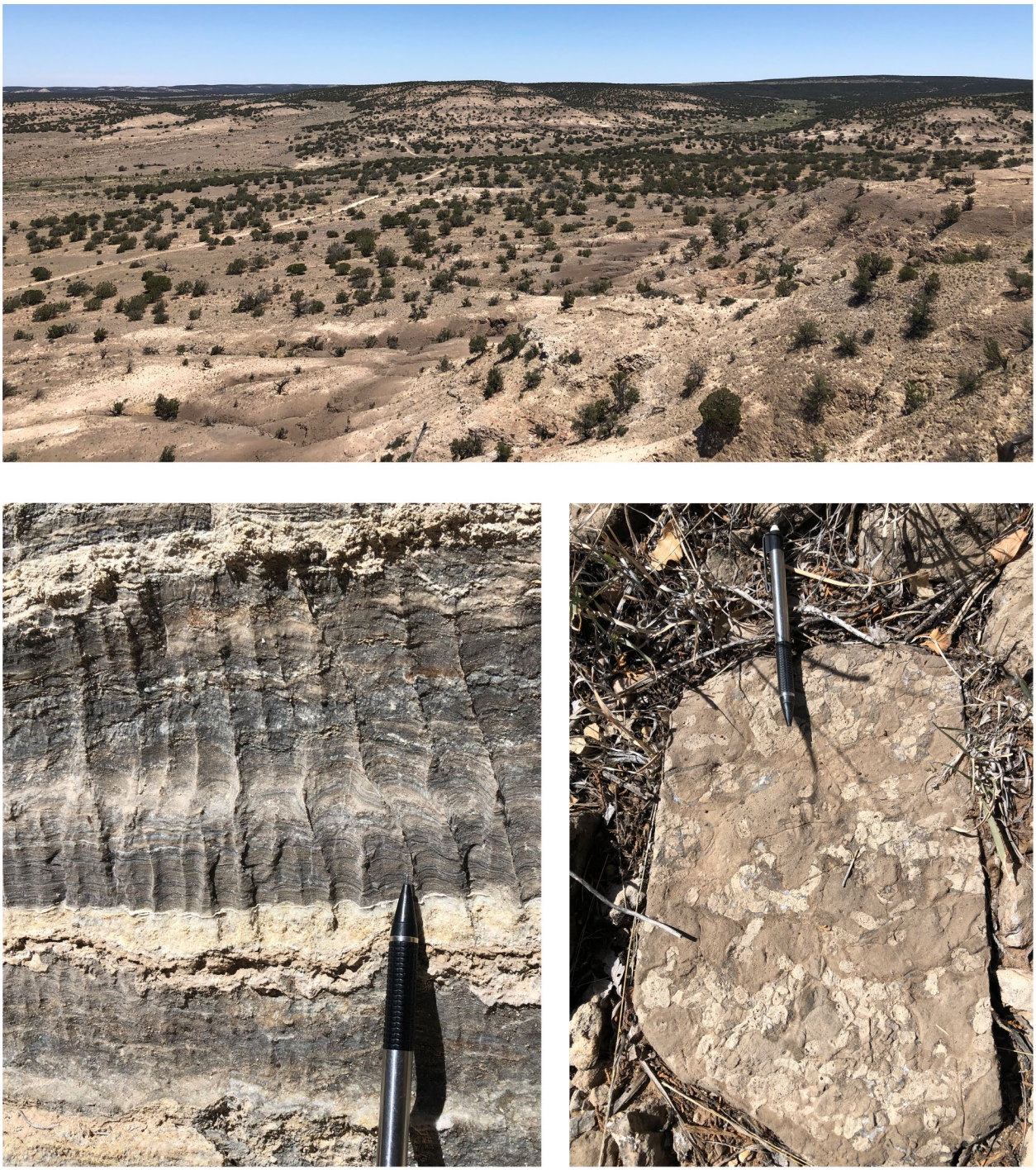

Figure 10—Photographs of the San Andres Formation east of the Quebradas highlands. **(A):** Gypsum-dominated strata in the upper half of the San Andres Formation, looking north along the Chupadera Mesa escarpment in the Mesa Well Canyon drainage. **(B):** Close-up view of laminated gypsum, from near where photograph A was taken. (UTM 13S 38733m E, 3764832m N, NAD83). **(C):** Burrow marks in micritic limestone of the lower San Andres Formation; burrows are 2–3 cm wide and several cm long. Photograph taken at the north edge of Mesa Chupadera about 8.5 km south of Mountainair (UTM 13S 386950m E, 3812010m N, NAD83).

The Artesia Formation is easily eroded and only rarely crops out. It consists of reddish-orange, reddish-brown, or pale-red siltstone and very fine- to fine-grained sandstone that is quartzose. There are minor beds of gypsum and carbonates (dolomite or limestone). It represents deposition on a relatively arid coastal margin during the Roadian–Wordian ages (271–266 Ma; Lucas et al., 2022b; Cather and Koning, 2024).

Triassic and Jurassic

The Triassic strata on the quadrangle consists of a 180- to 200-m-thick sequence of mudstones, sandstones, and minor conglomerate (Cather and Koning, 2024). This sequence is divided into two formations that are lumped together on the geologic map. Both were deposited in continental settings by rivers. The lower unit, the Moenkopi Formation (10–30 m thick), consists of reddish-brown to chocolate-brown mudstone, lithic-arenite sandstone, and minor conglomerate; the sandstone is ledge forming and commonly cross-stratified. The overlying Chinle Formation (Fig. 11A) is characterized by reddish-brown, gray, and purplish-gray fluvial mudstone with subordinate sandstone, limestone-pebble intraformational conglomerate, and freshwater limestone. The Shinarump Member is locally observed at the base of the Chinle Formation. It consists of discontinuous, lenticular beds of reddish-brown to grayish-red, fine- to coarse-grained sandstone with well-rounded pebbles of chert, quartzite, and limestone up to a few centimeters long (Fig. 12A). Although Cather and Koning (2024) estimate a thickness of 0–30 m, typically only a few meters are exposed. These strata were deposited during the Middle to Late Triassic time (ca. 240–210 Ma).

Triassic strata are unconformably overlain by the Morrison Formation, which pinches out to the southwest and is only found east of the Joyita Hills on this quadrangle. The Morrison consists of a fine- to medium-grained lithic arenite sandstone that is commonly kaolinitic (Cather and Koning, 2024). The sandstone is interbedded with greenish-gray mudstone and sandy siltstone that represent fluvial deposition.

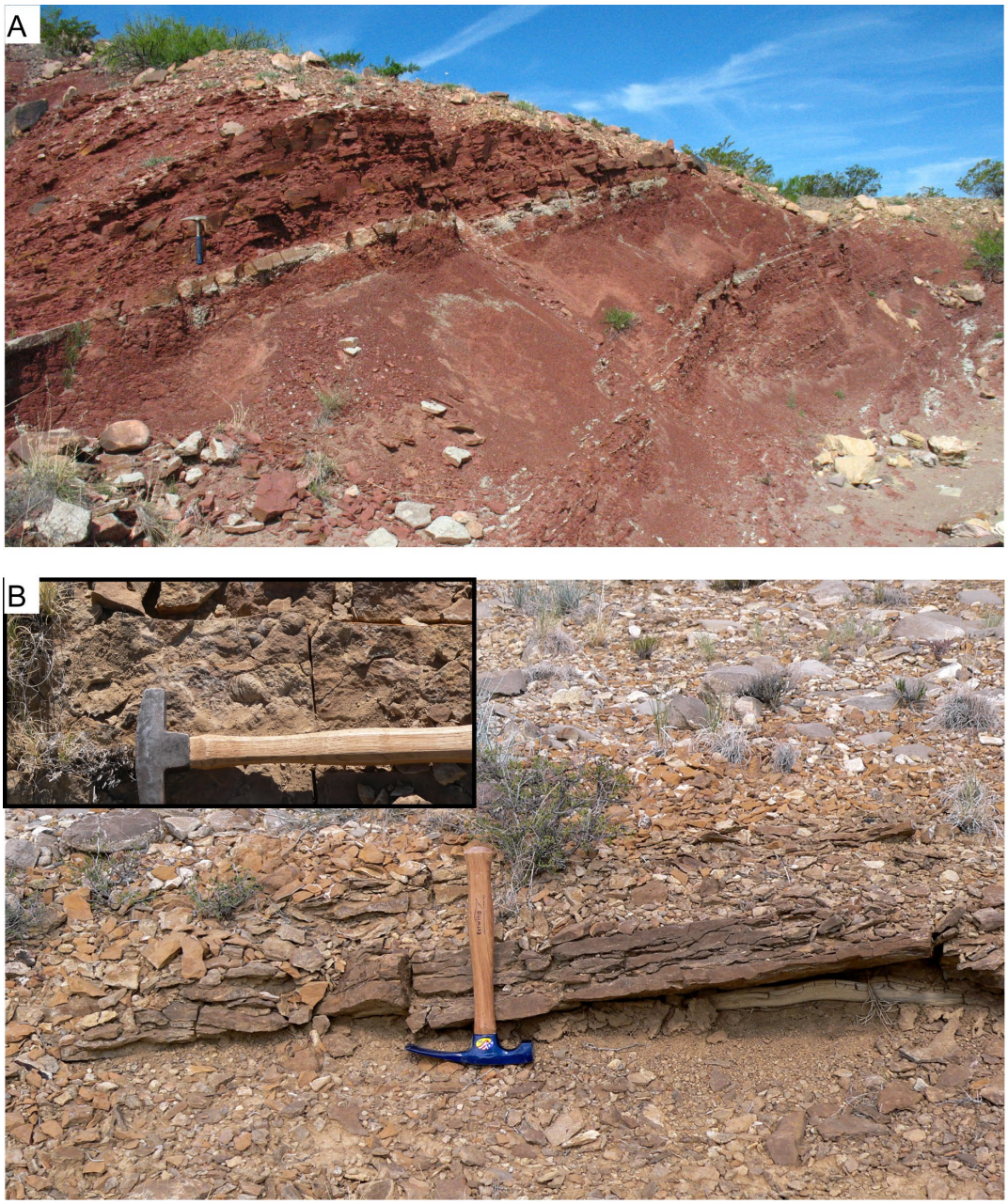

Figure 11—(A): Reddish-brown mudstones, siltstones, and very fine- to fine-grained sandstones of the San Pedro Arroyo Member of the Chinle Formation. Photograph taken a short distance south of the southern quadrangle boundary (UTM 13S 338749m E, 3751747m N, NAD83). **(B):** A fossiliferous calcarenite bed near the base of the D-Cross Tongue of the Mancos Shale, correlated to the Juana Lopez beds by Hook and Cobban (2013, fig. 11, unit #18). Photographed in the northwestern Jornado del Muerto coal field, located about 20 km northeast of Carthage. The Juana Lopez beds are interbedded in noncalcareous, grayish marine shale, are 3.1 m thick, and their base lies 2.6 m above the disconformable lower contact of the D-Cross Member (Cather and Koning, 2024). Fossils depicted in the inset photograph (top left) are interpreted as Inoceramus perplexus Whitfield (from USGS Mesozoic Invertebrate Locality D10466 from NW1/4 sec. 5, T. 3 S., R. 3 E., New Mexico Meridian, Bustos Well quadrangle; per S. Hook, written communication, 2024). Cretaceous strata are commonly characterized by brownish sandstones and yellowish-brown to olive-brown mudstones, in contrast to the reddish mudstones to sandstones of the overlying Baca Formation and underlying Chinle Group (or, where present, the pastel-colored Morrison Formation).

Upper Cretaceous

The Cretaceous section consists of yellowish-tan to brownish, terrestrial, nearshore, and marine strata. Only the early part of the Late Cretaceous epoch is preserved. This interval includes the Dakota Sandstone, Mancos Shale, Tres Hermanos Formation, Gallup Sandstone, and Crevasse Canyon Formation. Collectively, these strata record three major marine transgression-regression cycles of the WIS, with the last transgression represented by a 30-m-thick tongue of the Mancos Shale (Mulatto Tongue) interbedded in the lower Crevasse Canyon Formation (Cather and Koning, 2024). A detailed overview of the Late Cretaceous in the map area is presented in Cather and Koning (2024). For the purposes of depiction on a 1:100,000-scale geologic map, we simply divide the Late Cretaceous strata into lower and upper intervals.

Lower Interval of the Upper Cretaceous

The lower map unit of the Upper Cretaceous is 300–360 m thick and includes the Dakota Sandstone, Mancos Shale (lower tongue and D-Cross Tongue), and Tres Hermanos Formation (Cather and Koning, 2024, and references therein). The lowest of this sequence, the Dakota Sandstone, features a 5- to 20-m-thick interval of gray to yellow, medium- to coarse-grained, quartz-rich sandstone and minor mudstone deposited in a fluvial depositional environment that grades upsection to marginal marine. The Mancos Shale is calcareous to noncalcareous, gray, marine shale that commonly weathers to yellowish colors. The lower Mancos (Tokay) tongue (between the Dakota Sandstone and Tres Hermanos Formation) contains minor, thin, fine-grained sandstone beds near the base and top of the unit; the Tokay Tongue also has the 19-m-thick Bridge Creek Limestone Beds about one-third from the base. The upper Mancos tongue (D-Cross) lies between the Tres Hermanos Formation and Gallup Sandstone and is noncalcareous but locally contains scattered calcrete concretions near its base and top. At the base of the Mancos lie fossiliferous calcarenites of the Juana Lopez beds (Fig. 11B).

The Tres Hermanos Formation contains three undifferentiated members (not mapped) deposited during a marine regression and subsequent transgression. We list these members in ascending stratigraphic order using descriptions from Cather and Koning (2024). The Atarque Sandstone is composed of light-gray to dark-brown or buff-colored sandstones that form ridges. Its base is transitional with underlying shale. The Atarque Sandstone was deposited in a coastal barrier-island environment during the regression phase. The Carthage Member consists of sandstone and shale that commonly form slopes. The lower two-thirds of the Carthage Member contains thin, fine-grained sandstone beds (of paludal-lacustrine or crevasse splay origin) and discontinuous cross-bedded channel-fill sandstones. It was deposited in a coastal plain at the culmination of the regression. The upper third of the Carthage Member was deposited in the ensuing transgression and consists of marine shale with fossiliferous concretions. The Fite Ranch Sandstone Member is a ridge-forming unit composed of light-gray (weathering light to dark brown), highly bioturbated sandstones that coarsen upward from very fine grained to fine grained. The Fite Ranch Member was deposited in a coastal barrier-island paleoenvironment.

Upper Interval of the Late Cretaceous

The upper interval records a retreat of the WIS ca. 90–85 Ma. The upper interval varies from 20 to 300 m thick. The ridge-forming nature of the Gallup Sandstone makes it a logical choice to demarcate the lower part of the upper interval. This formation is a gray to yellowish-gray, fine-grained sandstone and mudstone that is 5–15 m thick and was deposited during the aforementioned regression in a coastal barrier-island depositional environment. The overlying Crevasse Canyon Formation is composed of a coarsening-upward sequence characterized by tan to gray to olive-brown sandstone, mudstone, and siltstone deposited in coastal plain, brackish lagoon, and fluvial depositional paleoenvironments. Local coal seams are found near the base and were targets for local coal mining, including Carthage to the south of the map area (Cather and Koning, 2024) and the Jornada coal field east of the Blackington Hills (see below; Cather and Koning, 2024). About 50 m above the top of the Gallup Sandstone, a 30-m-thick tongue of marine shale (Mulatto Tongue of the Mancos Shale) is intercalated within the lower Crevasse Canyon Formation (Cather and Koning, 2024).

Cenozoic

The Cenozoic strata on the quadrangle reflect relatively continuous deposition since ca. 55 Ma. Terrestrial deposits in the Paleogene record the transition from Laramide basin fill (Baca Formation) to voluminous volcaniclastic deposition (Spears Group). Proceeding upsection, the volcaniclastic sands and gravels are increasingly interbedded with rhyolitic ignimbrites and basaltic andesite flows of the Datil and Mogollon Groups. The voluminous Hells Mesa Tuff, which erupted from the Socorro caldera at 32.35 Ma, makes up the uppermost part of the Datil Group. The lower Oligocene strata (31–28 Ma) overlie a contact corresponding to an unconformity (2–3 Myr lacuna) or compressed section; these strata include thick, high-silica ignimbrites interbedded with La Jara Basaltic Andesite flows and subordinate conglomerates and sandstones of the upper Spears Group. Wedge-like thickening of La Jara tongues and the Lemitar Tuff in fault-bounded half grabens indicates extension during 34–28 Ma (Cather et al., 1994a; Chamberlin et al., 2001).

Major extension from ca. 25 Ma to the present has allowed for the deposition of a thick sequence (up to 2 km) of sandstones, siltstones, claystones, and conglomerates of the Santa Fe Group within the Rio Grande rift. The Santa Fe Group in the Socorro 30 x 60-minute quadrangle can be divided into two formations: the Popotosa Formation overlain by the Sierra Ladrones Formation. Where exposed, the boundary between the two is an angular unconformity on the margins of the Socorro Basin but may be conformable near the center of the basin.

Santa Fe Group deposition culminated at 850–800 ka (Sion et al., 2020). Since then, deposition has been characterized by a complex montage of allostratigraphic units whose deposition is controlled largely by paleoclimate-modulated fluxes of sediment and water superimposed on the long-term incision of the Rio Grande. Post-Santa Fe Group sedimentary deposits are associated with alluvial activity along major valleys and drainages, sheetfloods on gently sloping bajadas

and basin floors, eolian activity, and mass wasting (landslides). The alluvial map units are divided into three general time periods: "older" (middle Pleistocene), "intermediate" (mainly late Pleistocene), "younger" (latest Pleistocene to Holocene), and "recent" (historic to present).

Baca Formation

The Baca Formation consists of grayish to reddish-brown conglomerates and conglomeratic sandstones. The Hart Mine Formation has been proposed for the Baca Formation east of the Rio Grande by Lucas and Williamson (1993), but we retain usage of Baca Formation for reasons listed in Cather et al. (2013) and because the majority of past studies have continued use of that name. On the west side of the Rio Grande, trough- and tabular-bedded conglomerates appear to fill a paleovalley cut into the underlying Madera Group limestone about 2 km south of Polvadera Mountain (Chamberlin et al., 2001). Baca Formation strata are also present near Corkscrew Canyon in the southern Lemitar Mountains. In the Quebradas region, the Baca Formation consists of sandstone, conglomerate, and minor reddish mudstone (Cather and Koning, 2024). Sandstone is commonly cross-bedded and subarkosic (Fig. 12B). The conglomerate consists of pebbles, cobbles, and boulders composed of Proterozoic lithotypes (granite, gneissic granite, schist, and quartzite) and Paleozoic lithotypes (limestone, sandstone, and siltstone; Fig. 12C). In the northern Quebradas region, there are intervals containing clasts of well-rounded quartzite and metavolcanics. The Baca Formation is ≈300 m thick in the Quebradas region, but only 0–30 m thick west of the Rio Grande valley.

Figure 12—Photographs of gravelly Triassic and Paleogene conglomeratic strata. **(A)** Upper Triassic Shinarump Member of the Chinle Formation, hammer for scale; photograph taken at UTM 13S 338504m E, 3752158m N, NAD83. The rounded pebbles are composed primarily of chert, quartz, and quartzites. **(B)** Arkosic, coarse to very coarse-grained sand of the Baca Formation. Pencil for scale. **(C)** Middle Eocene Baca Formation, hammer for scale. Gravel compositions are relatively diverse and include grayish Paleozoic limestones-dolomites (l-d), reddish Permian siltstones to very fine-grained sandstones (P), and Proterozoic gneiss and granitoids (g). **(D)** Grayish, conglomeratic sandstone of the Spears Group; photograph taken ≈1 km south of the southern quadrangle boundary in the Blackington Hills (Fig. 1). Rock hammer for scale. All photographs courtesy of Steven Cather.

Spears Group

In the Lemitar Mountains and Joyita Hills, the Spears Group (as defined in Cather et al., 1994b) consists of grayish-red to light-gray conglomerates, sandstones, siltstones, and reddish mudstones derived from intermediate-composition volcanic highlands (Figs. 12D and 13A; Chamberlin et al., 2001; Cather et al., 2004, 2014; de Moor et al., 2005). These highlands were located primarily to the southwest. Conglomeratic beds are lenticular to tabular and usually 1–3 m thick. Gravels range from boulders to pebbles and are composed of andesite (plagioclase and pyroxene phenocrysts) and dacites (plagioclase, hornblende, and biotite phenocrysts). In the lower ≈30 m of the unit, these volcanic clasts are mixed with gray micritic limestone and cobbles and pebbles composed of red siltstone to very fine-grained sandstone. Medium-grained pyroxene monzonite and dark-gray, aphanitic basaltic andesite clasts occur sparsely in the upper half of the formation in the Lemitar Mountains (Chamberlin et al., 2001). The Spears Group is 120–330 m thick near Polvadera Peak and 700–800 m thick east of the Rio Grande. This unit grades conformably downward into the underlying Baca Formation. The age of the Spears Group is 43–33 Ma, based on potassium-argon (K/Ar) and $^{40}Ar/^{39}Ar$ dates of volcanic clasts and interbedded tuffs (Osburn and Chapin, 1983; Cather and Koning, 2024).

In the Quebradas region, the Spears Group consists of a lower ≈760-m-thick unit and an upper 0- to 120-m-thick unit (Cather and Koning, 2024). The lower unit is composed of medium- to light-gray, volcaniclastic sandstone, conglomerate, debris-flow breccia, and minor muddy sandstone-mudstone (Figs. 12D and 13). Clasts are dominated by plagioclase- and amphibole-bearing andesite-dacite. The upper Spears Group in the Quebradas area consists of dark- to medium-gray volcaniclastic sandstone and conglomerate with local debris flows. Clasts are mostly basaltic andesite (plagioclase- and pyroxene-phyric) and andesite-dacite with plagioclase and amphibole phenocrysts.

Volcanic Rocks of the Datil and Mogollon Groups

The Datil Group comprises the lava flows and ignimbrites that include and lie below the Hells Mesa Tuff (Cather et al., 1994b). Some of these flows and practically all the ignimbrites have formal names which we use in this study (Cather et al., 1994b, fig. 3, synthesizing earlier work by Osburn and Chapin [1983], and McIntosh et al. [1992]). The volcanic deposits intertongue with volcaniclastic deposits of the Spears Group, together forming a sequence up to 150 m thick. In the map area, the lavas and ignimbrites of the Datil Group are volumetrically minor compared to the Spears Group.

The Datil Group is best exposed in two localities: the Joyita Hills and the Blackington Hills, and we describe it below at each of these localities. Note that all $^{40}Ar/^{39}Ar$ ages are from Cather and Koning (2024, table 3); descriptions are compiled from Cather and Koning (2024) and individual 7.5-minute quadrangles (appendix A). At the Joyita Hills, the Datil Group includes the following rocks: La Jara Peak Basaltic Andesites (**Tlp**), upper Spears Group of Cather and Koning (2024), and tuff of Arroyo Veranito (Chamberlin et al., 2022a. At the Blackington Hills, the Datil Group

contains the following ascending sequence: Datil Well Tuff, Rockhouse Canyon Tuff, Hells Mesa Tuff, and upper Spears Group of Cather and Koning (2024). There, the **Datil Well Tuff** is a 0- to 50-m-thick, medium-brownish-gray, crystal-rich, rhyolitic ignimbrite; its phenocrysts are composed mostly of sanidine with subordinate plagioclase and lesser quartz, biotite, and pyroxene(?). Sanidine $^{40}Ar/^{39}Ar$ ages from the Datil Well Tuff are 35.38 ± 0.01 to 35.32 ± 0.02 Ma. The **Rock House Canyon Tuff** is a light-gray, poorly to moderately welded, crystal-poor, rhyolitic ignimbrite. Phenocrysts are mostly sanidine with rare quartz, biotite, and hornblende(?). The Rock House Canyon tuff returned an $^{40}Ar/^{39}Ar$ sanidine age of 34.78 ± 0.01 Ma. Overlying the Rock House tuff is a **dacite flow near Blackington Hills** that is brownish-gray and contains plagioclase and amphibole phenocrysts. This dacite has an $^{40}Ar/^{39}Ar$ age of 34.04 ± 0.02 Ma. The **Hells Mesa Tuff** is found across the western map area and is a reddish-brown to purplish-gray, densely welded, phenocryst- and quartz-rich, rhyolitic ignimbrite. It has 40%–50% phenocrysts that are typically 1–3 mm and composed of sanidine, plagioclase, quartz, and minor biotite. Southwest of Socorro, the plagioclase is altered to chalky minerals and adularia in association with potassium metasomatism. In the Lemitar Mountains, the lower part of the Hells Mesa Tuff is a 30- to 60-m-thick, light-gray to grayish-red to light-brownish-gray, nonwelded to densely welded, moderately pumiceous, quartz-poor ignimbrite that contains 35%–45% phenocrysts composed of plagioclase (commonly replaced by adularia) with minor biotite, sanidine, altered hornblende, and clinopyroxene(?).The $^{40}Ar/^{39}Ar$ age for the Hells Mesa Tuff is 32.35 ± 0.01 Ma, and it was expelled from the Socorro caldera, located immediately southwest of Socorro (Fig. 14).

The Mogollon Group is up to 700 m thick and consists of ignimbrites interbedded with basaltic andesite lavas. Its large thickness allows it to be divided into a lower and upper unit. These are described separately below. All listed ages are from Cather and Koning (2024, table 3). Descriptions are compiled from Cather and Koning (2024) and individual 7.5-minute quadrangles (appendix A).

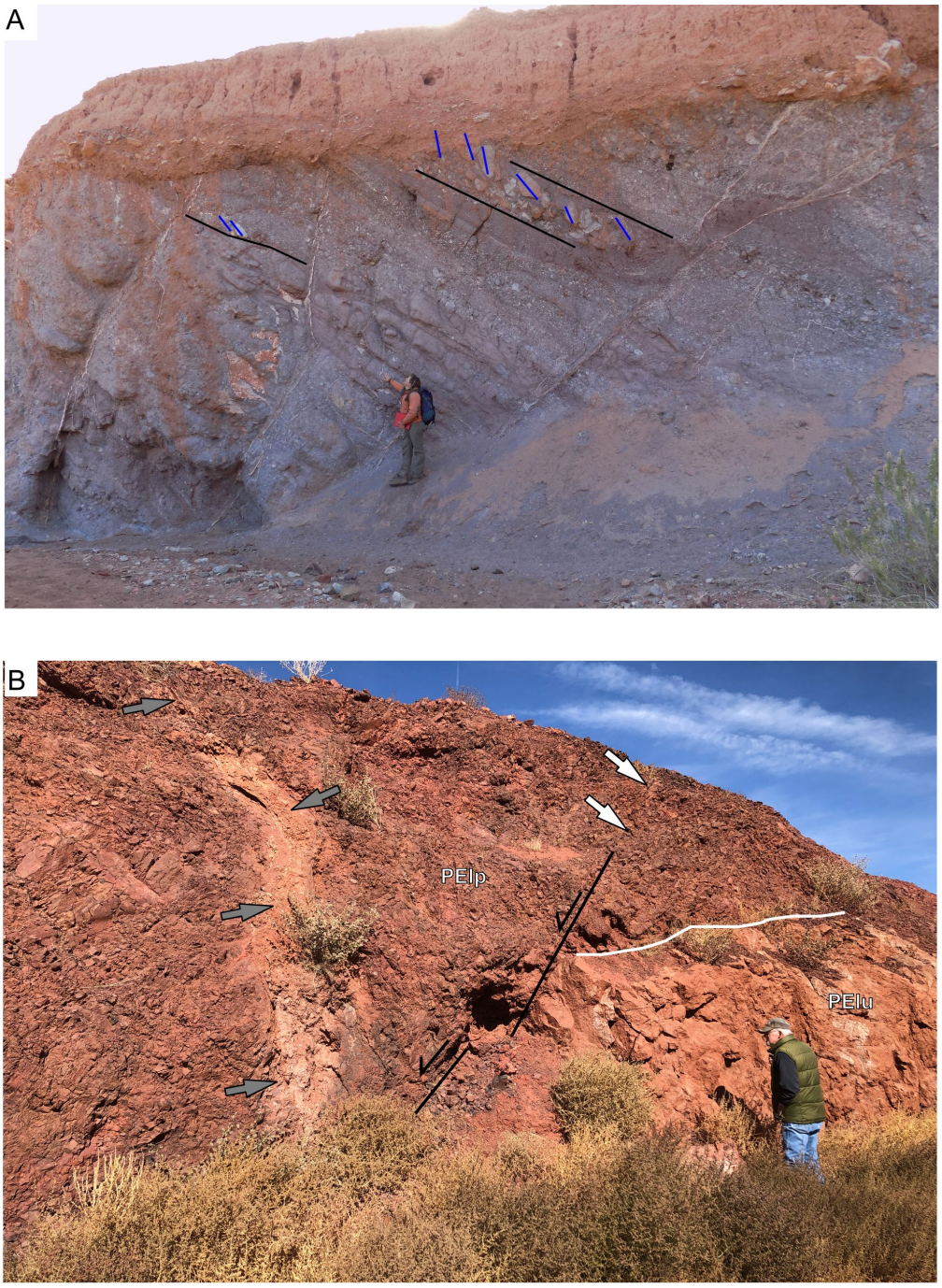

Figure 13—(A): Photograph of lower Spears Group conglomeratic strata 0.3 km southwest of Ojo de Amado Spring. View to the south-southwest. Note the tilting of outcrop-parallel gravel axes of certain gravelly intervals (blue lines) relative to bedding planes (black lines). We interpret these gravel tilts as resulting from fluvial imbrication; thus, paleoflow during the lower Spears Group was to the left (east). **(B):** Exposure of the upper Mogollon Group, located 1.8 km south of the southern quadrangle boundary in the southwestern corner of the quadrangle (UTM 13S 316000m E, 3762000m N, NAD83). **:lp** = La Jara Peak Basaltic Andesite and **Pelu** = upper part of Lemitar Tuff. The La Jara Peak Basaltic Andesite is unusually red here due to potassic metasomatism; most flows are medium-gray. A notable fault (black line) has downdropped **Pelp** against **Pelu**, whose outcrop extension is indicated by white arrows. Another fault zone is shown by the gray arrows. Many other small faults are present in the outcrop but not shown (cf. Koning et al., 2022a, fig. 2.25).

The lower unit of the Mogollon Group includes (in ascending order); tuffs of the Luis Lopez Formation, La Jencia Tuff, and Vicks Peak Tuff. **Tuffs of the Luis Lopez Formation** are light-brownish-gray to light-gray, poorly welded, pumiceous, rhyolitic ignimbrites representing primarily fallout deposition. The tuffs contain moderately abundant pumice (mostly aphyric) and sparse to moderately abundant, small lithic fragments (andesite, Hells Mesa Tuff) in a fine-grained matrix. Crystals are mostly sanidine, quartz, and plagioclase. There are two main tuffs: medial ($^{40}Ar/^{39}Ar$ age 30.43 ± 0.1 Ma; Chamberlin et al., 2004) and upper (29.03–29.00 Ma). The **La Jencia Tuff** is a light-gray to grayish-red, phenocryst poor, rhyolitic ignimbrite. The La Jencia Tuff contains 3%–5% phenocrysts of sanidine and quartz with traces of plagioclase and biotite. This tuff exhibits a distinctive, very densely welded, rheomorphic (flow-banded) zone in its middle part that grades upward and downward to a eutaxitic ignimbrite. It has an $^{40}Ar/^{39}Ar$ age (from sanidine) of 29.00 ± 0.01 Ma and was sourced from the Sawmill Canyon caldera in the Magdalena Mountains (Fig. 14; Osburn and Chapin, 1983). The La Jencia Tuff is as much as 120 m thick in the eastern Lemitar Mountains. The **Vicks Peak Tuff** (up to 75 m thick) is a light-gray to pale-red, phenocryst-poor, densely welded, rhyolitic ignimbrite that is up to 75 m thick. It is notably phenocryst-poor, containing only 1%–5% phenocrysts of sanidine and sparse quartz. It has an $^{40}Ar/^{39}Ar$ age of 28.77 ± 0.01 Ma and was sourced from the Nogal Canyon caldera in the southern San Mateo Mountains (Osburn and Chapin, 1983).

The upper unit of the Mogollon Group includes the La Jara Peak Basaltic Andesite flows, Lemitar Tuff, and South Canyon Tuff (Fig. 13B). The **La Jara Peak Basaltic Andesite** consists of tongues of medium-gray, purplish-gray, and grayish-red-purple basaltic andesite intercalated with Oligocene ignimbrite flows—particularly the Vicks Peak, Lemitar, and South Canyon Tuffs. Individual tongues are commonly 30–300 m thick and composed of many tens of flows, each about 3–10 m thick. The lava is massive to vesicular and contains 5%–10% fine-grained phenocrysts of olivine altered to reddish-brown iddingsite along with minor pyroxene phenocrysts. Phenocrystic plagioclase is absent or very sparse west of the Rio Grande, but the unit (as mapped) locally includes plagioclase phenocrysts east of the Rio Grande. The **Lemitar Tuff** is an ignimbrite containing a phenocryst-poor (5%–15%, increasing upsection), light-gray lower member and a densely welded, pink to dark-red, phenocryst-rich (30%–45%) dacitic to rhyolitic upper member. Phenocrysts include quartz, sanidine, plagioclase (locally altered), and biotite (trace augite and sphene). Lithics are minor. Phenocryst-poor (3%–5%) pumice is found in the lower member. Sparse, phenocryst-rich pumice and small (<2 cm), grayish-red "magma blobs" of dacite occur in the upper member. The Lemitar Tuff has an $^{40}Ar/^{39}Ar$ age of 28.24 ± 0.01 Ma (sanidine) and was sourced from the Hardy Ridge caldera in the southwestern Magdalena Mountains (Fig. 14; Ferguson et al., 2012). The tuff filled wedge-shaped paleovalleys and is up to 60–90 m thick. The **South Canyon Tuff** is a light-gray to pale-grayish-red to light-purple, pumiceous, densely welded, rhyolitic ignimbrite with common lithic fragments. Phenocryst content increases upsection from ≈5% in the ≈30-m-thick, partially welded base to ≈25% near the densely welded top. Phenocrysts are composed of subequal quartz and sanidine (the sanidine commonly being chatoyant). The South Canyon Tuff also has 5%–15% pumice (1–5 cm long).

Sanidine crystals have yielded an $^{40}Ar/^{39}Ar$ age of 27.67 ± 0.01 Ma (Cather and Koning, 2024). The South Canyon Tuff was sourced from the Mount Withington caldera (northern San Mateo Mountains, as shown in Fig. 14; Ferguson, 1991; Ferguson et al., 2012) and is up to 90 m thick.

Numerous dikes and sills occur in the Socorro 30 x 60-minute quadrangle (Figs. 14 and 15). Dikes are particularly common in the eastern half of the quadrangle, where they mostly trend northeast-southwest to slightly north of east. Relatively mafic sills are exposed east of the northern Joyita Hills. Along the east side of the Joyita Hills, a rhyolitic intrusion is found that contains phenocrysts of plagioclase, sanidine, biotite, and quartz. This intrusion crosscuts strata as young as the 32.35 Ma Hells Mesa Tuff, consistent with a K/Ar age of 31.3 ± 1.2 Ma (Aldrich et al., 1986).

Across the quadrangle, more than 90% of the dikes are intermediate to mafic in composition. Where described, the dikes are whitish to very light- to medium-gray (mostly medium-gray), weathering to medium- or dark-gray, nonvesicular, massive, and aphanitic to porphyritic. Where porphyritic, phenocrysts include plagioclase (subhedral), hornblende (subhedral to euhedral prisms, locally >10 mm long), minor biotite, and trace quartz; these minerals are relatively similar to those previously described by Bates et al. (1947), except they also note the presence of orthoclase, pyroxene, and magnetite in some samples. Locally, two feldspar types are present. Aphanitic to fine-grained intrusions are dark gray and contain <1-mm-long crystals of plagioclase and subordinate mafic grains (mostly amphibole). Some dikes contain occasional xenoliths, up to 7 cm in diameter, of mafic material with subequal plagioclase and pyroxene phenocrysts and rare biotite. Published compositional data from comparably few samples indicate silicic basalts or hornblende-bearing diorites (Aldrich et al., 1986; R.C. Chamberlin, written communication, 2024). Dikes exposed in the Yeso Group are commonly 45–75 m wide, but those penetrating Paleogene strata of the La Joya area are usually 1–20 m wide. In the eastern half of the quadrangle, most exposures show dikes and sills intruding Permian strata, primarily the Torres Member of the Los Vallos Formation. Sills are also present in Glorieta Sandstone in the ≈10-m-thick, fine-grained middle tongue. Diking on Chupadera Mesa and the Claunch uplands to the east is commonly manifested by narrow anticlines trending east-northeast. It is inferred that these anticlines are directly underlain in the upper Yeso Group by similarly trending dikes or aligned sills (Bates et al., 1947; Cather, 2009a). The presence of sills exposed at the western end of the anticline trending along Grumble Gulch support this interpretation (Fig. 15, site labeled GG).

We have compiled radiometric ages from nine samples of intrusions from the Quebradas highlands, Chupadera Mesa, Rayo Hills, and the Claunch uplands (Table 1, Fig. 15). Three of these samples came from sills and the other six from east- to northeast-trending dikes. Results indicate a clustering of ages between 33 and 30 Ma. One sample from a dike at Gran Quivira returned an age of 27.3 ± 0.04 Ma. A sill and dike in the Quebradas gave preferred ages of 21.25 ± 0.15 Ma and 20.34 ± 0.13 Ma (Table 1). How these ages might relate to regional tectonism and magmatism is discussed in the Geologic History section below.

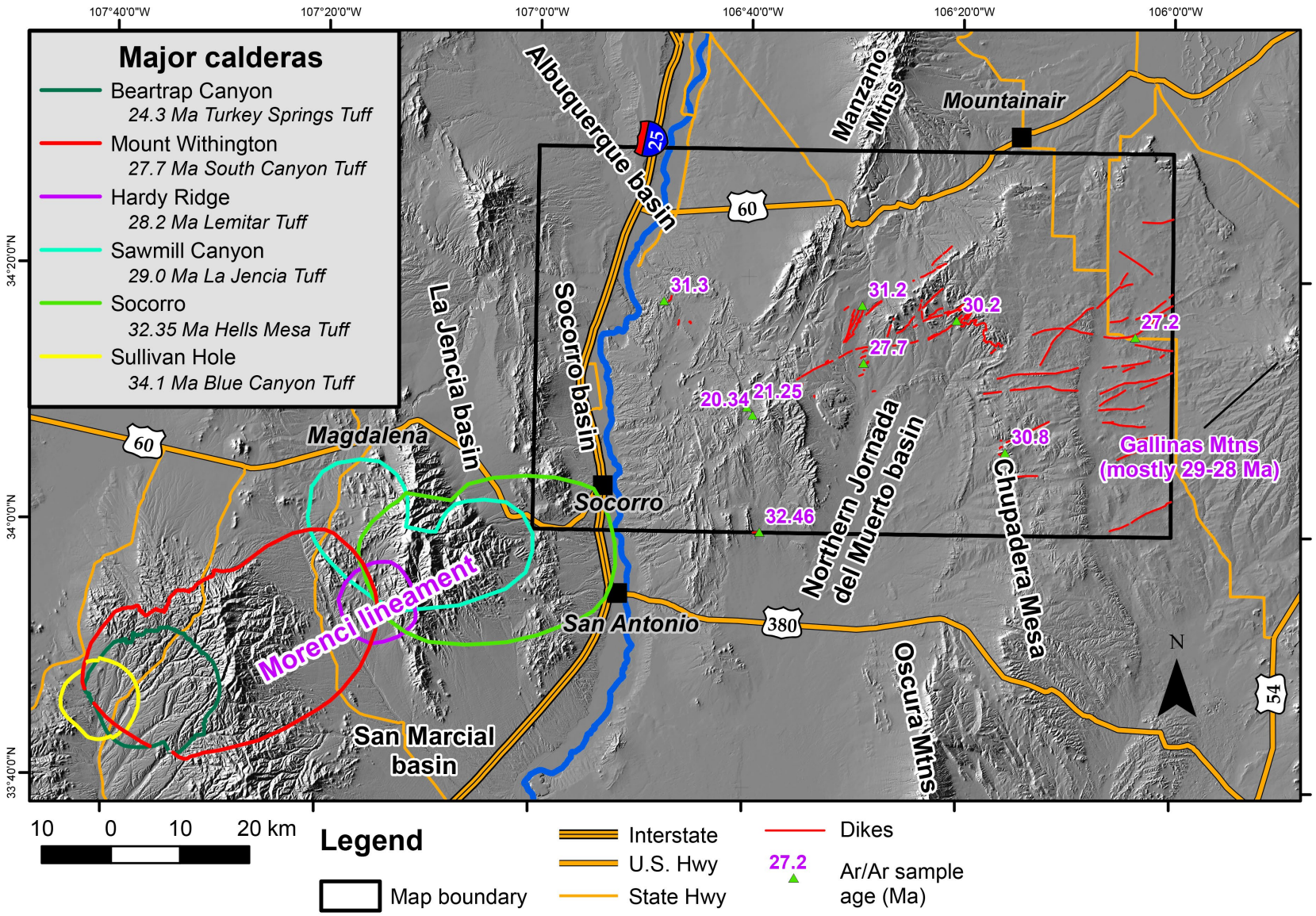

Figure 14—Map showing the location and orientation of dikes in the Socorro 30 x 60-minute quadrangle relative to the Gallinas Mountains intrusive center (right) and latest Eocene and Oligocene calderas (left). Locations and results (in Ma) of radiometric samples of dikes and sills are shown from Table 1.

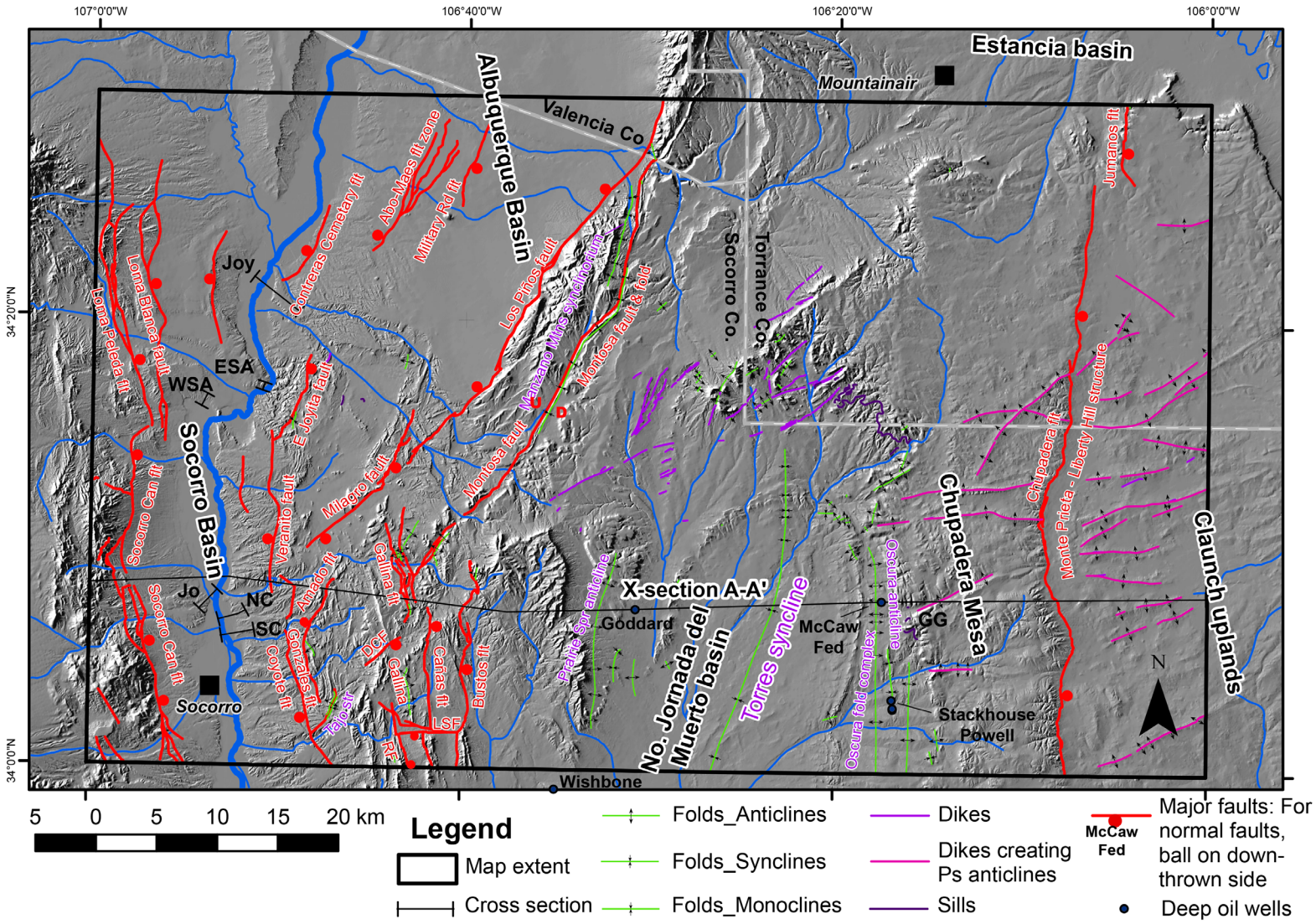

Figure 15—Map showing major faults, folds, and dikes in the Socorro 30 x 60-minute quadrangle. GG= Grumble Gulch. Abbreviations for terrace cross-section labels (appendix D) are ESA = East San Acacia, Jo = Journey, Joy = Joyita, NC = North Coyote, SC = South Coyote, WSA = West San Acacia. Abbreviations for fault labels are DCF = Del Curto fault, LSF = Landing Strip fault, RF = Ranchito fault. Note that there are additional dikes in the eastern part of the Joyita Hills, mainly trending northeast, but these are too small to show at this scale (see de Moor et al., 2005).

Table 1—Geochronology samples and analyses of mid-Cenozoic intrusions in central and eastern Socorro 30- x 60-minute quadrangle.

Sample	Lab ID	Location	UTM coord. (13S, NAD83)		Lithology	Orientation	Intruded interval	Material dated	Age (Ma), bold value is preferred	± 2σ (Ma)	Age type	Notes
			Easting	Northing								
SL-2*	61121-01	Sierra Larga	347154	3780362	andesite dike	50°	upper Yeso	whole rock	**20.34**	0.13	plateau	
	61128-01							biotite	*34.15*	0.02	integrated	Some complexity in spectra
SL-1*	61122-01	western La Cebolla	346343	3781485	intermediate sill	-	upper Yeso	whole rock	**21.25**	0.15	plateau	Potential age of alteration?
22RH-093A	70036	Rayo Hills, U Butte	363079	3796214	monzonitic dike (possible sill?)	35–37°	Yeso	biotite	**31.23**	0.2	psuedo-plateau	
Aldrich86-322**	-	Chupadera/Cañon Torcido	376657	3794015	intermediate dike	~43°	Yeso?	whole rock?	**30.2**	2.0	K-Ar	
Aldrich86-324***	-	Los Canoñcitos	334350	3796887	felsic (rhyolitic) dike	37–43°	Glorieta-Spears Fm.	whole rock?	**31.3**	1.2	K-Ar	
CHM100	71437	Grumble Gulch	383703	3774913	intermediate sill	Sill to SW of 65° str dike	Yeso	feldspar	**31.8**	0.6	psuedo-plateau	Mean age from two similar dates: 32.3 ± 0.9 and 31.5 ± 0.7 Ma. Messy spectra; 3rd and 4th steps used.
SOC0811-3A	71450	Blackington Hills	348136	3763416	intermediate-mafic; small feld and amph phenos	86°	Spears Fm.-Oligocene volcanics	groundmass	**32.92**	0.02	integrated	No plateau determined. Isochron age at 32.74 +/- 0.30 Ma.
SQSA23-5	71451	Gran Quivira	402523	3791496	intermediate dike	~55°	San Andres	feldspar	**27.26**	0.04	psuedo-plateau	Mean age using 27 ± 0.1 and 27.3 ± 0.04 Ma. Excess Ar; used first 3 steps in both.
SQSA23-9	71443	Patterson Draw	363233	3787845	amphibole-rich intermediate dike	63°	upper Yeso	feldspar	27.6	0.2	plateau	Isochron age of 27.45 +/- 0.23 Ma
									28.3	0.2	plateau	Isochron age of 27.99 +/- 0.46 Ma
								hornblende	**33.98**	0.05	plateau	Plateau age; isochron age of 33.8 +/- 0.02 Ma.

*From Cather et al. (2012), Green et al. (2013), and Cather et al. (in press).

** From Aldrich et al. (1986).

*** From Aldrich et al. (1986) and de Moor (2005).

Socorro Volcanic Field

The Socorro volcanic field was active from 10 to 7 Ma, well after Mogollon-Datil volcanism ceased. It is preserved mainly on Socorro Peak, ≈5 km west of the city of Socorro. The oldest map unit (**Nsd**) lumps slightly older dacites with rhyodacites (9.7–9.5 Ma). These porphyritic lavas are light- to medium-gray to pale-red to reddish-brown and contain ≈10% fine to medium phenocrysts of plagioclase and minor to subequal hornblende ± biotite.

After a hiatus of ≈1 Myr, a second episode of volcanism occurred 8.8–7.0 Ma that was dominated by various flow-banded rhyolites and minor tephras. This second episode occurred in three general areas at different times (Chamberlin, 1999). The **rhyolite lava dome at Signal Flag Hill** (UTM 13S 320270m E, 3768630m N, NAD83) is a light-gray to light-brownish-gray to pale-red, high-silica rhyolite lava (75%–76% SiO_2) inferred to have ruptured from a north-trending fissure event at 8.71 ± 0.05 Ma. It contains 15%–20% medium-grained phenocrysts of sanidine, plagioclase, and quartz along with minor biotite. The rhyolite lava dome at the Dicaperl Minerals perlite mine (UTM 13S 320620m E, 3766570m N, NAD83) is a light-gray, glassy, high-silica rhyolite lava (76%–77% SiO_2) forming a dome ≈1 km across that is currently being mined. This dome has a glassy core >90 m thick, and a granophyric felsite zone is present on its northeast flank. It has an $^{40}Ar/^{39}Ar$ age of 7.90 ± 0.03 Ma. The rhyolite contains <1% fine phenocrysts of sanidine and plagioclase with traces of quartz and biotite. The original microvesicular, obsidian lava has been uniformly altered by hydration to commercial-quality perlite (Barker et al., 1994). **Domes 3–4 km west-southwest of Socorro Peak** are a light-gray to light-brownish-gray to pinkish-gray, low-silica rhyolite containing ≈15% medium-grained phenocrysts of plagioclase, sanidine, and biotite with minor quartz. $^{40}Ar/^{39}Ar$ ages span 7.5–7.0 Ma (Chamberlin, 1999; D.J. Koning and M. Heizler, unpublished detrital sanidine $^{40}Ar/^{39}Ar$ data).

Pliocene Volcanic Flows

Three Pliocene-age volcanic flows are mapped and dated by $^{40}Ar/^{39}Ar$ techniques (Table 2). The **trachyandesite of San Acacia** is the oldest of these flows and is located immediately east and northeast of San Acacia. The rock is medium-gray to light-brownish-gray and contains 1%–2% phenocrysts of plagioclase, augite, and reddish-brown iddingsite. There are traces of xenocrystic quartz. The lava attains a maximum thickness of 40 m and is inferred to have erupted from a north-trending fissure vent near San Acacia dam (Machette, 1978). It appears to be disconformably overlapped by ancestral Rio Grande sediment (**Nsa**), and overlies fine sands and silts deposited on the eastern edge of the ancestral Rio Grande floodplain. $^{40}Ar/^{39}Ar$ dating has returned an age of 4.93 ± 0.04 Ma (Table 2, age converted from that listed in Chamberlin et al., 2001, using Fish Canyon standard of 28.201 Ma per Kuiper et al. [2008]).

Basalt rocks cap both Black Mesa and Mesa Redonda in the west-central part of the Socorro 30 x 60-minute quadrangle. These rocks consist of a dark- to very dark-gray or nearly black, aphanitic, very fine- to fine-grained olivine basalt having a composite thickness of 15–18 m. It does not appear to have been buried by younger sediment. Phenocrysts include 2%–5% olivine and 1%–

3% pyroxene. The lava is dense to somewhat vesicular with a few amygdules filled by zeolites or calcite. Samples from Mesa Redonda and Black Mesa returned respective $^{40}Ar/^{39}Ar$ ages of 3.680 ± 0.343 Ma and 3.652 ± 0.014 Ma (Table 2).

The **basalt of Socorro Canyon** is a dark-gray, massive to vesicular, olivine basalt flow. This rock contains 1%–2% phenocrysts of olivine (1–2 mm) and sparse to rare glomerophenocrysts of plagioclase. The lava flowed down an easterly paleoslope of ancestral Socorro/Six Mile Canyon and is down-faulted into the subsurface east of the Socorro Canyon fault zone. It has an $^{40}Ar/^{39}Ar$ age of 3.78 ± 0.1 Ma (Table 2) and an average thickness of 6–9 m.

Table 2—Geochronology of Pliocene volcanic flows in the western Socorro 30- x 60-minute quadrangle.

Sample	Location	Coordinates**		Map unit	Material dated	Age (Ma)***	± 2σ (Ma)	Reference(s)	Notes
		Easting	Northing						
22MR-087*	SE corner of Mesa Redonda	360674	3779358	Tb	groundmass	3.652	0.014	Chamberlin and Zimmerer, unpublished	
see notes	Socorro Canyon basalt	see notes	see notes	Tb	groundmass	3.78	0.1	Chamberlin (1999)	Average age of four youngest samples (out of five total); see Chamberlin (1999) report and map.
NM1522	NE of San Acacia Dam	326308	3792470	Tas	groundmass	4.93	0.04	Chamberlin et al. (2001)	Originally used Fish Canyon Tuff standard age of 27.84 Ma; age of 4.75 Ma listed in Chamberlin et al. (2001) is a typo and instead should be 4.87 ± 0.04 Ma per R.C. Chamberlin (written communication, July 9, 2024).
BLKMS-1	Upper flow on SE side of Black Mesa	350488	3788371	Tb	groundmass	3.68	0.343	Cather and Koning (in press, App 2)	Complex spectrum. Sampled by R.M. Chamberlin.

* $^{40}Ar/^{39}Ar$ ages obtained for this work and plotted on the accompanying geologic map.

** Coordinates given in North American Datum of 1983 (NAD83) and zone 13.

*** Ages incorporate recalibration to a Fish Canyon sanidine standard to an age of 28.201 Ma (Kuiper et al., 2008).

Santa Fe Group

The Santa Fe Group refers to the siliciclastic fill of the Rio Grande rift and includes relatively thin, volcanic flows interbedded in this sediment. Many key stratigraphic observations regarding the Santa Fe Group were made in the western part of the map quadrangle, where it is relatively well exposed in the San Acacia and La Joya areas (Denny, 1940; Bruning, 1973; Machette, 1978). Note that we exclude thinner basin-fill deposits in the eastern quadrangle from the Santa Fe Group, although they coincide in age with the upper Santa Fe Group in the main part of the rift. The Santa Fe Group includes the Popotosa Formation and the overlying Sierra Ladrones Formation.

Popotosa Formation

The Popotosa Formation was defined by Denny (1940) and redefined by Machette (1978). Popotosa Formation strata underlie the basaltic andesite of Sedillo Hill (7.0 Ma; Chamberlin and Osburn, 2006). Near the Rio Salado, immediately west of the map boundary, the Popotosa Formation overlies the La Jara Peak Basaltic Andesite. Popotosa strata there contain rhyolitic ash-fall beds deposited 14.5 Ma (Cather et al., 1994a), and, lower in the section, these strata contain a tongue of Silver Creek basaltic andesite (≈15.5 Ma; Cather et al., 1994a; Cather and Read, 2003). Numerous volcanic flows and tephra provide age control in the late Miocene part of the section (Koning et al., in preparation).

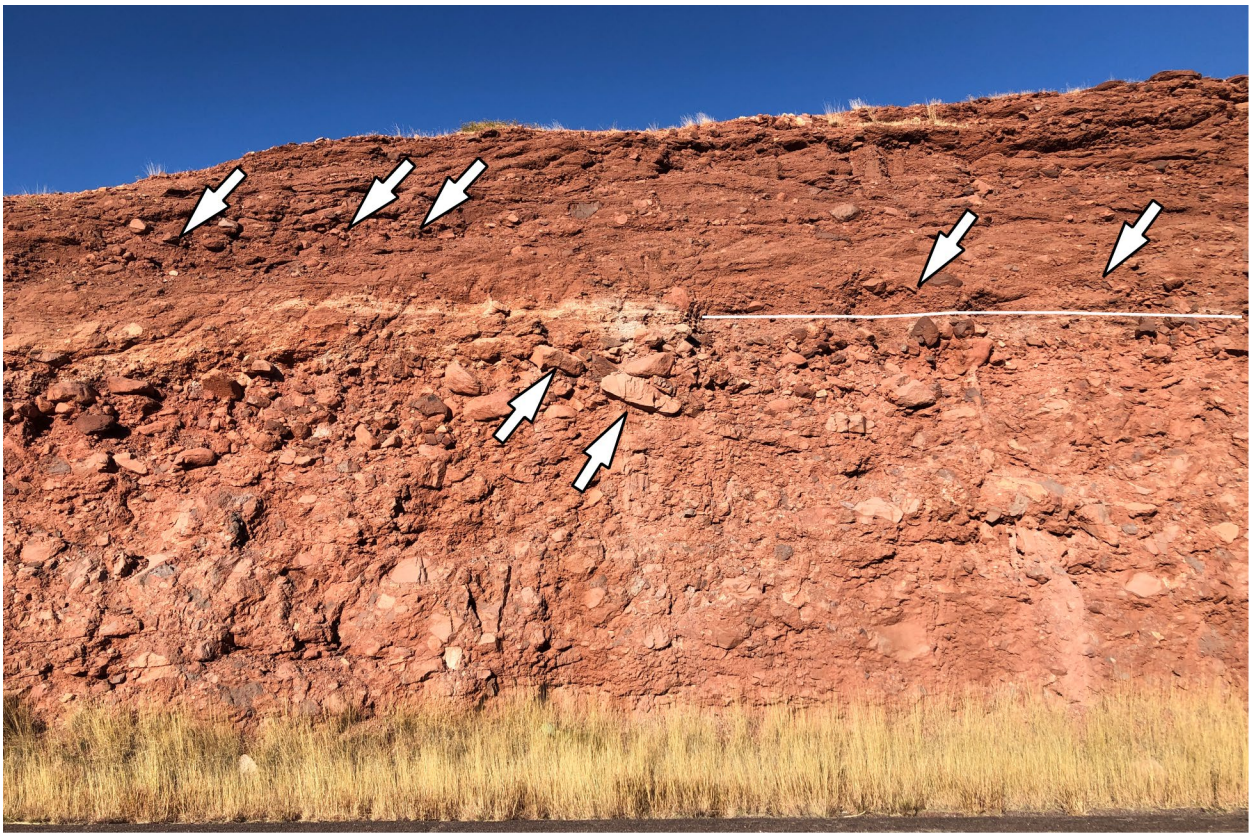

Figure 16—Photograph of the lower Popotosa Formation and Luis Lopez Formation in the southwestern corner of the quadrangle. The view is to the northeast. There are two subunits defined by clast sizes, whose boundary corresponds with the white line. The lower unit is a well-graded, mainly matrix-supported pebble–boulder conglomerate lacking defined bedding. The upper unit is redder, lacks boulders, and exhibits more defined bedding. The lower unit was deposited by debris-flow and hyperconcentrated-flow processes and the upper by stream-flow processes. Imbricated clasts in both units (white arrows) are mainly tilted to the right (southeast), indicating northwest-directed paleoflow toward the La Jencia Basin.

The Popotosa Formation is 1.5–3.0 km thick and composed of closed (endorheic) basin deposits consisting of playa mudstones flanked by sandy and conglomeratic piedmont deposits (Fig. 16). Playa mudstones (Fig. 17) are unique to the Popotosa Formation (in contrast to the Sierra Ladrones Formation). Conglomerates lack clasts of dark-red, jasperoid-cemented (potassium metasomatized) conglomerates-sandstones. Maximum thickness is ≈1.6 km along cross section A–A′ and >2.5 km west of San Lorenzo (Cather and Read, 2003).

The Popotosa Formation in the Socorro 30 x 60-minute quadrangle can be divided into (1) a lower part (>12 Ma) dominated by piedmont deposits to the south and containing many playa mudstones northwest and north of San Lorenzo Canyon, including the Rio Salado area and (2) and an upper part (12–7 Ma) with extensive playa deposits south of San Lorenzo Canyon that are flanked by piedmont deposits. Piedmont deposits in both the lower and upper parts are moderately to well consolidated, better cemented, and redder than those of the Sierra Ladrones Formation (Figs. 16 and 17A). In the lower part of the Popotosa Formation south of San Lorenzo Canyon, piedmont facies can be divided into lower red and overlying gray fanglomerate facies that predate late Miocene basaltic to dacitic volcanism in the Socorro Peak area (ca. 9.8–9.5 Ma); fanglomerates near Socorro are commonly red and strongly cemented by jasperoidal silica (Chamberlin, 1999; Chamberlin et al., 2001, 2022b). The basal part of the Popotosa Formation contains abundant conglomeratic, debris-flow deposits derived from local uplifts (Fig. 17A); the locations and configurations of these uplifts are poorly understood, but presumably, they are fault-bounded, small horsts. Predominately northwestward paleoflow in the lower piedmont deposits near Socorro is consistent with a playa lake in the La Jencia Basin to the northwest and the southernmost Albuquerque Basin.

A notable feature of the Popotosa Formation is clayey mudstone deposited on a playa (Fig. 17C). This playa was located south of the Rio Puerco and west of the modern course of the Rio Grande. During its existence (15? to 7 Ma), it progressively shifted south so that its southern shoreline, ca. 8.5–7.0 Ma, was located a few kilometers south of U.S. Highway 60 (Koning, in preparation). Playa sediment predating ≈8.5 Ma consists of reddish-brown to pinkish-gray mudstone and claystone with local thin, tan to light-gray tongues of siltstones and fine-grained to medium-grained sandstones and, in older strata, ≈1% beds of gypsum. A series of alluvial fans at the termini of southeast-trending drainages rimmed the northwestern side of the playa, depositing buff-colored, conglomeratic sandstones that interfinger with playa mudstones. Older playa muds contain greater than 1% gypsum beds composed of both primary (originally precipitated) and redissolved gypsum varieties (Fig. 17B). The buff-colored, conglomeratic sandstone features pebbles and minor cobbles of about subequal (±20%) felsic versus intermediate volcanic rock types; clast imbrication indicates a southeast paleoflow near the Lemitar Mountains. The sand is relatively brown to light-gray and relatively rich in volcanic lithic grains (≈25%–30%).

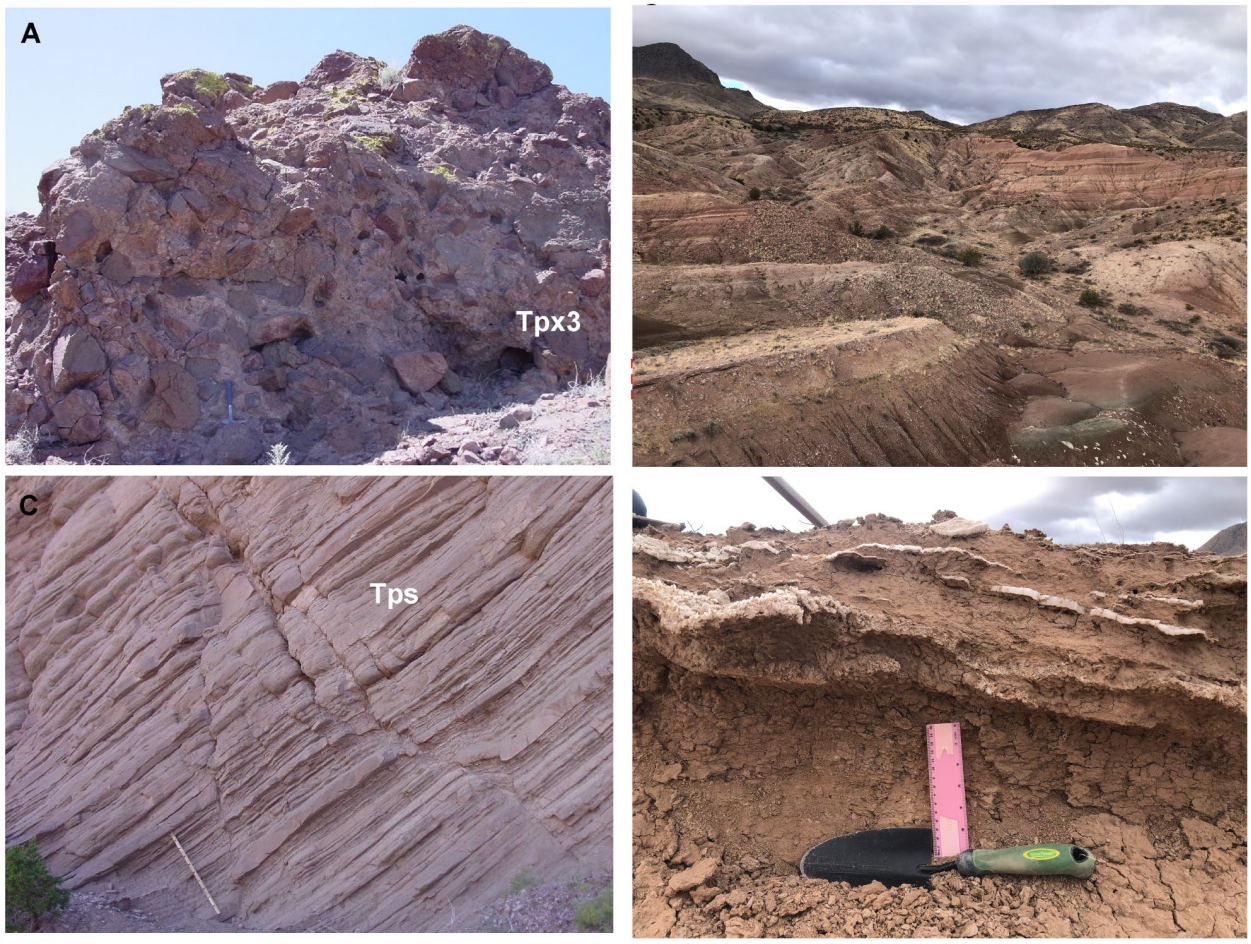

Figure 17—Photographs of the Popotosa Formation between Socorro and the Rio Salado. **(A)** Monolithic (andesite porphyry) breccia at the base of the Popotosa Formation (map unit **Npb**). It represents erosion and colluvial deposition from an early Miocene fault scarp (Chamberlin et al., 2022b). **(B)** Thinly bedded, tabular sandstones deposited on the toe of alluvial fan(s) or a bajada, probably adjacent to a playa to the north. Staff at lower right is 1 m long. Outcrop located on the north side of "unconformity butte" in San Lorenzo Canyon (UTM 13S 317640m E, 3790730m N, NAD83). It is located about 700 stratigraphic feet (210 m) above a 14.7 Ma ash located 2 km to the southwest (Chamberlin et al., 2022b). **(C)** View of layered, clayey sediments deposited in Lake Socorro. These strata lie 220 to ≈300 m above the 9.9 Ma basalt of Kelly Ranch and possibly are 9.5–9 Ma. The white, ledge-forming bed in the left foreground (red, dashed box) is gypsum and is shown more closely in panel D. **(D)** Photograph of gypsum beds that characterize the older part of playa lake sediment mapped between Socorro and San Lorenzo Canyon. The gypsum is found in two types of beds. The first type (labeled gy-1) is illustrated in the lower two wavy beds (each 1–3 cm thick), just above the pink ruler; those beds are composed of randomly oriented, blade-shaped gypsum crystals (selenite?) one to several millimeters long. The second type (labeled gy-2) is represented by the white beds about one ruler length above the top of the ruler, where the gypsum crystals are fibrous (satin spar?) and oriented at right angles to the bedding. The first type probably reflects primary deposition of gypsum in the playa, whereas the second type is a secondary precipitate that fills fractures. Gypsum is the main precipitate found in this ancient playa, and is probably due, at least in part, to high-sulfate groundwater that discharged into the lake at the time.

There is a transitional zone between the Popotosa and Sierra Ladrones Formations, which includes ≈8.5–7.0 Ma strata and is an ongoing focus of study by the lead author (unit **Npdp**). This zone is characterized by 10%–30% tongues of light-colored, very fine (lower)- to medium (lower)-grained, quartzo-feldspathic sands that are interbedded in reddish-brown clay that lacks gypsum beds. These sands generally have southward paleoflow directions and are interpreted to be fluvio-deltaic sands that periodically extended southward across a shallow playa floor. The top of the transition zone is overlain by the earliest/lowest Rio Grande deposits (unit **Nsa**). These axial-fluvial deposits are light-brownish-gray to pinkish-gray, quartz-rich sandstone and conglomeratic sandstone. The sand is fine- to coarse-grained and commonly cross-bedded. Gravel is mostly pebble-sized and dominated by volcanic clasts. There are also abundant clay rip-ups in the lowest fluvial strata, presumably derived from the reworking of floodplain deposits or the underlying playa deposits. Floodplain deposits are typically subordinate but are more common than those found upsection in the axial-fluvial deposits of the Sierra Ladrones Formation. These fine-grained deposits (mudstones to clayey fine-grained sandstones) often feature calcium carbonate nodules.

Sierra Ladrones Formation

The Sierra Ladrones Formation (defined by Machette, 1978) was deposited after the Rio Grande integrated through the Socorro Basin after 7.4–7.0 Ma (Koning et al., in preparation). These open-basin (exorheic) deposits are characterized by a central axial-fluvial facies flanked by piedmont deposits both at the foot of the Quebradas highlands to the east and the Socorro-Lemitar Mountains to the west. The axial-fluvial deposits commonly consist of predominately light-colored, cross-stratified sand that erodes readily. The piedmont deposits are less red than their counterparts in the underlying Popotosa Formation, are poorly to moderately cemented, and typically dip less than a few degrees.

Post-Santa Fe Group, Quaternary Deposits

About one-third of the map units in the Socorro 30 x 60-minute quadrangle postdate the Santa Fe Group and are less than ≈820,000 years old. After the culmination of Santa Fe Group deposition, ca. 820 ka, whose geomorphic level corresponds to the Las Cañas surface, there was progressive incision of the Rio Grande (Sion et al., 2020). Periodically, major aggradation events occurred along the river that resulted in the rise of the local base level by tens of meters, which in turn was accompanied by aggradation of the tributary drainages. Whether these shifts in base level were controlled more by erosion and sedimentation in the headwaters of the axial river versus those in local tributaries probably varied with time depending on paleoclimatic factors, and this subject warrants further study. Post-Santa Fe Group units are associated with deposition controlled by alluvial activity along major valleys and drainages, sheetfloods on gently sloping bajadas and basin floors, eolian activity, and mass wasting (landslides).

Alluvium

Alluvial units are differentiated based on landform position: valley floor deposits, Rio Grande terrace deposits, and alluvial fan deposits. We also recognize a relatively fine-grained sand unit (**Qas**) inferred to have formed via sheetflooding on wide valley floors or small basins. In each of these geomorphic positions, deposits are further subdivided according to inferred age. The four main age brackets are "recent" (historic [≈100 years ago] to present), "younger" (latest Pleistocene to Holocene), "intermediate" (mainly late Pleistocene), and "older" (middle Pleistocene). Whereas associating deposits with landscape position is straightforward, dividing deposits based on age is a more uncertain endeavor. Particularly uncertain is separating "intermediate" versus "older" deposits. The large area of the Socorro 30 x 60-minute quadrangle limited the number of field checks, so mapping was based largely on interpretations of aerial photographs as well as interpretations of previous mappers.

Recent Alluvium

Recent alluvium (**Qar**) is present as valley floor deposits. It is relatively easy to identify on aerial photographs since its surface is associated with obvious bar-and-swale topography, scour features, and a relative lack of vegetation in active arroyos or river bottoms. The deposit is mostly fine- to very coarse-grained sand and pebbles with minor to very little clay to silt. Alluvium associated with the Rio Grande (**Qarg**) is designated as a unique map unit that is up to ≈30–40 m thick since it includes floodplain deposits composed of clay, silt, and very fine- to fine-grained sand. The modern floodplain is commonly tilled or covered by riparian woodlands. Deeper sediment under the Rio Grande floodplain, included in the **Qarg** unit, is composed of sand interlayered with subordinate silt and clay. Much of the Rio Grande alluvium is inferred to be sheet-like deposits deposited during flood-related avulsion events (e.g., Happ, 1948).

Younger Alluvium

Younger alluvium (**Qay**) underlies low, valley-bottom terraces and includes subordinate valley-margin alluvial fans. This allostratigraphic unit is also found under alluvial fans, where for mapping purposes it includes subordinate recent deposits (**Qfyr**). The sediment consists of brownish-gray to reddish sand, silty-clayey sand, and gravelly sand to sandy gravel. The overall texture is finer-grained than found on recent alluvium. The corresponding geomorphic surface lacks bar-and-swale topography, may have weak clast varnish, and has a surface soil characterized by a weak calcic horizon (Stage I) locally capped by a dark, somewhat organic-rich A horizon.

Intermediate and Older Alluvium

Intermediate and older alluvium are present as terrace and alluvial fan deposits (Figs. 18–20). Both are mainly composed of sandy gravel, gravelly sand, and sand, with silt to clay being a minor constituent. The two allostratigraphic units are differentiated based on their relative height above the floors of the adjoining valley bottom (e.g., Rio Grande valley or its tributaries) and the degree of soil development. Intermediate deposits have mainly Stage II to Stage III carbonate morphologies, whereas older deposits commonly (but not always) feature Stage III through Stage IV morphologies. Note that factors such as eolian burial and erosion affect soil development and produce lateral variability.

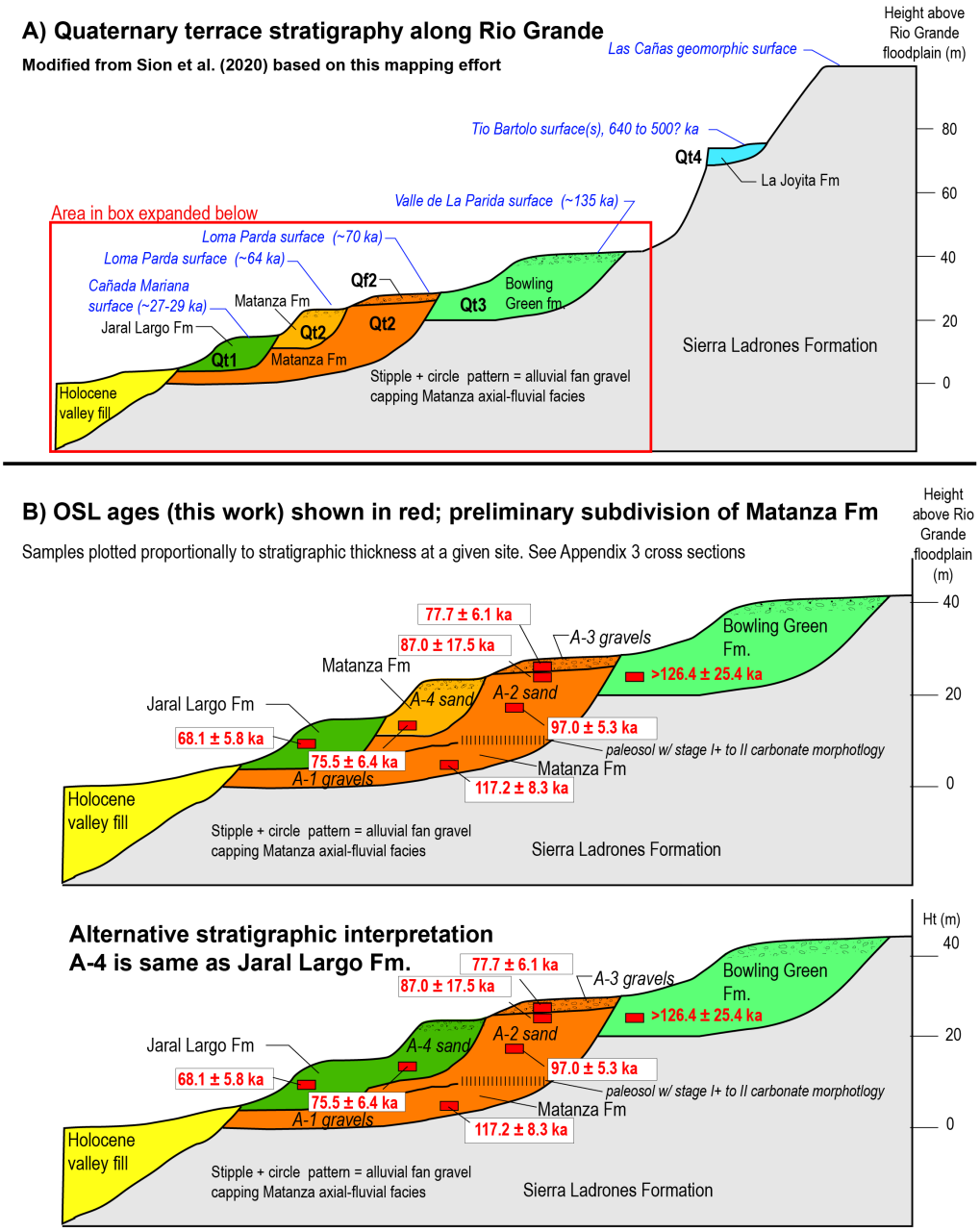

Figure 18—(A) Schematic diagram illustrating the stratigraphic relations and relative heights above the modern floodplain of the four allostratigraphic units in the middle to late Quaternary alluvium in the study area (slightly modified from Sion et al. [2020]). These units and their capping geomorphic surfaces are labeled with informal names from Sion et al. (2020). **(B)** An enlarged view of the lower three allostratigraphic units (**Qt1**, **Qt2**, **Qf2**, and **Qt3**) in addition to the relative position of our OSL samples. Note that the OSL age result for SanAcac-02 (79.8 ± 23.8 ka) is not shown due to its high error. Four hypothesized allostratigraphic units, based on outcrop observations at OSL sample sites and OSL age results, are noted (oldest to youngest): A-1 through A-4. Note that the relatively young Coyote sample (76 ka) is located slightly lower than the 97-ka sample and notably lower than the 78-ka sample. This suggests that, locally, the youngest allostratigraphic unit (A-4) backfilled a paleovalley during 78–70 ka; unit A-4 is inset into older allostratigraphic units A-1 through A-3, which were deposited between 125 and 90–80 ka. The lowest diagram shows an alternative stratigraphic interpretation, where the A-4 unit is equivalent to the dated lower–middle Jaral Largo formation at the Journey stratigraphic section.

Along the Rio Grande valley, recent work has differentiated and dated four geomorphic surfaces that overlie four allostratigraphic units that correspond to alloformations (Fig. 18A; Sion et al., 2020, 2021; NACSN, 2021; Phillips and Sion, 2022). The dating was accomplished using terrestrial cosmogenic nuclide chlorine-36 surface exposure dating (Sion et al., 2020). The two younger (lower) allostratigraphic units (**Qt1** and **Qt2**; **Qf1** and **Qf2**) are included in the intermediate alluvium. The two older (higher) allostratigraphic units (**Qt3** and **Qt4**; **Qf3** and **Qf4**) are included in the older alluvium. The "**Qt**" prefix is for terraces and the "**Qf**" prefix is for alluvial fans of a given allostratigraphic unit. Note that two ages were obtained from the Loma Parda surface that caps **Qt2** and **Qf2**: 64 ka for a surface projecting 24 m above the modern floodplain (see East San Acacia site, appendix C) and 70 ka for a surface projecting ≈28 m above the modern floodplain (north side of Nogal Canyon, west of San Antonio; see Sion et al., 2020).

Based on Sion et al. (2020) and Phillips and Sion (2022), the intermediate alluvium is divided into two allostratigraphic units underlying the two geomorphic surfaces (Figs. 17–20). Alluvium under the lower, younger Cañada Mariana surface is called **Qt1** or **Qf1**, correlative to the Jaral Largo formation of Sion et al. (2020). The tread height of the geomorphic surface (relative to adjoining valley floors) is typically 10–15 m but may range from 5–15 m. Its topsoil commonly has a Stage II carbonate morphology (Phillips and Sion, 2022). On aerial imagery, the surface has a relatively gray color compared to older (higher) terrace deposits, and subdued, meter-scale bar-and-channel patterns can commonly be observed in areas with low eolian activity.

Intermediate alluvium underlying the higher, older Loma Parda surface (ca. 70 ka) is designated as **Qt2** or **Qf2** (Figs. 17–19) and is correlative to the Matanza formation of Sion et al. (2020). The tread height of the geomorphic surface (relative to adjoining valley floors) is 18–30 m. The associated geomorphic surface is characterized by a topsoil with Stage II+ to Stage III carbonate morphology (Phillips and Sion, 2022). On aerial imagery, the surface is smooth and varnished where not buried by eolian sand. Along the Rio Grande, the gravelly alluvial fan sediment interfingers with axial-fluvial deposits. The axial-fluvial deposits are composed of light-brownish-gray, relatively massive and loosely consolidated, fine- to coarse-grained sand that locally grades east and west into a noncemented, weakly to moderately consolidated floodplain facies composed of light-brown to brown, very fine- to fine-grained sand, silt, and clay. Because gravelly fan sediment typically has prograded over the axial-fluvial sediment (Fig. 18), mapping the latter separately is not practical at 1:100,000 scale. The base of the Matanza formation generally lies below, or close to, the elevation of adjacent valley floors.

The lower of the two older alluvium units (**Qt3**) corresponds to the Bowling Green formation of Sion et al. (2020) (Figs. 18–20). The corresponding Valle de La Parida surface is 135 ka and typically projects 35–45 m above the Rio Grande. This surface is characterized by a topsoil with Stage III to Stage III+ (locally IV) carbonate morphology (field observations by the author and Phillips and Sion [2022]). On aerial imagery, the surface is smooth and varnished. Alongside the Rio Grande, the aforementioned gravelly sediment interfingers with axial-fluvial deposits (similar to that described for the intermediate alluvium). Because the gravelly fan sediment

typically has prograded over the axial-fluvial sediment, differentiating the latter is generally not practical at 1:100,000 scale. On aerial imagery, the surface has a relatively varnished, smooth surface where not buried by eolian sand.

The upper of the two older alluvium units (**Qt4** and **Qf4**) corresponds to the La Joyita formation of Sion et al. (2020). The La Joyita formation of Sion et al. (2020) has a tread height of 68–82 m above the Rio Grande. The associated geomorphic surface is characterized by a topsoil with Stage III+ carbonate morphology (Phillips and Sion, 2022). In many areas, two surfaces are present, separated by 3–7 vertical meters. We assume different deposits (unique allostratigraphic units) underlie the two surfaces, and we designate **Qf4a** as the lower unit and **Qf4b** as the upper unit (Figs. 19–20).

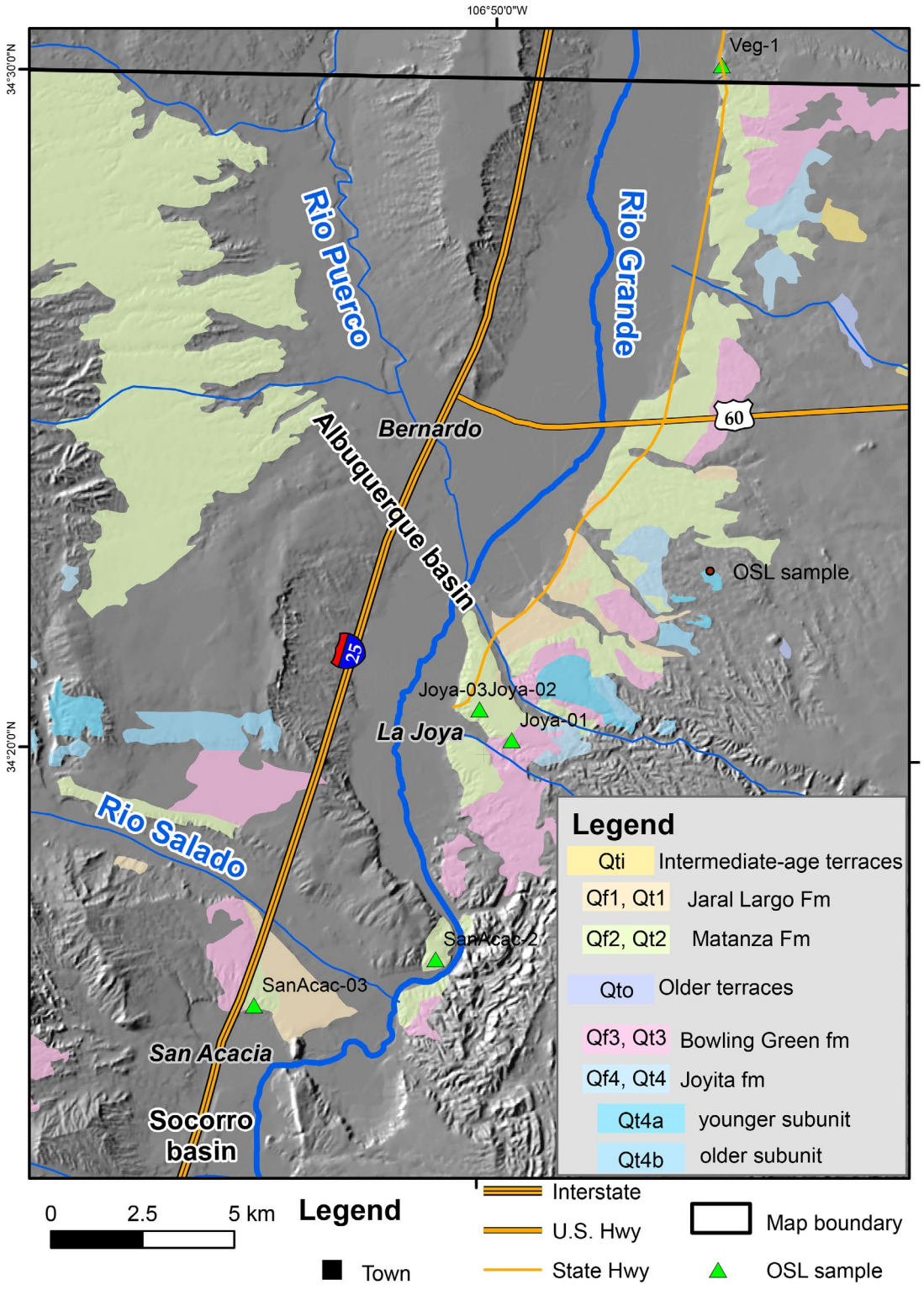

Figure 19—Map of the northern Rio Grande valley in the map area, showing the mapped location of intermediate- and older-age alluvium. These include both alluvial fan and terrace deposits (prefixed by **Qf** and **Qt**). Terrace deposits underlie relatively narrow and elongate geomorphic surfaces that are associated with incision along a particular ephemeral stream or the Rio Grande.

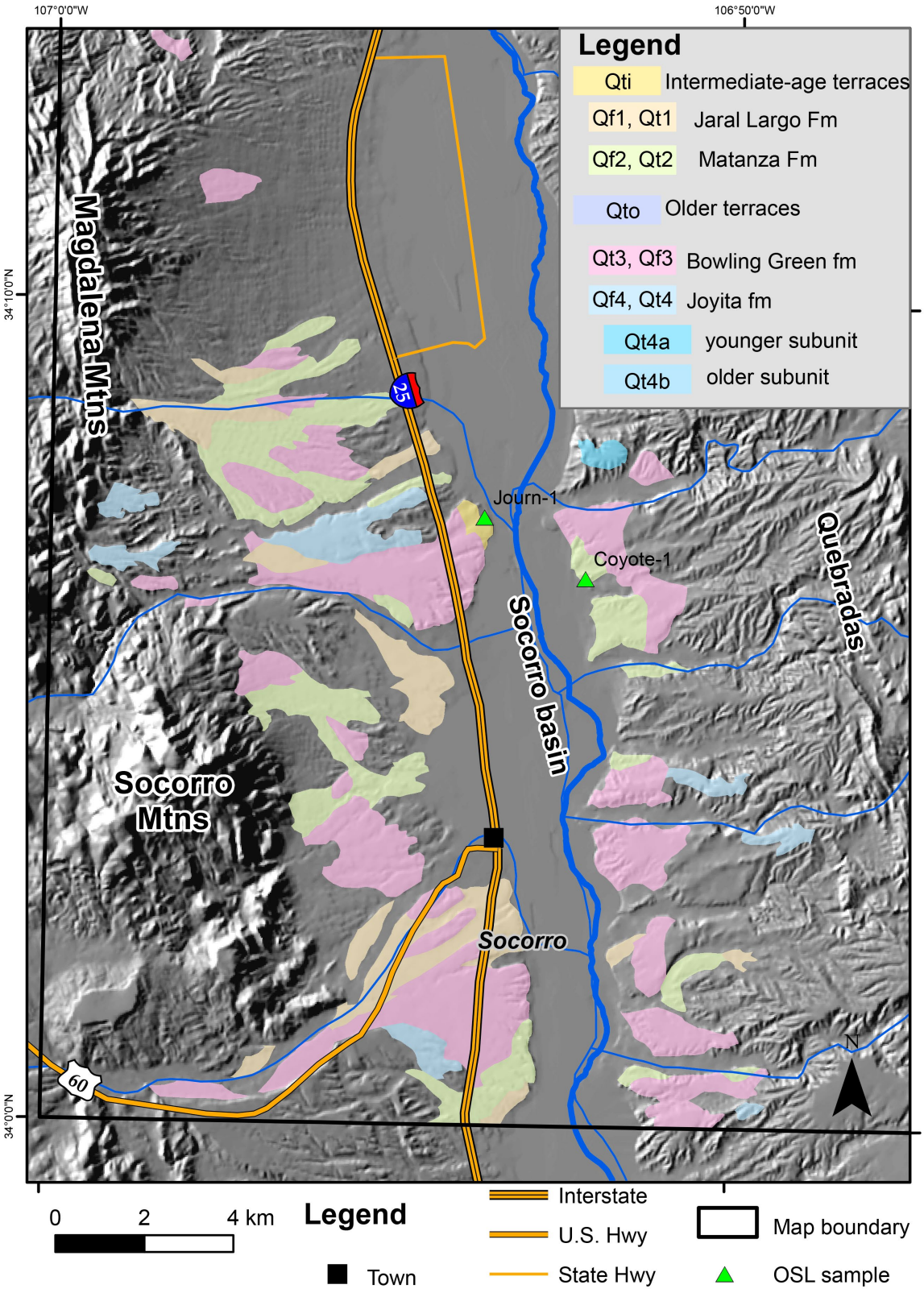

Figure 20—Map of the southern Rio Grande valley in the map area, showing the mapped location of intermediate- and older-age alluvium. These include both alluvial fan and terrace deposits (prefixed by **Qf** and **Qt**).

Age Control, Late Pleistocene Allostratigraphic Units

In order to more effectively map the Rio Grande alluvial allostratigraphic units northward across the study area (i.e., axial terraces **Qt1**–**Qt4** and alluvial fan terraces **Qf1**–**Qf4**), eight optically stimulated luminescence (OSL) samples were taken from units corresponding to the Jaral Largo (**Qt1**, **Qf1**), Matanza (**Qt2**, **Qf2**), and Bowling Green (**Qt3**, **Qf3**) formations (Figs. 19–20, Table 3). Appendix C contains stratigraphic descriptions for the stratigraphic and sedimentologic context of these samples. Stratigraphic sections (appendix C) were measured north of Socorro (Journey and Coyote sections), northwest of San Acacia (West San Acacia section), northeast of San Acacia (East San Acacia section), and east of the town of Joyita (Joyita sections). The Journey stratigraphic section is illustrated graphically in Figure 21. Table 3 summarizes the OSL ages. Appendix D shows topographic profiles and quasi-cross sections constructed transverse to the valley margin at each sample site. Appendix E contains the laboratory report regarding details of the methodologies and interpretations of results. The OSL samples were analyzed using multi-grain aliquots of potassium feldspar following a post-infrared infrared (post-IRIR) single-aliquot regenerative dose (SAR) protocol (Murray and Wintle, 2000; Thiel et al., 2011).

Appendix D and Figure 18 summarize the stratigraphic context of the allostratigraphic units and the relative height of the OSL samples above the elevation of the Rio Grande floodplain. We begin the discussion with the Bowling Green and Jaral Largo formations and then treat the Matanza formation. The Bowling Green formation (**Qt3**) OSL sample (Joya-1, Fig. 19) returned a minimum age of 126 ± 25 ka (Table 3). This minimum age is consistent with the age of the overlying Valle de la Parida surface (135 ka) obtained by Sion et al. (2020). Together, these two data indicate that the Bowling Green formation is older than 135–130 ka.

The OSL sample (Journ-1) from the lowest allostratigraphic unit (Jaral Largo formation, **Qt1**), collected 1.6 m above the base of the Journey stratigraphic section, yielded a relatively tight age of 68.1 ± 5.8 (Figs. 17, 20, and 21). The Cañada Mariana geomorphic surface capping the Jaral Largo formation is 29–27 ka (Sion et al., 2020), so the underlying deposit must be older than 30 ka but younger than the age of the Loma Parda surface (70–64 ka) capping the Matanza formation (Fig. 17). These data suggest deposition of the Jaral Largo formation started very soon after major incision at ≈70 ka that isolated the Loma Parda geomorphic surface. Alternatively, the Journey stratigraphic section sample may mostly represent the youngest allostratigraphic unit of the Matanza formation (A-4, see below; units 1–8 of Fig. 21), which was then beveled by erosion after 75–65 ka and followed by 1–3 m of deposition of coarse, locally derived fan gravels (e.g., units 9–11 of Fig. 21). In this alternative, the Jaral Largo sediment would be restricted to relatively thin and coarse fan gravel underlying the Cañada Mariana surface. More work is needed to test this stratigraphic alternative for the lower-middle Jaral Largo deposit.

Table 3—New OSL ages for Jaral Largo, Matanza, and Bowling Green Formations.

Field sample ID	Sample lab ID	Map unit and internal stratigraphic position	Relative height above floodplain (m)	UTM coordinates (NAD83, zone 13) Easting	Northing	Age (ka)
Joya-1	FC001	Bowling Green Fm., axial-fluvial sediment.	~60	332108	3801060	>126.4 ± 25.4
Joya-02	FC002	Top of Matanza Fm. ~4 m below a 36-m-high geomorphic surface, at top of A-2 axial-fluvial unit.	42	331238	3801890	87.0 ± 17.5
Joya-03	FC003	Top of Matanza Fm. ~2 m below a 36-m-high geomorphic surface, within A-3 fan gravel.	44	331229	3801890	77.7 ± 6.1
SanAcac-02	FC004	Top of Matanza Fm. 3.3 m below a 24-m-high geomorphic surface dated at 64 ka (Sion et al., 2020).	20	330022	3795069	79.8 ± 23.8
SanAcac-03	FC005	Within Matanza Fm. axial-fluvial sand (probably A-2 unit) at 61% of the tread height (as measured at the floodplain); tread projects 28 m above the floodplain.	20–21	325078	3793808	97.0 ± 5.3
Veg-01	FC006	Collected 7 m below the top of the lower cobble layer at the base of the Matanza Fm. (unit A-1).	~5?	337831	3819475	117.2 ± 8.3
Journ-01	FC007	Qt1, 8 m above the floodplain.	8	325298	3777467	68.1 ± 5.8
Coyote-1	FC008	Qt2, Matanza Fm. 18 m above floodplain.	18	327572	3776069	75.5 ± 6.4

Notes: UTM locations have error of +/- 3 m.

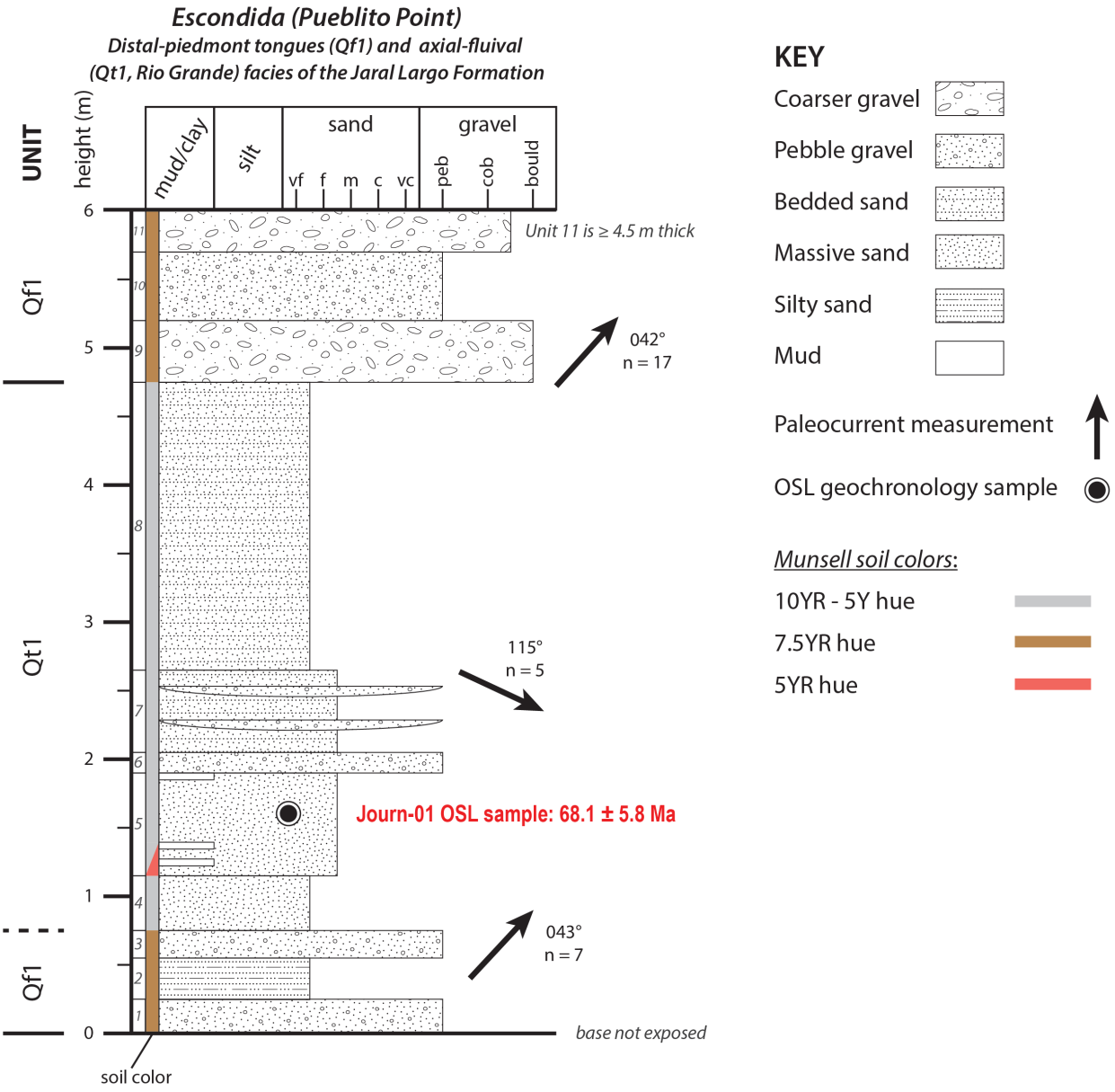

Figure 21—Stratigraphic section of the Jaral Largo formation at the Journey sample site, located 4.1 km south-southeast of Lemitar (UTM 13S 325298m E, 3777467m N, NAD83).

The remaining OSL samples were from within the Qt2 unit (samples Veg-1, Joya-02 and -03, SanAcac-02 and -03, and Coyote-1, Figs. 19 and 20), correlative to the Matanza formation of Sion et al. (2020). These five samples returned OSL ages of 125–71 ka (Table 3), indicating deposition during marine isotope Stage 5 (MIS 5; age of 130 to ≈70 ka; Lisiecki and Raymo, 2005). The ages of this allostratigraphic unit fall nicely in the maximum and minimum age constraints provided by the Valle de la Parida (135 ka) and Cañada Mariana (30–29 ka) geomorphic surfaces (Fig. 18).

Stratigraphic and chronologic study of the outcrops near the OSL sample sites, combined with cross sections across these sites, give indications that the Matanza unit is composed of multiple allostratigraphic units (Fig. 18, Appendices 3 and 4). The deepest sample was obtained from the Veguita quarry, where a 10- to 15-m-thick cobbly gravel lies at the base of the Matanza formation (Fig. 22). A low-error OSL age of 117.2 ± 8.3 ka was obtained from a sand lens within the gravel (Veg-01, Fig. 22C). The gravel extends ≈7 m above the sample, where it is disconformably overlain by a paleosol (Stage I+ to Stage II). The paleosol is cut out by an erosional surface (Figs. 22B and 22C). The amount of calcium carbonate precipitation in the paleosol is consistent with ≈10 kyr of soil formation in an arid environment (Gile et al., 1981). The overlying deposit is a well-bedded, slightly orangish sand and muddy sand (≈10 m thick), which in turn is overlain by ≈5 m of loosely consolidated, light-gray, axial-fluvial sand (Figs. 22A and 22B). The paleosol and erosional surface therefore separate two allostratigraphic units at this site, which we call A-1 and A-2. Whether these allostratigraphic units extend across the study area remains to be confirmed, but it is suggestive since elsewhere cobbly alluvium is not found higher up in the deposit.

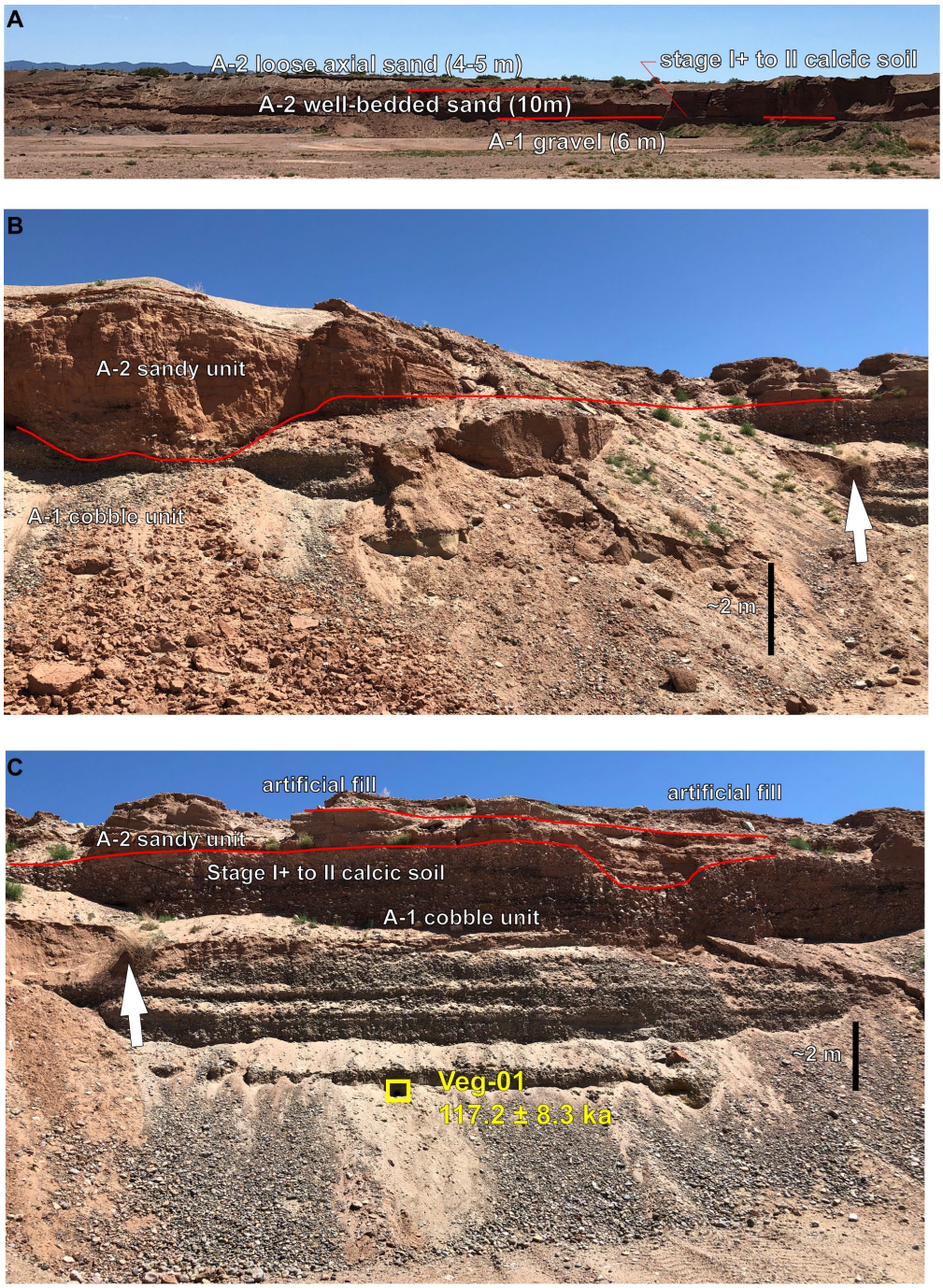

Figure 22—Annotated photographs of the Veguita sample site, located in an active quarry east of the Rio Grande, 0.5 km north of the quadrangle border. **(A):** Eastern quarry wall as it looked in July 2022 (approx. UTM 13S 337940m E, 3819530m N, NAD83). The A-1 cobbly gravel seen at the OSL sample site has a paleosol developed on it (Stage I+ to Stage II) and is disconformably overlain by well-bedded, slightly orangish sand (10 m) followed by 4–5 m of loosely consolidated, light-gray sand. Both lithologic units above the paleosol are grouped into allostratigraphic unit A-2. **(B)** and **(C)**: Quarry wall at the OSL sample site (as it looked in July 2022), looking north to north-northeast. Photo B is to the left (west) and photo C is to the right (east); the white arrow points to the same bush in both photographs. In photo C, the Veg-01 sample location is shown by the yellow box (UTM 13S 337831m E, 3819475m N, NAD83). Allostratigraphic units A-1 and A-2 are the same as in photo A. The paleosol is labeled in photo C. Note the paleosol is locally cut out by a scour surface (red line), corresponding to paleogullies up to about 1.5 m deep.

.

The Joya-02 and -03 sites sample the highest 4 m of the Matanza formation where it underlies a particularly high geomorphic surface (projecting 36 m above the modern floodplain; Fig. 23, appendix D). The topsoil is characterized by Stage III carbonate morphology, which is typical for the Loma Parda geomorphic surface. Allostatigraphic unit A-2 is inferred to be the same as what is seen in the Veguita quarry due to its sandy nature and lack of cobbles. The sandy, axial-fluvial sediment of unit A-2 is overlain by a scoured contact that probably represents a slight disconformity between A-2 and A-3 (Fig. 23). Unit A-3 is characterized by very poorly sorted pebbles to boulders that have northwest paleoflow indicators (imbrication) and a gravel composition consistent with derivation from the highlands to the east-southeast. Given the OSL ages of 87.7 ± 17.5 ka at the top of A-2 and 77.7 ± 6.1 ka in A-3, we infer that A-3 alluvial fan deposition occurred 83–77 ka after a period of slight(?) erosion. Thus, 83–77 ka is the culmination of the main phase of Matanza formation deposition.

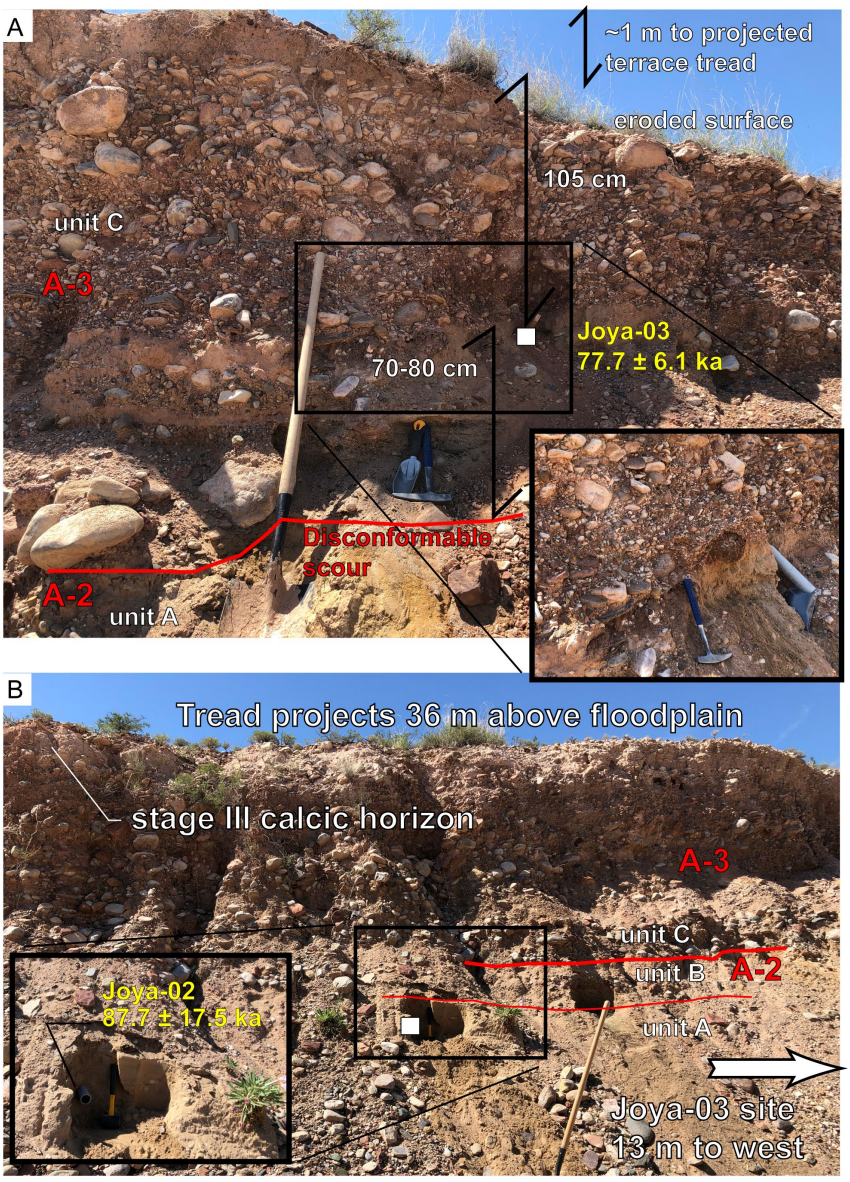

Figure 23—Annotated photographs of the Joya-02 and Joya-03 sites, which sampled the top 4 m of the Matanza formation. Here, the Matanza is overlain by a particularly high geomorphic surface (projecting 36 m above the modern floodplain; appendix D). Considering this high geomorphic position, it is inferred that these samples represent the end of the main phase of deposition of the Matanza formation. Interpreted allostratigraphic units A-2 and A-3 are labeled in red, the OSL samples are labeled in yellow, and local lithologic units are labeled in white. **(A):** The coarse-grained gravelly unit (A-3, unit C) represents alluvial fan deposition that prograded over underlying axial-fluvial deposits (A-2, unit A). These fan deposits overlie a scoured contact that likely represents a disconformity. The lower 80 cm of A-3 contains lenses of axial-fluvial sand and cobbles of reworked clay; these represent fluvial reworking of the underlying A-2 unit during early alluvial fan progradation. Sample Joya-03 came from a reworked axial-fluvial sand, and returned a low-error age of 77.7 ± 6.1 ka (UTM 13S 331229m E, 3801890m N, NAD83). The lack of cemented sediment suggests that a strong soil did not have time to develop on A-2 before it was eroded during early A3 time. **(B):** Sample Joya-02 was collected 80 cm below the A-3/A-2 contact (same as the unit C/unit B contact). It returned a high-error age of 87.7 ± 17.5 ka (UTM 13S 331238m E, 3801890m N, NAD83). We infer the true age is closer to 90–80 ka due to lack of cemented sediment in the base of the A-3 allostratigraphic unit (indicating lack of a strong paleosol). Therefore, A-2 deposition probably culminated 90–80 ka, and coarse fan gravel was able to prograde and aggrade (3 m thick) across the terrace surface at ca. 80–77 ka. Incision probably occurred ca. 78 ka.

A fourth allostratigraphic unit in the Matanza formation is suggested by a young OSL age of 75.5 ± 6.4 ka relatively low in the Coyote Canyon stratigraphic section (Coyote-01 sample in Fig. 24; Table 3, Fig. 18, appendix D). This sample is 40% of the tread height, whereas two samples in the A-2 unit are higher. Specifically, SanAcac-03 (97.0 ± 5.3 ka) is at 61% of the tread height and Joya-03 (77.6 ± 6.1 ka) is 94% of the tread height (appendix D, Fig. 18). We infer that the Coyote Canyon stratigraphic section is measured in younger, inset alluvium filling a paleovalley (Fig. 18B). The sharp, scoured contact at the base of the axial-fluvial pebbly sand at the Coyote Canyon stratigraphic section might represent a disconformity (Fig. 24), but that remains to be confirmed. The well-bedded, orangish sand below the possible disconformity does look similar, however, to the A-2 orangish sand overlying the cobbly gravel at the Veguita site (compare Figs. 22C and 24). Given the similarity of ages between Joya-03 and Coyote-01 (77.7 ± 6.1 ka and 75.5 ± 6.4 ka, respectively), it appears that the incision event creating the paleovalley occurred between 77 and 75 ka, and then the A-4 deposit would have aggraded between 77 and 70–64 ka (70–64 ka being the age range of the Loma Parda surface given in Sion et al. [2020]). It is noteworthy that the geomorphic surface overlying A-4 at the Coyote Canyon OSL site projects to 24–25 m above the modern floodplain (North Coyote profile in appendix D), whereas a geomorphic surface developed on the Matanza formation 1.5 km to the south projects to 32 m above the floodplain (South Coyote Canyon profile in appendix D). North-south topographic profiles between these geomorphic surfaces also indicate that the northern Coyote surface is 3–4 m lower. The 3- to 8-m-lower geomorphic surface (projecting to 24 m above the modern floodplain) overlying the Matanza formation where the anomalously young Coyote-01 OSL sample was collected is consistent with the Matanza deposit there being a separate allostratigraphic unit. Another alternative is that the A-4 allostratigraphic unit of the Matanza formation is actually correlative to the lower–middle Jaral Largo formation; such an interpretation is allowed by the overlap in errors in the Journey-01 and Coyote-01 OSL ages (Fig. 17, lower part of B panel). More detailed mapping of the Matanza formation plus more dating (OSL ages of sediment and cosmogenic ages of geomorphic surfaces) is needed to test this alternative and to further elucidate the nature and number of allostratigraphic units within the Matanza formation.

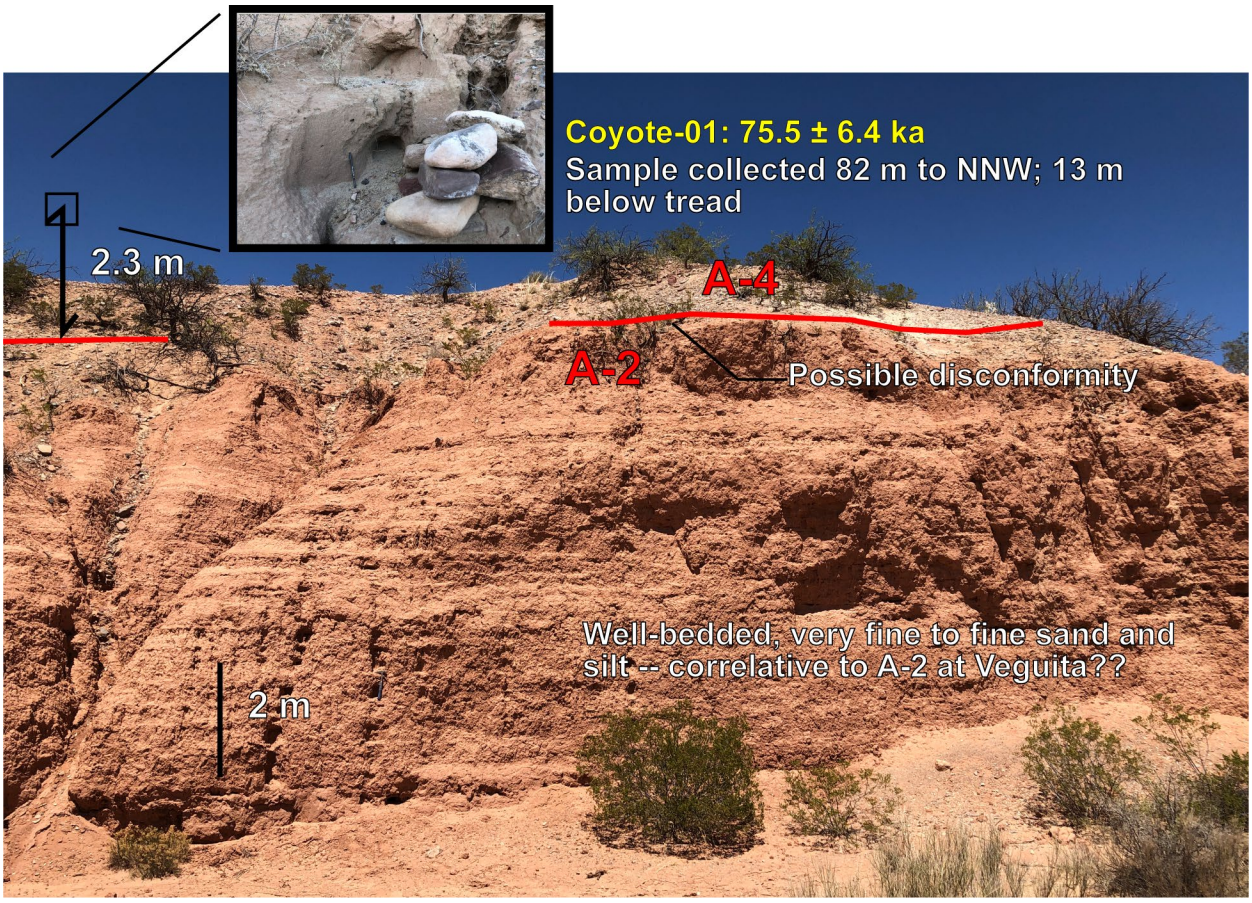

Figure 24—Annotated photograph of the lower part of the North Coyote Canyon stratigraphic section (UTM 13S 327595m E, 3775978m N, NAD83). The inferred disconformity between the A-3 and A-4 allostratigraphic units is shown by the red line. The alluvium above the red line is inferred to fill a paleovalley because the low-error age of 75.5 ± 6.4 ka is located relatively low in the Matanza formation, below the relative heights of samples yielding ages of 97.0 ± 5.3 ka and 77.7 ± 6.1 ka (Fig. 18B). This younger paleovalley fill (A-4) may possibly be correlative to the lower–middle Jaral Largo formation (bottom diagram in Fig. 18B).

In summary, data collected thus far suggest four allostratigraphic units between 130 and 60 ka. Cobbly aggradation of the first unit (A-1) occurred during high stream power of the axial river at 117.2 ± 8.3 ka, probably at the start of MIS 5d (5d is a substage of MIS postdating substage 5e) but possibly at the end of MIS 6. Deposition of A-1 ended with a base-level fall that formed a terrace tread and allowed soil development for ≈10 kyr, followed by incision of the tread. Relatively sandy A-2 deposition occurred between ≈105 and 80 ka. Slight scouring and coarse deposition of side-stream sediment characterized A-3 deposition ca. 77 ka. Notable base-level drop along the main river occurred between 77 and 75 ka, followed by aggradation of A-4 in the Matanza formation at 75–70 ka. Unit A-4 could possibly be correlative to the lower–middle Jaral Largo formation, but for now, we assume that its relatively higher tread surface denotes an older underlying deposit. If so, then another deep incisional event occurred ca. 70 ka, at the start of MIS 4 and immediately followed by aggradation of the Jaral Largo formation 70–60 ka.

Sheetflood Deposits Mainly Reworking Eolian Sand

A common surficial unit on the eastern side of the quadrangle is composed of sand sheets that reflect local reworking of eolian and loessic deposits on gently sloping geomorphic surfaces by sheetfloods (unit **Qs**). These sheetfloods are probably associated with intense rainfall events during the summer monsoons. These deposits do not include alluvial sheetflood deposits associated with the valley bottoms or alluvial fans of major drainages (e.g., **Qas**, **Qasy**, or **Qasyr**). The mapped deposits consist of brownish, massive, and bioturbated sand with minor scattered granules and pebbles. No dune forms (including coppice dunes) are obvious in aerial photos. Sand is very fine- to medium-grained, subrounded to subangular, and composed of quartz, minor feldspar, and 1%–10% lithic and mafic grains; locally the sand is silty to clayey. The deposit contains minor, scattered coarse- to very coarse-grained sand and pebbles. In the deposit, there is a very low proportion of gravel beds, and where present these tend to be very thin and lensoidal. The topsoil and buried soils are characterized by weak ped and calcic horizon development (typically Stage I carbonate morphology). In the easternmost part of the quadrangle, we have mapped a combined unit where surficial sheetflood deposits overlie similarly textured basin fill (i.e., the Claunch basin fill), where differentiating the two was not practical due to poor exposure.

Eolian Deposits

Sandy eolian deposits (**Qe**) cover a notable proportion of the map area. Based on their geomorphic position (i.e., lee-side accumulations of thick eolian sand) and quartz-rich composition, the eolian sand was transported mainly by northeast-directed winds, and the Rio Grande valley was an important source area (together with sandy alluvium in tributary drainages east of the Rio Grande). The eolian deposits consist of unconsolidated to weakly consolidated sheets of light-brown to tan sand that drapes topography. Sand typically features low coppice dunes or mounds (mostly <1 m tall), differentiating it from unit **Qs**. Sand grains are mainly fine- to medium-grained, subrounded to rounded, well- to moderately sorted, and quartz-rich. Buried soils with weak calcic horizons occur at depth. Eolian sand dunes are mapped on the northern side of the

lower Rio Salado (**Qed**), where the dune forms are mainly parabolic, 100–150 m wide, and up to 3–5 m tall.

Mass-Wasting Deposits

Landslides are concentrated on uplifted terrain on the west side of the Socorro Canyon fault zone, but most are inactive and relatively stable. They are particularly common around Socorro Peak, where their associated surfaces are characterized by hummocky topography. The deposits consist of displaced, deformed, and disrupted Santa Fe Group sediment, mainly Popotosa playa clays (Npp), capped by a variety of Neogene volcanic rocks. Many landslides can be characterized as Toreva-type (rotational) slides, where strata are tilted backward toward the headscarp. Most landslides are currently stable or inactive and were presumably active during wetter periods in the Pleistocene.

Age Control, Holocene Allostratigraphic Units

Charcoal sampled from Holocene alluvium (map unit Qay) has been dated in two general areas. Along the lower Rio Salado, samples were ca. 3 ka (Sion et al., 2020). Valley-floor alluvium in the Rayo Hills was sampled in two drainages, returning radiocarbon ages ranging from 3.5 to 0.1 ka (Aby and Jochems, 2022).

STRUCTURE

Figure 15 shows structural basins and major faults, folds, and dikes; more faults and stratal attitudes are shown on the geologic map. The overall geologic structure of the Socorro 30 x 60-minute quadrangle becomes more complex in a westward direction. In the eastern half of the quadrangle, strata are relatively flat-lying under the Chupadera Mesa and the Claunch uplands. The most notable structures in the eastern quadrangle are the east-down Chupadera fault (part of the Monte Prieta-Liberty Hill structure) and east- to northeast-trending anticlines likely cored by dikes (Cather, 2009a). In the south-central quadrangle lies the >30-km-long, south-plunging Torres syncline, which is flanked on the east by the Oscura anticline and on the west by the Prairie Springs anticline. Strata are elevated in the Quebradas highlands (cross section A–A′), and faulting density increases westward. Most structures in the Quebradas highlands are extensional, but many have evidence of Laramide ancestry. A particularly long fault, the 020° striking Montosa fault, is a Laramide-age, east-verging, fault-bend propagation fold structure cored by a west-dipping dextral reverse fault. Only the southern part of the Montosa fault has been notably reactivated by extension. The Rio Grande rift in the western quadrangle includes the southern Albuquerque Basin and the Socorro Basin. The Socorro Basin represents the inversion of a Laramide highland called the Sierra uplift (Cather, 1983, 2009b). The Socorro and the Albuquerque Basins are separated by a structural high near San Acacia, where extensional strain steps 1–3 km eastward from the west-down Socorro Canyon fault to the west-down Loma Peleda and Loma Blanca faults. The Lemitar and Socorro Mountains represent west-tilted, footwall uplifts along the Socorro Canyon fault system. These features are explained in detail below from west to east.

Rio Grande Rift

Socorro Basin

The Socorro Basin is a down-dropped half-graben lying between the Socorro and Lemitar Mountains on its west side and the Quebradas highlands on its east side. Tectonic subsidence of the basin allowed sand, clay, silt, and gravels of the Santa Fe Group to accumulate in the Socorro Basin during the Miocene through Quaternary. Based on old but high-resolution gravity surveys by Alan Sanford (1968), the bedrock floor of the Socorro Basin near the city of Socorro is tilted to the west toward these mountains. Sanford (1968) estimated the top of the Precambrian basement in the Socorro Basin to be about ≈1,000 m below sea level. The structural configuration of the Socorro Basin prior to 10 Ma is poorly understood. Northwestward paleoflow directions in the Popotosa Formation in the eastern San Lorenzo Canyon area and in U.S. Highway 60 roadcuts (Fig. 16) suggest that major depocenters ca. 20–10 Ma may have been the La Jencia Basin to the west and a playa north of San Lorenzo Canyon in the southernmost Albuquerque Basin.

The east side of the Lemitar and Socorro Mountains are bounded by the east-down Socorro Canyon fault zone. This fault may have been active since the early Miocene, but throw rates likely increased since 7.5 Ma, given the fact that thick, playa clays deposited before 7.5 Ma have accumulated on the footwall (west side) of the Socorro Canyon fault zone (see cross section A–A′ in Chamberlin [1999] and its revision in Koning et al. [2022b], fig 2.5). About 1.3 km of stratigraphic separation (1.0 km of vertical displacement) of the older playa muds has occurred across the fault, as evidenced by the elevation of the top of the playa muds preserved on Socorro Mountain and the top of playa muds at 356 m depth in the Evergreen well (Koning et al., 2022b, fig. 2.5). This gives a stratigraphic displacement rate of 130 m/Myr. Close to the same location, the Las Cañas surface is offset by about 30 m (Phillips and Sion, 2022), giving a vertical displacement rate of ≈30 m/Myr since ≈820 ka. Thus, the Socorro Canyon fault was notably less active after 800 ka than during 7.5–0.8 Ma.

Strata in the Socorro and Lemitar Mountains, on the footwall of the Socorro Canyon fault, are mainly tilted between 40° and 60° to the west. Spatial relations between these strata and faults have been used to interpret three generational sets of faults (Chamberlin, 1983; Chamberlin et al., 2001; Chamberlin et al., 2022b). Faults of the first set now dip near-horizontal, crosscut lower Oligocene volcanic rocks, and are inferred to be Oligocene. The second fault set dips about 30°–40° and is inferred to be about mid-Miocene. The third fault set is steeply dipping (50°–80°) and includes the Socorro Canyon fault. Relations between fault dips, stratal dips, and strata ages indicate that extension-related, domino-style tilting has occurred since the early Oligocene and explain the three aforementioned generations of faults in the Lemitar Mountains (Chamberlin, 1983; Cather et al., 1994a; Chamberlin et al., 2022b). In domino-style tilting, blocks bound by normal faults progressively rotate to shallower dips. At about 35°–40°, frictional resistance becomes too great on these faults, and a new generation of steeper faults form that truncate older, shallow-dipping faults. An example of an older, tilted fault is found in the Woods Tunnel at the foot of Socorro Peak. This tunnel cuts across a shallow-dipping fault named, appropriately, the

Woods Tunnel fault zone, which is inferred to be offset by the Socorro Canyon fault at the foot of the range (Koning et al., 2022b, figs. 2.5 and 2.7). Another place the Socorro Canyon fault may crosscut an older, low-dipping fault is at the foot of the east-central Lemitar Mountains, where the general mountain front slopes only 12°–15° to the east and may correspond to an exhumed, low-angle fault plane.

Immediately across (east of) the topographic low between the Lemitar and Socorro Mountains (located 10 km northwest of Socorro) is a corresponding residual Bouguer gravity high in the Socorro Basin, separating lower Bouguer values to the north and south (Sanford, 1968). So there appear to be two subbasins in the Socorro Basin in the Socorro 30 x 60-minute quadrangle that are separated by a slight bedrock high, corresponding to this relative gravity high, about 5–6 km north of Socorro.

There are four relatively long faults on the eastern side of the Socorro Basin (Fig. 15). These include the Fite Ranch fault (south of the map area) and the 17-km-long Coyote fault (in the map area). There is a 2 km left step-over between the northern Coyote fault and the southern Veranito fault. Along cross section A–A′, the northern part of the Coyote fault has 250 m of vertical displacement and the Veranito fault has 90 m of vertical displacement. Displacement along these faults likely increases toward their respective centers away from the cross-section line. That is, slip likely increases northward for the Veranito fault and southward for the Coyote fault.

The fourth fault along the eastern side of the Socorro Basin is the East Joyita fault, which is 8 km long and strikes 030° along the eastern side of the Joyita Hills (Fig. 15). The southern end of this east-down fault has a pronounced "zigzag" pattern (on a scale of tens of meters; see de Moor et al. [2005]) and is truncated by the west-down Veranito fault. At its north end, in the northern Joyita Hills, the East Joyita fault horsetails, with most faults trending northeast but one strand bending to the northwest (de Moor et al., 2005). These splaying faults offset rocks as young as early Oligocene volcanics (i.e., the 29.0-Ma La Jencia Tuff). Late Pliocene to early Pleistocene strata of the Sierra Ladrones Formation are not offset at the northern end of the fault zone. Dip-slip offset is at least 600–700 m, down to the east (de Moor et al., 2005). Measured dips on the East Joyita fault range from 35° to 50° and the fault is described as moderately dipping by de Moor et al. (2005). These workers also interpret the East Joyita fault as a rotated, planar normal fault related to rifting, experiencing the aforementioned domino-tilt style of extensional tectonics. However, other workers have suggested the fault is an eastward-flattening detachment (Beck, 1993) or related to the Quebradas detachment fault system (Cather and Koning, 2024).

The Socorro Basin reflects the extensional inversion of a contractional Laramide uplift, called the Sierra uplift (Cather, 1983, 2009a, 2009b). The presence of the former Laramide uplift is well-illustrated by stratigraphic relations in the Socorro and Lemitar Mountains. There, the Gray Mesa Formation (Pennsylvanian age) is unconformably overlain by upper Eocene strata (Spears Group and Datil Group). In the Quebradas highlands, however, 1.5–1.9 km of upper Paleozoic and Mesozoic strata overlie the Gray Mesa Formation. Thus, 1.5–1.9 km of exhumation occurred in

the Sierra uplift between ≈80 and 55 Ma. Additional evidence for the Sierra uplift is found in the Baca Formation in the Quebradas highlands, whose piedmont facies exhibit eastward paleoflow data and associated conglomerates containing abundant Madera Group limestones and granite clasts. These lithologic types are consistent with the Pennsylvanian and Proterozoic rocks that underlie the Datil and Spears Groups in the Socorro and Lemitar Mountains. We infer that the main contractional faults producing the Sierra uplift were located on the eastern side of what is now the Socorro Basin, probably corresponding to the eastern fault zone of the basin (i.e., Veranito and Coyote faults, and the Fite fault to the south of the quadrangle).

Southern Albuquerque Basin

The structure of the southern Albuquerque Basin is relatively complex and controversial. Based on the integration of geophysical data (primarily gravity data) with well data, the structurally deepest part of the basin is near the intersection of the Rio Puerco and Rio Grande; this low zone extends southward to the hanging-wall area flanked by the west-down Cliff fault and east-down Loma Blanca fault (Grauch and Connell, 2013). To the west of this synclinal low lie the east-down Loma Blanca fault and the Loma Peleda fault (east to west). One controversy is whether these faults are low-angle detachments (Ricketts et al., 2015) or extend down to mid-crustal depths at moderate to high angles (Grauch and Connell, 2013; Chamberlin et al., 2016, fig. 0.33). To the east of the synclinal low lies the Joyita structural bench, where basin fill is interpreted to be largely <500 m thick (Grauch and Connell, 2013). The west side of the Joyita bench is partly bounded by the northeast-trending, northwest-down Abo-Maes fault zone (Fig. 15). This fault zone projects to the northwestern tip of the Joyita Hills, but there is no evidence for related offset in the Plio-Pleistocene Sierra Ladrones Formation. An alternative is that the west-northwest-down monocline characterizing the northern Joyita Hills continues northward in the subsurface (under the Sierra Ladrones Formation), and this monocline demarcates the western end of the Joyita Bench. Since the Sierra Ladrones Formation is not folded, this postulated, subsurface monocline would have been active prior to 5–1 Ma. Near U.S. Highway 60, a volcanic-cored, topographic knob known as Black Butte (Fig. 1) is bounded on the west by the aforementioned Abo-Maes fault (northwest-down) and the east-down Military Road fault (Fig. 15). Between the Military Road fault and the Los Pinos Mountains, structural modeling by Grauch and Connell (2013) indicates a deepening of basin fill. The eastern side of the southern Albuquerque Basin is flanked by the Manzano and Los Pinos Mountains. These are bounded on their western foot by east-down, normal fault systems (i.e., Los Pinos fault on this quadrangle). However, these faults have not offset Quaternary surfaces. It appears that in the middle to late Quaternary, extensional strain has shifted westward from these basin-margin faults to the Contreras Cemetery and Abo-Maes fault zones near the interior of the basin. In contrast, the two major faults on the west side of the southern Albuquerque Basin, the Loma Peleda and Loma Blanca faults, do show notable evidence of middle to late Quaternary vertical offset, ranging from 5–35 m (Personius and Jochems, 2016a, 2016b; Williams et al., 2017). `

Structures in the Quebradas Highlands

In the Quebradas highlands, the density of faults decreases eastward. Most faults are interpreted to be normal faults related to Rio Grande rift extension, but several structures are contractional or represent extensionally reactivated, former Laramide structures. This section summarizes the structural data and related discussion of Cather and Koning (2024), and the reader is referred to that work for a more thorough treatment of the fascinating structures here.

Quebradas Detachment Fault

A regionally extensive detachment fault system is interpreted by Cather (2009a) and Cather and Koning (2024). This interpretation is mainly based on exposures of low-angle faults, angular relations of strata across hanging wall and footwall ramps, and local removal (excision) of strata in the upper Yeso Group (upper Torres, Cañas, and/or Joyita Members of the Los Vallos Formation). An example of such angular relations is shown in Figure 25. Also, in numerous places hanging wall strata exhibit reverse-drag folds (roll-over anticline) where an inclined fault (fault ramp) connects two horizontal faults (fault flats). However, mapping indicates that many roll-over, asymmetric anticlines are likely associated with listric splay faults rather than detachment fault ramps (Cather and Koning, 2024). Throughout the study area, the principal slip surface of the detachment fault is interpreted to be one or more faults within the Los Vallos Formation. Study of the geometry of roll-over anticline orientations, inferred to develop above listric splay faults, and a single exposure of asymmetric shear fabric indicate an eastward slip direction of the upper block of the detachment fault. Movement is interpreted to have occurred episodically in the ≈25-Myr interval between the middle Eocene and early Miocene, and was driven by structural relief generated during the Laramide (Fig. 26; Cather and Koning, 2024).

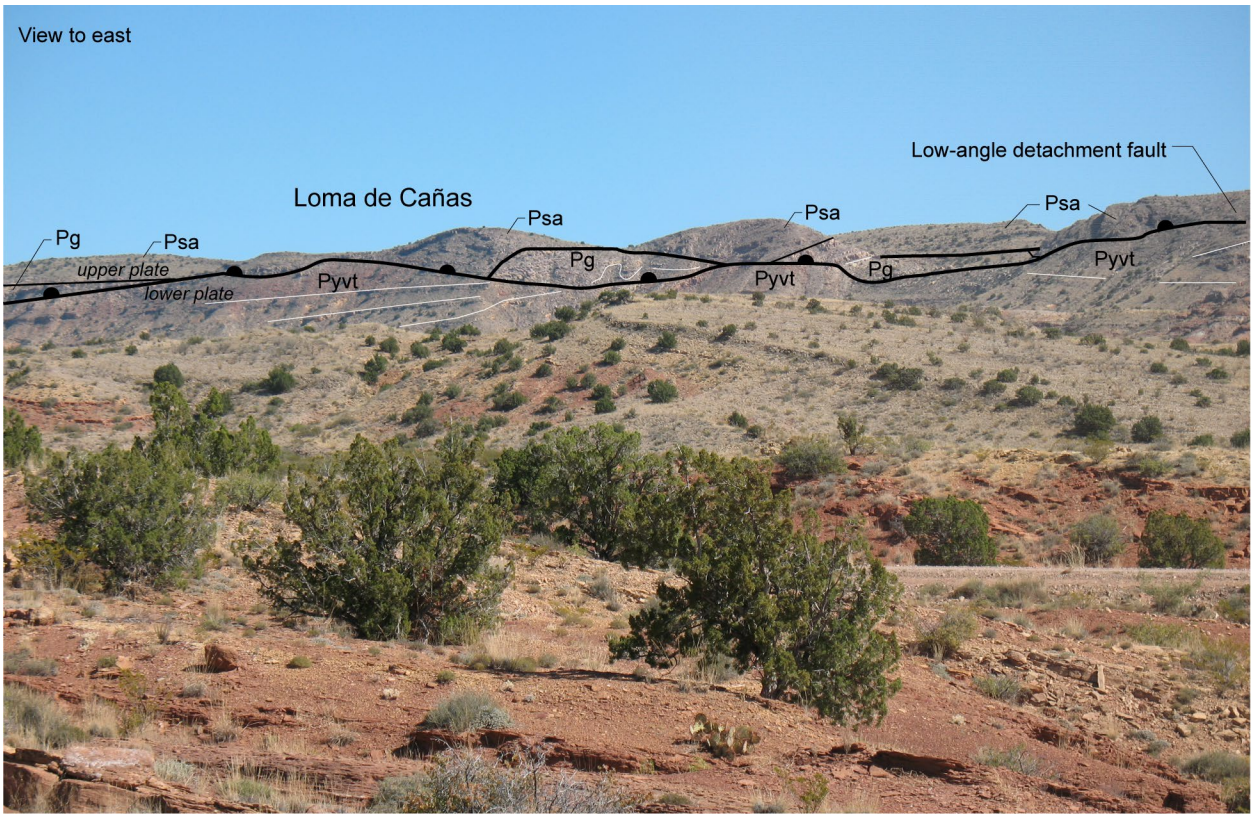

Figure 25—View toward the east of the low-angle faults that are observed in the uppermost Yeso Group, where they juxtapose either the San Andres Formation or Glorieta Sandstone against the middle to upper Yeso Group strata. These faults are part of the Quebradas detachment fault, which is typically found in the interval occupied by the Cañas and Joyita Members of the Los Vallos Formation. Faults are represented by heavy black lines with semicircles on the upper block. White lines are bedding contacts. Figure used with permission from the New Mexico Geological Society (Koning et al., 2022a, fig. 1.46).

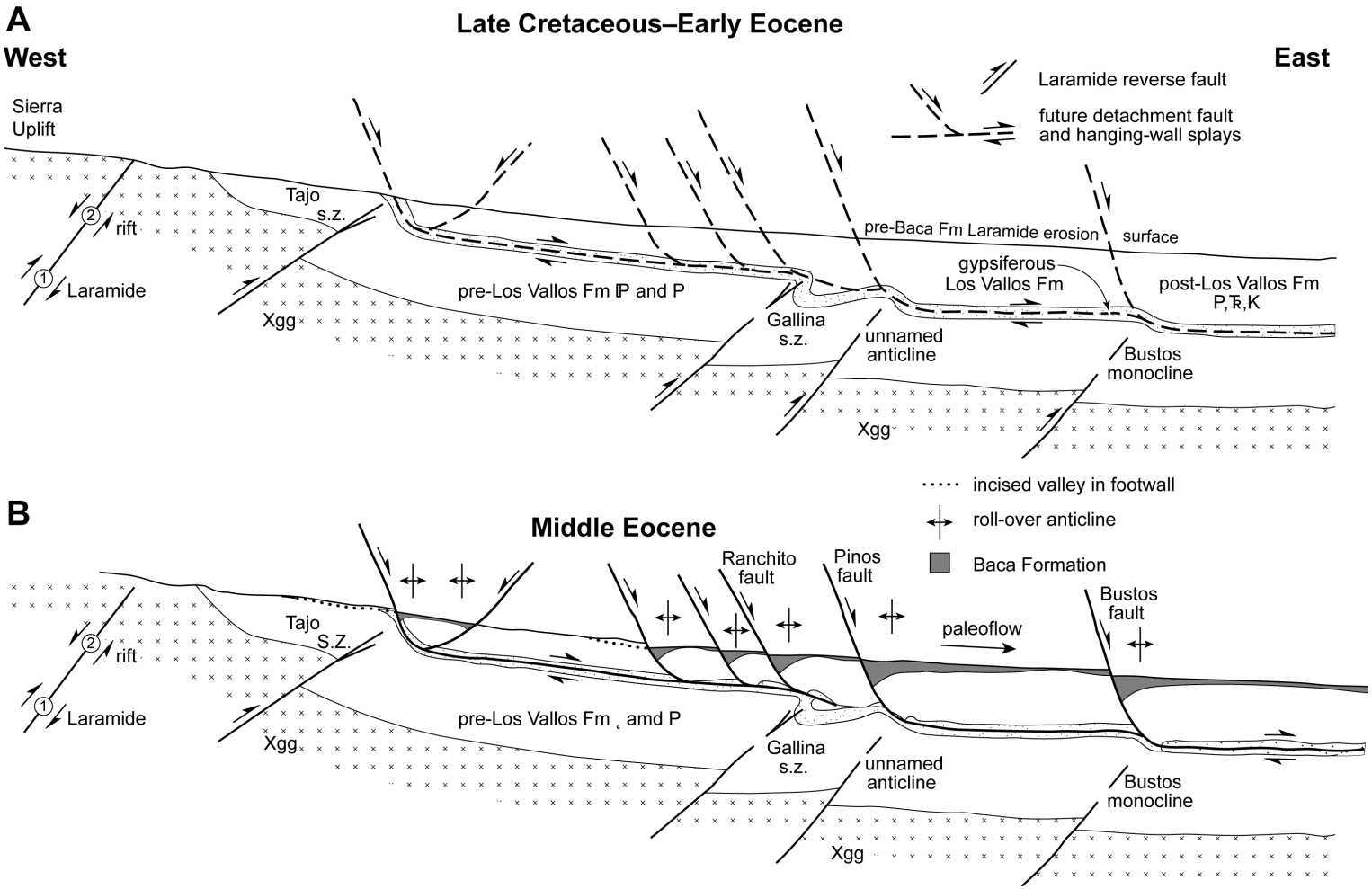

Figure 26—Schematic cross-sectional model for the development of the Quebradas detachment system. The cross-section line is approximately along 34°03' in the Loma de las Cañas and Bustos Well quadrangles (≈3 km north of the Landing Strip fault zone). Scale is approximate. s.z. = structural zone. **(A)** East vergence during Laramide contraction resulted in Laramide basement wedges. **(B)** The structural relief generated in the Laramide allowed gravity-driven detachment to occur in the middle Eocene through the Oligocene to the early Miocene. Note the top-east slip on the Quebradas detachment and associated hanging-wall splay faults and rollover anticlines. Note that depositional control of the Baca Formation by splay faults has only been demonstrated for the Ranchito fault zone, south of the Landing Strip fault zone. Figure used with permission from Cather and Koning (2024).

We accept the interpretation for this detachment complex (Cather, 2009a; Cather and Koning, 2024) and consequently draw a low-angle fault at the Glorieta-San Andres formation contact in the Quebradas highlands on the geologic map and cross section A–A′. In reality, the fault shifts in stratigraphic position within the Los Vallos Formation, sometimes even extending above the base of the Glorieta Sandstone to the base of the San Andres Formation. However, most of the slip appears to occur in the upper half of the Los Vallos Formation, where the gypsum layers of the Cañas Member are located.

The Quebradas detachment fault is not directly observed east of the Quebradas region in the Rayo Hills or Chupadera Mesa, but a wide zone of tight folds near the axis of the northern Oscura anticline (Oscura fold complex, Fig. 15) may be related to contraction at the eastern end of the detachment. No sign of a detachment fault was observed at the base of the Glorieta Sandstone in the east-dipping ridge on the west side of the Torres syncline (e.g., UTM 13S 362802m E, 3774559m N, NAD83). However, the Oscura fold complex along the northern Oscura anticline (Cather, 2009a, fig. 3), near the Stackhouse Powell Government Permit wells and the McCaw Federal 01 well, in addition to thickened Yeso Group in these wells, indicates that detachment-style faulting and contraction within the Los Vallos Formation probably extended eastward to that location, as inferred by Cather (2009a). Whether contractional structures are focused just below the Los Vallos-Glorieta contact or are distributed throughout the gypsum-rich part of the Vallos Formation is not known.

Montosa Fault and Fold

The main contractional structure in the Quebradas highlands is the Montosa fault and related folding, which comprises one of the most notable Laramide structures in central New Mexico. Striking along the eastern flank of the Los Pinos Mountains and extending into the southern Manzano Mountains, this structure is 90 km long, trends ≈020°, and is characterized by an east-verging, fault-propagation fold. This fold is cored by a reverse fault that dips 45°–70° west (Cather, 2009c). Stratigraphic separation is up to ≈600 m (Reiche, 1949). Throw diminishes to the south. At its southern end, where the fault trends relatively north-south, the fault exhibits normal right-oblique motion (W.J. Nelson, written communication, 2024)—we refer to this segment as the "southern Montosa fault." Elsewhere, several workers have noted evidence for a dextral component of slip on the fault (Cabezas, 1991; Hayden, 1991; Behr, 1999). In the northern Los Pinos Mountains, the fault juxtaposes Proterozoic rocks against the Pennsylvanian Madera Group. To the south, strata as young as Permian age are offset, but the basalt capping Black Mesa (3.68 ± 0.343 Ma) shows no displacement (Cather, 2009c; age from Table 2). These stratigraphic and structural relations indicate that most of the fault was active in the Laramide, consistent with fission-track cooling ages for the Los Pinos and Manzano Mountains (Kelley et al., 1992), but the southern part was reactivated during Rio Grande extension. This fault is inferred to have kinematically linked Laramide contractional uplifts to the south and north (Cather, 2009c).

Milagro Fault Zone

The somewhat enigmatic Milagro fault zone is present in the Valle de Ojo de la Parida and extends northeast (020°–040°) to a location 5–10 km east of the Joyita Hills. Its total length is ≈15 km and it is as much as 1 km wide. The sense of throw is mainly down to the southeast. Although generally concealed in the Valle de Ojo de la Parida, stratigraphic relations among scattered Upper Cretaceous strata indicate numerous intervening, buried faults. The fault zone extends southwestward to the southern Joyita Hills. There, it is buried by Paleogene strata, indicating a Laramide history. Locally, the fault exhibits Neogene movement, such as where it appears to offset the Quebradas detachment (UTM 13S 341900m E, 3788400m N, NAD27; Cather and Koning, 2024).

Amado-Gonzales Faults

The Amado fault strikes 030°–045° and exhibits 900 m of northwest-down, stratigraphic displacement (see cross section A–A′). The structure was named by Rejas (1965) and is at least 17 km long and 1–2 km wide. The dip of the fault is poorly constrained. To the south, this fault may tie into the west-down, 340°–350° striking Gonzales fault, located on the western edge of the Quebradas, 9 km east of Socorro. Parts of this fault zone were termed the Cañoncito de la Uva fault zone and Stapleton-Alamillo fault zone by Colpitts (1986) and the Parida structural zone by Cather (2009b), but subsequent mapping shows that they are continuous with the Amado fault zone first defined by Rejas in 1965 (Cather and Koning, 2024). At its northeastern end, the Amado fault zone is truncated by north-northwest-trending normal faults. At one location, the Amado fault is offset by the Quebradas detachment fault ≈2.5 km southeast of Mesa del Yeso (Cather and Koning, 2024). In other places, the Amado fault cuts across the detachment fault, reflecting activity during Rio Grande rifting (e.g., NE1/4 sec. 23 and NW1/4 sec. 24, T. 2 S., R. 1 E., New Mexico Meridian; Cather and Koning, 2024). Our depiction of the fault in cross section A–A′ suggests it has primarily experienced extensional strain. As inferred by Cather and Koning (2024) and Cather (2009a), this fault could have served as a dextral transpressional fault in the Laramide orogeny.

Gallina Fault and Fold Structure

The Gallina fault is denoted for a complex series of roughly north-trending faults in the central part of the Quebradas. These faults are associated with short north- to northeast-striking anticlines. The collective structure is viewed as a faulted anticlinorium in Cather and Koning (2024). Many of these faults exhibit normal throw, likely related to the Rio Grande rift extension. The anticlines and larger anticlinorium, however, likely reflect older Laramide contraction (Cather and Koning, 2024). Further evidence for Laramide contraction includes local observations that beds as young as the Yeso Group (which post-date ARM tectonism) are locally overturned and offset by reverse faults, and locally, the structure does not appear to offset the Quebradas detachment (Cather and Konging, 2024), so it must predate that structure (Cather and Koning, 2024).

The Gallina structural zone is 17 km long and 0.5–1 km wide. From the Landing Strip fault zone on its southern end, this structure extends slightly west of north and terminates about 5 km north of the Montosa fault. The northeast-striking Montosa fault zone terminates southwestward against the Gallina structural zone (Brown, 1987). North of this intersection, the Gallina structural zone consists of steep faults bounding gently tilted blocks. Parallel to these faults are open folds, typically with gentle limb dips. South of this intersection strata dip more steeply and, in places, are overturned and offset by reverse faults. The short folds generally trend north (Behr, 1999), are mostly east-verging, and are locally overturned (Brown, 1987). The axial plane of this part of the anticlinorium dips west (Brown, 1987). Note that cross section A–A′ runs across the southernmost end of the Gallinas structural zone, and this anticlinorium is not obvious (see cross sections of the geologic map of Cather and Koning [2024]).

We agree with the interpretation by Cather and Koning (2024) that the Gallina structural zone is a fault-propagation fold complex that formed above a blind, west-dipping Laramide reverse fault—analogous to some folds in the Tajo structural zone. Support for this interpretation includes the observation that deeper stratigraphic levels are exposed west of the Gallina structural zone compared to immediately to the east. Cather and Koning (2024) agree with Brown (1987) that much of the Gallina structural zone acted as a restraining step-over between the Montosa fault and Del Curto fault.

Tajo structure

The Tajo structure is a noteworthy, arcuate, fault-propagation and fault-bend fold complex located in the western Quebradas, 11 km west of Socorro. The southern end of the structure is cut out by the Coyote fault; from there it can be mapped 4–5 km northeastward to where it is readily accessible near Arroyo del Tajo (using the Quebradas Backcountry Byway). A particularly spectacular example of these folds is found where the complex crosses Arroyo del Tajo (Fig. 26). An exposure located ≈0.2 km south of Arroyo del Tajo indicates the fold complex is cored by a westward dipping reverse fault (G. Axen, written communication, 2022). Other smaller reverse faults are also present. The folds of the Tajo structure are open to tight, commonly asymmetric, and in places are overturned toward the east or northeast (Fig. 27). Folds are locally Z-shaped (Rejas, 1965) and have axial planes that dip ≈30° to 70° to the west (Fig. 27). Within the large fault-propagation syncline to the east of the anticline(s) are smaller-scale and somewhat chaotic folds within the lower Yeso Group and Abo Formation. Throw on the Tajo structure decreases dramatically within 1–2 km north of Arroyo del Tajo, perhaps because some strain is partitioned onto a northeast-striking, dextral slip fault immediately north of this arroyo.

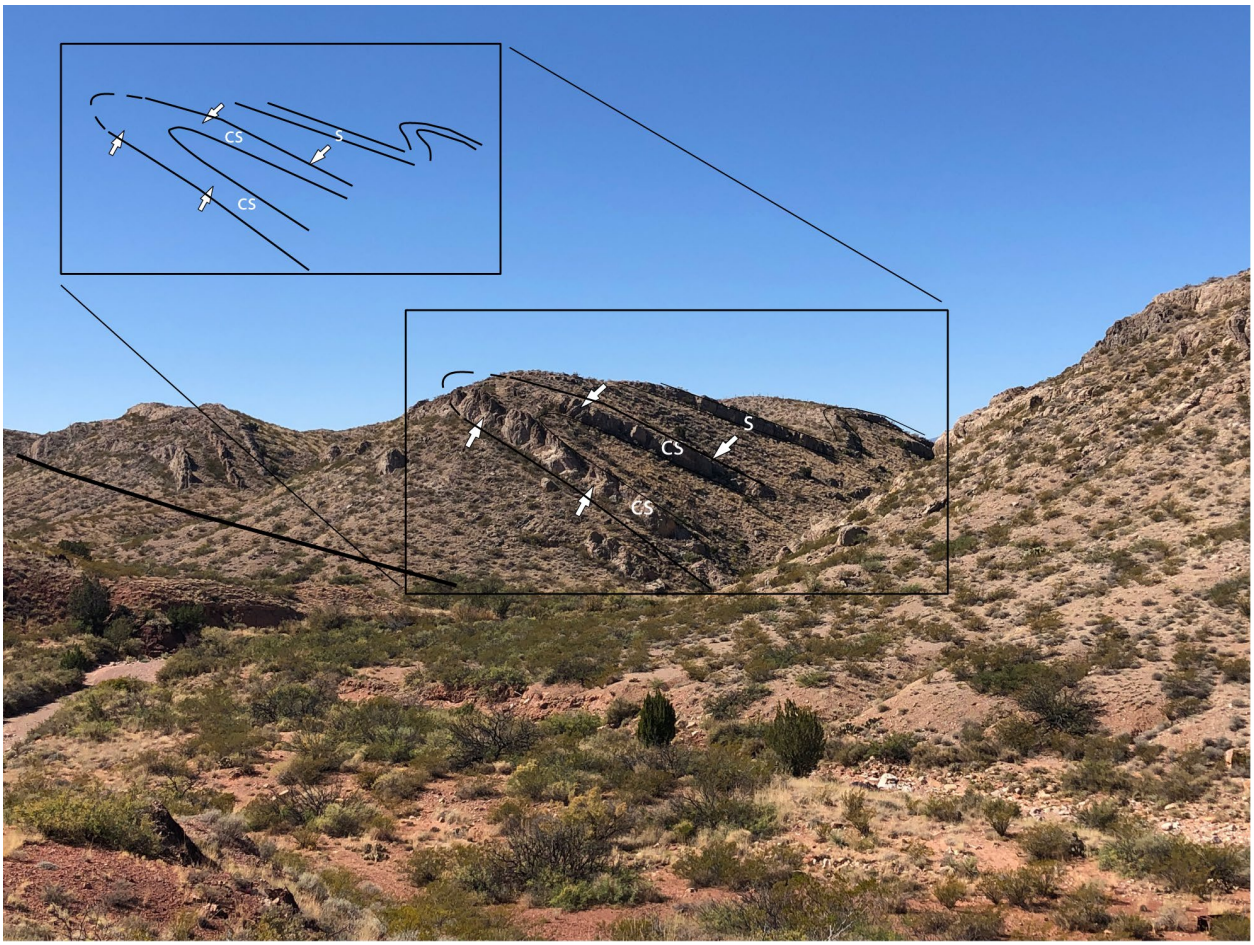

Figure 27—View to the southwest along the upper part of the Tajo fold. Here, it is a tight, asymmetric anticline with an overturned eastern limb. Observed deformed strata include the upper Atrasado Formation (cs = Council Spring Member, s = Story Member). To the right (west), a broader syncline and anticline developed in these same strata. White arrows denote the Council Spring Member on either side of the eastern fold. In the foreground, on either side of the arroyo, reddish-brown Abo Formation strata are tilted to the west and overturned. Figure used with permission from the New Mexico Geological Society (Koning et al., 2022a, fig. 1.47).

The Tajo structure is largely interpreted to be Laramide in age because it deforms strata as young as the Leonardian-age Yeso Group, which post-dates the Ancestral Rocky Mountain orogeny (e.g., Kues and Giles, 2004). Cather and Koning (2024) infer that the Tajo structural zone is a remnant salient on the eastern front of the transpressional Laramide Sierra uplift, which was structurally inverted to form the Socorro Basin of the Rio Grande rift (Cather, 1983, 2009b).

A northern extension of the Tajo structure, as interpreted by Cather and Koning (2024), is observed at Ojo de Amado Spring. Here, the Atrasado Formation has been tilted vertically at the spring but warped to shallow northward dips only 100–200 m to the east, forming a north-dipping, asymmetric syncline (Fig. 28). Westward rollover of beds to the southeast indicates an anticline located ≈250 m west of, and parallel to, the aforementioned syncline axis. A smaller anticline-syncline pair is found ≈0.4 km south-southeast of the spring (Fig. 28). This collective structure is consistent with an east-verging fault-propagation fold on the eastern flank of the Sierra uplift. At the spring, the irregular map trace of the upper contact of Pennsylvanian strata indicates that paleovalleys were eroded on the eastern flank of the uplift, although a sinuous fault cannot be ruled out and one west-down, normal fault exposure is observed near the spring (Fig. 30). We interpret that the paleovalley was backfilled first by a few meters of conglomeratic Baca Formation (very poorly sorted pebbles to boulders that could be paleo-colluvium) and then by several meters of basal Spears Group, where the clast composition is mixed limestone, intermediate volcanic rocks, and minor Proterozoic rocks. Eastward paleoflow based on clast imbrication in the Spears Group (Figs. 13B and 28) supports an east-draining paleovalley. In summary, at Ojo de Amado Spring, there is evidence of a middle(?) to late Eocene paleovalley incised into an asymmetric synclinal warp probably associated with fault-propagation folding on the eastern flank of the Sierra uplift; this paleovalley then funneled late Eocene Spears Group sediment eastward into the Joya-Carthage basin.

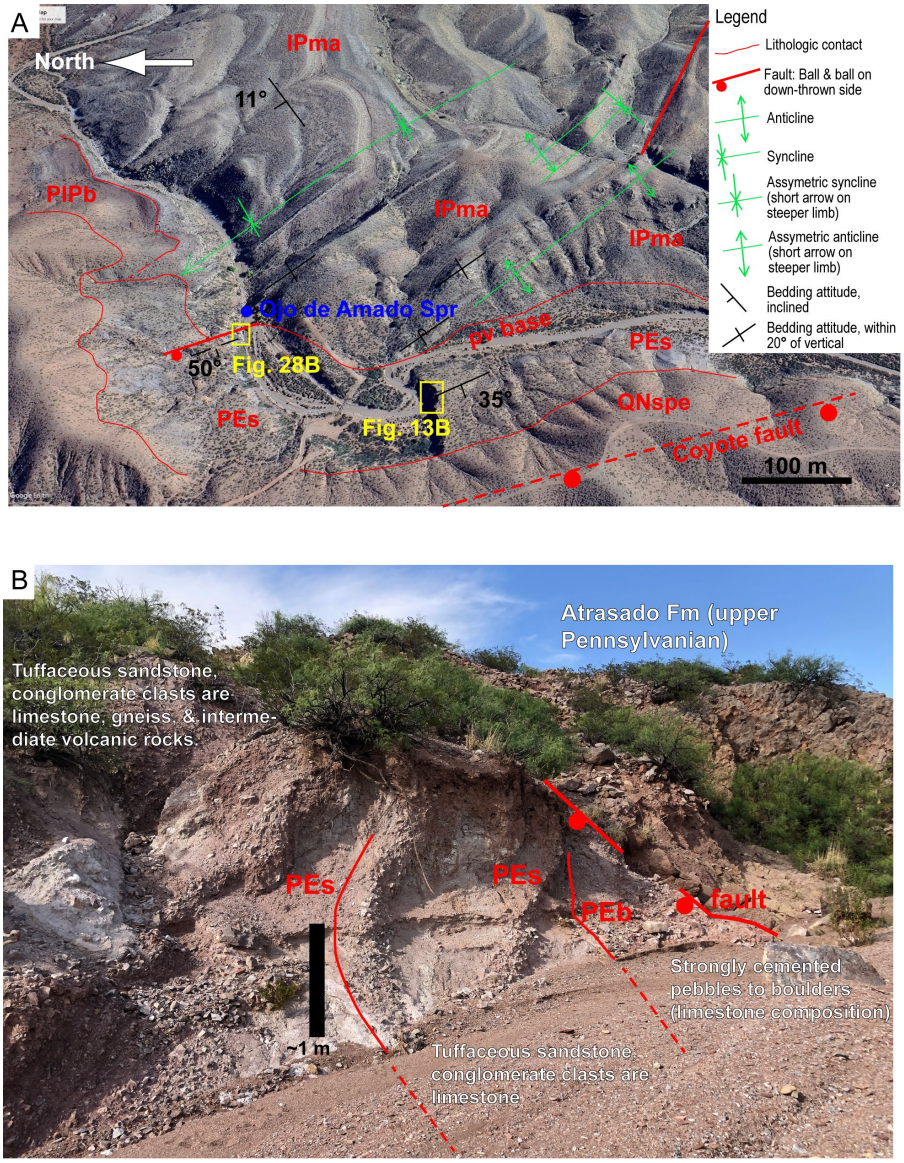

Figure 28—Structural and stratigraphic relations at Ojo de Amado Spring, located 9 km northeast of Socorro (UTM 13S 332025m E, 3775620m N, NAD83). These relations are interpreted to reflect (1) the development of an east-vergent fault-propagation fold in the Laramide, (2) erosion of the fold to produce a paleovalley, (3) backfilling of the paleovalley by a few meters of Baca Formation followed by >100 m of Spears Group, and (4) normal faulting and westward tilting (30°–50°) during Rio Grande rifting after 25–20 Ma. **(A):** Annotated Google Earth image showing contacts (red), structures (green), and photo locations (yellow). Map units (red text) are abbreviated as follows: **IPma** = Atrasado Formation, **PIPb** = Bursum Formation, **Pes** = Spears Group, and **QNspe** = eastern piedmont facies of the Sierra Ladrones Formation. Note the highly sinuous trace of the base of the Spears Group, which we infer is a paleovalley (labeled "pv base") backfilled by Spears Group sediment; however, the contact does correspond to a fault immediately northwest of the spring. **(B):** Photograph of an outcrop on the north side of Arroyo de los Pinos, 30 m northwest of the pool at the spring, bounded on the right (east) by a small(?), west-down fault. Immediately adjacent to the fault are 3 meters of very poorly sorted, strongly cemented, angular to subangular pebbles to boulders that we interpret as paleocolluvium or debris flow of the Baca Formation (**PEb**). Above lie tuffaceous sandstones interbedded with conglomerates, the lower conglomerates being composed wholly of limestone clasts, but upsection (to the left) the clasts are composed of limestone, granitic gneiss, and plagioclase-phyric intermediate volcanic rocks. This stratigraphic succession is characteristic of the gradational Baca (**PEb**) vs. Spears (**PEs**) contact.

Landing Strip Fault

The Landing Strip fault is a 5- to 6-km-long, south-down fault located northwest of the northern tip of the Blackington Hills. To the immediate north is a south-facing monocline that may be related to the Laramide uplift. The Cañas fault terminates southward against the Landing Strip fault. There appears to be more contractional strain north of the Landing Strip fault than to the south; if so, the differential strain across it suggests a component of dextral slip during the Laramide (Cather and Koning, 2024).

Bustos Fault and Monocline

The Bustos fault and monocline, located north of the Blackington Hills, consists of an east-down monocline on the west and an east-down fault a short distance to the east (cross section A–A′). The monocline is apparent only north of the Landing Strip fault zone; east-down flexure explains a ≈100–150 m discrepancy in elevation of the Quebradas detachment across it (Cather and Koning, 2024). The mapped fault is east-down. Steep dips in the immediate hanging wall suggest a listric fault geometry. Consistent with Cather and Koning (2024), we have this fault flatten in the upper Los Vallos Formation (cross section A–A′).

Structures in the Northern Jornada del Muerto Basin

We extend the northern Jornada del Muerto Basin into the south-central part of the Socorro 30 x 60-minute quadrangle, between Sierra Larga on the west and Chupadera Mesa on the east (Fig. 1). It is largely coincident with the Torres syncline (Fig. 15). Consistent with Cather (2009a), we restrict the Trinity basin to the south of the quadrangle, in the structurally low area west of the Oscura Mountains. There, the Trinity basin is coincident with low Bouguer gravity values, whose northern boundary corresponds to a northwest-trending gravity gradient likely coincident with a southwest-down normal fault (Cather, 2009a). Within the study area, Neogene basin-fill deposits are <20 m thick and bedrock is commonly exposed.

Torres Syncline

The Torres syncline is clearly demarcated by two parallel ridges of inward-dipping San Andres-Glorieta Sandstone (Fig. 15; geologic map; Bates et al., 1947). This ridge strikes 010° for a distance of 18 km north of the southern quadrangle boundary. North of there, the two ridges curve toward each other and meet, indicating that the syncline plunges southward along a bearing of 190°. In the center of the syncline, reddish-brown mudstones and minor sandstones of the Chinle Formation are intermittently to poorly exposed. About 500–550 m of structural relief is interpreted where cross section A–A′ extends across the syncline. We queried a west-dipping fault in the subsurface under the eastern San Andres-Glorieta ridge—an inferred northward continuation of the fault structure bounding the western foot of the Oscura Mountains.

Although more study is needed, we favor an interpretation that the Torres syncline is related to Neogene extension rather than Laramide contraction. First, the syncline aligns with the deeper Trinity basin to the south, where $^{40}Ar/^{39}Ar$ dating of the mineral jarosite indicates faulting on its

eastern flank from 8 to 3 Ma (Lueth, 2009). Second, the absence of Paleogene to early Neogene strata in the core of the Torres syncline argues that it did not form in the Laramide. There is no notable accumulation of Baca Formation, Spears Group, and Mogollon-Datil Group strata preserved in the syncline, which would be expected if there was a structurally low area here in the middle to late Eocene. Erosionally resistant volcanic units, in particular, might be expected to be preserved in a late Eocene to early Oligocene structurally low area. Finally, we note that other large and relatively symmetrical synclinal basins, similar in scale and size to this one, have formed during Neogene extension in nearby areas, but we are unaware of symmetrical synclinal structures developing in the region in the Laramide. Comparable extensional sags include the Jornada del Muerto synclinal-horst basin to the south (Mack et al., 2003) and the Estancia Basin 70 km to the north (Newton et al., 2020, fig. 4b). Other extensional synclinal-horst basins farther south-southwest in New Mexico include the Miocene Gila Wilderness and Uvas Valley basins (Mack et al., 2003). As illustrated by cross section A–A′, we infer that the Torres syncline may be a similar synclinal-horst basin, with flanking horst blocks on the west (immediately east of the Prairie Springs anticline, although the anticline itself may be mostly related to Quebradas detachment faulting) and east (northward continuation of the horst block-anticline from the northern Oscura Mountains).

Prairie Spring anticline

The Prairie Spring anticline is present 5 km west of the aforementioned San Andres-Glorieta ridge rimming the west side of the Torres syncline (Fig. 15). We interpret that this anticline extends only 5 km north of cross section A–A′, about half of that shown by Wilpolt and Wanek (1951). Additionally, our mapping indicates a local horst block about 1.4 km to the east of the anticline axis along the cross-section line. Given inferred stratigraphic levels near the horst block and anticline, it is difficult to construct a deep-seated, anticlinal structure coincident with the axis of the anticline. Consequently, we favor an interpretation that the Prairie Springs anticline is related to contractional thickening at the eastward toe of the Quebradas detachment structure, as proposed by Cather and Koning (2024). No oil wells have been drilled on the anticline axis.

Oscura anticline-horst block

Bates et al. (1947), Wilpolt and Wanek (1951) and Broadhead and Jones (2004) mapped the Oscura anticline as extending 32–33 km northward from the Oscura Mountains along the western flank of Chupadera Mesa. Numerous wells were drilled near the axis, including McCaw Federal 01 and Stackhouse Powell Government. Subsurface elevations of pre-Yeso strata, such as the Abo Formation and Proterozoic rocks, are relatively higher on the anticline axis than to the west or east (Broadhead and Jones, 2004, fig. 6; cross section A–A′). We argue that it is possible that the west-down fault at the foot of the eastern Oscura Mountains continues northward alongside the western part of the anticline, perhaps at depth as shown in cross section A–A′. If so, this structure may be a hybrid between an anticline and horst block.

The anticline component likely originated in the Laramide, but we argue that two younger structural sets may have been superimposed on it. One is the aforementioned, postulated west-

down fault that was postulated by Bates et al. (1947) to give a slight asymmetry to the anticline (i.e., slightly steeper west limb). Another is contractional structures at the eastern toe of the Quebradas detachment fault (Cather, 2009a). Evidence for contraction and thickening includes (1) the Los Vallos Formation is notably thicker here than in the Quebradas highlands (520 m versus 240 m; cross section A–A′) and (2) near the anticline hinge is a complex of tight folds developed in exposed Los Vallos Formation strata (Cather, 2009a, fig. 3). Thus, overprinted on this Laramide fold is contraction and thickening (and possible thrusting) arguably associated with the eastern end of the Quebradas detachment system. Near where the San Andres-Glorieta-cored ridge on the eastern limb of the syncline begins bending to the northwest, relatively small, north-trending anticlines and synclines were mapped. These folds may be upsection manifestations of the detachment-related contractional structures in the Los Vallos Formation, although it is also plausible they are Laramide in age.

Chupadera fault

The Chupadera fault extends northward 50 km in the Socorro 30 x 60-minute quadrangle (Fig. 15). Based on cross section A–A′, it has produced 180–210 m of east-down throw, much of it due to flexure. Previous workers have posited that the Chupadera fault is either a reverse structure or normal fault (e.g., Cather, 2009a). We favor a normal fault interpretation for the following reasons. First, no contractional structures have been verified on the immediate west side of the fault, but more detailed field work could still be done. Second, we infer that relatively low and laid-back fault scarps are present in middle to late Quaternary alluvium near the center of the fault zone (see the geologic map, UTM 13S 394965m E, 3777725m N, NAD83); the Quaternary age suggests normal faulting given the extensional stress regime that prevailed in the Neogene. Finally, an en echelon fault to the north, the Jumanos fault, is definitively a normal fault structure (Fig. 29). Structural contouring by Broadhead and Jones (2004) has the top of Proterozoic rocks and overlying Paleozoic strata dip gently toward the Chupadera fault from both the east and the west. Detailed mapping in bedrock north of the mapped north end of the Chupadera fault (UTM 13S 398621m E, 3812383m N, NAD83) found no evidence of west-east displacement of strata across the projected trace of the fault, no stratal folding, nor evidence of intense fracturing. Previous workers have suggested the Chupadera fault represents a southward continuation of the Picuris-Pecos fault (of north-central New Mexico) and has hosted major strike-slip (Harrison and Cather, 2004; Cather, 2004, 2009a; Cather et al., 2006). If such a strike-slip fault exists, we argue it was pre-Laramide since Permian strata are not demonstrably deformed.

Jumanos fault and monocline

The Jumanos fault (new name) offsets exposed San Andres-Glorieta strata on the northern edge of Mesa Jumanos, about 10 km east of New Mexico State Highway 55. This east-down fault extends 7 km south of the northern boundary of the quadrangle. At its southern end, topographic gradients suggest the fault bends to the southeast and vertical displacement rapidly diminishes. There is high certainty that this is a normal fault due to a graben structure and normal fault drag

(Fig. 29) at a location ≈4 km north of its southern end (UTM 13S 401128m E, 3816056m N, NAD83). Here, there is 50 m of east-down throw (including normal-drag flexure and offset). At the latitude where this fault appears to terminate, the Chupadera fault terminates northward. We thus interpret the southerly topographic slope in this area as reflecting a relay ramp between these two faults, and the Jumanos fault represents an en echelon continuation of the Chupadera fault system. The Jumanos fault may continue northward and tie into the west-down faults bounding the Perro subbasin of the Estancia Basin (Newton et al., 2020, fig. 6).

Figure 29—View to the NNE of the Jumanos fault, located ≈4 km north of its southern end (UTM 13S 401128m E, 3816056m N, NAD83). Here, mapping of the San Andres-Glorieta contact indicates the fault zone has a narrow graben exhibiting normal drag folding along its eastern fault. Including east-down flexure on its footwall, the total throw of the fault is 50 m. Inset photo: Slickenstria lineations and Riedel shears of a subsidiary fault exposure, located 0.3 km to the south, indicate east-down, normal slip.

EXTRACTIVE RESOURCES

Minerals and coal

Portions of eight mining districts and one coal field lie within the Socorro 30 x 60-minute quadrangle (Fig. 30). Most mining districts in the quadrangle are inactive, with little production (appendix F); however, one major mine, the Dicaperl Minerals perlite mine, and three aggregate (sand and gravel) mines (PG Veguita, San Antonio, and South Socorro I-25) are active in the quadrangle. Summaries of the mining districts are arranged below in alphabetical order, with more details on history, production, and types of deposits in appendix F. Descriptions of the types of mineral deposits are found in McLemore and Lueth (2017), McLemore and Austin (2017), and McLemore and Chenoweth (2017). The locations of these districts are shown in Figure 30. Aggregate mines are not described in this report.

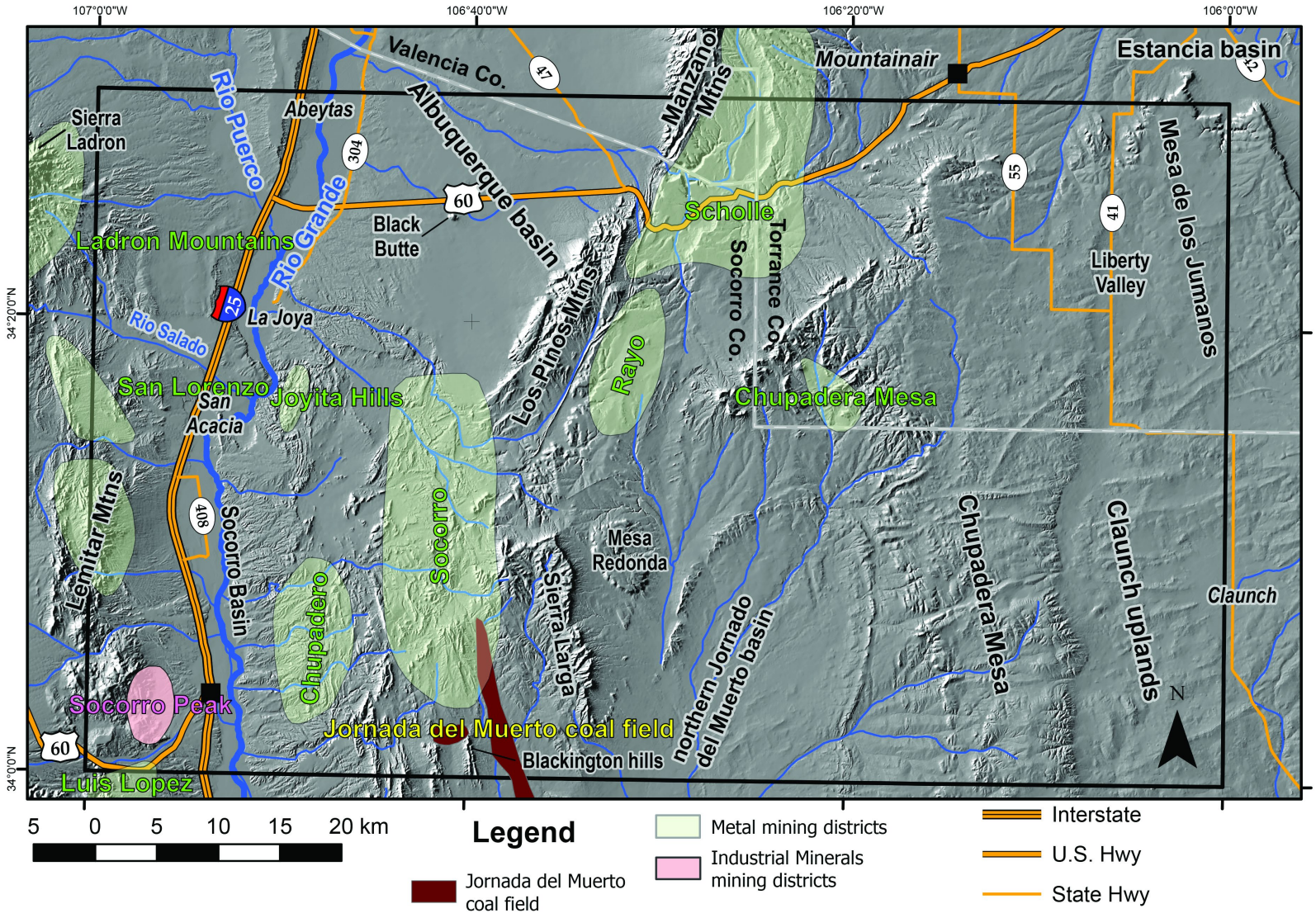

Figure 30—Map of mining districts and coal fields in the Socorro 30 x 60-minute quadrangle.

Chupadera Mesa Mining District

The Blackington and Harris iron deposits in the Chupadera Mesa district in the north-central portion of the quadrangle were mined between 1964 and 1975; approximately 100 tons of iron ore worth $125 was produced (McLemore, 1984; value not adjusted to inflation). The iron deposits are small, of intermediate grade, and are found adjacent to Cenozoic dikes in Yeso Group sedimentary rocks as replacement bodies. The largest bodies are only 30 m long and 2 m wide and assayed 39.6% to 47% total iron, with trace amounts of gold (McLemore, 1984).

Chupadera Mining District

A variety of mineral deposits are found in the Chupadera district east of Socorro, including stratabound sedimentary-copper deposits, Rio Grande rift (RGR) barite-fluorite-galena veins, disseminated uranium-rare earth elements (REE) in Proterozoic rocks, gypsum, limestone, and fire clay (Cather and Koning, 2024). Less than $2,000 worth of copper, silver, fluorite, barite, and fire clay were produced before 1960 (appendix E). Six outcrops of medium- to coarse-grained Proterozoic Tajo granite that are exposed along north-trending faults in the Quebradas area were originally prospected for uranium in the 1970s by Rocky Mountain Energy Company (McLemore, 1983b; Cather and Koning, 2024). Recent sampling of the Tajo granite indicated as much as 262 ppm uranium and 282 ppm total REE, which are uneconomic (Dietz and McLemore, 2022). Future economic development of any of these deposits is low.

Joyita Hills Mining District

RGR barite-fluorite-galena veins were first prospected around 1880 in the Joyita Hills district, northeast of Socorro. A mill was constructed in 1915 to process silver from galena, but was not very successful (North, 1983); only an estimated 50 ounces of silver were produced (McLemore, 2017). Veins are found in fissures in Proterozoic gneiss and along the contact of Proterozoic rocks with Oligocene volcanic rocks and Pennsylvanian and Permian sedimentary rocks. Later, small sandstone uranium and RGR copper-silver (uranium) veins were found but no production occurred (McLemore, 1983a, 1983b). The economic potential is low.

Jornada del Muerto Coal Field

The Jornada del Muerto coal field is a small field in the center of the quadrangle. Two small mines operated here prior to 1927, where as much as 1.2-m-thick coal beds are found in the Dilco Coal Member of the Crevasse Canyon Formation. Most of the coal in the district is uneconomic because it is too thin, faulted, steeply dipping (24°–45°), and overlain by thick overburden.

Lemitar Mountains Mining District

Five types of mineral deposits are found in the Lemitar Mountains: carbonatite, episyenites (metasomatites), REE-thorium-uranium veins, RGR barite-fluorite-galena, and vein and replacement deposits in Proterozoic rocks, but production has been from only the RGR barite-fluorite-galena deposits (McLemore, 1983c, 2017). The carbonatites have been examined for REE potential; some samples are as much as 1.1% REE. Carbonatites are carbonate-rich rocks of apparent magmatic derivation containing more than 50% magmatic carbonate minerals and less

than 20% SiO_2. These carbonatites are composed of dolomite, calcite, apatite, magnetite, fluorite, and other minerals. Carbonatites generally contain REE, uranium, thorium, niobium, tantalum, zirconium, hafnium, iron, titanium, vanadium, copper, and strontium.

Luis Lopez Mining District

Only the northernmost portion of the Luis Lopez district lies within the quadrangle in the northern Chupadera Mountains. The Luis Lopez district consists of epithermal manganese veins. The district was one of the largest producers of manganese in New Mexico; total production from 1952 to 1958 was 97,000 short tons of concentrate that averaged 41% manganese and 18,000 short tons of crude ore that averaged 28% manganese (Farnham, 1961; Willard, 1973). Production continued until the early 1970s, but this later production was not reported. Manganese veins and breccias follow steeply dipping faults and fracture zones (Eggleston et al., 1983).

Rayo and Scholle Mining Districts

Stratabound sedimentary-copper deposits containing copper, silver, and locally lead, zinc, uranium, vanadium, and molybdenum are found in the Scholle and Rayo districts in the northern portion of the quadrangle (McLemore, 2016, 2017). Spanish explorers likely found copper in the area in 1629. The Scholle deposits were rediscovered by modern prospectors as early as 1902 (McLemore, 1984), but production did not begin until 1915. From 1915 to 1961, 15,037 short tons of ore were produced from the Abo Formation in the Scholle district and yielded 1,122,468 lbs copper, 8,147 oz silver, and 426 lbs lead (appendix A). In 1916, approximately $700 worth of radium was produced from this district (McLemore, 1984). Less than $1,000 worth of copper and silver were produced from the Rayo district, which also came from the Abo Formation (McLemore, 2017). Many of the stratabound sedimentary-copper deposits are being reexamined for critical minerals potential, especially heavy REE, vanadium, cobalt, and arsenic (McLemore et al., 2024); the Scholle and Rayo deposits require additional sampling to evaluate the critical minerals potential.

San Lorenzo Mining District

The San Lorenzo district is within the Sevilleta National Wildlife Refuge and was withdrawn from mineral entry. An unknown amount of copper and silver has been produced from the district (appendix A). Uranium is associated with the copper-silver veins (Lasky, 1932; North, 1983; Eveleth et al., 2009). Numerous, small prospects are found throughout the district (V.T. McLemore, field investigations).

Socorro Mining District

The Socorro mining district is east of Socorro and was first prospected in the 1950s. An estimated $70,000 worth of uranium and vanadium was produced from RGR copper-silver (± uranium) vein deposits (McLemore, 1983a, 1983b, 2017; Cather and Koning, 2024). Small sandstone uranium, volcanogenic uranium, stratabound sedimentary-copper, RGR barite-fluorite-galena (± silver, copper) vein, and gypsum deposits also are found in the district (Cather and Koning, 2024). Future economic development of any of these deposits is unlikely.

Socorro Peak Mining District

The Dicaperl Minerals perlite mine, operated by the Dicalite Management Group, is one of the largest perlite deposits in the United States, with more than 15 million short tons of active and proven reserves and an estimated mine life of 60 years (https://www.dicalite.com/location/socorro-nm/, accessed June 23, 2024). Perlite is a natural siliceous volcanic glass, characterized by abundant concentric fractures, commonly has a pearly luster, and expands appreciably by vesiculation under appropriate heat treatment. Perlite is used in construction (tiles, insulation boards, and aggregate), filtering material, filler (carrier of herbicides, insecticides, and chemical fertilizers), and as a soil additive. The mine opened in 1949 but closed in 1961 because of decreased demand. However, market conditions improved in 1975 when the mine reopened and it remains in operation today.

Volcanic epithermal silver-gold veins are found north of the perlite mine in the Socorro Peak district that were mined in the late 1880s until the silver crash of 1893 (North, 1983; Eveleth et al., 2009). The Torrance 10-stamp mill and New Orleans and La Joya smelters processed the silver-gold ores. Ore was later shipped to the Billings smelter in Socorro east of the district. The Billings smelter processed an estimated $18 million of silver from Magdalena, Socorro Peak, and other mining districts throughout New Mexico from 1883 to 1894 (Eveleth, 1983). None of the smelters remain today.

Oil and Natural Gas

Information presented here regarding oil and gas resources in the Socorro 30 x 60-minute quadrangle is from Broadhead and Jones (2004). These workers conclude that favorable potential for oil and gas exists in two areas: (1) the west-central part of the southern quadrangle, between the central Quebradas and the Torres syncline and (2) near the southern half of the eastern quadrangle boundary, south of the town of Claunch. This inference is made by comparing various oil and gas potential indicators between a limited number of wells. In the Torres syncline, these wells include the JK Anderson Wishbone well and Yates Petroleum McCaw Federal (labeled Wishbone and McCaw Fed in Figure 15). The McCaw Federal well is located in the quadrangle near the northern tip of the Oscura anticline (UTM 13S 380911m E, 3777073m N, NAD83). The Wishbone well is located 1 km south of the southern quadrangle boundary, at a distance 6 km east of the southern Blackington Hills (UTM 13S 353640m E, 3761529 m N, NAD83). Neither of these wells nor any wells in the larger regions record any production.

Although source rock characteristics are relatively similar across the quadrangle, a higher degree of maturation and total organic content is present west of the Torres syncline in the southern Socorro 30 x 60-minute quadrangle. The primary reservoirs for oil and gas are marine and nearshore strata associated with Gray Mesa, Atrasado, and Yeso strata (Pennsylvanian to early Permian). Terrestrial sandstones of the Abo Formation may also serve as reservoirs. Petroleum source rocks are dark-gray to black organic shales in marine Pennsylvanian strata that could have a high kerogen concentration. Algal, herbaceous, and amorphous kerogens can generate oil and

associated gas given a certain degree of maturation (Brooks et al., 1987; Tyson, 1987; Hunt, 1996), and woody kerogens can produce gas. With increasing maturation, kerogen color changes from yellow to orange to brown to black (Staplin, 1969). Broadhead and Jones (2004) calibrated color with inferred maturity levels using a thermal alteration index (TAI). Comparison of the TAI and total organics indicates that the area near the Oscura anticline (east limb of Torres syncline) has lower maturity levels, whereas maturity increases westward in the southern Socorro 30 x 60-minute quadrangle between the Torres syncline and the middle of the southern Quebradas highlands (based on data from the Wishbone well). This westward increase in maturation is likely due to crustal heating associated with late Eocene to Oligocene igneous events near the southwestern corner of the Socorro 30 x 60-minute quadrangle. Broadhead and Jones (2004) hypothesize that the Torres syncline may be an economic oil play.

Increasing eastward, thermal maturity and eastward pinchouts of Pennsylvanian strata near Claunch suggest favorable oil and gas prospects along the southern half of the eastern quadrangle boundary. This inference is based on well data located south and southeast of the Socorro 30 x 60-minute quadrangle. Here, thermal maturation increases eastward due to voluminous mid-Cenozoic intrusions between Capitan and Corona, and the Pennsylvanian sandstones truncated by a basal Permian unconformity could form a trap ("eastern Pennsylvanian boundary play" in Broadhead and Jones [2004]).

GEOLOGIC HISTORY AND SUMMARY

Here, we overview the stratigraphy and structural features of the Socorro 30 x 60-minute quadrangle by giving a brief narrative of the geologic history. Chapters in this history are organized as (1) early to middle Proterozoic sediment accumulation and igneous activity related to back-arc spreading of a subduction zone, metamorphosed by tectonism between 1,660–1,430 Ma of the Mazatzal and early Picuris orogenies; (2) late Paleozoic sedimentation during and postdating ARM tectonism; (3) Triassic to Jurassic terrigenous sedimentation related to west-northwest-flowing rivers; (4) Late Cretaceous marine, nearshore, and coastal plain sedimentation; (5) middle to late Eocene sedimentation during late stages of the Laramide orogeny; (6) late Eocene to late Oligocene sedimentation and igneous rocks (primarily ignimbrites) related to intermediate volcanism followed by bimodal felsic-mafic volcanism; and (7) Miocene to Quaternary sedimentation in the Rio Grande rift. Strata are described in more detail above (under the Stratigraphy section). Even more detailed descriptions of lithologic units are found in appendix A.

Paleoproterozoic to Mesoproterozoic Sedimentation, Intrusions, and Metamorphism

Notable sedimentation, volcanism, and intrusive activity occurred from 1,670 to 1,600 Ma during the Mazatzal orogeny, producing the bulk of the Proterozoic rocks seen in the Socorro 30 x 60-minute quadrangle. These sediments and volcanic rocks were subsequently metamorphosed and

preserved as the Manzano group of the Los Pinos Mountains, which are likely correlative to the Proterozoic rocks observed on the east flank of the Lemitar Mountains.

The earliest deposits in the Socorro quadrangle belong to the >150-m-thick Bootleg Canyon sequence. An interpreted protolith composed of clayey sediment and various sandstones was later metamorphosed into amphibolites, pelitic and "layered" schists, and quartzites. Based on the age of overlying units, the Bootleg Canyon sequence is probably 1,670–1,665 Ma. The Bootleg Canyon sequence is overlain by 1,200–1,250 m of the Sevilleta metarhyolites (**Xsr**), which yielded zircon U-Pb ages of 1,665 ± 161,660 ± 19 Ma and 1,660 ± 19 Ma (Holland et al., 2020) and 1,662 ± 2 Ma (Shastri, 1993). The overlying Abajo unit is 250–280 m thick and interpreted to have a protolith of sandstone, clayey sediment, and relatively mafic lavas + dikes, which were metamorphosed into metalithic arenites, "impure" quartzite, pelitic schist, greenschist, and metaigneous rocks. The age of the Abajo unit is ≈1,660 Ma based on constraints from the subjacent Sevilleta metarhyolites and maximum depositional ages from detrital zircons within and above the unit. A 450-m-thick sequence of quartz-rich sands overlying the Abajo was later metamorphosed into the White Ridge (lower) and Sais Quartzites (upper), which are lumped together as **Xq** on the compilation map. The youngest detrital zircon ages from the lower Sais Quartzite indicate a maximum depositional age of 1,660–1,653 Ma. The protolith of the stratigraphically highest unit in the Manzano group, the Blue Springs Formation, is interpreted to be characterized by clayey to sandy sediment (metamorphosed to schist and quartzite) interlayered with rhyolite (transformed to metarhyolites) that yielded U-Pb ages (zircons) of 1,601 +4/-3 Ma (Luther et al., 2005) to 1,588 ± 7 Ma (Holland et al., 2020).

The Manzano group is interpreted to have formed above a north-dipping, southward retreating subduction zone (Holland et al., 2020). These strata were emplaced on older Yavapai crust and were initially associated with isotopically juvenile volcanic rocks; with time, igneous activity reflected both juvenile-crustal and asthenospheric sources, possibly due to crustal thinning over an extending arc system. An upsection change in provenance is interpreted for the Manzano group. Sediments of the Sais Quartzite and underlying/older strata are inferred to reflect reworking from local highlands into rapidly subsiding intra- and/or back-arc basins. The upper part of the quartzite package (White Ridge) and overlying strata are characterized by older U-Pb detrital zircon ages (the youngest suite being 1,785–1,737 Ma) compared to underlying sediment and interbedded rhyolites. These older ages probably reflect increasing contributions of sediment sourced from the relatively distant Yavapai and Mojave crustal terrains (Holland et al., 2020), but the tectonic setting remained more or less the same; in intra- and/or back-arc basins. This distal provenance, combined with the younger ages of interbedded metarhyolites (1,588 ± 7 Ma), led Holland et al. (2020) to infer a possible unconformity at the base of the Blue Springs Formation or within the formation.

The ca. 1,680–1,590 Ma sediments and rhyolites of the Manzano group were intruded by granites exhibiting differing degrees of foliation development. Strongly foliated, granitic rocks (**Xgf**) on

the east side of Polvadera peak yielded a U-Pb zircon age of 1,648 ± 6 Ma (Bowring et al., 1983), but strongly foliated granites in the Los Pinos Mountains are probably older than the 1,659–1,655 Ma non- to weakly foliated Los Pinos Granite (Luther et al., 2005; see age discussion below). Most granites are non- to weakly foliated and include the Los Pinos, Polvadera, and Tajo Granites, lumped together into the **Xg** map unit. The Los Pinos Granite has yielded a U-Pb age of 1,668 ± 13 Ma and a Pb-Pb age of 1,655 ± 3 Ma (Holland et al., 2020). Because this granite crosscuts 1,660–1,653 Ma strata, its age is probably closer to 1,659–1,655 Ma (within error of the U-Pb age). An important Mesoproterozoic intrusion is the Priest Granite, which exhibits no to weak tectonic foliation and intrudes into the isoclinal, tilted Manzano Peak synclinorium in the Los Pinos and Manzano Mountains. The age of the Priest Granite ranges from 1,459 ± 13 Ma (Holland et al., 2020) to 1,430 Ma (Bauer et al., 1993). The Tajo Granite, crops out locally along the western flank of the Quebradas highlands, does not crosscut other Proterozoic units, and has not been directly dated.

Three main periods of deformation are interpreted for the Manzano group and related granites (Luther et al., 2005; Holland et al., 2020). The first (D1) involved west-directed thrusting that folded an earlier foliation orientated subparallel to compositional layering and inferred bedding. The second deformation event (D2) refolded D1 folds into larger upright folds, including the Manzano Peak synclinorium (Baer et al., 2004) and created prominent northeast-striking foliation and fabrics. In most places, the dominant rock fabric is a composite of D1 and D2, where the D1 fabric is deformed to be semi-parallel with D2 by the isoclinal nature of folds. Locally, however, D2 fabric crosscuts D1 fabric and compositional layering (Holland et al., 2020). The composite D1-D2 fabric probably developed during progressive and/or polyphase deformation events that were largely coaxial and began 1,665–1,660 Ma and extended past the 1,588 Ma emplacement of the Blue Ridge metarhyolites. Older Paleoproterozoic granites (**Xgf**) became more foliated than younger Paleoproterozoic granites (**Xg**) during this protracted deformation. Deformation is interpreted to be related to pulses of tectonism (e.g., contractional deformation) associated with the northward-dipping paleosubduction zone. Deformation probably culminated in the early part of the 1,460–1,400 Ma Picuris orogeny, after the emplacement of the 1,588 Ma Blue Ridge Formation but prior to the emplacement of the 1,460–1,430 Ma Priest Mountain Granite that crosscuts the Manzano Mountain synclinorium. S-C fabrics and porphyroblast-matrix textures in the contact aureole of the Priest Mountain Granite (map unit **Yg**) may be interpreted as preserving regional stress fields at the time of intrusion (Holland et al., 2020) or shortening related to pluton emplacement (Luther et al., 2005).

Late Paleozoic Sedimentation

A major unconformity (whose lacuna spans ≈1.2 billion years) separates Proterozoic rocks from late Paleozoic strata. The earliest Paleozoic unit preserved in the Socorro 30 x 60-minute quadrangle consists of relatively thin Mississippian strata (up to 30 m thick) found in the Lemitar and Socorro Mountains. These strata were deposited in a paleo-embayment on the west side of a northeast-striking paleotopographic high in central New Mexico (Armstrong and Mamet, 1988;

Armstrong et al., 2004). Mississippian strata are characterized by marine limestones and shales, with probable fluvial deposition in basal conglomeratic sandstones.

Pennsylvanian sedimentation in the study area occurred during the following stages (oldest to youngest): Atokan, Desmoinesian, Missourian, and Virgilian. Sedimentation was influenced by base-level fluctuations controlled by ARM tectonism (regional epeirogeny and local uplifts), glacioeustacy, and regional climate change (Kues and Giles, 2004; Cather and Koning, 2024, and references therein). The lowest unit, the 140- to 180-m-thick Sandia Formation, is Atokan in age (312–308 Ma) and was deposited in or near a seaway following a marine regression during the preceding Morrowan age (Kues and Giles, 2004). The Sandia Formation reflects sedimentation in open marine, marginal marine (nearshore), and coastal plain environments (Kues and Giles, 2004; Cather and Koning, 2024, and references therein). It is widespread across the map area, pinching out eastward near the Chupadera fault (see cross section A–A′). The formation is dominated by shale, siltstone, and quartzose sandstone, with minor quartz-conglomeratic sandstone and 5–25% limestone. Later, relatively high sea levels during the Desmoinesian (308–306 Ma) were conducive to the deposition of limestones and shales characterizing the 130- to 235-m-thick Gray Mesa Formation (Fig. 4A; Rejas, 1965; Lucas and Estep, 2000). More clastic material (shales and sandstones) is found in the overlying Atrasado Formation (225–270 m thick), probably reflecting the onset of pronounced tectonism and associated paleogeographic relief in the late Desmoinesian, Missourian, and Virgilian (Kues and Giles, 2004). Episodic sea level rises allowed for the accumulation of marine shales and limestones, whereas arkosic sandstones and minor conglomerates were probably deposited by rivers, lakes, deltas, and minor lakes (Lerner et al., 2009; Falcon-Lang et al., 2011; DiMichele et al., 2017; Cather and Koning, 2024). An overall upward transitioning to reddish and greenish clastic sedimentation signaled waning marine influence and a transition to the terrestrial sedimentation that characterizes the Wolfcampian stage (Kues and Giles, 2004). Only a thin Missourian section (i.e., the upper Atrasado Formation) is preserved in the Joyita Hills, due to localized ARM tectonic uplift and associated erosion in that area (Kottlowski and Stewart, 1970).

Most Permian sedimentation in the Socorro quadrangle occurred during the Wolfcampian and Leonardian ages. The 25- to 120-m-thick Bursum Formation (which may extend into the underlying Pennsylvanian, depending on how one defines the Pennsylvanian–Permian boundary) reflects a continuation of the transition from relatively thick intervals of marine strata in the uppermost Atrasado Formation to the wholly terrestrial Abo Formation. The Bursum Formation consists of purplish-red to variegated greenish-gray mudstones, arkosic sandstone, and conglomerates that are interbedded with marine limestones that decrease in abundance upsection. The conglomerates contain clasts of quartz, feldspar, and granite fragments eroded from local uplifts, including the Joyita Hills and an uplift under the modern Socorro Basin south of Socorro (Cather, 2018). The Bursum is primarily early Wolfcampian (ca. 299–295 Ma) based on fusulinids collected in its lower part (Kottlowski and Stewart, 1970; Altares, 1990; Beck and Johnson, 1992; Allen et al., 2013). The underlying contact is a disconformity whose lacuna

encompasses up to a few million years in the late Virgilian (Cather, 2018; Cather and Koning, 2024), and the oldest Bursum strata were deposited in wide paleovalleys (Krainer and Lucas, 2009). Alternating terrestrial and marine beds indicate cyclical transgression-regression sequences 10–50 m thick controlled by tectonism and eustacy (Krainer and Lucas, 2009). The Bursum onlaps with an angular unconformity over pre-Virgilian Paleozoic strata on the western margin of the Joyita uplift (Kottlowski and Stewart, 1970), indicating Virgilian tectonic activity. Paleocurrent analyses on conglomeratic sediments in the Quebradas highlands suggest three fluvial systems: (1) a north- to east-directed fluvial system south of the Joyita Hills that transported eroded Proterozoic detritus from an uplift now buried under the southern Socorro Basin, (2) westward rivers/streams on the western slope of the Joyita uplift, and (3) northeastward- to southeastward-directed rivers/streams east of the Joyita uplift and near Abo Pass that primarily reworked upper Madera Group (Cather, 2018).

By the middle Wolfcampian, ARM uplifts had sufficient paleotopographic relief to shed copious sediment to northern and central New Mexico (Kues and Gile, 2004). South- to southwest-directed fluvial systems (Cappa, 1975; Cappa and McMillan, 1983) deposited the Abo Formation from the Wolfcampian to early Leonardian, corresponding to about 295–275 Ma (Lucas et al., 2022b; Cather and Koning, 2024). Floodplain deposits are composed of brick-red, nonfissile mudstones and bedded siltstones to very fine-grained sandstones (Fig. 5). Channel deposits are mostly medium- to coarse-grained, arkosic to subarkosic sandstone; local lateral accretion bedding is interpreted as point-bars of meandering rivers, whose channels were as much as ≈5 m deep (Cather and Koning, 2024). Mudstones and floodplain deposits with interspersed lenticular fluvial channel fills are more abundant in the lower Abo (Scholle Member); sheet-like, very fine- to medium-grained sand bodies are more common in the overlying Cañon de Espinosa member (Lucas et al., 2022b; Cather and Koning, 2024). Interpretation of paleosols, vertebrate fossils, plant fossils, and fluvial-channel architecture suggests a warm, subhumid to semi-arid paleoclimate characterized by seasonal precipitation (Mack, 2003).

ARM tectonism had ceased by the close of the Wolfcampian (Ye et al., 1996). The Leonardian (280–271 Ma), in contrast, was characterized by tectonic stability and erosion of ARM uplifts that lowered paleogeographic relief (Kues and Giles, 2004). Coastal plain sedimentation alternated with shallow marine conditions in a relatively arid climate (Mack and Dinterman, 2002; Kues and Giles, 2004). Colorful (reddish-orange and red to pastel-colored) and well-sorted fine-grained sandstones, siltstones, and silty mudstones characterize the 70- to 110-m-thick Meseta Blanca Formation of the Yeso Group (Fig. 6), which were likely deposited by eolian sand and silt sheets reworked by floods and marine inundations (Cather and Koning, 2024). The overlying Los Vallos Formation consists of grayish-red to grayish-yellow sandstone, siltstone, and claystone interbedded with gypsum and ledge-forming carbonates up to a few meters thick (Fig. 7). Like in the underlying Meseta Blanca Formation, sandstones are mainly very fine- to fine-grained and quartzose. Carbonates are restricted to the lower ≈145–160 m of the formation (Torres Member). The upper part of the Los Vallos is overlain by gypsum-dominated strata (Cañas Member), which

in turn is overlain by ≈12–20 m of orangish- to light-reddish-brown siltstone and very fine- to fine-grained sandstone (Joyita Member). The Cañas and Torres Members were deposited in a shallow-marine to coastal-sabhka environment; the Joyita was deposited as eolian sand sheets with modest reworking by ephemeral(?) rivers (Cather and Koning, 2024).

A transgression followed by regression occurred during the late Leonardian (275–271 Ma). Early in this transgression, notable eolian activity deposited the 70- to 90-m-thick Glorieta Sandstone. This fine- to medium-grained sand was deposited by eolian processes, as indicated by local dune forms (e.g., Fig. 8), but much of this sand was reworked in shallow marine environments (Lucas et al., 2013). The Glorieta is onlapped by the 140- to 150-m-thick, marine San Andres Formation (Figs. 9 and 10). The San Andres consists mainly of limestone (minor dolomite) interbedded with intervals composed of gypsum and variable siltstone-mudstone. Limestone dominates in the lower 60 m, whereas shallowing marine conditions in the latter part of San Andres deposition led to gypsum, dolomite, and siltstone to mudstone being more abundant in the upper 80–90 m (Figs. 10A and 10B). The contact between these two formations is characterized by interfingering east of the Quebradas highlands, with sandstone tongues becoming thicker and more common to the north.

The youngest preserved Permian unit is the relatively thin (0–30 m thick) Artesia Formation. These strata are composed of reddish to orangish siltstone and very fine- to fine-grained sandstones, with minor beds of gypsum and dolomite or limestone. The base of the deposit is a disconformity, where karstic brecciation is locally observed in the underlying San Andres Formation. The Artesia Formation was deposited during the Roadian to Wordian ages (271–266 Ma) on an arid coastal plain, probably as loess and eolian sand sheets that were occasionally reworked by sheet floods and shallow-marine inundations (Cather and Koning, 2024).

Ancestral Rocky Mountain Tectonism

Locally coarse-grained sediment in the Sandia, Atrasado, and Bursum Formations attests to relatively close uplifts. These arkosic coarse sandstones and conglomerates give indirect evidence for ARM tectonism. Direct evidence for this tectonism is very sparse. A northeast-trending thrust fault (Polvadera thrust) in the Lemitar Mountains (east of Polvadera Peak), where the Sandia Formation is of unequal thickness on either side, illustrates a structure directly related to ARM tectonism. Another example is found along the western flank of the Joyita Hills, where an angular unconformity is present at the base of the Bursum Formation and there is thinning of the underlying Atrasado Formation (Kottlwoski and Stewart, 1970; Cather and Koning, 2024).

Triassic–Jurassic Continental Sedimentation

Triassic strata in the Socorro quadrangle comprise two formations (grouped together as a single map unit). These rocks were fluvially deposited in a broad basin that covered central and northern New Mexico but extended into Nevada, Colorado, Oklahoma, and Texas. This tectonic

feature is interpreted as a back-bulge basin that lay well east of an arc-trench system that existed along the western margin of Pangea (Dickinson, 1976; Lawton, 1994).

The older/lower Moenkopi Formation is of early Anisian age (between 245 and 240 Ma) and 10–30 m thick (Lucas, 1991, 2004; Spielmann and Lucas, 2009). These strata disconformably overlie either the Artesia or San Andres Formations. The Moenkopi Formation consists of reddish-brown to "chocolate-brown" mudstones, lithic-arenite sandstones, and minor conglomerates. This fluvial sediment was deposited by rivers flowing north to northwest from the Mogollon highlands and from uplifts south-southeast of the state in the Ouachita fold belt of Texas (Lucas, 2004).

The Chinle Formation disconformably overlies the Moeknopi Formation and is late Carnian to Norian in age, ca. 220–205 Ma (Lucas, 2004; Spielmann and Lucas, 2009; Dickinson, 2018). The Chinle Formation is 170–190 m thick and consists of a lower Shinarump Member and the overlying San Pedro Arroyo Member. The Shinarump Member is 0–30 m thick and is typically a ledge-former, where only a few meters are typically exposed. It consists of discontinuous, lenticular beds of reddish-brown to grayish-red, fine- to coarse-grained sandstone with well-rounded pebbles of chert, quartzite, and limestone (Fig. 12). The San Pedro Arroyo Member is reddish-brown, gray, and purplish-gray fluvial mudstone with subordinate sandstone, limestone-pebble intraformational conglomerate, and freshwater limestones (Fig. 11). Both members were deposited by paleorivers flowing north and northwest from the eastern end of the Mogollon highlands; some laminated mudstones possibly accumulated in floodplain lakes and ponds in this basin (Lucas, 2004; Cather and Koning, 2024).

An unconformity encompassing ≈50 million years separates the Triassic and Jurassic strata in the Socorro 30 x 60-minute quadrangle. The only preserved Jurassic unit is the Morrison Formation, whose age is Late Jurassic (Kimmeridgian–Tithonian ages, ≈155–145 Ma; Lucas, 2004). The Morrison is composed of fine- to medium-grained lithic-arenite sandstone that is commonly kaolinitic (Cather and Koning, 2024). The sandstones are interbedded with greenish-gray mudstone and sandy siltstone. It was deposited by northeast-flowing rivers within a retroarc basin that extended from central New Mexico to southern Saskatchewan (Turner and Peterson, 2004). In the map area, the rivers are interpreted to have headed in the Mogollon highlands (Lucas, 2004, fig. 12).

Late Cretaceous Western Interior Seaway Coastal Margin

During the Late Cretaceous, the WIS flooded a back-arc, foreland basin the interior of the North American continent (Armstrong, 1968; Price, 1973; DeCelles, 1994), whose western margin was characterized by a subduction zone and associated volcanic arc. The western shoreline of the WIS trended approximately northwest-southeast, with rivers and associated deltas flowing northeast into the WIS (Blakey, 2023; Nummedal, 2004; Lin et al., 2019). The seaway likely formed due to (1) dynamic regional subsidence caused by a shallowing angle of the subducting Farallon flat slab (Pang and Nummedal, 1995; Liu and Nummedal, 2004; Liu et al., 2011; Chang and Liu, 2021); (2)

crustal loading during the Sevier orogeny, which generated a wide foreland basin east of the Sevier highlands (Beaumont, 1981; Jordan, 1981; Pang and Nummedal, 1995; Liu and Nummedal, 2004; Miall et al., 2008); (3) globally high sea levels related to a greenhouse climate (resulting in minimal, if any, glacial ice and thermal expansion of seawater); and (4) extensive mid-ocean ridge volcanism displacing seawater onto continents (Hay, 2008). The maximum extent of the seaway occurred 95–92 Ma. The long-term east-northeastward retreat that followed (in the remainder of the Late Cretaceous) was punctuated by many transgressions and regressions on the scale of 0.1–1 Myr (Haq, 2014), many of which could be ca. 400 kyr eccentricity cycles (Mack et al., 2016) that many workers interpret to be related to climatically controlled eustacy influenced by astronomical forcings (e.g., Nummedal, 2004; Gale et al., 2008; Mack et al., 2016; Lin et al., 2019;). Lithologic descriptions and environmental and eustacy interpretations below are mainly from Cather and Koning (2024). Important earlier work synthesized in Cather and Koning (2024) regarding Cretaceous stratigraphy and biostratigraphy in the map area includes (Hook, 1983, 1984, 2010; Molenaar, 1983; Hook et al., 1983, 2012; Hook and Cobban, 2007, 2011, 2013, 2015).

The stratigraphically lower Cretaceous interval (**Kl**) is associated with the T-1 transgression, R-1 regression, T-2 transgression, and R-2 regression. The lowest Cretaceous unit in this interval is the Dakota Sandstone (middle Cenomanian), characterized by 5–20 m of gray to yellow, medium- to coarse-grained, quartz-rich sandstones and minor mudstones. Most of the unit is fluvial, but near the top sandstones are deposited in a nearshore environment. The overlying Mancos Shale is gray but commonly weathers yellowish. It consists of two shale tongues separated by the Tres Hermanos Formation. The lower (Tokay) tongue contains fine-grained sandstone beds near the base and top of the unit. About one-third up from the base of the Tokay tongue is a 19-m-thick interval with abundant limestone beds, correlated to the Bridge Creek Limestone. The Tres Hermanos Formation is composed of sandstone and shales and has three members (listed in ascending order); the Atarque Sandstone Member (light-gray to dark-brown or buff-colored sandstone), the Carthage Member (sandstone and shale), and the Fite Ranch Sandstone (light-gray to dark brown, highly bioturbated sandstones that coarsen upward from very fine-grained to fine-grained). The upper tongue of the Mancos is called the D-Cross Tongue, and it has scattered concretions of calcium carbonate near its base and top. The Tokay tongue records a major transgression (T-1), whose maximum water depth is near the center of the tongue at the base of the Bridge Creek Limestone Beds. Subsequent R-1 regression is recorded consecutively in (1) the upper part of the shale-dominated, marine Tokay Tongue; (2) the overlying Atarque Sandstone Member, deposited in a regressive barrier island environment or shoreface complex that prograded to the northeast; and (3) the lower two-thirds of the Carthage Member, which was laid down during the culmination of the regression (Hook and Cobban, 2011) on a broad, low-relief coastal or delta plain by rivers (channel fills and floodplain deposits) or ponds and lakes. The upper 15–30% of the Carthage Member was deposited in the ensuing T-2 transgression and consists of marine shale with fossiliferous concretions. The Fite Ranch Sandstone is associated with a coastal barrier-island paleoenvironment and its upper contact is a disconformity. T-2 led

to deeper-water conditions of the marine shales of the D-Cross Tongue, within which (near the middle of the tongue) is the start of the R-2 regression (Cather and Koning, 2024).

The upper Cretaceous interval in the Socorro 30 x 60-minute quadrangle (**Ku**) records the culmination of the R-2 regression and a final transgression (T-3), followed by permanent terrestrial sedimentation. The transition from marine into nearshore deposits is observed in the Gallup Sandstone, a gray to yellowish-gray, fine-grained sandstone and mudstone that is 5–15 m thick. It was mainly deposited in a regressive coastal barrier-island setting that experienced periodic minor transgressions. The overlying Crevasse Canyon Formation is composed of a coarsening-upward sequence characterized by tan to gray to olive-brown sandstone, mudstone, and siltstone. These strata were deposited in coastal plain, brackish lagoon, and fluvial paleoenvironments. T-3 marine strata are located about 50 m above the top of the Gallup Sandstone, where a 30-m-thick tongue of Mancos Shale (Mulatto Tongue) is intercalated within the lower Crevasse Canyon Formation. R-3 terrestrial strata of the Crevasse Canyon Formation overlie this marine tongue (Cather and Koning, 2024).

Paleogene Laramide Orogeny and Related Sedimentation

The Laramide orogeny in central New Mexico started ca. 75–70 Ma (Thacker et al., 2023) and ended ca. 45 Ma (Kelley et al., 1992, 2009; Cather, 2009b). Many structures in the map area were active during the Laramide. However, the reactivation of most of those structures during the Rio Grande extension complicates interpretations of earlier Laramide strains. Major structures described above that exhibit notable contractional folding and involve post-Bursum strata (post-ARM tectonism), consistent with Laramide-age tectonism, include the Montosa and Gallinas fault-and-fold structures and the Tajo structure (Cather, 2009a; Cather and Koning, 2024). The Bustos monocline is also very likely a Laramide structure. Northeast-striking structures, which may have served as strike-slip or transpressional faults that link various north-south-striking fault-fold structures, include the Amado and Milagro faults (Cather and Koning, 2024). The west-striking Landing Strip fault may also have acted as a strike-slip fault during the Laramide. The Oscura anticline on the east side of the Trinity basin is inferred by us to be Laramide, but it alternatively may be due to contraction at the termini of gypsum-rooted, east-directed detachment faults (Cather, 2009a; Cather and Koning, 2024)—similar to what we tentatively infer for the Prairie Spring anticline (cross section A–A′).

Two large-scale tectonic features formed during the Laramide: the Sierra uplift west of the Quebradas highlands and the Carthage-La Joya basin within what is now the Quebradas highlands. The absence of post-Madera Group, upper Paleozoic, and Mesozoic strata on the Sierra uplift (e.g., as exposed in the Lemitar Mountains) indicates 1.5–1.9 km of exhumation occurred between the Late Cretaceous and the deposition of upper Eocene strata mapped as Spears and Datil Groups. These time constraints coincide well with the age range of Laramide tectonism. The structural zone defining the eastern edge of the Sierra uplift probably coincides with the Coyote-Veranito faults that have been reactivated as normal faults defining the eastern side of the Socorro

Basin; the Tajo fold structure may also be part of this eastern structural zone. Evidence for this being the structural boundary includes an overall increase in clast sizes westward toward this boundary in the piedmont lithofacies (with Proterozoic clast compositions observed) and overturned bedding and fault-propagation folding along the Tajo structural zone (Figs. 27 and 28). The aforementioned fault-propagation fold at Ojo de Amado, on which lies an inferred paleovalley backfilled by Spears Group, is consistent with Laramide tectonism of the Sierra uplift. There, the Spears Group was subsequently tilted westward 30°–50° during rifting, implying that Atrasado Formation beds at Ojo de Amado Spring were once overturned before being rotated westward to their current vertical position.

The presence of scattered outcrops of Baca Formation in the western Quebradas highlands is used to interpret a Laramide-age basin there called the Carthage-La Joya basin. The Baca Formation in this basin consists of sandstone, conglomerate, and minor reddish mudstone. The sandstone is commonly cross-bedded and subarkosic. The conglomerate consists of pebbles, cobbles, and boulders composed of Proterozoic lithotypes (granites, gneissic granite, schist, and quartzite) and Paleozoic lithotypes (limestone, sandstone, and siltstone). The age of the overlying Datil Group volcanics (i.e., late Eocene) and the presence of Bridgerian fossils in its lower part, near Carthage (Gardner, 1910; Lucas and Williamson, 1993, indicate a middle Eocene age for the Baca Formation. Both piedmont and axial lithofacies have been recognized (Cather, 2009b). Piedmont deposits contain mostly Proterozoic and Paleozoic detritus. Paleocurrent analyses indicate derivation from the Sierra uplift to the west (east-northeast paleoflow) and from a paleo-uplift along the west side of the Montosa fault-fold structure (southwest paleoflow). Between these two piedmont deposits lie axial-river lithofacies, which are comparably more texturally and compositionally mature than the piedmont deposits and contain unique clasts composed of felsic metavolcanic rocks, chert, quartz, and petrified wood; less than 10% of the clasts are upper Paleozoic lithotypes similar to those observed in the piedmont lithofacies. The unique gravels are inferred to be sourced in central Arizona from the Mogollon highlands (Cather, 2009b). Paleoflow indicators for axial-fluvial deposits at one location south of the map area (Rancho Ojo del Llano) suggest an overall southeast-directed paleoflow within the Carthage-La Joya basin. Based on gravel maturity and composition, Cather (2009b) infers that the axial-fluvial facies in this basin were deposited by an east-flowing river with its head in the Mogollon highlands of Arizona. This river commonly terminated in a middle Eocene lake northwest of the Socorro Basin, but periodically flowed eastward across the Sierra uplift and into the Carthage-La Joya basin.

Late Eocene to Oligocene Volcanism and Tectonism

Volcanism, Intrusions, and Sedimentation

The period between about 42 and 26 Ma was marked by a high degree of volcanic activity and related sedimentation. Prior to 36 Ma, volcanism was intermediate in composition based on associated volcaniclastic detritus. Lava flows are relatively sparse and presumably concentrated near eruptive centers buried under the Socorro Basin, or else located farther to the southwest. However, erosion of these eruptive centers produced a thick volcaniclastic apron deposited in the

Carthage-La Joya basin (Cather, 2009b), which eventually onlapped westward onto the Sierra uplift.

The volcaniclastic sediment is mapped as the Spears Group, consisting of grayish-red to medium- or light-gray conglomerates, sandstones, siltstones, and reddish mudstones. Debris flows and lahars are common. Conglomerate clasts range from pebbles to boulders. The base of the unit is gradational with the underlying, nonvolcanic Baca Formation (e.g., Fig. 28). In the Quebradas highlands, the Spears Group below the Hells Mesa Tuff consists of a lower unit ≈760 m thick and an upper unit 0–120 m thick. Clasts in the lower unit are dominated by plagioclase- and amphibole-bearing andesite-dacite. Clasts in the upper unit are mostly basaltic andesite (plagioclase- and pyroxene-phyric) and andesite-dacite with plagioclase and amphibole phenocrysts. In the Lemitar Mountains, the Spears Group thickens rapidly northward from 120 to 330 m. East of the Rio Grande, the Spears Group is 700–800 m thick.

Volcanic rocks of the Datil and Mogollon Groups mainly overlie the Spears Group, but tongues of volcaniclastic sediment are found throughout the section. Early volcanic rocks include the Datil Well Tuff, present only near the southern quadrangle border (35.38 ± 0.01 Ma to 35.32 ± 0.02 Ma); the Rockhouse Canyon Tuff (34.78 ± 0.01 Ma), overlain by andesite (Joyita Hills) or dacite (Blackington Hills) flows; and the La Jara Peak Basaltic Andesite. The Hells Mesa Tuff is a regional marker bed at the top of the Datil Group; it is readily recognizable by its coarse grains and quartz-rich phenocryst assemblage. The Hells Mesa Tuff (32.35 ± 0.01 Ma) erupted from a caldera that occupied the southwest corner of the quadrangle (Fig. 14; Chamberlin et al., 2004). The east-west-trending northern caldera boundary can be seen in Socorro Peak (Koning et al., 2022b, figs. 2.3 and 2.6) and the boundary curved southward southwest of the peak, not visible due to later burial by the Santa Fe Group.

A ≈2-Myr apparent lacuna corresponds to an unconformity or compressed section at the top of the Hells Mesa Tuff. The Luis Lopez Formation of the Mogollon Group (30–29 Ma) overlies the Hells Mesa Tuff and records mafic, intermediate, and felsic volcanism and sedimentation within the Socorro caldera southwest of Socorro (Chamberlin et al., 2002). Two tuffs associated with rhyolitic eruptions (30.43 ± 0.1 Ma and 29.00 ± 0.01 Ma) are preserved as far northeast as the Joyita Hills. Within the caldera, the Luis Lopez Formation is up to 700 m thick, and sediments intercalated with the tuffs and volcanic flows are derived mostly from erosion of the caldera walls.

Between 29 and 27 Ma, much volcanic activity occurred on the southwestern part of the quadrangle. Ignimbrite tuffs sourced from the northwestern Mogollon-Datil volcanic field are intercalated with copious flows of La Jara Peak Basaltic Andesite derived from the southeastern Colorado Plateau (Chamberlin et al., 2001). The sequence of Mogollon Group ignimbrites is (oldest to youngest): the La Jencia Tuff (29.00 ± 0.01 Ma), the Vicks Peak Tuff (28.77 ± 0.01 Ma), the Lemitar Tuff (28.24 ± 0.01 Ma), and South Canyon Tuff (27.67 ± 0.01 Ma). Individual tongues of the La Jara Peak Basaltic Andesite are commonly 30–300 m thick and composed of many tens

of flows, each about 3–10 m thick. Wedge-shaped geometries in the Lemitar Mountains indicate the basaltic andesites were concomitant with early extension and domino-style block rotation (Chamberlin, 1983).

Various intrusive activities accompanied late Eocene to Oligocene volcanism. Pyroxene-phyric, gray mafic rocks occur as sills 5–10 km east of the Joyita Hills, where they intrude the Yeso Group, Baca Formation, and Cretaceous strata (Allen et al., 2013). An east-west-trending, intermediate to mafic dike at the south end of the Blackington Hills returned an age of 32.98 ± 0.05 Ma (Fig. 15), which is somewhat older than the age of the Hells Mesa Tuff. Since that dike is orientated toward the Socorro caldera, it may possibly relate to pre-caldera intrusions.

An impressive dike swarm is found east of the Quebradas highlands, particularly in the Rayo Hills, Chupadera Mesa, and Claunch uplands (Figs. 14 and 15). The dikes here trend 050°–070° and, locally, are adjacent to sills of similar composition that intrude the Los Vallos Formation or the fine-grained interval in the middle of the Glorieta Sandstone. These intrusions are intermediate to mafic in composition and spatially associated with two sets. The first is found in the Rayo Hills, where a dense collection of northeast-southwest-trending dikes project southwestward toward the Socorro caldera (Fig. 14). The second set is a more distributed collection of dikes within and east of the central-southern part of Chupadera Mesa—inferred by subparallel, tight anticlinal folds. Dikes in both sets project southwestward to the Morenci lineament and associated calderas (Figs. 14 and 15). The dikes east of the Joyita Hills (de Moor et al., 2005) project to the Sawmill and Socorro calderas.

Samples collected from both sets of dikes (Table 1) mainly yield $^{40}Ar/^{39}Ar$ ages of 33–30 Ma. The remaining samples returned ages of 34.0 (n=1), 27.3 (n=1), and 21.3–20.3 Ma (n=2). Age values are scattered spatially. The cluster of ages at 33–30 Ma may possibly be associated with pre- and post-eruption intrusions of the Socorro caldera, and perhaps associated magmatic inflation created the unconformity or compressed section outside of that caldera. The 34.0 and 27.3 Ma ages closely follow the eruptions of the Blue Canyon Tuff and South Canyon Tuff, respectively, from the Sullivan Hole and Mount Withington calderas. We hypothesize that most of the intermediate to mafic dikes (and related sills) in the central to the eastern part of the Socorro 30 x 60-minute quadrangle occurred in response to voluminous magma generation associated with these caldera eruptions, which traveled several tens of kilometers to 100 km northeastward away from these centers following a relatively wide zone of preexisting crustal weaknesses aligned with the Morenci lineament to the southwest (Fig. 14). Further dating efforts of these dikes may possibly find temporal correlations to other caldera eruptions.

Late Eocene to Oligocene Tectonism and Faulting

Extensional faulting characterized the latest Eocene through Oligocene, consistent with what has been inferred in adjoining regions (Cather, 1990; Koning et al., 2014). Half-graben, extensional faulting in the southwestern Socorro quadrangle is evidenced by (1) wedge-shaped thickness geometries of the Lemitar Tuff and the adjoining La Jara Peak Basaltic Andesite and (2) evidence

of normal faulting in the southern end of the Joyita Hills between the 34.4 Ma tuff of Arroyo Veranito and the 32.4 Ma Hells Mesa Tuff (Chamberlin et al., 2022a).

A particularly interesting structural phenomenon that occurred during the late Eocene through Oligocene is detachment faulting observed east of the Rio Grande (Cather, 2009a; Cather and Koning, 2024). This detachment and related splay faults developed mostly in the Los Vallos Formation, primarily in the Cañas Member (Figs. 25 and 26). Large-scale fault movement along these planes excised strata, commonly reducing the thickness of the Los Vallos Formation. For example, the Joyita Member may be removed down-slip of where a fault flat at the base of the Glorieta Sandstone ramps down to a fault flat lower in the Yeso Group, allowing translation of Glorieta Sandstone directly over pre-Joyita strata. It is inferred that the thickened Yeso Group observed on the east side of the Torres syncline may reflect contraction (thrust faults and folding) and related thickening of the Los Vallos Formation at the lower (eastern) end of these detachments (Cather, 2009a; Cather and Koning, 2024). We have elected to depict the Prairie Springs anticline as being related to this contraction based on adjoining stratigraphic relations, as explained above, but that is not certain. Very steep bedding dips and folding (seen best in aerial imagery) define the Oscura fold complex near the Oscura anticline axis and the western Chupadera Mesa escarpment (Fig. 15). This fold complex is probably a manifestation of the contraction at the toe of the east-directed detachment faults.

Miocene through Quaternary rifting and sedimentation

The Miocene through early Pleistocene is when relatively high subsidence was occurring in the Rio Grande rift, allowing preservation of several hundred meters to >1,000-m-thick clastic strata assigned to the Santa Fe Group. Multiple models have been invoked to explain the creation of the Rio Grande rift: (1) rotation of the Colorado Plateau (Hamilton, 1981; Chapin and Cather, 1994; Landman and Flowers, 2012), (2) collapse of over-thickened Laramide crust (Cordell, 1978; Eaton, 1987), and (3) mantle convective upwelling (Moucha et al., 2008; van Wijk et al., 2008). Note that extension probably started in the latest Eocene through Oligocene (Cather, 1990; Chamberlin et al., 2022a; van Wijk et al., 2018), but exhumation of adjoining mountain ranges notably accelerated after 25 Ma based on thermochronology data (Ricketts et al., 2016; Abbey and Niemi, 2019). Note that some workers have advocated for a post-21 Ma initiation for rifting (e.g., Ingersoll, 2001). In the Albuquerque and Socorro Basins, earliest Santa Fe Group sediment generally ranges from ≈20–16 Ma (Gawne, 1981; Tedford and Barghoorn, 1997, 1999; Connell et al., 2002; Cather and Read, 2003; Tedford et al., 2004; Cikoski, 2010).

In the Socorro 30 x 60-minute quadrangle, four phases in the history of rifting are recognized: (1) closed-basin deposition in the Popotosa Formation, (2) transition from closed- to open-basin conditions; (3) widespread aggradation of the Sierra Ladrones Formation in an exoheric basin, and (4) post-Santa Fe Group erosion and localized deposition. East of the Rio Grande rift, Pleistocene deposition occurred in the northern Jornada del Muerto Basin and Pliocene(?) to Pleistocene deposition occurred in the Claunch platform and southernmost Estancia Basin. Two

episodes of volcanic activity also occurred: 10–7 Ma Socorro Peak volcanic field (dacite progressing to rhyolite) and ca. 3.5 Ma basaltic volcanism.

Closed-basin deposition in lower Popotosa Formation

Conglomerates and sandstones characterize the lower Popotosa Formation in the Rio Grande rift. Particularly good exposures are seen in San Lorenzo Canyon, where the following succession of units is observed: (1) locally derived conglomeratic sediment associated with much debris-flow deposition, up to a few hundred meters thick, and (2) a 1- to 2-km-thick interval where sandstone and mudstones (basin-floor deposits, probably near the southeastern margin of a playa) interfinger with conglomeratic piedmont deposits. Paleocurrents in conglomeratic sediment in San Lorenzo Canyon are northwestward and those in basin-floor deposits range from northeast to northwest (Chamberlin et al., 2001; Cather and Read, 2003). These basin-floor paleoflow directions indicate the main playa was located north of San Lorenzo Canyon, likely corresponding, in part, to the thick, clayey playa sediments mapped near the Rio Salado (Machette, 1978). West-southwest of Socorro, strata are composed of conglomerate to sandstone that were eroded from late Eocene to Oligocene volcanic rocks that include the South Canyon, Lemitar, and Hells Mesa Tuffs. In these exposures, paleoflow ranges from west to north (Chamberlin, 1999), suggesting that the La Jencia Basin to the west experienced higher subsidence rates than the modern-day Socorro Basin. These southerly Popotosa deposits are tilted up to 25° and generally well-cemented. Strong cementation is commonly associated with jasperoid silicification and potassic metasomatism (see discussion in Koning et al. [2022b], p. 77–81; Dunbar et al. [1994]; Dunbar and Miggins [1996]; and Chamberlin and Eggleston [1996]). These deposits are older than ca. 11 Ma based on age constraints of the upper Popotosa Formation, although jasperoid silicification occurred in the late Miocene ca. 8.7–7.4 Ma (Dunbar et al., 1994; Dunbar and Miggins, 1996; Wilks and Chapin, 1997).

Transition from Closed- to Open-Basin Conditions in the Upper Popotosa Formation

Widespread playa deposits are observed in the upper Popotosa Formation that interfinger with adjoining fan-delta and alluvial-fan sediments. The alluvial-fan sediments are composed of conglomeratic sandstones, where the gravel composition is strictly volcanic and reflective of erosion and reworking of the late Eocene–Oligocene volcanic sequence. A distinctive, buff-colored conglomeratic sandstone located west of Lemitar contains southeastward paleoflow indicators and interfingers southward with clayey playa-lake sediment. Tongues of alluvial fan deposits derived from the Quebradas highlands to the east consist wholly of felsic-volcanic-dominated gravel and sand. This indicates that the Quebradas highlands were covered by the late Eocene to Oligocene volcanic sequence described above.

Where mapped near Socorro and Lemitar, the playa-lake sediment is likely younger than that mapped along the Rio Salado. Here, it is termed “Lake Socorro” and has three subunits, the uppermost of which is overlain by throughgoing Rio Grande deposits (Koning et al., 2024). The **lower Lake Socorro unit** is characterized by pinkish-reddish-gray to reddish-brown to pastel-

colored (including greenish) clays, minor interbedded sandstones, and local gypsum precipitation. These strata are interbedded with the 9.9 Ma basalt of Kelly Ranch (not mapped). The sandstones are tabular, fine- to medium-grained, and lack cross-stratification (including ripple marks). Mud cracks and other desiccation features are absent or very sparse, and no signs of microfauna were observed in exposures 5–10 km north of Socorro. There are 12% green clays, 2–3% relatively thin sand bodies, 1% gypsum beds, and evidence of a persistently wet playa surface but not necessarily standing water. A tongue of the 9.9 Ma basalt of Kelly Ranch provides age control for the lower Lake Socorro unit (Chamberlin et al., 2001; age converted using a 28.201 Ma Fish Canyon Tuff monitor age per Kuiper et al. [2008]). The **middle Lake Socorro unit** consists of reddish-brown clays interbedded with <3% sand bodies and <1% gypsum. The **upper Lake Socorro unit** lacks gypsum and green clays and has 10–30% fluvio-deltaic sand tongues with southward paleoflow indicators. The sand locally coarsens upward and exhibits intricate microlamination with clays (horizontal-planar and ripple-marked, with thicker cross-stratification to the north). Gypsum precipitation is notably sparser than in the first stage. Paleoflow indicators in the sands are generally to the south. The reddish-brown clay has 0–3% scattered sand grains and desiccation features are not obvious. A tongue of the 8.5 Ma basalt of Broken Tank (not mapped) indicates that the middle Lake Socorro unit is about that age. $^{40}Ar/^{39}Ar$ dating of detrital sanidine in the fluvio-deltaic sand tongues and the 7.0 Ma trachybasalt of Sedillo Hill indicate that the upper Lake Socorro unit is roughly 8.5–7.0 Ma (Koning et al., 2024).

Aggradation of Sierra Ladrones Formation in an Exoheric Basin

The Sierra Ladrones Formation constitutes the upper part of the Santa Fe Group. It consists of a central axial-fluvial facies flanked laterally by piedmont deposits. Both are relatively non- to weakly cemented and tilts are generally <5°.

The eastern piedmont deposits are composed of reddish-brown sandy gravel, gravelly sand, and sand. The gravel is predominately of sedimentary rock types (e.g., limestone, sandstone, and siltstones) derived from erosion of Paleozoic–Mesozoic strata, but north of Arroyo de la Parida the gravel is a mix of sedimentary and volcanic rock types. The change from volcanic gravel to sedimentary-dominated gravel in the eastern piedmont facies indicates notable exhumation of the Quebradas highlands in the latest Miocene through early Pliocene, probably facilitated by a shifting or concentration of extensional strain onto Socorro Basin faults after ≈8.5 Ma.

The western piedmont deposits consist of reddish-brown to light-brown sandy conglomerate, conglomeratic sandstone, and sandstone between the Rio Grande and the Socorro and Lemitar Mountains. In contrast to the eastern piedmont, gravel is composed predominately of volcanic rock types that include sparse clasts of dark-red jasperoid-cemented (potassium metasomatized) lower Popotosa Formation. North of the Rio Salado, volcanic-dominant gravels grade northward to those composed of limestone and gneiss (derived from Ladron Peak).

The axial-fluvial facies exhibits a notable upsection change. Its lower part (map unit **Nsa**) is somewhat darker and grayer and contains less gravel than the upper part. Also, the gravel in the

lower unit has a higher proportion of volcanic clasts and less extrabasinal gravel (e.g., granite and quartzite). In the upper axial-fluvial unit, gravel is composed of felsic-intermediate volcanic rocks, rounded chert, various sedimentary clasts, quartzite, and granite. This may reflect an increased discharge of the Rio Grande in the later Pliocene through Pleistocene compared to the late Miocene through early Pliocene, allowing it to more effectively carry extrabasinal gravel.

Post-Santa Fe Group erosion and localized deposition

Across much of the southern to central Rio Grande rift, Santa Fe Group deposition ended by ≈0.8 Ma (Mack et al., 1998; Sion et al., 2020). Since then, the Rio Grande has been progressively downcutting. However, notable episodes of aggradation occurred during this period of overall incision. These valley fills were later incised by younger incisional events, where the aggradation-incision cycle would repeat itself. Aggradation and incision were probably controlled by paleoclimatic-modulated discharge and hillslope erosion of local tributaries and the trunk river system, with the premise that the paleoclimatic changes were mainly related to shifts between glacial-interglacial regimes (Gile et al., 1991; Connell et al., 2005; Sion et al., 2020). Whether base level near the Rio Grande valley is largely controlled by upstream factors or local factors remains unresolved. This geomorphic activity left a series of geomorphic surfaces that generally decrease in age downward. Four allostratigraphic units have been mapped that usually underlie a given geomorphic surface and are correlated to the Jaral Largo, Matanza, Bowling Green, and Joyita alloformations of Sion et al. (2020). These deposits incorporate both axial-fluvial sediment deposited by the Rio Grande (**Qt4**–**Qt1**) and interfingering alluvial fan deposits (**Qf4**–**Qf1**). In many areas, the fan deposits have prograded over the axial-fluvial deposits, and the latter could not be differentiated.

As summarized above, the Rio Grande valley has at least four mappable allostratigraphic units. The older Joyita formation (**Qt4** and **Qf4**) is not directly dated and appears to have two subunits associated with it (mapped as **Qt4a** and **Qt4b**) at different geomorphic levels. We agree with Phillips and Sion (2022) that base level was relatively more stable, or the rate of incision by the Rio Grande was slower, than later in the Pleistocene. The Matanza formation, whose tread lies 120 m above the modern floodplain, is greater than 130 ka (sample Joyita-1) and underlies a 134-ka surface (Valle de Parida).

We are able to refine the geologic history associated with the Matanza formation (**Qt2**) and the paleogeomorphic-temporal transition between this formation and the Jaral Largo formation (**Qt1**). The Matanza formation appears to have four allostratigraphic subunits separated by intraformational disconformities. In the first allostratigraphic unit (A-1 in Figs. 18 and 22), periodically high discharges by the Rio Grande laid down cobbly alluvium with abundant clasts derived from northern New Mexico sometime between 125 and 110 ka. At the locality from which an OSL age of 117.2 ± 8.3 ka was obtained (Veguita Quarry), this lower unit is capped by a paleosol (Stage II carbonate morphology) and an erosional surface, suggesting that increasing discharge along the Rio Grande eventually led to incision and terrace-tread formation, where the terrace

tread was relatively stable for ≈10 kyr. After ca. 100 ka, aggradation of relatively sandy sediment occurred until 80 ka (allostratigraphic unit A-2, Figs. 18 and 23). Coarse-grained sediment derived from side canyons prograded onto the culmination surface during 77.7 ± 6 ka (subunit A-3, Fig. 23), after which base level fell by >20 m, probably driven by Rio Grande incision. This incision was relatively quick, and aggradation of the last allostratigraphic unit (A-4) was underway by 75.5 ± 6 ka. It is possible that the fourth subunit represents early Jaral Largo deposition (bottom diagram in Fig. 18B). But since the overlying geomorphic surfaces of these two deposits are notably different in height, for now we prefer the interpretation that they represent unique cut and fill events.

If our preferred interpretation is correct, then another incision event that dropped the Rio Grande base level occurred within 75–68 ka, followed by deposition of the 6-m-thick Jaral Largo formation by ≈68 ka based on sampling of the terrace deposit (**Qt1** and **Qf1**). Aggradation of the Jaral Largo ended by ca. 30 ka, and then incision occurred that is inferred to be related to the onset of marine isotope stage 2 (MIS 2) glaciation (Sion et al., 2020). It is possible that intraformational disconformities are present in the Jaral Largo alluvium (**Qt1** and **Qf1**).

Modern valley fill is up to 30–40 m thick in the larger drainages. Aggradation likely started in the latest Pleistocene and continued into the late Holocene (Hawley and Kottlowski, 1969; Sion et al., 2020). Where sampled in the Rio Salado and near the Rayo Hills, radiocarbon ages of sandy Holocene alluvium exposed in recently incised arroyos range from 3.5–0.1 ka (radiocarbon years before present; Sion et al., 2020; Aby and Jochems, 2022).

An important geomorphic process for the late Pleistocene–Holocene, and probably the middle Pleistocene as well, is the reworking of eolian sand sheets by sheetflooding on broad, gentle geomorphic slopes. This process has resulted in a surficial sand sheet that mantles the landscape in much of the central to eastern parts of the 30 x 60-minute Socorro quadrangle (unit **Qs**). Locally, **Qs** grades laterally into eolian sand featuring dune development (**Qe**). The relatively consistent quartzo-feldspathic composition of the sand (i.e., the lack of lithic grains comparable to local bedrock) is consistent with a hypothesis that much of the eolian sand is blown east-northeast from the Rio Grande valley and its large, eastern tributaries.

ACKNOWLEDGEMENTS

We wish to thank Steve Cather, Richard Chamberlin, and Fred Phillips for their reviews of the manuscript. We thank several property owners that allowed us access on their lands: Art Buckanum (CA Bar Ranch), Keith and Donna Banks, Gary Vega, Jayson Moore, Bill Luther, Molly Baldridge, Tony Sanchez, and Thomas Carroll (Deer Canyon Preserve).

APPENDIX A—DESCRIPTION OF MAP UNITS

POST-SANTA FE GROUP SEDIMENTARY DEPOSITS

Eolian Deposits

Qe

Eolian sand, undivided (recent to Holocene)

Sheets of light-brown to tan sand draping topography; mostly mapped in the central and eastern areas of the quadrangle and near the Rio Salado. The deposit typically features low coppice dunes or mounds (mostly <1 m tall), differentiating it from unit **Qs**, and may accumulate up to several meters thick on the lee (commonly northeast) sides of ridges. Composed of mainly fine- to medium-grained, subrounded to rounded, and moderately to well-sorted, quartz-rich sand. Buried soils, characterized by weak calcic horizons (Bk), structural development or reddening (Bw), or minor illuviated clay (Bt), may occur at depth. Loosely to weakly consolidated near the surface. The deposit is 0.5 to several meters thick.

Qed

Eolian sand with tall dunes (recent to Holocene)

Parabolic dunes north of the lower Rio Salado. Dune forms are mainly parabolic, 100–150 m wide, and up to 3–5 m tall. Dune geometry indicates a northeast transport direction; sand is sourced from the adjoining Rio Salado. Light-brown to brown (7.5YR 5–6/4), medium-grained, subrounded to subangular, well-sorted, loosely consolidated dune sand composed of clear grains (mostly quartz, plagioclase, and sanidine), 15% lithic grains (mainly volcanic), 10% orangish grains (potassium feldspar, granite, chert), and 2–4% mafic grains. Underlying these dunes is a sand sheet correlative to **Qe**. The deposit is 1–4(?) m thick.

Sheetflood Deposits

Qs

Sheetflood deposits, mainly reworking eolian sand (Holocene)

Light–brown to brown to strong–brown, massive sand with minor scattered granules and pebbles. Occurs as a bioturbated, surficial sheet covering relatively flat to low-sloping areas of the landscape. No coppice dunes nor other dune forms are obvious in aerial photos. The deposit contains minor, scattered coarse- to very coarse-grained sand and pebbles; variable pebble coverage on the surface (mainly <20%). There is a very low proportion of gravel beds. Mostly very fine (upper)- to medium (lower)-grained (ranging from very fine [lower] to medium [upper]-grained), subrounded to subangular, moderately to well-sorted sand that is composed of quartz, minor feldspar, and 1–10% lithic and mafic grains; locally silty to clayey. Topsoil and buried soils are characterized by ped development (weak to moderate, fine- to coarse-grained, subangular, blocky peds), weak calcic horizons (typically Stage I), and weak illuviated clay horizons (few, faint, silt to clay films on ped faces). Locally, buried soils have stronger calcic horizons (up to Stage II+). Moderately to well-consolidated. The deposit is 0.5–4 m thick.

Qscl

Sheetflood deposits, mainly reworking eolian sand that overlies and includes Claunch basin fill (Holocene to Pleistocene)

Deposit as described in unit **Qs** that overlies and includes sandy Claunch basin fill (**QNcl**). Units are combined on this map due to the difficulty in assessing the thickness of the similarly textured surficial sand (**Qs**). The deposit is tens of meters thick.

Interbedded Surficial Deposits

Qae

Interbedded alluvial, sheetflood, and eolian deposits (Holocene)

Interbedding, observed or inferred, of younger alluvium (**Qay**, **Qasy**), sheetflood (**Qs**), or eolian deposits (**Qes**). See descriptions of those individual units. The deposit is 1–5(?) m thick.

Qfaey

Younger alluvial-fan sediment interbedded with eolian tongues along the eastern margin of the Rio Grande valley (Holocene to latest Pleistocene)

Light-reddish-brown to light-brown, fine- to medium-grained sand and silty sand with scattered pebbles. Deposited mainly by sheetflooding processes on alluvial fans flanking the eastern margin of the Rio Grande floodplain. The sand is compositionally similar to **Qarg** sand; poorly to moderately sorted, and is relatively massive. General sedimentologic features are similar to unit **Qs** but likely include eolian tongues and underlie alluvial fans. The deposit is 1–4 m thick. This description is synthesized from McCraw et al. (2006).

Alluvium

Valley Floor

Qa

Alluvium, undivided (Holocene to middle Pleistocene)
Alluvium that includes a collection of various younger and older units that cannot be differentiated at 1:100,000 scale. May include the following units: **Qayr**, **Qasyr**, **Qasi**, and **Qao**. See descriptions of those individual units. A few to several meters thick.

Qar

Recent alluvium (<150 years old)
Sand and subordinate gravel (mainly pebbles and cobbles). Coarse-grained sediment that underlies bars and channel floors on arroyo bottoms (i.e., braided stream patterns) or is found as sand sheets or small fans at the mouths of channels or gullies. Mostly medium- to very coarse-grained and poorly sorted sand. Bar-and-swale topography is commonly observed, and vegetation is sparse. The sediment is loosely consolidated and is 1–3 m thick.

Qarg

Alluvium of the Rio Grande (recent to latest Pleistocene)
Tan to light-gray sand, clay, and silt underlying the floodplain and active channel of the Rio Grande, with variable but minor proportions of pebbles. The active channel is characterized by longitudinal bars separated by 0.5- to 1.5-m-deep channels. Fine- to very coarse-grained sand that is composed of quartz, clear feldspars (sanidine and plagioclase), lithic grains (volcanic, chert, sedimentary, and granite), and potassium feldspar. Very fine- to coarse-grained, moderately to poorly sorted, and heterolithic pebbles (including volcanic rocks, chert, quartzite, quartz, limestone, and red-bed siltstones and very fine- to fine-grained sandstones derived from Permian strata). Relatively abundant pebbles are found at the mouths of major tributary arroyos. The modern floodplain is commonly tilled or covered by riparian woodlands. Deeper sediment is composed of sand interlayered with subordinate silt and clay. Much of the sand is inferred to be sheet-like deposits that accumulated during flood-related avulsion events (e.g., Happ, 1948). Weakly consolidated and non-cemented. The deposit may be up to 20–30 m thick (McCraw et al., 2006).

Qay

Younger alluvium underlying low terraces (Holocene to latest Pleistocene)
Sand, silty to clayey sand, and gravelly sand to sandy gravel underlying low, valley-bottom terraces and subordinate valley-margin alluvial fans. The alluvium consists of brownish-gray to reddish sand, silty to clayey sand, and gravelly sand to sandy gravel. Somewhat darker tones than nearby **Qar** deposits are visible on aerial photos. The gravel consists of pebbles with subordinate cobbles. The overall finer-grained texture than found on **Qar**. One or more weakly developed buried soils are commonly present (characterized by Stage I calcic horizons and locally overlying A or Bw horizons). Horizontally laminated or massive sand and silty to clayey sand beds that contain variable proportions of scattered pebbles (typically <50%). The gravelly beds are commonly lenticular to broadly lenticular or U-shaped. The geomorphic surface lacks bar-and-swale topography and is weakly varnished. The surface soil is characterized by a weak calcic horizon locally capped by a dark, somewhat organic-rich A horizon. Includes the recently proposed Polvadera formation of Sion et al. (2020), which returned radiocarbon ages of ca. 3 ka. Weakly to well-consolidated and non- to poorly cemented. The deposit is 1–15 m thick.

Qayr

Younger alluvium underlying low terraces with subordinate recent alluvium (recent to latest Pleistocene)
Unit **Qay** with subordinate proportions of recent alluvium (**Qar**). See descriptions of those individual units. The deposit is 1–15 m thick.

Qayrp

Younger alluvium and subordinate recent alluvium in the Rio Puerco valley (recent to latest Pleistocene)
Pale-brown to yellowish-brown to reddish-brown sand, silt, clay, and pebbly sand. Sparse pebbles composed of chert, volcanic rocks, granite, siltstones to sandstones, and possibly limestone. The alluvium underlies the upper Holocene, maximum aggradational surface of the Rio Puerco valley, and grades laterally into alluvial-fan deposits (**Qfyr**). Tabular-bedded and weakly to well-consolidated. The deposit is 20–30 m thick. This description is synthesized from McCraw et al. (2006).

Qas

Sandy alluvium, mainly deposited by sheetflooding on wide valley floors (Holocene to late Pleistocene)
Light-brown to brown to strong-brown, massive sand and slightly clayey to silty (estimated 1–15% fines) sand with 0–5% scattered coarse- to very coarse-grained sand and pebbles. Mainly fine- to medium-grained (ranging from very fine- to medium-grained), subrounded to subangular, moderately sorted sand that is composed of quartz and very minor to minor feldspar with 1–10% mafic lithic grains. There are <20% very thin to thin lenses of clast-supported, sandy pebbles (minor cobbles). Subangular to subrounded gravel. The sandy sediment may be overprinted by a weakly cumulic soil (subangular, relatively coarse, subangular blocky, soft to slightly hard peds that lack clay films and exhibit a Stage I calcic horizon). Modern channels are not notable on the surface; sheetflood deposition dominates. The deposit is a few to several meters thick.

Qasy

Sandy alluvium, mainly deposited by sheetflooding and occupying low-level terraces (Holocene to late Pleistocene)
Deposit as described in unit **Qas** but correlative in geomorphic position and age to alluvial unit **Qay** (i.e., occupying a low, valley-bottom terrace position). See descriptions of those individual units. The sediment is a few to several meters thick.

Qasyr

Sandy alluvium, mainly deposited by sheetflooding and occupying low-level terraces with subordinate recent alluvium (recent to late Pleistocene)
Deposit as described in unit **Qas** but correlative in geomorphic position and age to alluvial unit **Qay** (i.e., occupying a low, valley-bottom terrace position). Includes subordinate amounts of recent alluvium (**Qayr**). See descriptions of those individual units. The deposit is a few to several meters thick.

Qasi

Sandy alluvium, mainly deposited by sheetflooding and occupying intermediate-level terraces (early Holocene to late Pleistocene)
Deposit as described in unit **Qas** but is underlying a terrace whose tread is 2–5 m above adjoining drainages. Light-brown to reddish-yellow, very fine- to fine-grained, quartzo-feldspathic sand with Stage I to Stage II gypsic horizon(s) in the topsoil. The deposit is a few to possibly several meters thick.

Qaiyr

Intermediate-age alluvium and younger and recent alluvium, undivided (recent to late Pleistocene)
Valley-bottom deposits forming low terraces. Composed of an unmappable (due to 1:100,000 scale) combination of alluvium that is correlative to intermediate-age terrace deposits (**Qti**), younger alluvium (**Qay**), and minor recent alluvium (**Qar**). See descriptions of those individual units. The undivided deposit is 1–10 m thick.

Qao

Older alluvium (late to middle Pleistocene)
Sand and variable sandy gravel to gravelly sand occupying relatively high geomorphic levels in the northern Trinity basin (several meters above local drainages); underlies broad valley floors, low-sloping piedmonts, and local terraces. Gravel mainly consists of clasts eroded from the San Andres and Glorieta Formations. Crust-forming, strongly developed gypsic topsoils. The deposit is 1–10(?) m thick.

Terrace Deposits Along Major Drainages, Largely Excludes Alluvial-Fan Deposits

"Younger" terraces correspond to the valley floor unit **Qay**, where there has been recent incision by the active channel. However, in some areas, the valley floor is not incised and the same unit is receiving periodic deposition during floods. Because of the dynamic nature of channel incision (e.g., many channels are headward propagating), we have elected to place these younger terraces into **Qay** and **Qfy**.

Qti

Intermediate-age terrace deposits, undivided (late Pleistocene)
Sandy gravel, gravelly sand, and sand underlying intermediate-level terraces whose treads slope parallel to the adjoining drainage. Inferred to correlate to either the Jaral Largo or Matanza formations of Sion et al. (2020) based on relatively weak calcic soil horizon development underlying the surface (mainly Stage II to Stage III carbonate morphologies); however, the relatively far distance of these deposits to the Rio Grande makes specific correlations with the stratigraphy of Sion et al. (2020) uncertain. The deposit is 1–10 m thick.

Qt1

Lower of the intermediate-age terrace deposits (late Pleistocene)
Tabular- to lenticular-bedded sandy gravel and gravelly sand. Correlative to the Jaral Largo formation of Sion et al. (2020). The composition and color of the sediment are dependent on local source areas. Includes axial-fluvial facies similar to unit **Qarg**. The surface has a relatively weak desert varnish and locally vague bar-and-channel topography. The tread height is 3–14 m. The surface soil is characterized by a Stage II calcic horizon (Phillips and Sion, 2022). The deposit is 1–5 m thick. This description is synthesized from Sion et al. (2020, 2021) and Phillips and Sion (2022).

Qt2

Upper of the intermediate-age terrace deposits (late Pleistocene)
Tabular- to lenticular-bedded sandy gravel and gravelly sand. The composition and color of the sediment are dependent on local source areas. Includes axial-fluvial facies similar to unit **Qarg**: very pale-brown to light-brown, medium- to very coarse-grained sand interbedded with beds composed of clast-supported and rounded, sandy cobbles and pebbles of heterolithic composition (volcanic rocks, locally derived Mesozoic to Paleozoic sedimentary clasts, along with extra-basinal clasts of igneous and metamorphic rocks, orthoquartzite, granite, and polished chert); trough-cross stratification is common. The surface may have moderate to strong desert varnish and lacks bar-and-swale topography. The tread height is 18-30 m. The surface soil is characterized by a Stage II+ to Stage III calcic horizon (Phillips and Sion, 2022). The deposit is ≈20–30 m thick. This description is synthesized from Sion et al. (2020, 2021) and Phillips and Sion (2022).

Qto

Older terrace deposits, undivided (middle Pleistocene)
Sandy gravel, gravelly sand, and sand underlying high-level terraces whose treads slope parallel to the adjoining drainage. Inferred to correlate to either the Bowling Green or La Joyita formations of Sion et al. (2020) based on relatively strong calcic soil horizon development underlying the surface (common Stage III+ to Stage IV carbonate morphologies); however, the far distance of these deposits from the Rio Grande makes specific correlations with the stratigraphy of Sion et al. (2020) uncertain. The deposit is 1–10 m thick.

Qt3

Lower of the older terrace deposits (late middle Pleistocene)
Tabular- to lenticular-bedded sandy gravel and gravelly sand. Correlative to the Bowling Green formation of Sion et al. (2020). The composition and color of the sediment are dependent on local source areas. Includes axial-fluvial facies similar to unit **Qarg**: white to pale-brown, pebbly to cobbly sand, and clast-supported gravel containing abundant rounded orthoquartzite, chert pebbles, and igneous and metamorphic extra-basinal clasts. The surface may have moderate to strong desert varnish and lacks bar-and-swale topography. The tread height is ≈25–45 m above the local stream level. The surface soil is characterized by a Stage III to Stage III+ calcic horizon. The deposit is 1–10 m thick. This description is synthesized from Sion et al. (2020, 2021) and Phillips and Sion (2022).

Qt4

Upper of the older terrace deposits (middle Pleistocene)
Tabular- to lenticular-bedded sandy gravel and gravelly sand. Correlative to the La Joyita formation of Sion et al. (2020). The composition and color of the sediment are dependent on local source areas. Includes local axial-fluvial sediment that is mapped in the northern map area and characterized by white to pale-brown, pebbly to cobbly sand and clast-supported gravel. Consists of well-rounded, extra-basinal gravel clasts of igneous and metamorphic rocks, orthoquartzite, and polished chert. The tread height is 60–75 m above the elevation of the Rio Grande and >25 m above local drainages. The surface soil has a Stage III+ calcic horizon. The deposit is 1–10 m thick. This description is synthesized from Sion et al. (2020, 2021) and Phillips and Sion (2022).

Qt4a

Lower subunit of the older terrace deposits (middle Pleistocene)
Deposit as described in unit **Qt4** but underlying a slightly lower geomorphic surface (by 3–6 vertical m) compared to the surface capping **Qt4b**. Correlative to the La Joyita formation of Sion et al. (2020). The deposit is 5–6 m thick. This description is synthesized from Sion et al. (2020, 2021) and Phillips and Sion (2022).

Qt4b

Upper subunit of the older terrace deposits (middle Pleistocene)
Deposit as described in unit **Qt4** but underlying a slightly higher geomorphic surface (by 3–6 vertical m) compared to the surface capping **Qt4a**. Correlative to the La Joyita formation of Sion et al. (2020). The deposit is 5–6 m thick. This description is synthesized from Sion et al. (2020, 2021) and Phillips and Sion (2022).

Deposits Related to Alluvial-Fan Landforms (Includes Alluvial Slopes)

Four items are important to note regarding Pleistocene alluvial-fan deposits. First, most of the deposits underlie surfaces that have alluvial-fan morphologies (e.g., contour lines are convex towards the Rio Grande); however, in a few areas, such as west of Polvadera, the deposits underlie alluvial slopes (e.g., contour lines parallel the Rio Grande). Second, these deposits are near the modern stream gradient on fans located relatively far from the Rio Grande (>10 km). Within 10 km of the modern Rio Grande, dynamic changes in the elevation of the valley bottom, in addition to variable sedimentation flux through time (from both the Rio Grande and its tributaries), have created a set of four geomorphic surfaces commonly associated with four allostratigraphic, inset alluvial-fan units. Differences in relative height of these fan surfaces are most notable near the river, but the surfaces converge away from the river, and correlation of the surfaces and associated allostratigraphic units is more difficult and uncertain. Third, the alluvial-fan deposits interfinger with Rio Grande alluvium (axial-fluvial facies) near the margins of the modern floodplain. In addition, the fan deposits typically prograde over the axial-fluvial facies. This interfingering is depicted on the 1:24,000 geologic maps of the area, but differentiation of the axial-fluvial deposits cannot be shown in most of this study area, due to the smaller map scale. Two allostratigraphic units of axial-fluvial sediment can be differentiated near San Acacia and the towns of Contreras and La Joya. Fourth, we follow the allostratigraphic unit scheme noted by Sion et al. (2020), but for the general reader, label the allostratigraphic units using **Qf1**, **Qf2**, **Qf3**, and **Qf4**. The number following the "**Qf**" denotes the allostratigraphic unit, with **Qf1** being the youngest and **Qf4** being the oldest. Specific correlations with the Sion et al. (2020) formations (corresponding to allostratigraphic units) are noted below.

Qf

Alluvial-fan deposits, undivided (recent to middle Pleistocene)
Alluvium that includes a combination of various younger and older units that cannot be differentiated at 1:100,000 scale. May include the following units: **Qfr**, **Qfyr**, **Qfi**, **Qfo**. See descriptions of those individual units. This combination of deposits is a few to several meters thick.

Qfyr

Younger alluvium with subordinate recent deposits on alluvial fans (recent to latest Pleistocene)
Brownish to reddish sand, silty to clayey sand, and gravelly sand to sandy gravel. Includes subordinate recent alluvium (**Qar**). The overall texture is finer-grained than **Qar** sediment. The gravel consists of pebbles with subordinate cobbles. The composition and color of the sediment are dependent on local source areas. One or more weakly developed buried soils are commonly present (characterized by Stage I calcic horizons). Sand and silty to clayey sand beds are horizontally laminated or massive and contain variable proportions of scattered pebbles. The gravelly beds are lenticular to broadly lenticular or U-shaped. Bar-and-swale topography is lacking or subdued (<10 cm). The surface exhibits somewhat darker tones than found in nearby **Qar** deposits and is weakly varnished. The surface soil is characterized by a weak calcic horizon (Stage I to Stage II) locally capped by a dark, somewhat organic-rich A horizon. Weakly to well-consolidated and non- to poorly cemented. Includes what Sion et al. (2020) map as the Polvadera formation. The deposit is 1–10(?) m thick.

Qfy

Younger alluvial-fan deposits (Holocene to latest Pleistocene)
Brownish to reddish sand, silty to clayey sand, and gravelly sand to sandy gravel. Commonly occupies low terraces. The overall texture is finer-grained than **Qar** sediment. The gravel consists of pebbles with subordinate cobbles. The composition and color of the sediment are dependent on local source areas. One or more weakly developed buried soils are commonly present (characterized by Stage I calcic horizons). Sand and silty to clayey sand beds are horizontally laminated or massive and contain variable proportions of scattered pebbles. The gravelly beds are lenticular to broadly lenticular or U-shaped. Bar-and-swale topography is lacking or subdued (<10 cm). The surface exhibits somewhat darker tones than found in nearby **Qar** deposits and is weakly varnished. The surface soil is characterized by a weak calcic horizon (Stage I to Stage II) locally capped by a dark, somewhat organic-rich A horizon. Weakly

to well-consolidated and non- to poorly cemented. Includes what Sion et al. (2020) map as the Polvadera formation. The deposit is 1–10(?) m thick.

Younger and intermediate-age alluvial-fan deposits with subordinate recent alluvium (recent to late Pleistocene)
A combination of units **Qfy**, **Qfi**, and **Qar** that cannot be differentiated at 1:100,000 scale. See descriptions of those individual units. Correlates to the Polvadera, Jaral Largo, and Matanza formations of Sion et al. (2020). The deposit combination is 1–10(?) m thick.

Younger and intermediate-age alluvial-fan deposits (Holocene to late Pleistocene)
A combination of units **Qfy** and **Qfi** that cannot be differentiated at 1:100,000 scale. See descriptions of those individual units. Correlates to the Polvadera, Jaral Largo, and Matanza formations of Sion et al. (2020). The deposit combination is 1–10(?) m thick.

Intermediate-age alluvial-fan deposits (late Pleistocene)
Sandy gravel, gravelly sand, and sand underlying intermediate-level fan surfaces on alluvial-fan landforms. Inferred to correlate to either the Jaral Largo or Matanza formations of Sion et al. (2020) based on the relatively weak calcic soil horizon underlying the surface (mainly Stage II to Stage III carbonate morphologies); however, the relatively far distance of these deposits to the Rio Grande makes specific correlations with the stratigraphy of Sion et al. (2020) uncertain. See descriptions for **Qf1** and **Qf2**. The deposit is 1–10 m thick.

Intermediate-age and older alluvial-fan deposits (late to middle Pleistocene)
The surficial units on the alluvial fan are a combination of units **Qfi** and **Qfo** that cannot be differentiated at 1:100,000 scale. See descriptions of those individual units. The deposit combination is 1–10 m thick.

Lower of the intermediate-age fan deposits near the Rio Grande (late Pleistocene)
Sandy gravel and gravelly sand; mainly in very thin to medium, tabular to lenticular beds. Correlative to the Jaral Largo formation of Sion et al. (2020). West of the Rio Grande, the gravel is mostly subrounded and mainly composed of a variety of volcanic types. East of the Rio Grande, subangular sedimentary clasts dominate (eroded mainly from Permian–Pennsylvanian formations), with volcanic gravel common near the Joyita Hills. The deposit is correlated to the Jaral Largo formation of Sion et al. (2020). The associated geomorphic surface is characterized by a topsoil with Stage II carbonate morphology (Phillips and Sion, 2022). On aerial imagery, the surface color is relatively gray, compared to older (higher) terrace deposits, and subdued and meter-scale bar-and-channel patterns can commonly be observed in areas with low eolian activity. The geomorphic surface is 29–27 ka (Sion et al., 2020), so the deposit is older. An optically stimulated luminescence age in the lower part returned an age of 68.1 ± 5.8 ka (this work). The tread height above the Rio Grande is 5-15 m. The deposit is 1-8 m thick. This description is synthesized from Sion et al. (2020, 2021) and Phillips and Sion (2022).

Upper of the intermediate-age fan deposits, includes axial-fluvial facies near the Rio Grande (late Pleistocene)
Sandy gravel and gravelly sand; mainly in very thin to medium, tabular to lenticular beds. Correlative to the Matanza formation of Sion et al. (2020). West of the Rio Grande, the gravel is mostly subrounded and mainly composed of a variety of volcanic types. East of the Rio Grande, subangular sedimentary clasts dominate (eroded mainly from Permian–Pennsylvanian formations), with volcanic gravel common near the Joyita Hills. The deposit is correlated to the Matanza formation of Sion et al. (2020). The associated geomorphic surface is characterized by a topsoil with Stage II+ to Stage III carbonate morphology (Phillips and Sion, 2022). Alongside the Rio Grande, the aforementioned gravelly sediment interfingers with axial-fluvial deposits composed of light-brownish-gray, relatively massive and loosely consolidated, fine- to coarse-grained sand that grades east and west into a non-cemented, weakly to moderately consolidated floodplain facies composed of light-brown to brown, very fine- to fine-grained sand, silt, and clay. Because the gravelly fan sediment typically has prograded over the axial-fluvial sediment, mapping the latter is generally not practical at 1:100,000 scale. On aerial imagery, the surface

has a relatively varnished, smooth surface where not buried by eolian sand. The associated geomorphic surface is ca. 70 ka (Sion et al., 2020). Optically stimulated luminescence analyses conducted as part of this mapping returned an age of 125–70 ka, mainly oxygen isotope Stage V (130–70 ka). The tread height is 18-30 m above the Rio Grande. The deposit is ≈6–30 m thick. This description is synthesized from Sion et al. (2020, 2021) and Phillips and Sion (2022).

Qfo

Older alluvial-fan deposits (middle Pleistocene)
Sandy gravel, gravelly sand, and sand associated with relatively higher-level terraces found on obvious alluvial-fan forms. Inferred to correlate to either the Bowling Green or La Joyita formations of Sion et al. (2020) based on a relatively strong petrocalcic horizon (locally Stage III+ or greater carbonate morphology); however, the relatively far distance of these deposits to the Rio Grande makes specific correlations with the stratigraphy of Sion et al. (2020) uncertain. See descriptions for **Qf3** and **Qf4**. The deposit is 1–10 m thick.

Qf3

Lower of the older fan deposits, includes axial-fluvial facies near the Rio Grande (middle Pleistocene)
Sandy gravel and gravelly sand; mainly in very thin to medium, tabular to lenticular beds. West of the Rio Grande, the gravel is mostly subrounded and mainly composed of a variety of volcanic types. Correlative to the Bowling Green formation of Sion et al. (2020). East of the Rio Grande, subangular sedimentary clasts dominate (eroded mainly from Permian–Pennsylvanian formations), with volcanic gravel common near the Joyita Hills. The associated geomorphic surface is characterized by a topsoil with Stage III to Stage IV carbonate morphology (field observations and Phillips and Sion, 2022). Alongside the Rio Grande, the aforementioned gravelly sediment interfingers with axial-fluvial deposits composed of light-brownish-gray, relatively massive and loosely consolidated, fine- to coarse-grained sand that grades east and west into a non-cemented, weakly to moderately consolidated floodplain facies composed of light-brown to brown, very fine- to fine-grained sand, silt, and clay. Because the gravelly fan sediment typically has prograded over the axial-fluvial sediment, mapping the latter is generally not practical at 1:100,000 scale. On aerial imagery, the surface has a relatively varnished, smooth surface where not buried by eolian sand. The surface is ca. 135 ka (Sion et al., 2020) and the deposit age is inferred to be 200–135 ka. The tread height is 35–45 m above the Rio Grande. The deposit is 1–15 m thick. This description is synthesized from Sion et al. (2020, 2021) and Phillips and Sion (2022).

Qf4

Upper of the older fan deposits (middle Pleistocene)
Sandy gravel and gravelly sand; mainly in very thin to medium, tabular to lenticular beds. Correlative to the La Joyita formation of Sion et al. (2020). West of the Rio Grande, the gravel is mostly subrounded and mainly composed of a variety of volcanic types. East of the Rio Grande, subangular sedimentary clasts dominate (eroded mainly from Permian–Pennsylvanian formations), with volcanic gravel common near the Joyita Hills. The deposit fines toward the Rio Grande to a pebbly sand and sand intercalated with 1–10% gravel beds. The associated geomorphic surface is characterized by a topsoil with Stage III+ carbonate morphology (Phillips and Sion, 2022). In many areas, two surfaces are separated by 3-7 vertical m. We assume different deposits (unique allostratigraphic units) underlie the two surfaces, and we designate them as **Qf4a** (lower) and **Qf4b** (upper), and displayed in Figures 19 and 20 of the report. The tread height is 68–82 m above Rio Grande (Sion et al., 2020). The deposit is 1–8 m thick. This description is synthesized from Sion et al. (2020, 2021) and Phillips and Sion (2022).

Qfoa

Older fan alluvium associated with Abo Arroyo (middle Pleistocene)
Alluvial deposits along discrete paths of the Abo drainage after valley entrenchment began. The sediment consists of unconsolidated sand and subangular to subrounded pebbles and cobbles composed of limestone, sandstone, granitic, and metamorphic rock types (indicating derivation from uplands to the east). Rare clasts of rounded, Rio Grande-derived pebbles are reworked from ancestral Rio Grande facies in the upper Sierra Ladrones Formation. The sediment is inset against the Sierra Ladrones Formation. Pedogenic carbonate horizons on the topsoil reach Stage II to Stage III. Subdivided into nine units in Rinehart et al. (2014). The treads are about 30 m above the Abo Arroyo valley floor. The deposit is 3–7 m thick. This description is synthesized from Rinehart et al. (2014).

Qfoh

Older, gravelly fan alluvium at high geomorphic levels (middle Pleistocene)
Lithologically similar to unit **Qfo** and may be of similar age. This unit is mapped mainly in the upper Abo drainage, where gravel clasts range from small pebbles to large boulders. The gravel is derived from the northwestern Chupadera Mesa where it includes clasts eroded from the San Andres Limestone and Glorieta Sandstone. The gravel is derived from the Manzano Mountains where it includes Proterozoic gneiss, schist, and quartzite. Commonly capped by unit **Qs**. Underlies high geomorphic surfaces standing 18–30 m above adjoining, low-order drainages. The deposit is <10 m thick. This description is synthesized from Oviatt (2010).

Mass-Wasting Deposits

Qls

Landslide deposits (late to middle? Pleistocene)
Displaced, deformed, and disrupted Santa Fe Group related to gravity-driven, surficial processes. Particularly common near Socorro Peak. Surface characterized by hummocky topography. Displaced Santa Fe Group is mainly Popotosa Formation clays (**Npp**) that are locally capped by a variety of tilted Neogene volcanic rocks (units **Nsr**, **Nsd**, **Nb**). Includes numerous Toreva-type (rotational) slides, where strata are tilted downward toward the headscarp. Most landslides are relatively stable or inactive. The thickness is uncertain, but perhaps as much as 90 m. This description is synthesized from Chamberlin (1999) and Chamberlin et al. (2001).

BASIN-FILL DEPOSITS EAST OF THE RIO GRANDE RIFT

QNcl

Sand and minor gravel near Claunch (Pleistocene)
Mainly reddish-brown to light-brown-pink, massive, silty to clayey, very fine- to fine-grained sand, and silt to very fine-grained sand. Minor intervals (beds and channel-fills) of sandy gravel to gravelly sand. The gravel is composed of pebbles and variable proportions of cobbles (boulders to the west, near Chupadera fault) that are angular to subangular (minor subrounded) and composed of limestone to dolomite and locally sparse sandstone or volcanic rocks. Reddish-brown to light-reddish-brown to light-brown, fine- to very coarse-grained sand matrix occurs in the gravelly beds that are subrounded to subangular; the fine-grained sand is quartz-rich, and the medium- to very coarse-grained sand contains abundant limestone grains. Weakly consolidated. The deposit is tens of meters to possibly 200 m thick.

QNgs

Gravelly sand in the Trinity and southern Estancia basins (middle Pleistocene to Miocene)
Interbedded sand, gravelly sand, and sandy gravel in tabular to lenticular beds. The gravel consists of angular to subrounded, poorly sorted pebbles, cobbles, and boulders. Clasts are reworked mainly from Glorieta Sandstone and San Andres Limestone, and in the Trinity basin there is trace to 2% granite, chert, and green sandstone. Fine- to very coarse-grained, poorly sorted sand that is composed of quartz with variable sedimentary lithic grains. Variably thick petrocalcic or petrogypsic (in the Trinity basin) horizon developed on the surface. The deposit is 10 m thick in the Trinity basin, and possibly >100 m in the southern Estancia basin.

SANTA FE GROUP SEDIMENTARY DEPOSITS

Ceja Formation

The Ceja Formation was deposited by drainages flowing off of the southeastern Colorado Plateau, including the Rio Puerco and Rio San Jose.

QNc

Ceja Formation (early Pleistocene to latest Miocene?)
Light-brown, very pale-brown, brown, and yellowish-brown sandstone with subordinate mudstone to muddy sandstone and <15% pebbly sandstone-conglomerate. Gravels are composed of chert, quartzite, basalt and intermediate volcanic rocks, minor granite, and minor sedimentary clasts. Sandstone is mostly very fine- to medium-grained. Local paleosols with Stage I to Stage II carbonate morphology. The unit is 100-600(?) m thick. This description is synthesized from McCraw et al. (2006).

Sierra Ladrones Formation of the Santa Fe Group

Open-basin (exorheic) deposits characterized by central axial-fluvial facies flanked on either side by piedmont deposits at the foot of the Quebradas region (to the east) and the Socorro-Lemitar Mountains (to the west). The axial-fluvial deposits are characterized by abundant, light-colored, cross-stratified sand that erodes readily. The piedmont deposits are less red than their counterparts in the underlying Popotosa Formation, and are also poorly to moderately cemented and typically dip less than a few degrees.

QNspw

Western piedmont deposits of the Sierra Ladrones Formation (early Pleistocene to Pliocene)
Reddish-brown to light-brown sandy conglomerate, conglomeratic sandstone, and sandstone underlying the piedmont between the Rio Grande and the Socorro and Lemitar Mountains to the west. The bedding is tabular and lenticular with subordinate irregular to U-shaped channel forms. The gravel is subrounded to subangular, poorly to moderately sorted, and composed predominately of volcanic rock types that include dark-red clasts of jasperoid-cemented (potassium metasomatized) conglomeratic sandstone eroded from the lower Popotosa Formation (**Npc**). North of the Rio Salado, volcanic-dominant gravels grade northward to those composed of limestone and gneiss (derived from Ladron Peak). The gravel size and proportion decrease eastward. Mostly medium- to very coarse-grained volcanic litharenite sand. Buried calcic horizons are common. The unit grades eastward into unit **QNst** and downsection into unit **Nst** and **Nspw**. Weakly to well-consolidated and poorly to moderately cemented. The unit is 240–300 m thick. This description is synthesized from Chamberlin (1999) and Chamberlin et al. (2001).

QNspe

Eastern piedmont deposits of the Sierra Ladrones Formation (early Pleistocene to Pliocene)
Reddish-brown sandy gravel, gravelly sand, and sand underlying the piedmont between the Rio Grande and the Quebradas region. The bedding is tabular and lenticular with subordinate irregular or U-shaped channel forms. The gravel is subangular to subrounded, poorly to moderately sorted, and composed predominately of sedimentary rock types (e.g., limestone, sandstone, siltstone) derived from the erosion of Mesozoic to Paleozoic strata. North of Arroyo de la Parida, near Joyita Hills, the gravel is a mix of sedimentary and volcanic rock types. The gravel size and proportion decrease westward. Mostly medium- to very coarse-grained sedimentary-lithic arenite sand. The unit grades westward into unit **QNst**. Weakly to well-consolidated and poorly to strongly cemented. The unit is >100 m thick. This description is synthesized from Cather et al. (2004) and Cather and Colpitts (2005).

QNst

Transitional unit between the piedmont deposits and axial-fluvial facies of the Sierra Ladrones Formation (early Pleistocene to Pliocene)
Reddish-brown, brown, and light-brown gravel-poor sediment representing the intertonguing axial-fluvial deposits with piedmont deposits. The unit consists of tabular-bedded sandstone, siltstone, mudstone, and <10% conglomeratic sandstone. The tongues of axial-fluvial gravelly sandstone (**QNsa**) contain sparse pebbles of quartzite, chert, limestone, sandstone, granite, and volcanics. Primarily mapped east of the Rio Grande, piedmont gravels (**QNspe**) are derived from the east and are composed of red siltstone, sandstone, and limestone. Where mapped near the city of Socorro, piedmont gravels (**QNspw**) are derived from the west and are composed of subrounded volcanic types. Weakly to well-consolidated and poorly to strongly cemented. The unit is 100–300 m thick and probably thicker on the west side of the axial-fluvial facies. This description is synthesized from Chamberlin (1999) and Chamberlin et al. (2001).

QNsa

QNsa

Axial-fluvial deposits of the Rio Grande of the Sierra Ladrones Formation (early Pleistocene to Pliocene)
Buff-white, light-gray, and very pale-brown sand with minor gravelly sand that is locally well-cemented and minor mudstone. Medium- to coarse-grained sand that is commonly cross-stratified (mostly tangential foresets). The sand is angular to rounded, moderately sorted, and is composed of quartz, vitreous feldspar grains (e.g., sanidine, plagioclase), minor lithic grains (sedimentary rock fragments and chert), and <10% mafic grains. Heterolithic gravels are a mix of felsic to intermediate volcanic rocks, rounded chert, and Mesozoic- to Paleozoic-derived sedimentary clasts, quartzite, granite, and mafic volcanic rocks. Red or greenish-gray, poorly cemented minor mudstone that represents floodplain deposits. Mostly weakly to moderately consolidated and non- to weakly cemented (about 1–15% strong cementation) and erodes readily. The unit is ≈300 m thick. This description is synthesized from Chamberlin (1999) and Chamberlin et al. (2001).

Nspw

Older western piedmont deposits of the Sierra Ladrones Formation (early Pliocene to latest Miocene)
Conglomeratic strata conformably prograding over unit **Nsa**, mapped in the northwest part of the Socorro 30 x 60-minute quadrangle mainly on the footwall of the Loma Blanca fault. The strata consist of conglomerates, conglomeratic sandstones, and sandstones. Mostly clast-supported (locally matrix-supported) conglomerate that is composed of volcanic rocks, limestone, granite, and schist to gneiss. Medium- to very coarse-grained and typically horizontal-planar laminated to cross-bedded sandstone. The unit is >100 m thick. This description is synthesized from Connell and McCraw (2007).

Nst

Older transition and intertonguing zone between the piedmont and axial-fluvial facies of the Sierra Ladrones Formation (early Pliocene to latest Miocene)
Reddish-brown, thinly bedded, very fine- to fine-grained sandy mudstone containing 10- to 20-cm-thick bioturbated zones and less than 30% conglomeratic strata. The unit is mapped in the zone of overlap between the axial-fluvial deposits and the easternmost outcrops of piedmont sandstone and conglomerate. The unit is >15 m thick. This description is synthesized from Chamberlin et al. (2001).

Nsa

Older axial-fluvial deposits of the Rio Grande of the Sierra Ladrones Formation (early Pliocene to latest Miocene)
Light-brownish-gray to pinkish-gray, quartz-rich sandstone and conglomeratic sandstone. Similar to unit **QNsa** but contains less gravel. The gravel has a higher proportion of volcanic clasts than observed in **QNsa** and less extra-basinal gravel (e.g., granite and quartzite). Fine- to coarse-grained and planar to trough cross-bedded sand. The unit is mapped near the Rio Salado and is as much as 200 m thick. This description is synthesized from Chamberlin et al. (2001).

Popotosa Formation of the Santa Fe Group

Closed (endorheic) basin deposits consisting of playa muds near the basin center flanked by conglomeratic piedmont deposits. Playa muds are unique to the Popotosa Formation (in contrast to the Sierra Ladrones Formation). Conglomerates lack reworked clasts of dark-red, jasperoid-cemented (potassium metasomatized) conglomerate. Piedmont deposits are well-consolidated, better cemented, and redder than those of the Sierra Ladrones Formation. Piedmont facies can be divided into a lower red and an overlying gray fanglomerate facies, both predating late Miocene basaltic to dacitic volcanism in the Socorro Peak area (ca. 9.8–9.5 Ma). In situ conglomerates and conglomeratic sandstones near Socorro are commonly red and strongly cemented by jasperoidal silica. The lower part of the Popotosa Formation lacks playa clays, and instead contains abundant conglomeratic, debris-flow deposits derived from local uplifts. The locations and configurations of these uplifts are poorly understood, but presumably, they are fault-bounded, small horsts. The unit was defined by Denny (1940) and redefined by Machette (1978). Popotosa Formation strata underlie the basaltic andesite of Sedillo Hill (7.0 Ma; Chamberlin and Osburn, 2006). The base of the unit appears to be diachronous, becoming younger to the south (basal strata become older to the north). Near the Rio Salado, immediately west of the map boundary, lower Popotosa strata contain rhyolitic ash-fall beds deposited at 14.5 Ma (Cather et al., 1994a). Numerous volcanic flows and tephra provide age control in the upper Miocene part of the section.

Npdp

Fluvio-deltaic sands interbedded with playa clays of the Popotosa Formation (late Miocene)
Reddish-brown playa clays (as described in unit **Npp**) interbedded with tongues of tan to light-brown, very fine (lower)- to medium (lower)-grained sand. Subrounded to subangular, well-sorted, non- to weakly cemented sand that is composed of quartz, plagioclase, and sanidine with 1–5% orange grains composed of potassium feldspar, orange quartz, and orange chert. Commonly finely interlaminated with clay or clayey fine-grained sand (horizontal-planar to cross-stratified). This quartzo-feldspathic sand is interpreted as Rio Grande fluvio-deltaic lobes that extended southward across the Socorro basin playa. The unit is 200–250 m thick. This description is synthesized from Chamberlin (1999) and Chamberlin et al. (2001).

Npu

Upper Popotosa Formation (late Miocene)
Interbedded playa and easterly or westerly derived piedmont facies (**Npc** and **Npe**) that lie above the dacite member of the Socorro Peak Rhyolite and locally include tongues of the Socorro Peak Rhyolite. The unit is mapped west of the Dicaperl Minerals perlite mine and includes the perlitic sedimentary

apron surrounding the rhyolite dome and easterly derived piedmont sediment (described in **Npe**). The unit is 30–40 m thick.

Npp

Playa deposits of the Popotosa Formation (late to middle Miocene)
Reddish-brown mudstone and claystone with minor greenish clays; local thin, tan to light-gray tongues of siltstones to fine-grained sandstones. Thin beds of gypsum and selenite veinlets are found in the lower part of the unit north of the city of Socorro. To the north-northwest, the mudstones to claystones become increasingly interbedded with tan-colored, conglomeratic sandstones (**Npf**). Playa deposits are capped by the 7.0 Ma trachyandesite of Sedillo Hill. The unit is 390–750 m thick. This description is synthesized from Chamberlin (1999) and Chamberlin et al. (2001).

Npf

Upper alluvial-fan and fan-delta conglomeratic sands of the Popotosa Formation (late Miocene)
Pale-brownish-yellow (buff), conglomeratic sandstones. Mainly very thin to medium, tabular to lenticular beds of sandstone, pebbly sandstone, and sandy conglomerate. Locally, these beds exhibit low- to high-angle internal cross-stratification or horizontal-planar lamination. Composed of very fine- to very coarse-sized pebbles with minor fine- to coarse-sized cobbles. Subrounded, poorly to moderately sorted gravel that is composed of about subequal (±20%) felsic vs. intermediate volcanic rocks. Felsic rocks include identifiable regional ignimbrites (e.g., Vicks Peak, upper Lemitar, and Hells Mesa Tuffs). Mainly medium- to very coarse-grained sand in gravel beds that contains ≈25–30% volcanic lithics and ≈5% orange grains (including potassium feldspar). The gravel locally contains sparse to moderately abundant, subrounded clasts of hydrothermally altered, crystal-poor rhyolites (altered to a yellowish-brown to gray and speckled with small dots of yellow-brown goethite). The gravel is associated with southeasterly paleocurrent indicators. Brown to light-gray, very fine- to medium (lower)-grained, subangular to subrounded, and well-sorted sand occurs in the interfingering zone with the playa muds. The sand in this zone is composed of feldspar and quartz, 5–15% lithic grains, and up to 10% orange grains dominated by potassium feldspar. Detrital sanidine ages are consistent with a source area corresponding to much of the modern Rio Salado (D. Koning and M. Heizler, unpublished data). The unit intertongues with the lower to middle part of **Npp**. The unit is up to ≈450 m thick at Cañoncito del Lemitar. This description is synthesized from Chamberlin (1999) and Chamberlin et al. (2001).

Npe

Upper easterly derived piedmont deposits of the Popotosa Formation (late to middle Miocene)
The unit is mapped in the western margin of the Quebradas. Conglomeratic sandstones that include mostly clast-supported and poorly sorted conglomerates and medium- to very coarse-grained and horizontal-planar laminated to cross-bedded sandstones. The unit is present near the Dicaperl Minerals perlite mine, but it is subsumed into **Npu** at that location. At this location, this unit is composed of pale-reddish-orange to pale-red conglomeratic sandstones. Volcanic clasts are dominant in the gravel fraction, with sparse pebbles of Permian-derived, red siltstones and very fine- to fine-grained sandstones. Near the Dicaperl Minerals perlite mine, the unit overlies 7.9 Ma tuffs and intertongues with (1) gray, perlitic sandstones shed off the lava dome (**Npsr**) associated with the Dicaperl Minerals perlite mine, and (2) reddish-brown, playa claystones. The unit is >100 m thick. This description is synthesized from Chamberlin (1999), Chamberlin et al. (2001), and Cather and Colpitts (2005).

Npt

Npt

Transitional facies between distal piedmont and playa paleoenvironments of the Popotosa Formation (late to middle Miocene)
Approximately subequal reddish-brown mudstone vs. volcaniclastic sandstone. The unit is mapped near San Lorenzo Canyon and the Rio Salado. This description is synthesized from Chamberlin et al. (2001).

Npx

Fanglomerate derived from the Ladron Mountains of the Popotosa Formation (late? to middle Miocene)
Light-gray to light-brown, subangular fanglomerate interbedded with sandstone. The gravels are predominately composed of Pennsylvanian and Proterozoic rocks of the Ladron Mountains. Tertiary volcanic clasts become more abundant downsection. Inferred to grade laterally into unit **Npc**. Overlies playa beds of **Npp**. The unit is 60 m thick. This description is synthesized from Machette (1978).

Npl

Lower Popotosa Formation (middle Miocene)
Cross section only. Conglomerates, sandstones, and possibly mudstones that lie below units **Npf** and **Npp**. The upper part is probably of mixed provenance and correlative to **Npcs**, **Npss**, **Npc**, and possibly **Npp**; the unit grades downsection into locally sourced sediments correlative to **Npb**. Likely well-consolidated and relatively well-cemented. The unit is 700–750(?) m thick.

Npcs

Conglomeratic strata, at and near San Lorenzo Canyon, of the Popotosa Formation (middle Miocene)
Conglomeratic sandstone, sandstone, and conglomerate that grade/interfinger westward into a basin-floor facies (**Npss**). Moderately to well-cemented strata. Reddish mudstone beds are present near this interfingering contact. The gravel is derived from the erosion of Tertiary volcanic rocks. The unit extends northward to the eastern side of Cerritos de Las Minas, where it dips under the thick playa deposits near the Rio Salado (unit **Npp**). This description is synthesized from Chamberlin et al. (2001).

Npss

Sandstone and minor mudstone, at San Lorenzo Canyon, of the Popotosa Formation (middle Miocene)
Sandstone-dominated volcaniclastic deposits that contain subordinate to very sparse pebbly sandstone and locally subequal to subordinate reddish mudstone. Deposited on a northwest-sloping basin floor and the lateral, eastward transition from the basin floor to the adjoining distal, west-sloping piedmont slope. This description is synthesized from Chamberlin et al. (2001).

Npc

Lower conglomeratic piedmont deposits of the Popotosa Formation (middle Miocene)
Conglomeratic sandstone, sandstone, and conglomerate (or fanglomerate) derived mainly from the erosion of Tertiary volcanic rocks, namely the Luis Lopez Formation (**Pez**, andesite to rhyolite lavas) and regional tuffs (mostly South Canyon, Lemitar, and Hells Mesa Tuffs). The lower part of the unit is commonly composed of well-indurated, reddish-brown to dark-red, conglomeratic strata. The strong cementation and color are due to jasperoidal silica cements associated with potassium metasomatism of late Miocene age (Dunbar et al., 1994; Chamberlin and Eggleston, 1996; Dunbar and Miggins, 1996). Clast compositions and imbrications generally indicate a northerly transport direction in the reddened strata. These reddened strata locally grade upward into buff to gray conglomeratic sandstones or are disconformably overlain by these sandstones. On the east face of Socorro Peak, the metasomatized strata locally interfinger with gray, non-altered conglomeratic strata. The grayish conglomerates locally include light-purplish-gray sandstones and mudstones; in the gravel fraction, clasts of light-gray, crystal-poor ignimbrites and purplish basaltic andesites are dominant, and clast imbrications indicate northwesterly paleocurrents. The unit is 0–300 m thick. Except where noted, this description is synthesized from Chamberlin (1999) and Chamberlin et al. (2001).

Npb

Lower piedmont facies and basal debris flows, includes the South Canyon Tuff and Luis Lopez Formation near the base, of the Popotosa Formation (middle to early Miocene)
As in unit **Npc**, but the lower part includes reddish-brown, well-indurated, boulder-bearing, conglomeratic debris-flow deposits. Relatively monolithic. The gravel composition reflects first-cycle erosion of the upper part of the Oligocene-age volcanic sequence. This unit includes the upper andesites and rhyolites of the Luis Lopez Formation (**Pez**) and South Canyon Tuff (**Pmu**) near the base at the eastern foot of Socorro Peak. The unit is 150–300 m thick. This description is synthesized from Chamberlin (1999) and Chamberlin et al. (2001).

NEOGENE VOLCANIC ROCKS

Pliocene Basaltic to Andesitic Rocks of the Santa Fe Group

Nb

Basaltic rocks of the Santa Fe Group (middle Pliocene)
Includes basalts that cap Black Mesa and Mesa Redonda and the basalt of Socorro Canyon.

The **basalt of Black Mesa and Mesa Redonda** is a dark- to very dark-gray or nearly black, aphanitic, very fine- to fine-grained olivine basalt. This basalt forms ledges capping Mesa Redonda and Black Mesa in the south-central part of the map area. Phenocrysts include 2–5% olivine (fine-grained, anhedral to subhedral, occasionally glomerophyric) and 1–3% pyroxene (fine-grained, anhedral, commonly weathered). Dense to somewhat vesicular with a few amygdules filled by zeolites or calcite. Occasionally

exhibits platy to brecciated textures. The composite thickness of two to three flows is 15–30 m. This basalt has an $^{40}Ar/^{39}Ar$ age of 3.652 ± 0.014 Ma from Redonda Mesa.

The **basalt of Socorro Canyon** is a dark-gray, massive to vesicular, olivine basalt flow. Lava contains 1–2% phenocrysts of olivine (1–2 mm) and sparse to rare glomerophenocrysts of plagioclase. Lava flowed down an easterly paleoslope of ancestral Socorro/Six Mile Canyon and is down-faulted into the subsurface east of the Socorro Canyon fault zone. This basalt has an $^{40}Ar/^{39}Ar$ age of 3.75 ± 0.1 Ma. The basalt of Socorro Canyon's average thickness is 6–9 m.

The combined unit is 6–30 m thick. This description is synthesized from Chamberlin (1999) and Cather and Koning (2024).

Nta

Trachyandesite of San Acacia of the Santa Fe Group (early Pliocene)
Medium-gray to light-brownish-gray, phenocryst-poor, xenocrystic, trachyandesite flow near San Acacia. Contains 1–2% phenocrysts of plagioclase, greenish augite, and very fine-grained, reddish-brown iddingsite. The unit also has traces of xenocrystic quartz, rimmed with clinopyroxene, and sparse phenocrysts of hornblende. The lava was inferred to have erupted from a north-trending fissure vent near San Acacia dam (Machette, 1978). It appears to be disconformably overlapped by **QNsa** and **QNst** north of Bowling Green. The unit has an age of 4.79 Ma (Chamberlin et al., 2001; age converted using the Fish Canyon standard of 28.201 Ma per Kuiper et al., 2008). The maximum thickness is 40 m and thins to the south. This description is synthesized from Chamberlin et al. (2001).

Socorro Peak Rhyolite of the Santa Fe Group

A cluster of felsic lava domes centered near Socorro Peak (Osburn and Chapin, 1983). Individual domes vary in composition, from hornblende dacite (69–70% SiO2) to hornblende-biotite rhyodacite (70–73% SiO2) to high silica-rhyolite (75–77%) (Bobrow, 1984; Bobrow et al., 1983). Both the flows and associated eruptive tuffs are interbedded in the Popotosa Formation.

Nsr

Rhyolite member of the Socorro Peak Rhyolite of the Santa Fe Group (late Miocene)
Various flow-banded rhyolite domes near Socorro Peak (described from youngest to oldest):

The **domes 2-4 km southwest of Socorro Peak** are a light-gray to light-brownish-gray to pinkish-gray, flow-banded, low-silica rhyolite containing ≈15% medium-grained phenocrysts of plagioclase, sanidine, and biotite with minor quartz. This rhyolite has an $^{40}Ar/^{39}Ar$ age range from 8.8 to 7.0 Ma (Chamberlin, 1999; D.J. Koning and M. Heizler, unpublished detrital sanidine $^{40}Ar/^{39}Ar$ data).

The **rhyolite lava dome at the Dicaperl Minerals perlite mine** is a light-gray, glassy, flow-banded, high-silica rhyolite lava (76–77% SiO2) forming a dome ≈1 km across and is currently being mined. This dome has a glassy core >90 m thick; a granophyric felsite zone is present on its northeast flank. The rhyolite contains <1% fine-grained phenocrysts of sanidine and plagioclase with traces of quartz and biotite. The original microvesicular, obsidian lava has been uniformly altered by hydration to a commercial-quality perlite (Barker et al., 1994). This rhyolite has an $^{40}Ar/^{39}Ar$ age of 7.90 ± 0.03 Ma.

The **rhyolite lava dome at Signal Flag Hill** is a light-gray to light-brownish-gray to pale-red, flow-banded, high-silica rhyolite lava (75–76% SiO2). It contains 15–20% medium-grained phenocrysts of sanidine, plagioclase, and quartz, along with minor biotite. It was inferred to have erupted from a north-trending fissure vent. This rhyolite has an $^{40}Ar/^{39}Ar$ age of 8.71 ± 0.05 Ma (Chamberlin, 1999).

Nsd

Dacite and rhyodacite member of the Socorro Peak Rhyolite of the Santa Fe Group (late Miocene)
Light- to medium-gray to pale-red to reddish-brown, porphyritic, dacitic to rhyodacitic lavas. Contains ≈10% fine- to medium-grained phenocrysts of plagioclase and minor to subequal hornblende ± biotite. Dacite lava domes and associated shallow necks are in two north-northwest-trending belts; lavas extending away from this linear belt form flat-topped "tortas." The unit has an inferred age of 9.7 Ma. Rhyodacites have an $^{40}Ar/^{39}Ar$ age of 9.57 ± 0.06 Ma and are locally underlain by rhyodacitic tephra, and

abutt the western margin of the dacitic lavas. Individual flows average 60–120 m thick, with a range of 0–120 m. This description is synthesized from Chamberlin (1999).

OLIGOCENE TO EOCENE INTRUSIVE ROCKS

Pɛi

Intrusive rocks of intermediate to mafic composition (late? Oligocene to late Eocene)
Whitish to very light- to medium-gray, weathering to medium- or dark-gray, non-vesicular, massive, aphanitic to phaneritic, monzonite to intermediate to mafic rocks occurring as dikes and sills intruding Permian strata, primarily the Torres Member of the Los Vallos Formation (**Pyv**). Sills are also present in the Glorieta Sandstone (in fine-grained, medial interval), and east to east-northeast dikes crosscut the San Andres Formation on Chupadera Mesa. Spheroidal weathering is common. Where phaneritic, phenocrysts include plagioclase (subhedral), hornblende (subhedral to euhedral prisms, locally >10 mm long), minor biotite, and trace quartz. Locally, two feldspar types are present. Bates et al. (1947) noted the presence of orthoclase, pyroxene, and magnetite in some samples. Hornblende and biotite are commonly altered to greenish or yellowish, powdery secondary minerals. Aphanitic margins contain trace to 1% very fine, equant phenocrysts, inferred to be biotite based on their shape and luster, and they feature occasional to common splotches of very pale-green grainy alteration minerals forming diffuse boundaries with the groundmass. Aphanitic to fine-grained intrusions are dark-gray and contain <1-mm-long crystals of plagioclase and subordinate mafic grains (mostly amphibole). Some dikes contain occasional xenoliths of mafic material up to 7 cm in diameter with subequal plagioclase and pyroxene phenocrysts and rare biotite. Whole-rock geochemistry indicates a monzonitic composition (55.2–55.7 wt% SiO2, 8.3–8.8% Na2O + K2O). Aldrich et al. (1986) obtained a K/Ar age of 30.2 ± 2.0 Ma from one of these dikes. Dikes may be up to 160 m wide but are more commonly 45–75 m wide. Except where noted, this description is synthesized from Aby and Jochems (2022) and Jochems and Aby (2024).

Pɛir

Rhyolitic intrusive rocks (late? to early Oligocene)
Light-gray to pale-reddish-gray, flow-banded rhyolite occurring as plugs or dikes that intrude Spears Group (Cather et al., 1994b) strata on the east side of the Joyita Hills. The unit contains 5–15% phenocrysts that are fine- to medium-grained (1–4 mm) and composed of plagioclase, sanidine, biotite, and quartz. Hydrothermally altered except near dike margins. Flow folds and lineations indicate vertical to subhorizontal flow paths along dike margins. K/Ar age of 31.3 ± 1.2 Ma (Aldrich et al., 1986); the youngest unit is cross-cut by a rhyolite intrusion is the 32.35 Ma Hells Mesa Tuff. Except where noted, this description is synthesized from Allen et al. (2013).

Pɛim

Mafic intrusive rocks, occurring as sills (Oligocene to late Eocene)
Medium-gray, locally mottled to various shades of gray igneous rocks that contain ≈5% black pyroxene (0.5–1 mm) in a felted matrix of plagioclase microlites. Occurs as sills 5–10 km east of the Joyita Hills, where they intrude the Yeso Group, Baca Formation, and Cretaceous strata. The unit is 1–100 m thick. This description is synthesized from Allen et al. (2013).

PALEOGENE VOLCANIC ROCKS

Pɛva

Andesite at Cerritos de las Minas (late Oligocene)
Medium-gray or light-gray, weathering (oxidized) to reddish-brown, andesite flows that commonly have autobrecciated tops and bases. The lavas are fine to medium-grained and slightly porphyritic. Sparse andesitic sandstone and pebbly sandstone are present. Subangular, monolithic explosion breccias are interbedded with sparse debris flows. The unit is >45 m thick. This description is synthesized from Machette (1978).

Pɛmld

Combined lower Mogollon Group and Datil Group (early Oligocene to late Eocene)
Combined lower Mogollon Group and Datil Group for display at 1:100,000. See individual descriptions of **Pɛml** and **Pɛd**. Mapped locally in the Joyita Hills.

Pɛmds

Combined Mogollon Group, Datil Group, and Spears Group (late Oligocene to late Eocene)
Combined lower Mogollon Group, Datil Group, and Spears Group for display at 1:100,000. See individual descriptions of **Pɛds**, **Pɛml**, and **Pɛs**. Mapped mainly in Lemitar Mountains, where it includes the Spears

Group (Tes) and the tuff of Granite Mountain, Hells Mesa Tuff, Luis Lopez Formation, La Jencia Tuff, and Vicks Peak Tuff. At the north end of the Joyita Hills, the unit includes strata between the Vicks Peak Tuff and the lower Spears Group. The unit is 400–500 m thick.

Mogollon Group

Telp

La Jara Peak Basaltic Andesites (late Oligocene to late Eocene)
Medium-gray, purplish-gray to grayish-red-purple basaltic andesite tongues intercalated with the South Canyon, Lemitar, and Vicks Peak Tuffs. Individual tongues are commonly 30–300 m thick and composed of tens of flows, each about 3–10 m thick. The lava is massive to vesicular and contains 5–10% fine-grained phenocrysts of olivine altered to reddish-brown iddingsite, along with minor pyroxene phenocrysts. Phenocrystic plagioclase is absent or very sparse west of the Rio Grande, but the unit (as mapped) locally includes plagioclase phenocrysts east of the Rio Grande. Wedge-shaped geometries in the Lemitar Mountains indicate that the basaltic andesites were concomitant with early extension and domino-style block rotation. This description is synthesized from Chamberlin et al. (2001), de Moor et al (2005), Cather et al. (2014), and Cather and Koning (2024).

Temu

Upper Mogollon Group (late Oligocene)
Upper strata of the Mogollon Group. The unit includes (listed youngest to oldest) the South Canyon Tuff, which caps the La Jara Peak basaltic andesite flows that intertongue with the Lemitar Tuff and other Oligocene ignimbrite flows.

The **South Canyon Tuff** is a light-gray to pale-grayish-red to light-purple, pumiceous, densely welded, rhyolitic ignimbrite with common lithic fragments. Phenocryst content increases upsection from ≈5% in the ≈30-m-thick, partially welded base to ≈25% near the densely welded top. Phenocrysts are 1–3 mm and composed of subequal quartz and sanidine (commonly chatoyant). The tuff is lithic poor except near the base and in the Joyita Hills where lithics are 5–15% pumice (1–5 cm). The unit has an $^{40}Ar/^{39}Ar$ age of 27.67 ± 0.01 Ma (Cather and Koning, 2024) and is sourced from the Mount Withington caldera (northern San Mateo Mountains; Ferguson, 1991). The unit is up to 90 m thick.

The **La Jara Peak flows** consist of medium-gray, purplish-gray, to grayish-red-purple basaltic andesite tongues intercalated with the South Canyon, Lemitar, and Vicks Peak Tuffs. Individual tongues are commonly 30–300 m thick and composed of tens of flows, each about 3–10 m thick. The lava is massive to vesicular and contains 5–10% fine-grained phenocrysts of olivine altered to reddish-brown iddingsite, along with minor pyroxene phenocrysts. Phenocrystic plagioclase is absent or very sparse west of the Rio Grande, but the unit (as mapped) locally includes plagioclase phenocrysts east of the Rio Grande. Wedge-shaped geometries in the Lemitar Mountains indicate that the basaltic andesites were concomitant with early extension and domino-style block rotation.

The **Lemitar Tuff** is an ignimbrite containing a phenocryst-poor (5–15%, increasing upsection), and light-gray lower member and a densely welded, pink to dark-red, phenocryst-rich (30–45%) dacitic to rhyolitic upper member. Phenocrysts are 1–4 mm and include quartz, sanidine, plagioclase (locally altered), and biotite (trace augite and sphene). Lithics are minor. A phenocryst-poor pumice is found in the lower member (3–5%). Sparse, phenocryst-rich pumice and small (<2 cm), grayish-red "magma blobs" of dacite occur in the upper member. The unit has an $^{40}Ar/^{39}Ar$ age of 28.24 ± 0.01 Ma (Cather and Koning, 2024) and is sourced from the Hardy Ridge caldera in the southwestern Magdalena Mountains (Ferguson et al., 2012). The unit filled wedge-shaped paleovalleys and is up to 60–90 m thick.

The upper Mogollon Group is ≈500 m thick. This description is synthesized from Chamberlin et al. (2001), de Moor et al (2005), Cather et al. (2014), and Cather and Koning (2024).

Teml

Lower Mogollon Group (early Oligocene)
Lower strata of the Mogollon Group. Unit includes (listed youngest to oldest) the Vicks Peak Tuff, La Jencia Tuff, and the tuffs of the Luis Lopez Formation.

The **Vicks Peak Tuff** is light-gray to pale-red, phenocryst-poor, densely welded rhyolitic ignimbrite. Contains 1–5% phenocrysts of sanidine and sparse quartz. Exhibits a lithophysal zone near the base and large pumice lapilli (up to 30 cm long) near the top. The unit has an $^{40}Ar/^{39}Ar$ age of 28.77 ± 0.01 Ma and is sourced from the Nogal Canyon caldera in the southern San Mateo Mountains (Osburn and Chapin, 1983). Up to 75 m thick.

The **tuffs of the Luis Lopez Formation** are light-brownish-gray to light-gray, poorly welded, pumiceous, rhyolitic ignimbrites primarily representing fallout deposition. Contains moderately abundant pumice (mostly aphyric) and sparse to moderately abundant, small lithic fragments (andesite, Hells Mesa Tuff) in a fine-grained matrix. Crystals are mostly sanidine, quartz, and plagioclase. There are two main tuffs: medial, with an $^{40}Ar/^{39}Ar$ age of 30.43 ± 0.1 Ma (Chamberlin et al., 2004), and upper, with an age of 29.00–29.03 Ma. The unit is up to 60 m thick.

The **La Jencia Tuff** is a light-gray to grayish-red, phenocryst-poor, rhyolitic ignimbrite. It contains 3–5% phenocrysts of sanidine and quartz with traces of plagioclase and biotite. The tuff exhibits a distinctive, very densely welded, rheomorphic (flow-banded) zone in its middle part that grades upward and downward to a eutaxitic ignimbrite. The unit has an $^{40}Ar/^{39}Ar$ age of 29.00 ± 0.01 Ma and is sourced from the Sawmill-Magdalena caldera in the Magdalena Mountains (Osburn and Chapin, 1983). As much as 120 m thick in the eastern Lemitar Mountains.

Except where noted, ages are from Cather and Koning (2024). The lower Mogollon Group is ≈200 m thick. Except where noted, this description was synthesized from Chamberlin et al. (2001) and Cather and Koning (2024).

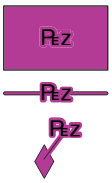

Luis Lopez Formation (early Oligocene)
Sedimentary rocks, volcanic flows, and rhyolitic tuffs that backfill the earlier (32.35 Ma) Socorro caldera; tuffs that extend beyond the caldera and are included in **Peml**. Sedimentary rocks are mainly derived from the erosion of the caldera wall. Lava flows range from mafic to intermediate to felsic. Away from the Socorro caldera there are light-brownish-gray to light-gray, poorly welded, pumiceous, rhyolitic ignimbrite tuffs primarily representing fallout depostion; this tuff contains variable (up to 50%) pebble- to cobble-sized, rounded to angular, lithic fragments of andesite lavas and variable Hells Mesa Tuff; sparse crystals of sanidine, quartz, plagioclase, and biotite in the fine-grained matrix are primary (lower part) to xenocrystic (upper part). In the Joyita Hills, the tuff is crystal poor, pumiceous, moderately to poorly welded, and contains sparse to abundant lithic clasts. There are two main tuffs: medial, with an $^{40}Ar/^{39}Ar$ age of 30.43 ± 0.1 Ma (Chamberlin et al., 2004), and upper, with an age of 29.00–29.03 Ma. The tuffs are up to 60 m thick. Primarily in the caldera south of Socorro Peak, the unit includes an upper rhyolite member and an upper andesite member. The upper rhyolite consists of flow-banded rhyolite lava domes and cogenetic, bedded tuffs; these are phenocryst-poor to moderately phenocryst-rich tuffs and contain 5–25% pearly sanidine, altered plagioclase, quartz, and traces of biotite. The upper andesite includes a dark-purplish-gray, gray, and reddish-brown andesite lava, flow breccia, and near-vent cinder deposit. The medium-grained (1-3 mm) andesite contains 5–20% phenocrysts of altered plagioclase and pyroxene, is massive to platey, locally vesicular, and the upper part of the unit has 5- to 15-mm-long plagioclase phenocrysts. The age is 30–29 Ma. Generally, the unit is 0-60 m thick outside of the caldera and up to 700 m thick within the caldera. Except where noted, this description is synthesized from Chamberlin (1999), Chamberlin et al. (2001), de Moor et al (2005), Cather et al. (2004), and Cather and Koning (2024).

Datil and Spears Groups

Ped

Datil Group (earliest Oligocene to late Eocene)
Lava flows and ignimbrites that include and lie below the Hells Mesa Tuff. The lavas and ignimbrites are volumetrically minor in the map area compared to the Spears Group. At La Joya, the Joyita Hills include the following units: the La Jara Peak Basaltic Andesites (**Pelp**), the upper Spears Group of Cather and Koning (2024), and the tuff of Arroyo Veranito (Chamberlin et al., 2022a). At the Blackington Hills is the following ascending stratigraphic sequence: the Datil Well Tuff, the Rock House Canyon Tuff, an informal dacite flow, the Hells Mesa Tuff, and the upper Spears Group.

There, the **Datil Well Tuff** is a medium-brownish-gray, crystal-rich, rhyolitic ignimbrite 0–50 m thick; its phenocrysts are composed mostly of sanidine with subordinate plagioclase and lesser quartz, biotite, and pyroxene(?). The unit has $^{40}Ar/^{39}Ar$ sanidine ages of 35.32 ± 0.02 Ma to 35.38 ± 0.01 Ma.

The **Rock House Canyon Tuff** is a light-gray, poorly to moderately welded, crystal-poor, rhyolitic ignimbrite. The phenocrysts are mostly sanidine with rare quartz, biotite, and hornblende(?). The unit has an $^{40}Ar/^{39}Ar$ sanidine age of 34.78 ± 0.01 Ma. The Rock House Canyon Tuff is 90–150 m thick.

The mapped **dacite flow near the Blackington Hills** is brownish-gray with plagioclase and amphibole phenocrysts. The unit has an $^{40}Ar/^{39}Ar$ age of 34.0 Ma. The dacite is up to 90 m thick.

The H**ells Mesa Tuff** is found across the western map area and is a reddish-brown to purplish-gray, densely welded, phenocryst- and quartz-rich, rhyolitic ignimbrite. It has 40–50% phenocrysts that are typically 1–3 mm and composed of sanidine, plagioclase, quartz, and minor biotite. The tuff has an $^{40}Ar/^{39}Ar$ age of 32.35 ± 0.01 Ma. In the Lemitar Mountains, the lower part of Hells Mesa Tuff is a light-gray to grayish-red to light-brownish-gray, non-welded to densely welded, moderately pumiceous, quartz-poor ignimbrite that contains 35–45% phenocrysts composed of plagioclase (commonly replaced by adularia) with minor biotite, sanidine, altered hornblende, and clinopyroxene(?). The lower part of the tuff is a 30–60 m-thick.

All $^{40}Ar/^{39}Ar$ ages from Cather and Koning (2024). Except where noted, this description is synthesized from Chamberlin et al. (2001), Cather et al. (2004), de Moor et al. (2005), Cather et al. (2014), and Cather and Koning (2024).

Tds

Datil and Spears Groups (earliest Oligocene to late Eocene)
Lava flows (including the flows of La Jara Peak) and ignimbrites below and including the Hells Mesa Tuff, which overlie and intertongue with Spears Group. The ignimbrites include the Datil Well and Rockhouse Canyon Tuffs and the tuff of Arroyo Veranito. The Hells Mesa Tuff contains phenocrysts of sanidine, plagioclase, quartz, and minor biotite. See descriptions for units **Ted** and **Tes**. This description is synthesized from Chamberlin et al. (2001), Cather et al. (2004), de Moor et al. (2005), Cather et al. (2014), and Cather and Koning (2024).

EARLY OLIGOCENE TO EOCENE SEDIMENTARY DEPOSITS

Ts

Spears Group (early Oligocene to late Eocene)
In the Lemitar Mountains and Joyita Hills, this unit consists of grayish-red, grayish-red-purple, light-brownish-gray, and light-gray conglomerates, sandstones, siltstones, and reddish-mudstones derived from intermediate-composition volcanic highlands located primarily to the southwest. The conglomeratic beds are lenticular to tabular and usually 1–3 m thick. The gravels range in size from boulders to pebbles, are subrounded to subangular, and are composed of andesites (plagioclase and pyroxene phenocrysts) and dacites (plagioclase, hornblende, and biotite phenocrysts). In the lower ≈30 m of the unit, these volcanic clasts are mixed with gray micritic limestone and red siltstone to very fine-grained sandstone cobbles and pebbles derived from Paleozoic rocks. Medium-grained pyroxene monzonite and dark-gray, aphanitic basaltic andesite clasts occur sparsely in the upper half of the formation in the Lemitar Mountains. Calcite and pinkish clays are the dominant cements; chalcedonic quartz is relatively rare. The age range from K/Ar dates of volcanic clasts and interbedded tuffs is approximately 39–33 Ma (Osburn and Chapin, 1983). Locally, this unit grades uncomformable into and includes relatively narrow outcrops of the underlying Baca Formation (≈25 m thick) near Polvadera Peak. The unit ranges from 120–330 m thick and appears to thicken rapidly to the north on the downside of an east-northeast-striking, high-angle fault exposed about 2 km south of Polvadera Mountain. In the Quebradas region, the Spears Group consists of a lower unit that is ≈760 m thick and an upper unit that is 0–120 m thick. The lower unit is composed of medium- to light-gray, volcaniclastic sandstone, conglomerate, debris-flow breccia, and minor muddy sandstone to mudstone. Clasts are dominated by plagioclase- and amphibole-bearing andesite to dacite. The lower part grades downward into the Baca Formation. The upper Spears Group in the Quebradas area consists of dark- to medium-gray, volcaniclastic sandstone

and conglomerate with local debris flows. Clasts are mostly basaltic andesite (plagioclase- and pyroxene-phyric) and andesite to dacite with plagioclase and amphibole phenocrysts. The unit is 120–330 m thick near Polvadera Peak and 700–800 m thick east of the Rio Grande. This description is synthesized from Chamberlin et al. (2001), deMoor et al. (2005), Cather et al. (2014), and Cather and Koning (2024).

Pb

Baca Formation (middle Eocene)
Grayish- to reddish-brown, limestone- and sandstone-clast conglomerates and conglomeratic sandstones. On the west side of the Rio Grande, trough- and tabular-bedded conglomerates appear to fill a paleovalley cut into the underlying Madera Group (Pennsylvanian) about 2 km south of Polvadera Mountain. These rocks are also present near Corkscrew Canyon (southern Lemitar Mountains). The unit is 0–30 m thick in the Lemitar Mountains. In the Quebradas region, this unit consists of sandstone, conglomerate, and minor reddish mudstone. The sandstone is commonly cross-bedded and subarkosic. The conglomerate consists of pebbles, cobbles, and boulders composed of Proterozoic lithoty¬¬pes (granites, gneissic granite, schist, and quartzite) and Paleozoic lithotypes (limestone, sandstone, and siltstone). In the northern Quebradas region, there are intervals containing clasts of well-rounded quartzite and metavolcanics from Proterozoic rocks. The unit is ≈300 m thick in the Quebradas region. This description is synthesized from Chamberlin et al. (2001) and Cather and Koning (2024).

MESOZOIC SEDIMENTARY ROCKS

KdTr

Dakota Sandstone capping Triassic strata (Late Cretaceous and Late to Middle Triassic)
See descriptions of the Dakota Sandstone (Kl) and Triassic strata (Tr); these units were combined for the purposes of mapping at 1:100,000 scale.

K

Cretaceous strata, undivided (Coniacian to Cenomanian, possibly as young as Santonian?)
Yellowish to tan-colored shales, siltstones, and sandstones that were deposited during three major transgressive-regressive cycles (see Hook [1983] and Hook et al. [2012] for summary papers). The marine strata include fossiliferous shales (commonly fissile), very fine- to fine-grained sandstones, and very minor limestones. The sandstones weather to pale-gray to yellowish to brownish-gray. The terrestrial strata are poorly fossiliferous and include non-fissile (blocky) mudstones as well as siltstones, and very fine- to medium-grained sandstones. The units include (listed from youngest to oldest, thicknesses from Hook et al. [2012] and Cather and Koning, [2024]) the Crevasse Canyon Formation and the Mulatto Tongue of the Mancos Shale (≈40 m), the Gallup Sandstone (13–42 m), The D-Cross Tongue of the Mancos Shale (61–110 m), the Tres Hermanos Formation (≈73 m), the Tokay Tongue of the Mancos Shale (61–110 m), and the Dakota Sandstone (≈20 m). The unit is mapped east of the Joyita Hills and north of Mesa del Yeso. The total unit thickness is ≈400–450 m. Except where noted, this description is synthesized from Allen et al. (2013) and Cather and Koning (2024).

Ku

Upper interval of Upper Cretaceous strata: Crevasse Canyon Formation, Mulatto Tongue of the Mancos Shale, and Gallup Sandstone (Coniacian, possibly Santonian?)
The **Crevasse Canyon Formation** is composed of a coarsening-upward sequence characterized by tan to gray to olive-brown sandstone, mudstone, and siltstone deposited in coastal plain, brackish lagoon, and fluvial depositional paleoenvironments; local coal seams occur near the base. About 50 m above the top of the Gallup Sandstone, a 30-m-thick tongue of **Mancos Shale (Mulatto Tongue)** is intercalated within the lower Crevasse Canyon Formation. The **Gallup Sandstone** is a gray to yellowish-gray, fine-grained sandstone and mudstone that is 5–15 m thick and was deposited during a regression in a coastal barrier-island depositional environment. The unit is 20–300 m thick (Cather et al., 2014). This description is synthesized from Cather et al. (2014) and Cather and Koning (2024).

Kl

Lower interval of Upper Cretaceous strata: Mancos Shale, Tres Hermanos Formation, and Dakota Sandstone (middle Cenomanian to middle Turonian)
This unit combines the Mancos Shale (lower Tokay and upper D-Cross Tongues), the Tres Hermanos Formation, and the Dakota Sandstone.

The **Mancos Shale** is a calcareous to non-calcareous, gray, marine shale that weathers yellowish. The upper Mancos tongue (**D-Cross**) lies between the Tres Hermanos Formation and Gallup Sandstone and is non-calcareous but locally contains scattered concretions composed of calcium carbonate near its base and top. The lower Mancos (**Tokay**) tongue (between the Dakota Sandstone and Tres Hermanos Formation) contains minor, thin, fine-grained sandstone beds near the base and top of the unit and the 19-m-thick Bridge Creek Limestone Beds about one-third of the way up from the base.

The **Tres Hermanos Formation** contains three unmapped members (listed from youngest to oldest). **Atarque Sandstone Member**: Light-gray to dark-brown or buff-colored sandstones; forms ridges, and the base is transitional with the underlying shale; deposited in a coastal barrier-island environment during the regression phase. **Carthage Member**: Sandstone and shale, slope-forming unit; lower two-thirds contains thin, fine-grained sandstone beds of paludal-lacustrine or crevasse splay origin and discontinuous cross-bedded, channel-fill sandstones. Both were deposited in a coastal plain at the culmination of the regression; the upper third was deposited in the following transgression and consists of marine shale with fossiliferous concretions. **Fite Ranch Sandstone Member**: Ridge-forming unit composed of light-gray (weathering light- to dark-brown), highly bioturbated sandstones that coarsen upward from very fine-grained to fine-grained; deposited in a coastal barrier-island paleoenvironment. The lowest unit, the Dakota Sandstone, includes a 5- to 20-m-thick interval of gray to yellow, medium- to coarse-grained, quartz-rich sandstones and minor mudstones deposited in fluvial to marginal marine depositional environments.

The lowest unit, the **Dakota Sandstone**, includes a 5- to 20-m-thick interval of gray to yellow, medium- to coarse-grained, quartz-rich sandstones, and minor mudstones deposited in fluvial to marginal marine depositional environments.

The combined unit is 300–360 m thick. This description is synthesized from Cather et al. (2014) and Cather and Koning (2024).

Jurassic and Triassic strata, undivided (Late Jurassic and Late to Middle Triassic)
See descriptions of the Morrison Formation (**Jm**) and Triassic strata (unit **Tr**); these units were combined for the purposes of mapping at 1:100,000 scale.

Morrison Formation (Late Jurassic)
Fine- to medium-grained lithic arenite interbedded with greenish-gray mudstone and sandy siltstone. The sandstones generally weather dark-brown to yellowish-brown and are commonly horizontal-planar laminated or cross-bedded and locally conglomeratic. The gravel clasts are mostly intraformational limestone. Mudstone intervals are typically covered. The unit is mapped east of the Joyita Hills where it is >60 m thick. This description is synthesized from Allen et al. (2013).

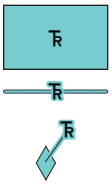

Triassic strata, undivided (Late to Middle Triassic)
Triassic strata include the Chinle Formation (Late Triassic) underlain by the Moenkopi Formation (Middle Triassic), both deposited in continental settings. The Chinle Formation is characterized by reddish-brown, gray, and purplish-gray fluvial mudstone with subordinate sandstone, limestone-pebble intraformational conglomerate, and freshwater limestones. The Shinarump Member is a few meters thick and is locally observed at the base of the Chinle Formation and consists of reddish-brown to grayish-red, fine- to coarse-grained sandstone with well-rounded pebbles of chert, quartzite, and limestone (up to a few centimeters long). The Moenkopi consists of reddish-brown to "chocolate-brown" mudstones, lithic arenite sandstones, and minor conglomerate; sandstones are ledge forming and commonly cross-stratified. The Moenkopi Formation is 10–30 m thick. The total unit thickness is 180–200 m. This description is synthesized from Cather et al. (2014); Allen et al. (2013).

PALEOZOIC SEDIMENTARY ROCKS

Permian Strata

P

Permian strata, undivided (Permian)
Cross section only. See descriptions of individual Permian units (e.g., San Andres Formation, Glorieta Sandstone).

Par

Par

Artesia Formation (Guadalupian)
Siltstone and very fine- to fine-grained sandstone. Quartzose and reddish-orange, reddish-brown, or pale-red and interbedded with minor beds of gypsum and dolomite/limestone. Tabular and internally horizontal-planar laminated, ripple-laminated, or bioturbated bedding. The disconformable lower contact is commonly marked by karstic brecciation. Mostly mapped east of the Joyita Hills. The unit is up to 20 m thick. This description is synthesized from Cather and Koning (2024) and Lucas et al. (2022b).

Psa

Psa

San Andres Formation (late Leonardian)
Gray to tannish-brownish-gray, tabular-bedded, ledge-forming limestone (minor dolomite) interbedded with intervals of gypsum, thin dolomites, and variable siltstone to mudstone. Limestone dominates in the lower 60 m, forming steep slopes. Gypsum, dolomite beds, and gypsiferous grayish-purple to reddish-brown siltstone to mudstone is more abundant in the upper 80–90 m, resulting in subdued topography. Gypsum intervals are commonly associated with dolomite beds. Sinkholes are commonly developed where the unit underlies the land surface. Limestone is thin- to thick-bedded (minor very thin beds) and mostly micritic (subordinate wackestone, floatstone, and rudstone); internally massive, bioturbated (mottled) with local burrows, or horizontal-planar laminated. Locally, fecal pellets (0.2–0.5 mm) are common. Locally, there are bivalves (brachiopods, pelecypods) and rare gastropods, bryozoans, scaphopods, rugose corals, crinoids, and phylloid algae. In the lower 30 meters of the formation, tongues of laterally extensive, ledge-forming, meter-scale-thick, quartzose sandstone beds from the Glorieta Sandstone (**Pg**) occur. Two sandstone-gypsum pairs are noted in the highlands north of the Trinity basin. White to light- or medium-gray and massive to vaguely medium- or thick-bedded (internally massive to laminated) gypsum. In most places on the map, the lower contact of the San Andres Formation is placed at base of first thick (≈30 cm) bed of limestone above the Glorieta Sandstone. However, on Mesa Jumanos, the lower limestone occurs as a relatively thin (meter-scale) tongue overlain by a thicker tongue of Glorieta Sandstone. There, the base of the San Andres Formation is placed at the top contact of this upper Glorieta tongue. In the lowest limestone bed, there is typically a gradational, progressively upward decrease of sand grains within a 0.2- to 1.0-m-thick zone above the base of the limestone bed. The San Andres Formation was deposited in various shallow-marine environments, including open-shelf, intertidal, and hypersaline lagoon settings, the latter particularly conducive for gypsum precipitation. The top contact is rarely preserved, but where present is an unconformity overlain by the Artesia Formation. Notable lateral variability is present in this formation. The unit is 140–150 m thick, but commonly eroded so that only the lower 50 m is preserved. This description is synthesized from Cather and Koning (2024) and Lucas et al. (2022b).

Pgi

Tongue of the Glorieta Sandstone in the lower San Andres Formation (late Leonardian)
A ledge-forming tongue of yellow-tan to white Glorieta Sandstone in the lower 30 m of the San Andres Formation. Locally this tongue is more varnished than the main Glorieta unit. The tongue is commonly 1–7 m thick and consists of quartzose sandstone similar to that of the main Glorieta unit (**Pg**), but slightly coarser (more commonly medium (lower)-grained compared to the fine (upper)-grained sandstone using eye estimate) and the grains are slightly more rounded. Actual sandstone thickness is probably greater than the ledge thickness, with local exposures indicating a thickness of up to 15 m. Locally, the lower part may be cross-stratified (≤60 cm foreset height), but the unit mainly exhibits very thin to very thick, tabular, horizontal-planar laminated or massive (likely bioturbated) beds. Locally, this sandstone is highly calcareous (limy sandstone) and grayish and several tongues are present. The proportion and thickness of the sandstone tongue(s) increases to the north-northeast, so that it is mapped with the main Glorieta Sandstone but separated from it by a meter-thick tongue of San Andres Formation. Mapped mainly in the Trinity basin and the north-northwest side of West Mesa. The tongue is up to 15 m thick. This map unit has been excluded from the cartographic product due to scale constraints, please reference the GIS data (MapUnitLines) available for download from the NMBGMR website (https://doi.org/10.58799/OF-GM-317).

Psai

Tongue of the San Andres Formation in the upper Glorieta Sandstone (late Leonardian)
Mapped in the northeast corner of the map area, this tongue of the lower San Andres Formation is within the upper Glorieta Sandstone. The tongue thins to the northeast as the overlying Glorieta (**Pgi**) tongue thickens. The rock consists of a light-gray to gray, micritic limestone or dolomite and sandy limestone to dolomite; fine (upper)- to medium (lower)-grained quartz sand. Very thin to thick, tabular bedding. There are local bivalves up to 20 mm long. Limestone locally contains rounded fecal(?) pellets up to 0.7 mm long. The tongue is commonly manifested as a 1-m-thick limestone ledge overlain by a gypsiferous(?), fine-grained slope former that is a few meters thick. The unit is 2–5 m thick. This map unit has been excluded from the cartographic product due to scale constraints, please reference the GIS data (MapUnitLines) available for download from the NMBGMR website (https://doi.org/10.58799/OF-GM-317).

Psag

San Andres Formation and Glorieta Sandstone, undivided (late Leonardian)
The San Andres Formation and Glorieta Sandstone are commonly combined on this map because the Glorieta Sandstone is typically too narrow to show at 1:100,000 scale. See individual descriptions of **Psa** (San Andres Formation) and **Pg** (Glorieta Sandstone). Together, the combined unit is up to 210 m thick.

Pg

Pg

Glorieta Sandstone (late Leonardian)
Light-gray to creamy-yellowish-white to white: weathering yellow, tan, or orange; ledge-forming sandstone. Medium to thick (minor thin, lesser very thing beds), tabular beds exhibiting internal horizontal-planar laminations with a variable amount of cross-stratification that is more common to the west (mostly <0.6 m thick sets with laminated to very thin foresets, but very locally, the foreset thickness is meter scale with thicker foresets), and local ripple marks. Bioturbation is common (disturbed, mottled textures) and locally includes sparse burrows. Foresets mainly dip to the southwest. Fine (lower)- to medium (lower)-grained sand (mostly fine [upper]- to medium [lower]-grained sand), subangular to subrounded (more rounded to the west), well-sorted, and quartzose. In the eastern part of the map area, the Glorieta consists of two tongues (each of comparable thickness) separated by ≈10 m of slope-forming gypsum, siltstone, and very fine-grained sandstone. Locally, relatively thin interbeds of reddish-brown to purplish-gray mudstones to siltstones are found in the lower 2–4 m of the unit. Variably cemented by silica and calcium carbonate, with silica cementation more common to the east. Interpreted as eolian sand sheets with locally preserved dune structures. The unit is 70–90 m thick. This description is synthesized from Aby and Jochems (2022) and Lucas et al. (2022b).

Py

Los Vallos and Meseta Blanca Formations of the Yeso Group, undivided (Leonardian)
See descriptions of units **Pyv** and **Pym**. The combined unit is 340 m thick.

Pyv

Pyv

Los Vallos Formation of the Yeso Group (middle Leonardian)
Grayish-red, grayish-yellow, or grayish-orange sandstone, siltstone, claystone, gypsiferous sandstone and siltstone, and muddy sandstone interbedded with gypsum and ledge-forming dolomite. Very fine- to fine-grained and quartzose sandstone, occurring as thin, tabular bodies. The upper part of the Los Vallos consists of ≈12–20 m of orangish to light-reddish-brown (locally gray, yellowish-gray), well-sorted siltstone and very fine- to fine-grained, quartz-rich sand and silty sand with <10% mudstone (Joyita Member) underlain by the variably thick (10–20 m, locally up to 100 m), gypsum-dominated strata (Cañas Member). The Joyita Member consists of very thin to thin, tabular to slightly irregular beds of sandstone that exhibits local low-angle cross-stratification to ripple lamination. There is locally a 5–6-m-thick vertical gradation between the Joyita Member and the Glorieta Sandstone, but the contact is sharp in other places. The Cañas Member includes subordinate buff to greenish-gray siltstone to very fine-grained sandstone and gray limestone to dolomite. The siltstone to very fine-grained sandstone is thinly bedded and exhibits horizontal laminations; carbonate beds are generally micritic and less than a few meters thick. The gypsum is thickly bedded and exhibits nodular mosaic textures or dark-gray horizontal to wavy laminations a few millimeters thick. Prominent, ledge-forming dolomite and limestone intervals are up to a few meters thick and are restricted to the lower ≈145–160 m (Torres Member); the carbonates are commonly horizontal-planar laminated to wavy laminated and range from micrite to wackestone. The

basal contact of the Torres Member is placed at the base of the lowest bed of limestone that is >1 m thick (mostly 2–3 m). The Cañas and Torres members reflect deposition in a shallow-marine to coastal-sabkha environment. The Joyita was deposited as eolian sand sheets with modest reworking by ephemeral(?) rivers. The uppermost strata (in the Cañas and Joyita Members) are commonly excised due to low-angle faulting associated with the Quebradas detachment fault system (Cather and Koning, 2024). Total thickness of the unit is 230–240 m. Except where noted, this description is synthesized from Cather and Koning (2024) and Lucas et al. (2022b).

Pym

Meseta Blanca Formation of the Yeso Group (early Leonardian)
This unit is named the Arroyo de Alamillo formation by Lucas et al. (2005). Red to reddish-orange and pastel-colored, tabular-bedded strata composed of fine-grained sandstones, siltstones, and minor silty mudstones. These strata commonly erode to form stair-step-like slopes. Very minor (<5%) thin beds of dolomite or limestone. Very fine- to fine-grained (minor medium-grained), well-sorted, subrounded to rounded, quartzose sandstones with horizontal-planar laminated beds and subordinate ripple laminations (including climbing ripples). Ripple marks (symmetric and asymmetric), halite pseudomorphs, and mud cracks are seen on bedding planes. Straight-crested or ladderback ripples are characteristic. The conformable lower contact is placed at the color change from brick-red and reddish-brown (Abo Formation, **Pa**) to more orangish and grayish colors. Depositional environment: eolian sheet sands and loessic silts that were reworked to varying degrees by floods and marine inundations. The unit is 70–110 m thick. This description is synthesized from Cather and Koning (2024) and Lucas et al. (2022b).

Pyma

Meseta Blanca and Abo Formations, undivided (early Leonardian to Wolfcampian)
The Meseta Blanca and Abo Formations are mapped undifferentiated in order to allow for depiction at the 1:100,000 map scale. See descriptions for units **Pym** and **Pa**. The combined unit is 210–350 m thick.

Pa

Abo Formation (early Leonardian to Wolfcampian)
The Abo is dominantly composed of brick-red, non-fissile mudstone, bedded siltstone to very fine-grained sandstone, and minor lenses of conglomerate. Two members, the Cañon de Espinoso and Scholle Members, can be recognized in many outcrops but have not been mapped separately. Sandstones in both members are arkosic to subarkosic, but the fine-grained sandstone and siltstone are more quartzose. Brick-red to dark-reddish-brown, non-fissile mudstontes are more abundant than sandstones. The overlying Cañon de Espinoso Member (≈50–175 m thick) has lower mudstone content and consists of mudstone, siltstone, and several laterally extensive, sheet-like, thin (<10 m) beds of very fine- to medium-grained sandstone exhibiting climbing-ripple laminations. The contact between the two members is conformable and gradational. The lower Scholle Member (37–69 m thick) consists of mudstone (some containing numerous calcrete nodules) with interbedded, relatively lenticular paleochannels (as much as 5 m thick) backfilled by cross-bedded sandstone and conglomerate. Conglomeratic strata are crudely stratified to trough cross-bedded and poorly sorted with a sandy matrix; clasts are commonly composed of intraformational limestone (ripped-up calcrete nodules) with only sparse extraformational clasts. The lower contact is placed at the color change, which is stratigraphically near the top of the uppermost limestone bed in the underlying Bursum Formation (**PIPb**). Deposited by south- to southwest-flowing rivers that were sourced from relict Ancestral Rocky Mountain uplifts. The unit is 140–240 m thick. This description is synthesized from Cather and Koning (2024) and Lucas et al. (2022b).

Permian and Pennsylvanian Strata

PIPbm

Bursum Formation and lower–middle Madera Group, undivided (Wolfcampian to Desmoinesian)
The Bursum Formation and underlying strata of the Madera Group are mapped undifferentiated in order to allow for depiction at the 1:100,000 scale. See descriptions for units **PIPb** and **IPm**. The combined unit is hundreds of meters thick.

PPams

Abo, Bursum, Atrasado, Gray Mesa, and Sandia Formations, undivided (early Leonardian to Atokan)
The Abo and Bursum Formations and the Madera Group (Atrasado and Gray Mesa Formations) are mapped undifferentiated in order to allow for depiction at the 1:100,000 scale where these units are steeply tilted in the Joyita Hills. See descriptions for units **Pa**, **PPb**, **PPm**, and **PPs**. The combined unit is 200–240 m thick.

PPb

PPb

Bursum Formation (early Wolfcampian)
Purplish-red to variegated greenish-gray mudstone, sandstone, and conglomerates that are interbedded with marine limestones. The limestones are micritic, nodular to massive, and most common in the lower part. The upper part contains local conglomeratic sandstones, where clasts are composed of quartz, granite, and reworked Pennsylvanian rocks (e.g., siltstone and limestone). Represents the transition between the terrestrial red beds (Abo Formation, **Pa**) and the dominantly shallow-marine deposition (Atrasado Formation, **PPma**). The unit has an unconformable lower contact that is locally angular. The unit is 25–120 m thick. This description is synthesized from Cather and Koning (2024) and Lucas et al. (2022b).

Pennsylvanian Strata

PPm

Madera Group (Virgilian to Desmoinesian)
Composed of the Atrasado Formation (**PPa**) underlain by the Gray Mesa (**PPg**) Formation. The presence of relatively abundant limestones distinguishes the Madera Group from the underlying Sandia Formation. The ledge-forming limestones are light- to medium-gray, micritic, and in medium to thick, tabular beds. These limestones are interbedded with dark-greenish-gray, limy shales and minor sandy limestones. Fossils include fusulinids, brachiopods, crinoids, and corals. The Madera Group is ≈580 m thick east of Rio Grande and ≈210 m (locally as thin as 60 m) west of Rio Grande due to erosion in the Paleogene prior to the deposition of the Baca Formation. This description is synthesized from Cather and Koning (2024), Chamberlin et al. (2001), and Lucas et al. (2022a).

PPma

PPma

Atrasado Formation of the Madera Group (Virgilian to Desmoinesian)
Intercalated shales and limestones with minor arkosic sandstones. Contains fewer limestone beds than the underlying Gray Mesa Formation (**PPmg**). The Atrasado Formation has been divided into the following members, from youngest to oldest: Moya, Del Cuerto, Story, Burrego, Council Spring, Tinajas, Amado, and Bartolo. The dominant presence of limestone in the Amado, Council Spring, Story, and Moya Members is a useful criterion in this subdivision. The uppermost part of the Atrasado, the Moya Member, is a relatively thick with a cliff- and ledge-forming interval composed of limestone with minor shale and arkosic sandstone. The Del Curto Member consists of interbedded shales (which may be reddish), sandstones, and carbonates. The Story Member is mainly composed of limestones which are about 19–20 m thick. The Burrego Member is mostly slope-forming shale and siltstone with minor ledge-forming beds of arkosic sandstone, conglomerate, and limestone; characteristic lithologies are red-bed mudstone and cross-bedded arkosic sandstone. The Council Spring Member is a laterally persistent, 6–13 m thick, light-gray to white limestone that forms ledges, cliffs, and ridges; it locally contains bioherms. The Tinajas Member consists of covered intervals (probably shales) intercalated with relatively thin sandstone and limestone to dolomite intervals. The Bartolo Member consists of shale-siltstone with intercalated layers of conglomerate, sandstone, and fossiliferous limestone. The limestone interval comprising the Amado Member is 8–11 m thick and laterally persistent. The unit is ≈225–270 m thick. This description is synthesized from Cather and Koning (2024) and Lucas et al. (2022a).

PPmg

Gray Mesa Formation of the Madera Group (Desmoinesian)
Intercalated grayish limestone and poorly exposed shale. Locally recognized but not mapped are three members (listed from youngest to oldest). The **Garcia Member** (61–103 m) is composed of diverse shale, limestone, sandstone, and conglomerate. The **Whiskey Canyon Member** (25–42 m) is mainly composed of very cherty limestone that is highly resistant to erosion and forms ridges. The **Elephant Butte Member** (40–93 m) at the base consists of limestone and

shale beds and has a 10-m-thick sandstone near its base. The lower contact of the formation is placed at the base of the first thick, chert-bearing limestone above the siliciclastic-dominated Sandia Formation. The entire unit is 130–235 m thick, but is commonly much thinner on the west side of the Rio Grande due to erosion accompanying the Laramide-Sierra Uplift. This description is synthesized from Cather and Koning (2024) and Lucas et al. (2022a).

IPs

Sandia Formation (Atokan)
A siliciclastic-dominated unit composed of intercalated shale, siltstone, quartzose sandstone, and minor quartz-conglomeratic sandstone and limestone. The proportion of limestone in the unit is 5–25% Cather and Koning (2024), and it is typically a coarse-grained, bioclastic, wackestone/packstone (Lucas et al., 2022a). Drab-brown to gray to dark-gray shales and siltstones that locally contain plant fossils. The lower three fifths of the unit consist of shales, siltstones, and very fine- to fine-grained sandstones intercalated with ledge-forming, fine- to coarse-grained sandstones. The siltstones and very fine- to fine-grained sandstones are horizontal-planar laminated to ripple laminated. The ledge-forming sandstones are in medium to thick, tabular beds that are internally massive or exhibit trough cross-bedding; minor limestone intervals are 0.3–3 m thick (5–30 cm bed thicknesses) that increase in abundance upsection in the lower three fifths of the formation. The limestones are mostly coarse-grained, sandy, and fossiliferous (abundant fragments of crinoids, brachiopods, bryozoans, solitary and rugose corals, fusulinids, gastropods, conodonts, and shark teeth (Bauch, unpublished thesis, 1982; Ivanov et al., 2009; Lucas et al., 2009; Krainer and Lucas, 2013). The sandstone intervals are up to 9 m thick, commonly fine upward, and are composed of multistoried channel fills. Within the sandstone intervals are local 1- to 2-m-thick interbeds of gray siltstone and limy mudstone. Reddish, fine- to coarse-grained quartz-arenite sandstone, although locally arkosic or lithic arenite sandstones are present (Rejas, 1965; Krainer and Lucas, 2013). West of the Rio Grande, feldspathic to micaceous sandstone has been observed (Chamberlin et al., 2001). Individual sandstone beds contain fossil-plant fragments, including some stem fragments >1 m long. Conglomerate clasts are composed of quartz 1–2 cm in diameter. Locally, a basal lag conglomerate contains granitic clasts as large as 20 cm. The upper one third of the Sandia Formation contains shales interbedded with several (but still proportionally minor) fossiliferous limestones (most commonly in the upper part) and fine-grained quartz arenites. Deposited in open marine, marginal marine, and coastal-plain paleoenvironments. The unit is 140–180 m thick. Except where noted, this description is synthesized from Cather and Koning (2024), Chamberlin et al. (2001), and Lucas et al. (2022a).

IPms

Madera Group and Sandia Formation, undivided (Virgilian to Atokan)
Limestone-bearing strata that underlies red-bedded Permian strata and overlies either bedrock or local Mississippian strata. See descriptions of units **IPs**, **IPmg**, and **IPma** above. The combined unit is up to 740 m thick, but generally only 100–200 m thick on the west side of the Rio Grande due to erosion accompanying the Laramide-Sierra Uplift (Cather, 1983) before burial by the Baca Formation. Except where noted, this description is synthesized from Cather and Koning (2024), Chamberlin et al. (2001), and Lucas et al. (2022a).

Pennsylvanian and Mississippian Strata

IPM

Pennsylvanian and Mississippian strata, undivided (Pennsylvanian to Mississippian)
The lower Madera Group (**IPm**) and Sandia Formation (**IPs**) underlain by the Mississippian strata of the Kelly Limestone. The upper Kelly Limestone (Ladron Member) consists of gray to buff, fine- to coarse-grained, bioclastic limestones. The lower Caloso Member conformably underlies the Ladron Member and consistes of micritic limestones, shales, and a basal conglomeratic sandstone. Mapped in the Lemitar Mountains. The Pennsylvanian and Mississippian strata are <400 m thick. This description is synthesized from Cather and Koning (2024), Chamberlin et al. (2001), and Lucas et al. (2022a).

PROTEROZOIC ROCKS

XY

Proterozoic rocks, undivided (Mesoproterosoic to Paleoproterozoic)
Cross section only. See descriptions of individual Proterozoic units.

Mesoproterozoic Rocks

Yg

Granite, non-foliated (Mesoproterozoic)
Gray to pink, porphyritic to megacrystic, coarse-grained quartz monzonite intrusion. Mineral assemblage: plagioclase, potassium feldspar, quartz ± muscovite, ± chlorite, and ± epidote granite. Microline phenocrysts are up to 4 cm long and plagioclase is 0.5-1.0 cm. Slightly foliated at the pluton margins; variably developed alignment of megacrysts is interpreted as magmatic flow foliation. Age of 1,430 Ma (Bauer et al., 1993). Except where noted, this description is synthesized from Scott et al. (2005); Luther et al. (2005); Thompson and Barnes (1999).

Paleoproterozoic Rocks

Intrusive Igneous Rocks

Xg

Granite, non- to weakly foliated (Paleoproterozoic)
Pink (weathering red), massive, medium- to coarse-grained granite with the following mineral assemblage: quartz + albite + potassium feldspar. Includes the Los Pinos Granite (1,653–1,659 Ma; Karlstrom et al., 2004), Tajo Granite, and Polvadera Granite. The Los Pinos Granite locally has a distinctive myrmekite texture. The Tajo and Polvadera Granites contain minor amounts of biotite + magnetite ± hornblende, and foliation is locally well-developed along contacts with mafic plutonic rocks. Except where noted, this description is synthesized from Luther et al. (2005), Allen et al. (2014), and Chamberlin et al. (2001).

Xgf

Foliated granites (Paleoproterozoic)
Strongly foliated granite composed of potassium feldspar + quartz + plagioclase ± biotite. The foliation is defined by aligned biotite grains, augen of potassium feldspar porphyroclasts, and quartz rods. Where mapped on the east side of Polvadera Peak, a U-Pb age from zircon is 1,648 ± 6 Ma (Bowring et al., 1983). Includes granite of the Sepultura Canyon in the Los Pinos Mountains that is likely older than 1,650 Ma. Except where noted, this description is synthesized Chamberlin et al. (2001) and Allen et al. (2014).

Xm

Mafic intrusive rocks (Paleoproterozoic)
Mostly dark-gray plutonic rocks that range from diorite and gabbro to quartz diorite and quartz gabbro. The mineral assemblage includes hornblende + plagioclase feldspar + quartz. The foliation is generally lacking, although locally well-developed along contacts with the Polvadera Granite complex. The unit is mapped east of Polvadera Peak, where it is 1 km wide and ≈3.5 km long. This description is synthesized from Chamberlin et al. (2001).

Manzano Group

The Manzano group is an informal stratigraphic term proposed by Holland et al. (2020) for Proterozoic metasedimentary and metavolcanic rocks found in the Los Pinos Mountains.

Xb

Blue Springs Formation of the Manzano Group (Paleoproterozoic)
Inter-layered metarhyolites, schists, and quartzites. Named by Stark and Dapples (1946). The metarhyolite is black, brown, or gray and contains lenticular, quartz-feldspar, and pink stripes within darker layers. It is interpreted as a metarhyolite due to the presence of potassium feldspar in the felsic lenses and a geochemical composition close to rhyolite. The schist is a green to white, garnet + chlorite ± quartz ± muscovite schist. Schists in the middle to lower part of the unit are crenulated and have well-preserved garnet. Interpreted to be 1,588 ± 7 Ma (Holland et al., 2020). The unit is 400–550 m thick. Except where noted, this description is synthesized from Luther et al. (2005), Allen et al. (2014), and Scott et al. (2005).

Xq

White Ridge and Sais Quartzites of the Manzano Group (Paleoproterozoic)
This map unit includes three subunits. The Sais Quartzite at the top, the Estadio schist in the middle, and the White Ridge Quartzite at the base. The quartzites are thinly bedded and exhibit cross-stratification. The White Ridge Quartzite is an orange to gray, coarse-grained, impure, and immature metasedimentary rock. The Estadio schist is a coarse-grained, staurolite + garnet + biotite schist that serves as a marker unit. The Sais Quartzite is a reddish, schistose quartzite with very fine- to coarse-grained quartz grains, and bedding planes commonly show mica concentrations. The age is interpreted to lie between 1,665 ± 14 Ma and 1,661 ± 17 Ma (Holland et al., 2020). The combined unit is ≈450 m thick. Except where noted, this description is synthesized from Luther et al. (2005), Allen et al. (2014), and Scott et al. (2005).

Xas

Abajo metasedimentary rocks of the Manzano Group (Paleoproterozoic)
Informally called the Abajo metasedimentary rocks. Composed of a variety of metasedimentary rocks, including metapelites, meta-arkose, and impure quartzite. Commonly interlayered with mafic meta-igneous dikes and flows. Metapelites include chlorite schist and schists rich in staurolite, garnet, and amphibole porphyroblasts. Schists and some quartzites that are interbedded with the metarhyolite are thinly bedded; more massive and quartzite domains are locally dominant. The age is interpreted to lie between 1,665 ± 16 Ma and 1,661 ± 17 Ma (Holland et al., 2020). Tentatively correlated to meta-arkoses, quartzites, and greenschist and pelitic schists on the eastern side of Polvadera Peak (1,659 ± 3 Ma; Bowring et al., 1983). The unit is 350-380 m thick. Except where noted, this description is synthesized from Luther et al. (2005).

Xsr

Sevilleta metarhyolite of the Manzano Group (Paleoproterozoic)
Felsic, meta-igneous rocks that are generally pink to gray, blocky fracturing, and porphyritic with quartz and feldspar phenocrysts. Named by Stark and Dapples (1946). The texture ranges from thin, well-developed compositional banding to massive. Planar features, such as ≈1 mm to ≈5 cm flow bands or shear bands, are common and range considerably in thickness. Quartz veins, pegmatite, and massive schistose units are present locally and generally parallel foliation. Unique characteristics of its three felsic subunits include a lower flow that is medium-gray to black, finely banded, has minor white mica and biotite, and contains 1.0–2.5 mm white feldspar crystals (commonly sericitized); a middle flow that is dark-gray to black, contains local flattened lapilli up to 3 cm long, and contains 0.5- to 2.0-mm-long quartz and feldspar phenocrysts; and an upper flow that is brown to pink, finely banded, and has 0.5–3.0 mm feldspar and quartz phenocrysts and rounded to subrounded porphyroclasts in a quartzo-feldspathic, fine-grained matrix. Olive to dark-green, aphanitic, vesicular, flow-banded rock (gneissic with feldspar augen in places) interfingers with the metarhyolites. The age is interpreted to lie between 1,665 ± 14 Ma and 1,661 ± 17 Ma (Holland et al., 2020). The unit is 1,200–1,250 m thick. Except where noted, this description is synthesized from Luther et al. (2005) and Allen et al. (2014).

Xbc

Bootleg Canyon sequence of the Manzano Group (Paleoproterozoic)
Interbedded amphibolite, pelitic schists, quartzites, and "layered" schists. The amphibolite is black and white to greenish-gray to black, coarse-grained, and contains hornblende, epidote, biotite, chlorite, and actinolite. Light-green to beige pelitic schist layers contain garnet, biotite, ± chlorite, muscovite, plagioclase, quartz, Fe-Ti oxides, ± potassium feldspar, and ± tourmaline. Greenish (epidotized?) quartzite layers are thinly bedded and micaceous and contain fine-grained, epidote-rich, 0.5–2 cm-scale pods of calc-alkaline material. The layered schist is an interbedded mafic and granitic schist. The age is older than the Sevilleta metarhyolite (>1,665±14 Ma; Holland et al., 2020). The unit is >150 m thick. Except where noted, this description is synthesized from Allen et al. (2014).

APPENDIX B—SPECTRUM AND ISOCHRON PLOTS PERTAINING TO NEW $^{40}AR/^{39}AR$ ANALYSES

For samples: CHM-100, Soco811-3, SQSA23-5, SQSA23-9, 22RH-093A

New Mexico Geochronology Research Laboratory

CHM-100
Feldspar

a)

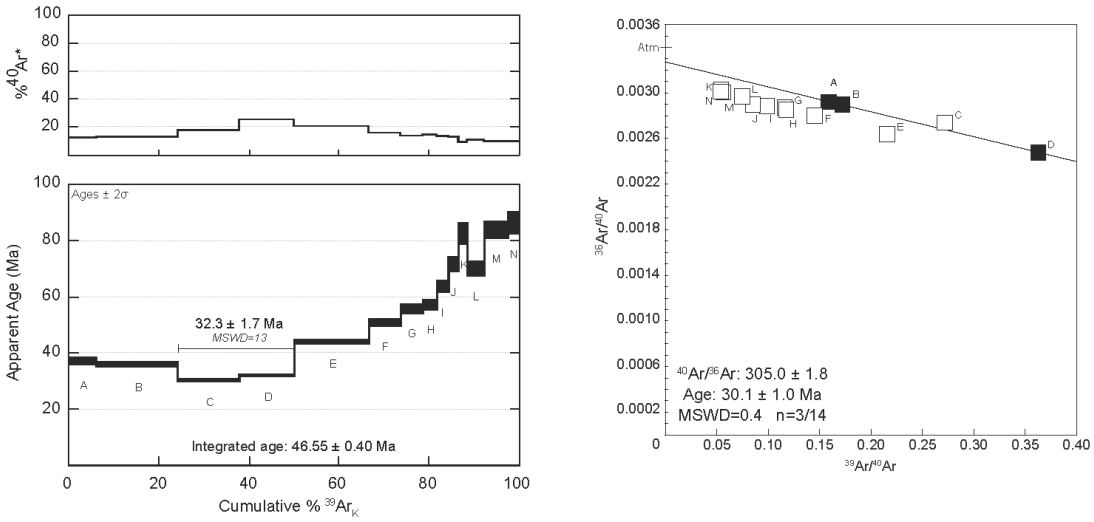

b)

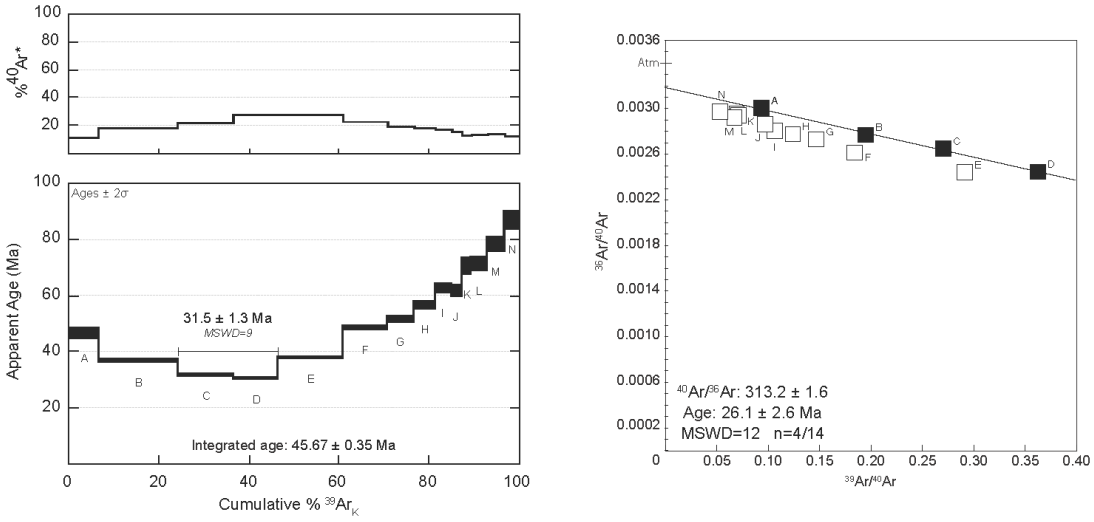

Soco811-3
Groundmass

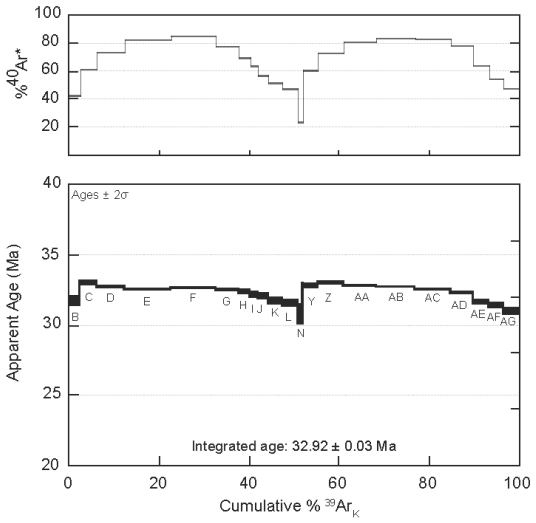

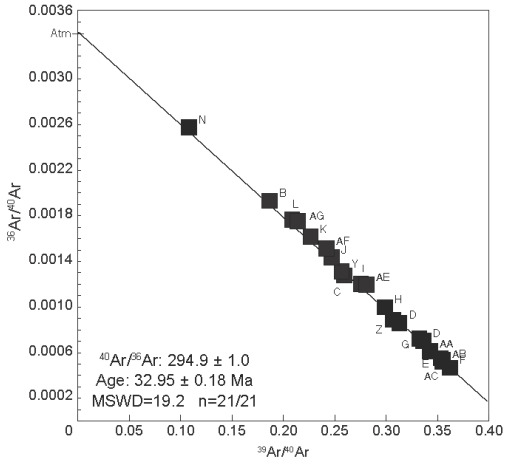

SQSA23-5
Feldspar

a)

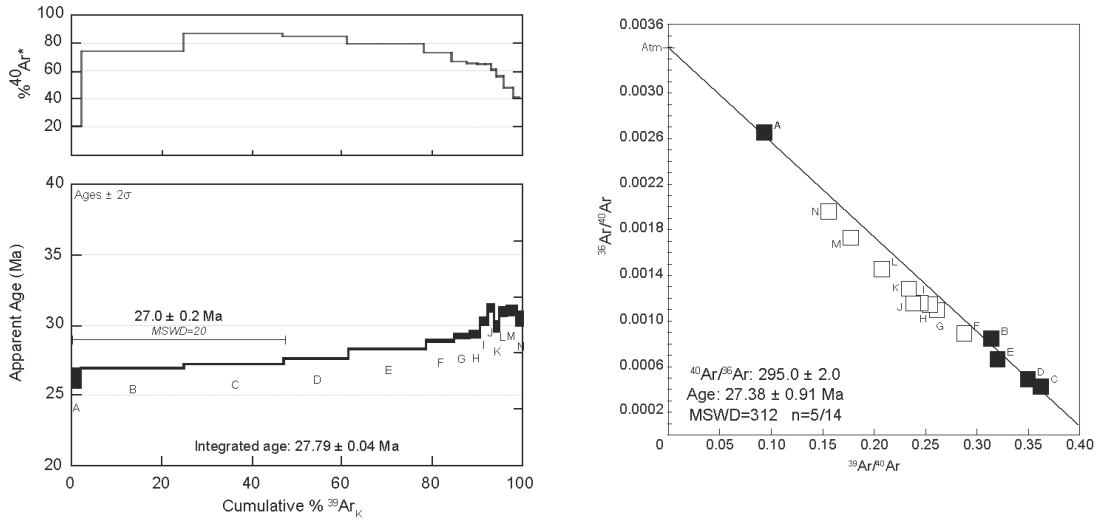

b)

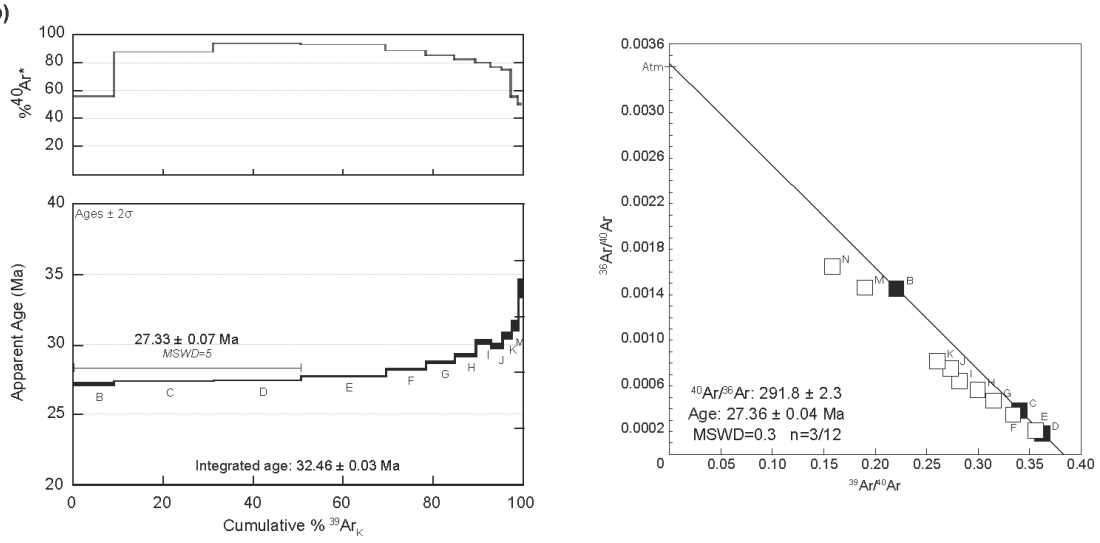

SQSA23-9
Feldspar

a)

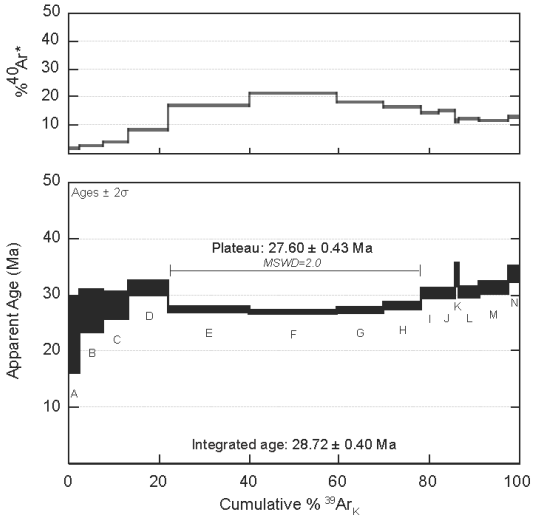

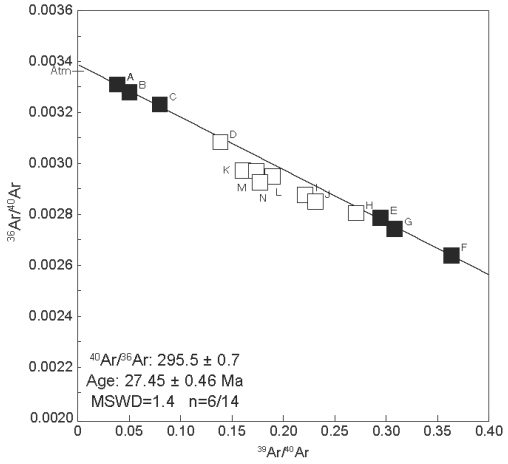

b)

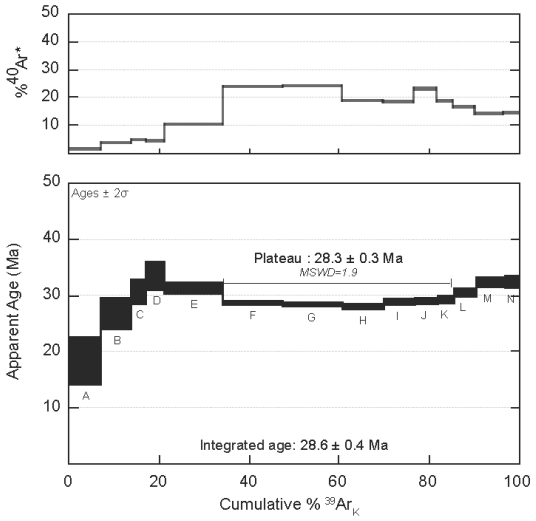

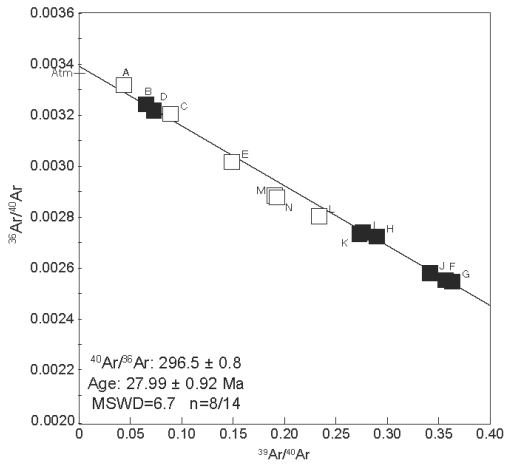

22RH-093A
Biotite

a)

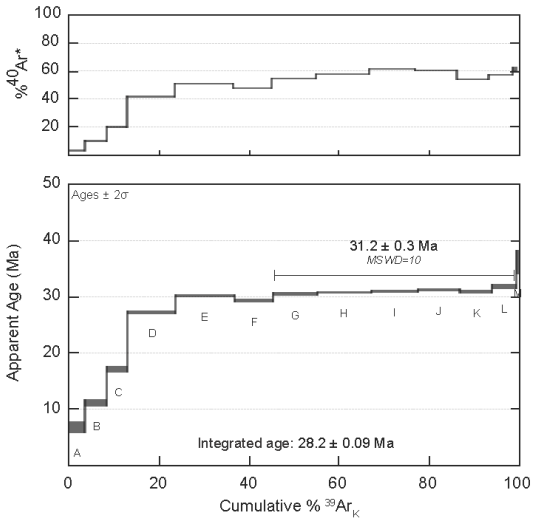

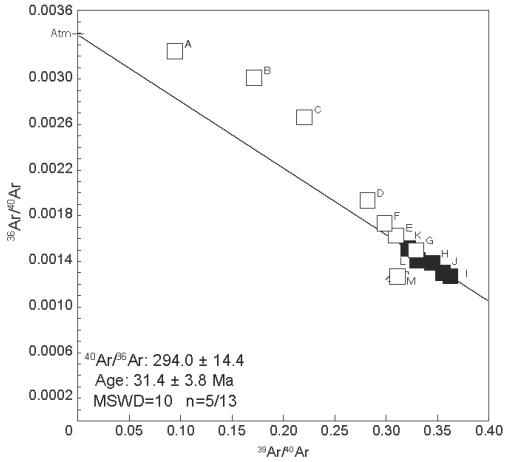

SQSA23-9
Hornblende

c)

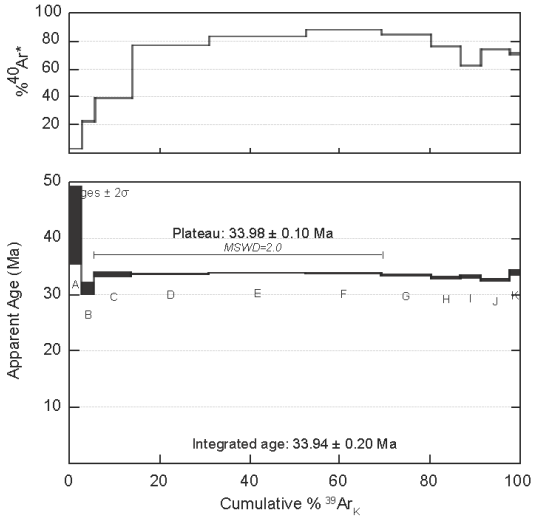

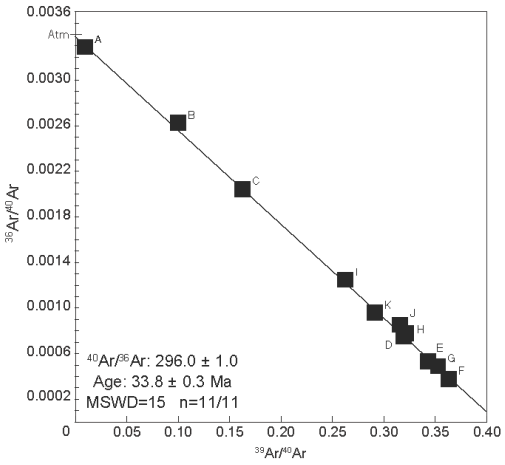

APPENDIX C—DESCRIPTIONS FOR RIO GRANDE TERRACE STRATIGRAPHIC SECTIONS

Grain sizes follow the Udden-Wentworth scale for clastic sediments (Udden, 1914; Wentworth, 1922) and are based on field estimates. Sand textures are abbreviated as follows: very fine-lower, vfL; very fine-upper, vfU; fine-lower, fL; fine-upper, fU; medium-lower, mL; medium-upper, mU; coarse-lower, cL; coarse-upper, cU; very coarse-lower, vcL; very coarse-upper, vcU. Pebble sizes are abbreviated as: very fine, vf; fine, f; medium, m; coarse, c; and very coarse, vc. The term "clast(s)" refers to the grain size fraction greater than 2 mm in diameter. Descriptions of bedding thickness follow Ingram (1954). Note that a stratigraphic section was not measured at the Veguita site.

Joya_01 stratigraphic section sampling Qt3. This section consists of **Bowling Green axial-fluvial sediment** overlying Sierra Ladrones Fm. No PLSS description is available because the site is in the middle of a former land grant. Measured and described by Dan Koning on July 10, 2022, using an Abney level, Brunton compass, Jacob's staff, and hand-held GPS unit.

Unit	Description	Thickness (cm)	Height (cm)
	Axial-fluvial facies of Qt3		
	Bottom and top of stratigraphic section: 332108 ± 3 m E; 3801060 ± 3 m N; zone 13, NAD83.		
G	CLAYEY SAND: 5YR 4/6, vfL to mL sand and clay mixed together in subequal proportions. To North (UTM coordinates 332101 E 3801077 N) sandy gravel is unconformaly. overlying this described sediment. Photo with hammer.	50	169
F	SLIGHTLY CLAYEY SAND: Weak to moderate consolidated and like E below, except reddened and has more clay	10	119
E	SAND: massive and mL-cL, moderately sorted, and weakly consolidated. Sand composed of clear grains (quartz, plagioclase, sanidine) with 15% orange grains and 12-15% mafic lithic grains.	30	109
D	SAND AND WEAK PEDOGENESIS: 7.5YR 6/4, massive, fU-mL sand with 10% f sand. 10% calcium carbonate splotches. Pedogenesis indicated by ped development (weak, coarse, subangular blocky and slightly hard). Weakly consolidated.	30	79
C	SAND: 20YR 7/2, massive sand that is mostly mL-mU. Sand is well sorted and composed of clear grains (quartz, sanidine, plagioclase) with 20% orange grains (Kspar, granite fragments, orange quartz) and 15% lithic grains.	25	49
B	SAND: 10YR 6/3, fU with trace 1% silt clay. Massive. 1-2% pebble size calcium carbonate modules that are relatively soft. Sediment is weak -moderately consolidated	12	24
A	SAND: 10YR 7/2, fU-mU (mostly mL), and low angle cross laminated (up to 12 cm tall), especially in upper 2-3 cm. Weakly consolidated. Sand is moderately to well sorted and composed of clear grains (quartz, sanidine, plagioclase) with 25% orange grains and 15% lithic mafic grains. Sand in not bioturbated. **@5-10 cm from base: OSL sample Joya-01.** UTM coordinates of: 13S 332108m E, 3801060m N (NAD 83).	12	12
1	SANDY COBBLES: vf-vc pebbles with 5% cobbles. Gravel are rounded to subround and composed of volcanics (intermediate-felsic compositions), 15-20%/ quartzite, 10% vf-f reddish sandstone (Yeso Group and Abo Fm), 10% granite. No Rabbit Mountain obsidian. Top goes to within 20 cm of ground surface (ground surface slopes 20 degrees west).	-100	-100

Joyita_02 stratigraphic section. This section consists of Matanza formation axial-fluvial sediment overlain by Matanza alluvial-fan sediment. The base is not exposed. No PLSS description is available because the site is in the middle of a former land grant. Measured and described by Dan Koning on July 11, 2023, using an Abney level, Brunton compass, Jacob's staff, and hand-held GPS unit.

Unit	Description	Thickness (m)	Height (m)
	Axial-fluvial facies of Qt2		
	Bottom and top of stratigraphic section: 331238 ± 3 m E; 3801890 ± 3 m N; zone 13, NAD83.		
C	ALLUVIAL FAN SANDY GRAVEL**:** Deposit is ~3 m (10 ft) thick with Stage 3 calcic soil on top (calcic horizon is ~1 m (3 ft thick) + (-0.5 ft), based on visual estimation). Bedding is very vague to nonexistent. Sand is 10YR 5/4 and medium to very coarse (mostly coarse to very coarse). The gravel is very poorly sorted and composed of very fine to very coarse pebbles, 30-40% cobbles, and 25% boulders. Gravel is mostly composed of Permian siltstones-fine sandstones, gray limestone, 20% granite and granitic gneiss, and 15% volcanic rocks. Imbrication is mostly to northwest. Slightly scoured, lower base.	~3.3	4.2
B	AXIAL-FLUVIAL GRAVELLY SAND: 10 YR 7/2 -6/3, coarse to very coarse, moderately sorted sand composed of clear grains (quartz, sanidine, plagioclase) with 15% orange grains [granite, Kspar, orange chert-quartz). Gravel comprised of vf-vc pebbles, 5% fine cobbles, and of Rio Grande provenance with much northerly derived clast types; gravel is rounded to poorly sorted. 1% cobble size rip ups of clay at base. sharp lower contact and scoured upper contact (20 cm of relief); upper contact interpreted as disconformity, and possible that lower contact is also disconformable.	0.6	0.9
A	AXIAL FLUVIAL SAND: Light yellowish brown (10YR 6/4), mL axial sand that is moderately to well sorted, composed of clear grains (quartz, plagioclase, sanidine) with 10-15% orange grains and 10% lithic grains. Massive in lower half and horizontally laminated in upper half. Moderately consolidated. **@ 10 cm from base of exposure: OSL sample Joya-02 collected.** UTM coord of: 13S 331238m E, 3801890 m N (NAD 83).	0.3	0.3

Joyita_03 stratigraphic section. This section consists of Matanza formation alluvial-fan sediment. Unit C here is the same as unit C in the Joyita 02 stratigraphic section. The base is not exposed. No PLSS description is available because the site is in the middle of a former land grant. Measured and described by Dan Koning on July 11, 2023, using an Abney level, Brunton compass, Jacob's staff, and hand-held GPS unit.

Unit	Description	Thickness (m)	Height (m)
	Axial-fluvial facies of Qt2		
	Bottom and top of stratigraphic section: 331229 ± 3 m E; 3801890 ± 3 m N; zone 13, NAD83.		
C	SANDY GRAVEL: thick–medium bedded sandy gravel derived from the east. Minor, thin beds of axial-fluvial sands that are likely reworked from the east. Gravel clasts include pebbles, ~30% cobbles, and 4-5% fine boulders that are subrounded to subangular and poorly sorted; gravel mainly composed of late-Paleozoic sedimentary clasts (e.g., limstones, sandstones, siltstones). Interpreted as an alluvial fan deposit. The sampled axial fluvial interbed within Unit C is 10 cm thick and the highest such bed; it dips 15 degrees to the east and is internally massive. The sand is 10YR 6/4, m-vc, has 1% very fine pebbles (granules), weakly consolidated like rest of Unit C, and composed of quartz 10-15% orange grains 10% lithics. Note that this and all sample sites had at least 20 cm outer cover removal sampled sand. **@ 70-80 cm above Unit C base is OSL sample Joya-03**. Sample located 13 m west of Joya 02. UTM coord of: 13S 331229m E, 3801890 m N (NAD 83).	~2.85	~2.85

East SanAcacia stratigraphic section. This section consists of Matanza formation axial-fluvial sediment. The base is not exposed. No PLSS description is available because the site is in the middle of a former land grant. Measured and described by Dan Koning on July 12, 2023, using an Abney level, Brunton compass, Jacob's staff, and hand-held GPS unit.

Unit	Description	Thickness (m)	Height (m)
	Axial-fluvial facies of Qt2		
G	COBBLE-RICH AND ROUNDED GRAVEL: Gravel composition: intermediate-felsic volcanic, 25% granite, 3-5% limestone, 15% -20% quartzite; 5% rounded (and polished) chert, 1% iron [siderite?] 1% K sandstone, 1% amphibolite, trace pedernal chert, trace to 1% Permian reddish siltstone-very fine sandstone. Inferred younger allostratigraphic unit, perhaps related to early incision. Inferred disconformity at base of unit.	2.7	5.7
F	SAND: 10YR 7/2-8/1, vaguely cross laminated sand that is loose; 10 YR 7/2-8/1, cL-cU; well sorted, subrounded- subangular and with 20-25% orange-colored grains and 15% lithics-mafics. **@2.4 m (3.3 m, 11 ft below tread): OSL sample SanAcac-02.** UTM coordinates of: 13S 330022m E, 3795069m N (NAD 83).	0.8	3.0
E	SILTY FINE SAND: 7.5 YR 6/2-3, well consolidated, silty vfL-fL sand; 5-20% scattered m-vc sand and vf-f pebbles1-3% thin to very thin lenses of pebbles (volcanic with minor granite and 1 quartzite). One gleyish horizon. . Interpreted as distal-piedmont - floodplain facies.	1.1	2.2
D	GRAVELLY SAND: Gravel clasts are matrix supported. Trace-0.5% clay in matrix, which makes the sediment consolidated. Gravels are poorly sorted, well rounded to subrounded, and contains Rio Grande gravels (intermediate-felsic volc 10% quartzite, 7-10% granite, 1% chert, 1-2% limestone). The sand is fl-vcu, subrounded, and mostly Rio Grande provenance. Massive with minor v thin- thin. lenticular beds. Lower 10 cm is particularly gravelly. Interpreted as fan sed mostly reworking axial sediment (maybe from an older terrace)?	0.70	1.10
C	SANd: Sand is massive and mU to vcU (mostly mU). Trace-7% scattered very fine to coarse pebbles, increasing up-section. Sand is Rio Grande sand with 10% lithics-mafics 10% - 12% orange-colored grains.	0.10	0.40
B	GRAVEL: Clast-supported, rounded to subrounded, vf-vc pebbles from Rio Grande. Moderately sorted and composed of volcanic rocks (felsic to intermediate), 1-3 % granite, 5-10% quartzite. 205 degree clast imbric, loose, massive . Upper contact is gradational over about 10 cm.	0.15	0.30
A	SAND: 10YR 6/3 mL-mU-cU sand (mostly mL-mU). Horizontal, very thin bedded and loose; sand is subrounded to lower well to upper moderately sorted; grains composed of clear grains (quartz, sanidine, plagioclase) with 20% orange-colored grains and 10% mafics to lithics. @0.05 m: OSL sample SanAcac-01. Not submitted for OSL dating. UTM coordinates: 13S 330023m E, 3795055m N (NAD 83).	0.15	0.15
	BASE OF SECTION: 330023 ± 3 m E; 3795055 ± 3 m		

West San Acacia stratigraphic section. This section consists of Matanza formation axial-fluvial sediment. The base is not exposed. No PLSS description is available because the site is in the middle of a former land grant. Measured and described by Dan Koning on July 12, 2023, using an Abney level, Brunton compass, Jacob's staff, and hand-held GPS unit.

Unit	Description	Thickness (m)	Height (m)
	Axial-fluvial facies of Qt2		
	Bottom and top of stratigraphic section: 325077 ± 3 m E; 3793807 ± 3 m N; zone 13, NAD83. **Terrace tread not reached.**		
D-7c	SILT AND VERY FINE SAND: Massive, slightly hard silt and very fine sand. Ph with orange shovel.	0.4	9.6
D-7b	BROWN CLAY	0.05	9.15
D-7a	FINE SAND: 10YR 5-6/3, fU sand composed of clear grains (quartz, plagioclase, sanidine), 10% orange-colored grains, and 3-5% mafics-lithics. 0.3-0.5 meters.	1.5	9.1
D-6	SAND: 10YR 6/4-7/3, fU-mU (mostly mL-mU), massive sand with 0.5% silt-clay. Sand is composed of clear grains (quartz, plagioclase, sanidine), 2-5% orange-colored grains, 3% lithics and 2% mafics. 5-10% orangish stains (10YR 7/6-8), often circular and seems to correspond with burrows; slight cementation differences also seen to outline accentuate old burrows. Upper contact gradual over 2-3 cm. @7.6 m: 3 cm thick, 10YR 6/2 clay bed.	0.9	7.6
D-5	SAND: 10YR 6/4 with one third to four-tenth mottling of 10YR -7.5YR 5/6. Sand is massive and composed of clear grains, 12-15% orange-colored grains, 3% volcanic rich lithics and 2-3% mafics. Sharp planer to slightly wavy upper contact.	0.9	6.7
D-4	SAND: 10YR 6/3, fU-mU (mostly ML), well sorted, subangular to subrounded sand composed of clear grains (quartz, sanidine, plagioclase), 15% orange-colored grains, 3% volcanic grains, 1-3% mafics. Weakly consolidated, much orange staining in lower half. Upper contact: gradual over 1-2 cm.	0.3	5.8
D-3	SAND: 10YR 6/3, horizontal planar-laminated, fL-mL (mostly fU) sand that is well sorted, subangular, and composed of clear grains, 15% orange-colored grains, 2-3% lithics, 2-3% mafics to weakly consolidated. Weakly consolidated. Photo with color book. @ 5.1-5.5 m: Laminations are more vague and sand is fU.	1.1	5.5
D-2	SAND: Cross laminated, medium-gr sand. Exhibits well-defined cross laminations 1-2 mm thick. 10YR 6/2-3 and 5/3 (moist). Sand is mL-cL, well sort, subangular to subrounded and composed of clear grains, 15% orangies, 2-5% volcanic dominated lithics and 1-2% mafics. Very minor volcanic, subrounded pebbles. @ 3.9 m: center of 15cm thick interval with abundant lamina having 5% CU-VCU sand and 3% clay rip-ups; weakly consolidated 1-3% vf-m pebbles. @ 3.2-3.7 m. 10YR 6/2, horizontal planer laminated sand that is mL-cL (mostly MU), well sort, subangular to subrounded. Sand is composed of clear grains (quartz, sanidine, plagioclase), 2-3% dk lithics, 2-3% mafics, and 15% orangies. Photo with pen.	1.2	4.4

	Note All units' "orange-colored grains" comprise mostly stained quartz with 5% kspar (including granite fragments) and 1-3% chert. Top contact is gradual over 1-2 cm.		
D-1c	SAND: 10YR 6/2-3 massive, mL-mU sand that is well sorted and subangular-subrounded (mostly subangular). Sand composed of clear grains, 15-17% orange-colored grains, 2% dark lithics and 3% mafics. @ 2.9 m: ~2 cm thick, orange-stained band, stratiformal.	0.7	3.2
D-1b	SAND: 10YR 6/3, fU-mL sand, as in D-1a. Top contact is gradual over a few cm.	0.3	2.5
D-1a	SAND: 10YR 6/3 (moist), massive, mL-mU sand (mostly mL): well sorted, subangular to subrounded, and composed of clear grains (quartz, sanidine, and plagioclase), 5% granite fragments and kspar, 10% orange-yellow quartz [minor chert], 3% dark volcanic and mafics. Sand is weakly consolidated and non-cemented. Top contact gradual over several cms. 1.4 -2.2 m	0.8	2.2
B	AXIAL-FLUVIAL SAND: 10YR 7/2-6/3 and vaguely horizontal-planar laminated. Sand is mU, well sorted, subrounded, and loose. **@130-140 cm: OSL sample SanAcac-03 (325078 ± 3 m E; 3793808 ± 3 m N; zone 13, NAD83.).**	0.20	1.40
A	AXIAL-FLUVIAL SAND: 10YR 6-7/2 and horizontal-planar laminated. Sand is mL-mU, subangular-subrounded, well sorted sand containing clear grains (quartz, sanidine, plagioclase, 10% orange grains, 10% lithic-mafics). **BASE OF TERRACE SEDIMENT NOT OBSERVED.**	1.20	1.20
	BASE OF SECTION: 325078 ± 3 m E; 3793808 ± 3 m N; zone 13, NAD83.		

North Coyote stratigraphic section. This section consists of Matanza formation axial-fluvial sediment. The base is not exposed. Measured in NW1/4NW1/4 of Sec. 28, T. 2 S., R. 1 E., New Mexico Meridian. Measured and described by Dan Koning on December 29, 2024, using an Abney level, Brunton compass, Jacob's staff, and hand-held GPS unit.

Unit	Description	Thickness (cm)	Height (m)
	Axial-fluvial facies of Qt2		
	Bottom and top of stratigraphic section: 325077 ± 3 m E; 3793807 ± 3 m N; zone 13, NAD83. Elev from 4.5 m DEM: 1432 m. Top elev using strat section thickness is 1436		
5	Axial-fluvial sand: Top: flat terrace surface of gravel pavement composed of medium to very coarse pebbles and 15% cobbles. Clasts are red siltstone – very fine sandstone with 25% limestones. Above 20.5: no exposure but probably gravel interbeds: pebbly on bottom but above ~22 m it coarsens upwards to be primarily cobbles and pebbles. Gravel is angular to subangular, poorly sorted, reddish siltstones and vf sandstones, with 25% grey limestone. Above 0.6 m above contact: reddish sand and brown to slightly reddish, muddy sand beds that are fL–fU–mL (mostly fU); poorly exposed. Lower 0.6 m of Unit 5 is fU axial fluvial sand interbedded with minor thin brown clay. Unit 5 is poorly exposed sand is fine grained, slightly reddish sand is FL-ML, summarily FU At 24.8: total thickness. 327559 E 3776105 N ph of 4/3/2 yellowish sand	5.8	24.8
4	Axial-fluvial, gravelly sand: Sand fraction is mU –vcU, moderately sorted, and subrounded to subangular. Sand is composed of quartz and other clear grains, including sanidine; 10-15% orange colored grains; 10-15% lithic grains. Lag gravel seen on surface consists of subrounded to poorly sorted, vf-vc pebbles of felsic volcanic to intermediate volcanic rocks, 1% pilar phyllite, 5% quartzite, 20-25% granite, 15% Abo-Yeso reddish clasts, 1-3% limestone, 1-5% tannish sandstone. @ 18-19 m: Abundant locally derived limestone and Abo-Yeso reddish clasts; much of these clasts are cobbles and boulders; the locally derived clasts are mixed with exotic Rio Grande gravel and axial-fluvial sand. Top of unit is an abrupt and scoured contact. Sample taken in basal 2 ft. Top of unit: UTM coordinates of 327558 m E, 3776090 m N: From here we head north	2.3	19
3	Floodplain clay: Reddish-brown clay in lower half mix with minor silt. Upper half slightly grey clay, less silt. Upper 10 cm is back to reddish-brown clay (med-thick tabular beds) upper contact scoured w/10 cm relief.	0.6	16.7
2	Axial-fluvial sand and pebbly sand, exposure to the northwest (above 1.5 m above base): B/t 15.4 and 16.1 m: Massive, mL-mU sand that shows signs of bioturbulation by burrows in upper 30 cm; burrow forms are up to 1 cm wide. Below 15..8 m. sediment is churned up and in a massive texture. Upper 15 cm has discontinuous red-clay blocks, 10-30 cm long, primarily clayey fL-fU sand. Upper Contact with unit 3 is sharp and relatively planer.	7.8	16.1

	@15.3-15.4 m: 10 cm of silt and very fine sand; sharply overlain by 10 cm of brownish clay; lower contact has 1 cm of wavy relief. Upper contact shows sand filled desiccation cracks. @14.7 m: mL-mU sand. @14.3 m: Horizontal planer laminated sand, size ranges from fU-mU and fU-cL (well to moderately sorted, respectively); 1% scattered vf-medium pebbles of volcanic rocks. 1-5% tangental cross laminations to 5 cm thick, facing SSE. Sand sample. Photo with hammer. **@ 12.1 m OSL sample taken called Coyote-01**. Below, sediment is a sand that is mU-cL and horizontal planer laminated. Sand has 10-12 % orange-colored grains, 10-12% volcanic lithic grains and mafics, subrounded to subangular. @ 9.8 m: UTM coordinates of 327580 ± 3 m E; 3776070 ± 3 m N; zone 13, Axial-fluvial sand and pebbly sand, exposure to the southeast (lower ~1.5 m of unit): Pale brown (10YR 6/3), massive, loose sand. Sand is mostly medium grained (1-10% coarse to very coarse sand grains and 1-10% pebbles), moderately sorted, subangular to subrounded, and composed of quartz and clear feldsp1424 m1421ar with 10-15% potassium feldspar grains and 10-15% lithic grains. Gravel is heterolithic and contains minor exotic clasts from the north, such as cherts and quartzites. Most gravel types are volcanic rocks, granite, or Paleozoic-Permian sedimentary rocks. Unit 2/ Unit 1 contact to south: UTM coordinates of 327582 ± 3 m E; 3775988 ± 3 m N; zone 13, NAD83. From here shoot to 315 degrees and gain 1.5 m, with an estimated vertical error of 0.4 m. Base of staff at the contact.		
1	Distal alluvial fan-marginal floodplain facies: Reddish, thin, tabular beds composed of silt and very fine sand (minor fine sand). Moderately to well consolidated bu no cementation. Upper Contact scoured, slightly wavy few centimeters scour relief. See Figure 1.24 of Day 1 field trip for 2022 FFC. **BASE OF UNIT NOT EXPOSED.**	8.3	8.3
	BASE OF SECTION: 327572 ± 3 m E; 3775977 ± 3 m N; zone 13, NAD83. Elev from 4.5 m DEM: 1412 m.		

Escondida – Jaral Largo Formation stratigraphic section. This section consists of two tongues of alluvial-fan or distal-piedmont facies and mainstem Rio Grande fluvial facies belonging to the Jaral Largo formation. The thickness of the upper distal-piedmont tongue is estimated at 4.5-5 m and was not included in the total section thickness. The base of the Jaral Largo Formation is not exposed locally. The section was measured at an exposure along an arroyo approximately 0.6 km west of the Rio Grande near Pueblito Point, Escondida, Socorro County, New Mexico (SW1/4SW1/4NE1/4 of sec. 24, T. 2 S., R. 1 W., New Mexico Meridian). Measured and described by Andy Jochems on August 5, 2022, using an Abney level and Jacob's staff.

Unit	Description	Thickness (m)	Unit Total (m)
	Total section	5.70	
	Top of stratigraphic section: UTM 13S 325300 m E, 3777473 m N.		
	JARAL LARGO FORMATION , DISTAL FAN FACIES OF TRIBUTARY DRAIANGE TO WEST		
ES-11	SANDY GRAVEL – Poorly to somewhat consolidated, non-calcareous, internally massive to moderately imbricated, very poorly sorted, subangular to rounded pebble-cobble or pebble-cobble-boulder gravel. Clasts consist of 50-90% pebbles, 10-30% cobbles, and 0-20% boulders of lithologies similar to unit 9 but lacking quartzite. Matrix consists of brown (7.5YR 4/3-4), very poorly sorted, angular to rounded, fL-vcL sand composed of 70-75% lithics (felsic > intermediate volcanics), 15-20% quartz, and 10-15% feldspar (pink potassium feldspar > plagioclase) with abundant reddish to purplish brown clay bridges.	>4.5	n/a
ES-10	SANDY PEBBLE GRAVEL – As unit 3 but lacking tangential cross-stratification.	0.50	5.70
ES-9	GRAVEL – Loose, imbricated, very poorly sorted, subangular to rounded pebble-cobble-boulder gravel. Clasts consist of 40-50% pebbles, 30-35% cobbles, and 15-25% boulders of felsic porphyry/volcanics, subordinate intermediate volcanics, and rare to minor breccia, fossiliferous limestone, and quartzite. Paleoflow (imbrication): 042° (n = 17)	0.45	5.20
	JARAL LARGO FORMATION OR POSSIBLE MATANZA FORMATION, RIO GRANDE AXIAL-FLUVIAL FACIES		
ES-8	Sand – Loose, non-calcareous, pale brown (10YR 6/3, moist), internally massive to horizontal-planar or low-angle cross-laminated, well-sorted, subangular to rounded, vfL-fU sand of similar composition as unit 5. Unit is pebbly and exhibits iron oxide staining in upper 0.6 m.	2.10	4.75
ES-7	Pebbly sand – Loose, non-calcareous, light brownish gray to pale brown (10YR 6/2-3, moist), internally massive to low-angle cross-laminated, moderately well-sorted,	0.60	2.65

	subangular to well-rounded, fL-mL sand composed of 60-65% quartz, 20-25% feldspar (pink or orange potassium feldspar > plagioclase), and 10-20% lithics (dark mafics). Occasional pebble stringers are thin, lenticular, and imbricated. Sand exhibits occasional iron oxide staining. Paleoflow (imbrication): 115° (n = 5)		
ES-6	Sandy pebble gravel – Loose, non-calcareous, broadly lenticular, moderately to well-imbricated, poorly sorted, subrounded to well-rounded, sandy pebble gravel. Pebble lithologies include granite, felsic porphyry/volcanics, quartzite, and chert. Sand is similar to unit 7. Iron oxide staining is common.	0.15	2.05
ES-5	Sand – Very poorly consolidated, very weakly calcareous, pale brown (10YR 6/3), internally massive, well-sorted, subangular to rounded, fL-mL sand composed of 50-60% quartz, 20-30% feldspar (plagioclase > orange potassium feldspar + glassy sanidine), and 15-20% lithics (dark mafics and reddish felsic volcanics). In lower 25 cm and upper 5 cm are dark reddish brown (5YR 3/3, moist), massive mud stringers up to 3 cm thick. Optically simulated luminescence (OSL) sample Journ-1 collected at waypoint 002 (see below) on July 12, 2022 by Dan Koning and Andy Jochems. Waypoint 002: shoot approximately 025° to base of unit ES-5 (UTM 13S 325297 m E, 3777466 m N).	0.75	1.90
ES-4	Sand – Poorly consolidated, very weakly calcareous, pale brown (10YR 6/3), internally massive, well- to very well-sorted, subangular to rounded, slightly silty to clayey vfU-fL sand composed of 85-90% quartz and feldspar, and 10-15% lithics (dark mafics). Iron oxide staining is common. Basal 3-5 cm consists of dark brown, fine, disseminated organic matter. JARAL LARGO FORMATION, DISTAL-PIEDMONT FACIES	0.40	1.15
ES-3	Sandy pebble gravel – As unit 1 but well-imbricated to tangentially cross-stratified and with iron and/or manganese oxide staining on subangular to rounded pebbles of mostly felsic volcanics. Paleoflow (imbrication): 043° (n = 7)	0.20	0.75
ES-2	Silty sand – Very poorly consolidated, weakly calcareous, light brown (7.5YR 6/4), massive to vaguely thin-bedded, internally massive, well-sorted, subangular, silty vfL-fL sand composed of 65-70% quartz and feldspar, and 30-35% lithic grains. Occasional stringers of cL sand to granules exhibit iron and/or manganese oxide staining.	0.30	0.55
ES-1	Sandy pebble gravel – Loose, non-calcareous, lenticular, weakly imbricated, poorly sorted, subrounded, sandy pebbly gravel. Pebbles are composed primarily of felsic volcanic lithologies. Sand consists of brown (7.5YR 4/3-4, moist), very poorly sorted, angular to subrounded, fU-vcL grains composed of 60-65% lithics (felsic volcanics with lesser intermediate volcanics and limestone), 20-25% quartz, and 15-20% feldspar. Iron oxide staining is common throughout the unit. **BASE OF UNIT NOT EXPOSED.**	0.25	0.25

Base of stratigraphic section: UTM 13S 325295 m E, 3777462 m N.

Photos of section: 20220805_163103, 20220805_163129, 20220805_163146

APPENDIX D—TOPOGRAPHIC PROFILES, OSL SAMPLE LOCATIONS, AND TERRACE STRATIGRAPHY AT STUDY SITES ALONG THE RIO GRAND

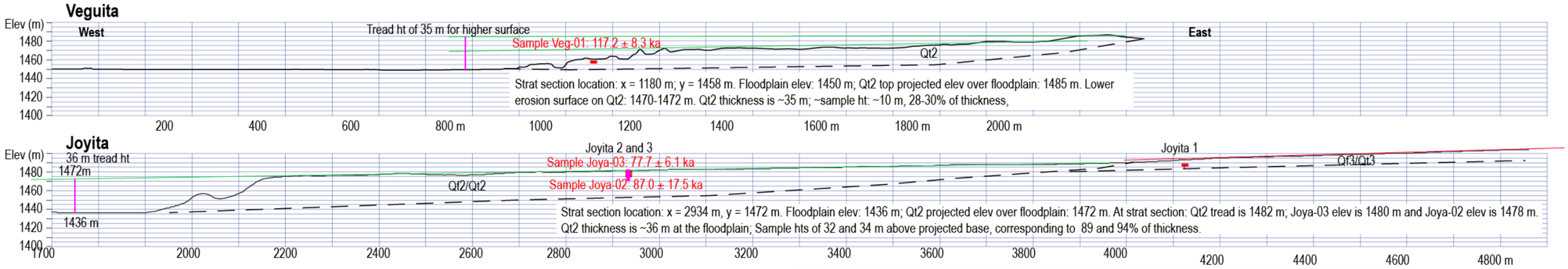

Endpoints of topographic profiles (UTM coordinates, NAD83, zone 13)

	SW end	Bend	NE end
Veguita	336711 E, 3819944 N		338964 E, 3819344 N
Joya	329179 E, 3804051 N (NW end)		332988 E, 3801056 N (SE end)
San Acacia East	329847 E, 3794557 N		330114 E, 3795338 N
San Acacia West	324786 E, 3793280 N		325405 E, 3794418 N
Journey	324549 E, 3776599 N		326162 E, 3778264 N
North Coyote	326095 E, 3775725 N	327856 E, 3776187 N	328476 E, 3776524 N
South Coyote	326323 E, 3774387 N		329200 E, 3774879 N

Explanation

- Topographic profile
- Inferred projection of base of terrace fill
- Best-filt line and projection of the Vallle de la Parida surface
- Best-filt line and projection of the Loma Parda surface
- OSL sample location
- Height or thickness measurement from plot
- Stratigraphic section

APPENDIX E—REPORT OF RESULTS FOR LUMINESCENCE DATING OF SEDIMENT FROM THE RIO GRANDE TERRACES, SOCORRO

For samples: Joya-01, Joya-02, Joya-03, SanAcac-02, SanAcac-03, Veg-01, Journ-01, Coyote-01

Luminescence Laboratory, Desert Research Institute

Report of Results

Rio Grande Terraces, Socorro, NM

Christina Neudorf, PhD
Assistant Research Professor-Geology
Manager of E.L. Cord Luminescence Lab
Desert Research Institute
2215 Raggio Parkway
Reno, NV 89512-1095
775-673-7407
Christina.Neudorf@dri.edu

07/19/2023

Dan Koning, Senior Field Geologist
New Mexico Bureau of Geology and Mineral Resources
New Mexico Institute of Mining and Technology
801 Leroy Place
Socorro, NM 87801

LUMINESCENCE DATING OF SEDIMENT FROM THE RIO GRANDE TERRACES, SOCORRO

Site: Socorro 100K sheet Rio Grande terraces

Estimated age or other age control: Middle-late Pleistocene

SUMMARY

Results from luminescence dating using multi-grain aliquots of K-feldspar following a post-infrared infrared (post-IRIR) single-aliquot regenerative dose (SAR) protocol (Murray and Wintle, 2000; Thiel et al., 2011) suggest that sample ages are as follows:

Sample Field ID	Sample Lab ID	Age (ka before 2022)
Joya-01	FC001	126.4 ± 25.4*
Joya-02	FC002	87.0 ± 17.5
Joya-03	FC003	77.7 ± 6.1
SanAcac-02	FC004	79.8 ± 23.8
SanAcac-03	FC005	97.0 ± 5.3
Veg-01	FC006	117.2 ± 8.3
Journ-01	FC007	68.1 ± 5.8
Coyote-01	FC008	75.5 ± 6.4

*Minimum age estimate. See text for explanation.

Laboratory Procedures and equipment

All laboratory procedures were conducted under dim red (>660 nm) lighting conditions specific to luminescence preparation and analysis.

Sample preparation

The sediment in both ends of the 30 cm long sample tube was removed to a depth of ~3 cm and used for dose rate and water content measurements. A reserve portion of the sample was removed and stored in safe light conditions. The remaining portion of the sample was prepared for analysis as follows:

- Treatment with sodium pyrophosphate decahydrate ($Na_4P_2O_7.10H_2O$) to deflocculate.
- Isolation of target grain size (180-250 μm or 250-355 μm) by wet sieving.
- Treatment with 10% HCl to remove carbonates.
- Treatment with 30% H_2O_2 to remove organics.
- Separation of magnetic sub-fraction using a hand magnet.
- Mineral density separation with heavy liquid (lithium heteropolytungstate) to isolate potassium (K) feldspar (ρ <2.58 gcm^{-3}).
- Feldspars were etched in 10% hydrofluoric acid (HF) for 10 min, followed by treatment with 10% HCl overnight to remove fluorides.
- Wet sieving to remove grains that were reduced to <180 μm (or <250 μm) by the HF etch.
- Mounting of 1 mm diameter aliquots of grains onto 9 mm stainless steel disc.

Instrument configuration for analysis

All measurements were made on Risø TL/OSL readers model DA-20, serial #243 or #244 using continuous wave measurements of the luminescence signal. Infrared stimulation (IR) on multi-grain aliquots was made with a cluster of Vishay TSFF 5210 IR diodes with peak emission at 870 nm, maximum power of 115 mW/cm^2 at the sample position. Single-grain stimulation was conducted using an IR diode (830 nm), 140 mW TTL modulated laser. Feldspar luminescence (410 nm) was detected through Corning/Kopp 7-59 and Schott BG39 filters.

The Post-$IRIR_{290}$ protocol

Feldspar luminescence signals were measured using the post-$IRIR_{290}$ single aliquot regenerative-dose protocol (Table 1). Because the IR stimulated luminescence (IRSL) signal from feldspar is known to fade over geological time periods, this fading rate must be measured and corrected for (Huntley and Lamothe, 2001; Huntley and Lian, 2006). More recently, post-IRIR luminescence dating protocols have been developed which measure the IRSL at an elevated temperature (e.g., 290°C, Table 1) after an IR stimulation at 50°C. The post-IRIR signal has been shown to fade less than the traditional IRSL signal, or not at all, which reduces error associated with fading corrections (Buylaert et al., 2009; Thiel et al., 2011).

Experiments were conducted to determine the suitability of the post-$IRIR_{290}$ signal for dating. Dose recovery tests were conducted on both multi-grain aliquots and single grains on sample FC001. Despite the high number of grains (52 out of 500) that passed SAR rejection criteria (below), only 71% of the original laboratory-administered dose was recovered during the single-

grain test. A dose recovery test on multi-grain aliquots (n=24) yielded a weighted mean measured/given dose ratio of 1.04 ± 0.02 and an overdispersion of <1%. This suggests that the protocol in Table 1 is suitable for multi-grain aliquots. Post-IRIR$_{290}$ signals from aliquots are adequately bright (thousands of counts per 0.1 second, Fig. 1A), and generate dose response curves that saturate at ~600-1000 Gy (Fig. 1B).

Table 1. The SAR measurement protocol used in this study.[1]

Step	Post-IRIR$_{290}$
1	Natural/Regenerative Dose
2	Preheat (320°C, 60 s)
3	IR diodes (50°C, 200 s)
4	IR diodes (290°C, 200 s) → L_n, L_x
5	Test dose (~6 Gy)
6	Preheat (320°C, 60 s)
7	IR diodes (50°C, 200 s)
8	IR diodes (290°C, 200 s) → T_n, T_x
9	IR diodes (325°C, 100 s)
10	Return to step 1.

[1]Ln = natural signal, Lx = regenerative dose signal. Tn = test dose signal measured after Ln, Tx = test dose signal measured after Lx. All steps of each protocol constitute one SAR cycle. The first SAR cycle measures the sensitivity corrected natural signal, and subsequent SAR cycles measure the Lx/Tx value after a series of successively increasing laboratory radiation doses (regeneration doses) administered to the sample. The regeneration doses are used to generate a dose-response curve (where 'x' values are the given radiation doses, and 'y' values are measured Lx/Tx signals) onto which the natural signal (Ln/Tn) is plotted to calculate the equivalent dose (De) value. Regeneration doses include: 1) one "zero-dose" point where no radiation dose is given to check for recuperation, and 2) one "repeat-dose" point (Rr), where a previous regeneration dose (R1) is given a second time to perform a recycling ratio test (Murray and Wintle, 2000).

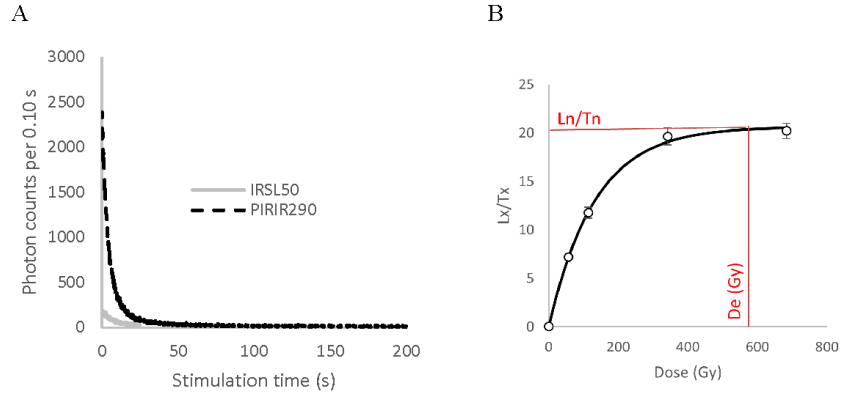

Figure 1. A) IRSL$_{50}$ and Post-IRIR$_{290}$ signals measured from one aliquot of sample FC001. B) A dose response curve measured from one aliquot of sample FC001. The De value is determined by where the sensitivity-corrected natural signal (Ln/Tn) intersects the dose response curve. Saturation occurs where the dose response curve flattens out at doses of ~600 to 1000 Gy.

Fading measurements and corrections

Fading rates were measured from samples FC002, -004, -006, -007 and -008 using the procedure of Auclair et al. (2003). These were found to be 0.83 ± 0.13, 0.07 ± 0.16, 0.67 ± 0.44, -0.04 ± 0.86, and 1.07 ± 0.11 %/decade for FC002, -004, -006, -007 and -008, respectively. Because the fading rates for samples FC004 and FC007 are equivalent to zero within 1 sigma, these are deemed negligible, and these samples were not corrected for fading. Due to their close geographic proximity, ages for samples FC001 & -003 were corrected using the fading rate of sample FC002, and the age for sample FC005 was corrected using the fading rate of sample FC008. Sample aliquot De values and ages were corrected for anomalous fading using the dose rate correction (DRC) method of Lamothe et al. (2003) and the calc_Lamothe2003 function of the Luminescence R package (Kreutzer and Mercier, 2020).

Bleaching tests

Bleaching tests were conducted on samples FC002 and FC008 to determine the rate of bleaching of the post-IRIR$_{290}$ signal. The signal is depleted to <3% of the natural signal in 28 hours (Fig. 2). These results suggest that grains that have experienced 28 h or more of sun exposure prior to their most recent burial event are likely to have a maximum residual dose of 0.3 Gy that is equivalent to a residual age of ~90 and 80 years for samples FC002 and -008, respectively. Even after only 1000 s (17 min) of sun exposure, aliquot doses are reduced to <6 Gy. This roughly equates to ~1730 and ~1190 years for FC002 and -008, respectively, which is insignificant relative to the age of the samples in this study.

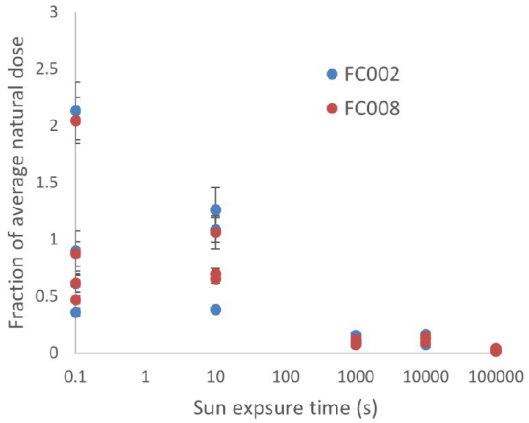

Figure 2. Bleaching rate for K-rich feldspar aliquots from samples FC002 and FC008 that were exposed to the sun for 10 s, 1000 s, 10,000, and 100,000 s (4 aliquots per sample per exposure time).

De measurement and age calculation

The final equivalent dose (De) for all samples was measured from multi-grain aliquots of ~15 grains each using the post-IRIR$_{290}$ signal (Table 2, Fig. 3). Dose response curves were fitted using an exponential curve (Fig. 1A). Routine screening criteria included rejection of aliquots that exhibited the following behavior:

- Poor signals as judged from net natural signals less than three standard deviations above the background.
- Failure to reproduce, to within 10%, the same signal from identical regeneration doses given at the beginning and end of the SAR sequence, which suggests inaccurate. sensitivity correction (recycling test).
- Maximum test dose error of > 10%.
- Recuperation values >5%.
- Saturation: i.e., the natural signal (Ln/Tn) is higher than the saturated part of the dose response curve.

The high irradiation doses required to measure samples of this age limited the amount of measurement time that could be allocated to each sample, so a maximum of 24 multi-grain aliquots were measured per sample. After screening, the total number of aliquots used for age calculation was reduced further, so resulting dose distributions and ages should be viewed with caution. The number of saturated aliquots per sample, i.e., aliquots where the natural signal failed to intersect the dose response curve because it was higher than the level of saturation, ranged from 0 to 18 (Table 2, column "n"). The majority of aliquots measured from sample FC001 (18 out of 24) were saturated, therefore the calculated age of this sample is considered to be a minimum age. Kernel density estimates (KDE) and abanico plots (Fig. 3) were used to examine the D_e distribution for evidence of partial bleaching or mixing and to determine the most appropriate dose model to use for age calculation for samples FC002-008. The central age model (CAM) of Galbraith et al. (1999), which assumes that all grains have been sufficiently bleached prior to burial, was applied to samples FC001, -003, -006, -007, and -008 (blue lines in Fig. 3). These samples had relatively low overdispersion, approximately symmetrical, unimodal De (age) distributions and/or dominent KDE peaks at the CAM dose. Ages were calculated using the dominant KDE peak for the rest of the samples (blue lines plotted for FC002, -004, -005 in Figure 3), as it is believed this peak most likely represents the most recent bleaching event.

Dose rate determination

Samples for dose rate measurements were dried and milled to a fine, flour consistency and sent to ALS Geochemistry in Reno, NV for geochemical analysis of U, Th, Rb and K_2O. U, Rb and Th samples were fused with lithium borate and measured with ICP-MS. K_2O was measured from the bulk sample with ICP-AES and converted to %K. Dose rates (Gy/ka) were calculated using the conversion factors of Liritzis et al. (2013) and are shown to 2 decimal places; ages were calculated prior to rounding.

Sample water contents were measured in the laboratory and average 2.3% (expressed as the percentage of the mass of dry sediment). Because the samples are suspected to have been relatively dry throughout most of their burial history, this value was used to calculate water-corrected dose rates, and a high estimated standard error of 5% was applied to account for variations in water content during sample burial. Cosmic dose rates (Gy/ka) were calculated according to Prescott and Hutton (1994). Dose rates were calculated using DRAC (Durcan et al., 2015).

Table 2. IRSL ages for Rio Grande Terraces, Socorro, NM.

Sample number	Fading rate[a] (%/decade)	Depth (cm)	n[b]	OD (%)	D_b (Gy)[c]	U (ppm)	Th (ppm)	Rb (ppm)	K (%)	External alpha dose rate wet (Gy/ka)	External beta dose rate wet (Gy/ka)	External gamma dose rate wet (Gy/ka)	Cosmic dose rate (Gy/ka)[d]	Total dose rate (Gy/ka)[e]	Age (ka)[c, f]
FC001	0.83 ± 0.13	1.6	3 (18, 24)	21	476.9 ± 100.4	1.64	4.56	71.1	1.93	0.09	1.69	0.86	0.23	3.77 ± 0.24	126.4 ± 25.4*
FC002	0.83 ± 0.13	3.8	15 (3, 24)	23	298.6 ± 63.0	1.44	3.68	67	1.76	0.08	1.52	0.76	0.18	3.43 ± 0.22	87.0 ± 17.5
FC003	0.83 ± 0.13	1.05	15 (6, 24)	19	288.5 ± 29.0	1.66	3.82	72	1.91	0.09	1.66	0.83	0.24	3.71 ± 0.24	77.7 ± 6.1
FC004	N/A	3.34	24 (0, 24)	26	275.0 ± 15.3	1.18	3.29	64.9	1.87	0.07	1.56	0.74	0.18	3.45 ± 0.23	79.8 ± 23.8
FC005	1.07 ± 0.11	8.23	16 (6, 24)	17	359.6 ± 31.4	1.11	3.18	68.2	1.94	0.06	1.61	0.74	0.11	3.42 ± 0.23	97.0 ± 5.3
FC006	0.67 ± 0.44	7.5	19 (4, 24)	23	456.3 ± 46.4	1.25	2.99	74.4	2.13	0.05	1.69	0.78	0.12	3.90 ± 0.29	117.2 ± 8.3
FC007	N/A	4.4	11 (2, 24)	11	303.4 ± 17.0	1.96	6.51	106	2.47	0.12	2.16	1.12	0.16	4.46 ± 0.28	68.1 ± 5.8
FC008	1.07 ± 0.11	4	18 (2, 24)	32	289.2 ± 31.7	1.38	6.16	64.7	1.73	0.07	1.49	0.86	0.17	3.83 ± 0.27	75.5 ± 6.4

[a] Ages were corrected for moisture using a laboratory-measured water content of 2.3 ± 5 %. Ages were corrected for fading using the Dose Rate Correction (DRC) model of Lamothe et al. (2003). Fading rates were measured from samples FC002, -004, -006, -007 and -008. Due to their close geographic proximity, ages for FC001 & -003 were corrected using the fading rate of sample FC002, and the age for sample FC005 was corrected using the fading rate of sample FC008.

[b] n is the number of D_e determinations accepted after screening and rejection of outliers; in parentheses are the number of saturated aliquots followed by the total number of aliquots measured.

[c] The burial dose, D_b, (or final fading-corrected age) was determined using either the Central Age Model (CAM) (Galbraith et al., 1999), or the most prominent peak in the Kernel Density Estimate plot. The error is the standard error. See text for explanation.

[d] Cosmic dose rates (Gy/ka) are calculated according to Prescott and Hutton (1994).

[e] Dose rates (Gy/ka) were corrected using a laboratory-measured sample-averaged water content of 2.3 ± 5%. Dose rates were calculated using the conversion factors of Liritzis et al. (2013) and are shown rounded to two decimal places; ages were calculated using values prior to rounding.

[f] Luminescence ages, rounded to the nearest 10 years, are expressed as thousands of years before AD 2022. Error is 1 sigma. Starred values are considered minimum ages due to a high number of aliquots in saturation.

FC002

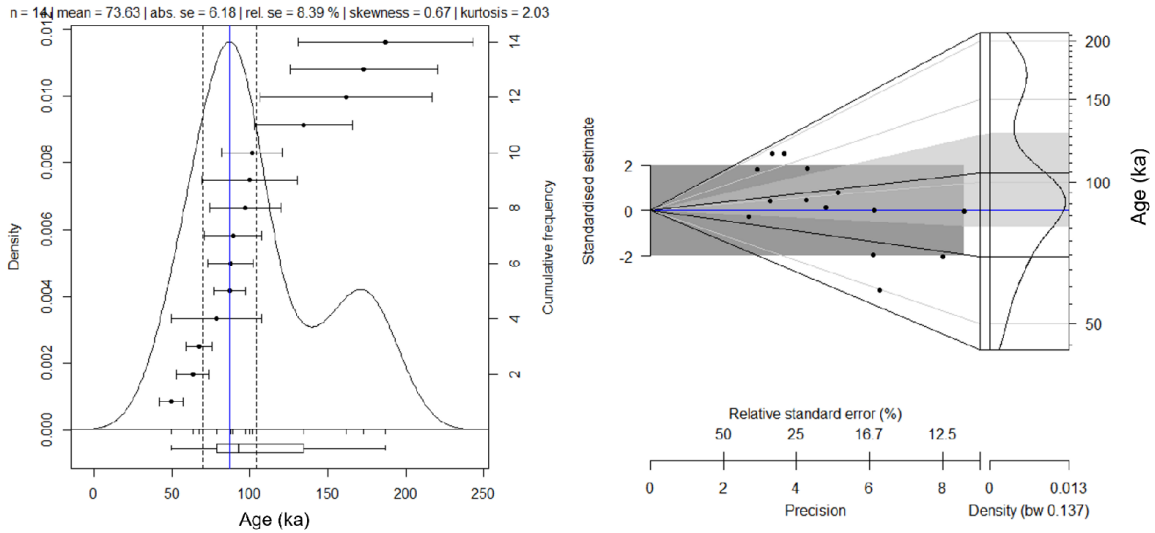

Figure 3. Kernel density estimate (KDE) (left) and abanico plots (right) for fading-corrected sample De (or age) values. Plots were generated using the Luminescence Package in R (Kreutzer et al., 2020). Blue lines (plus or minus 1 sigma marked as dashed black lines) represent the preferred De (or age) estimate. All abanico plots are centered on the preferred De (or age) value and points that lie within the shaded region are within 2 standard deviations of this value. See Appendix B for instructions on how to read an abanico plot.

FC003

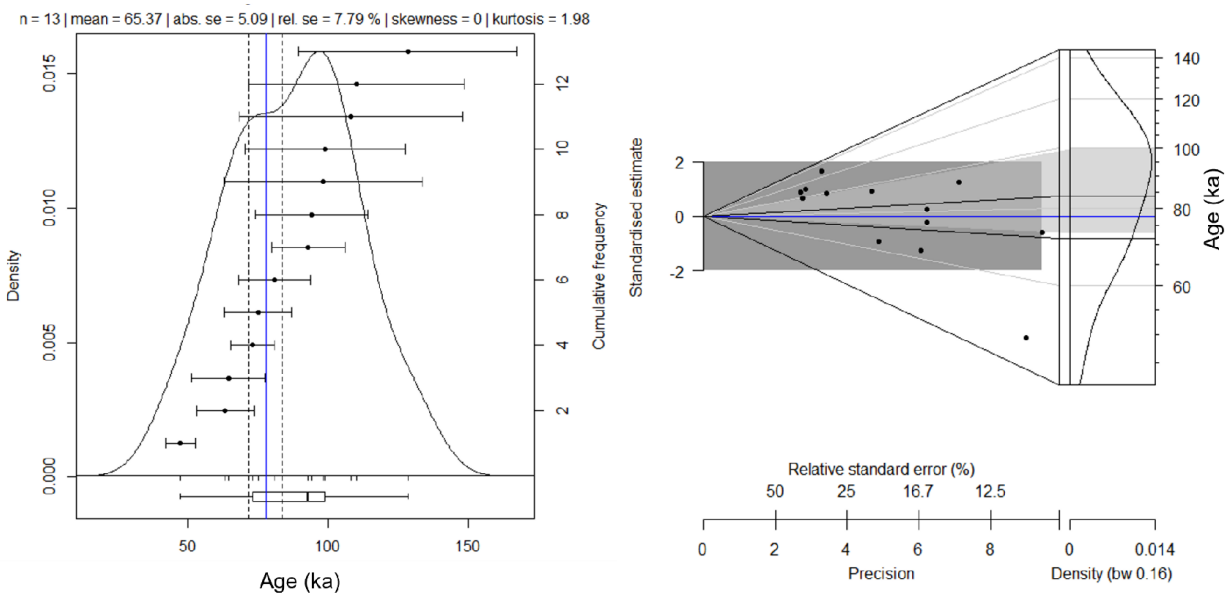

Figure 3. Continued...

FC004

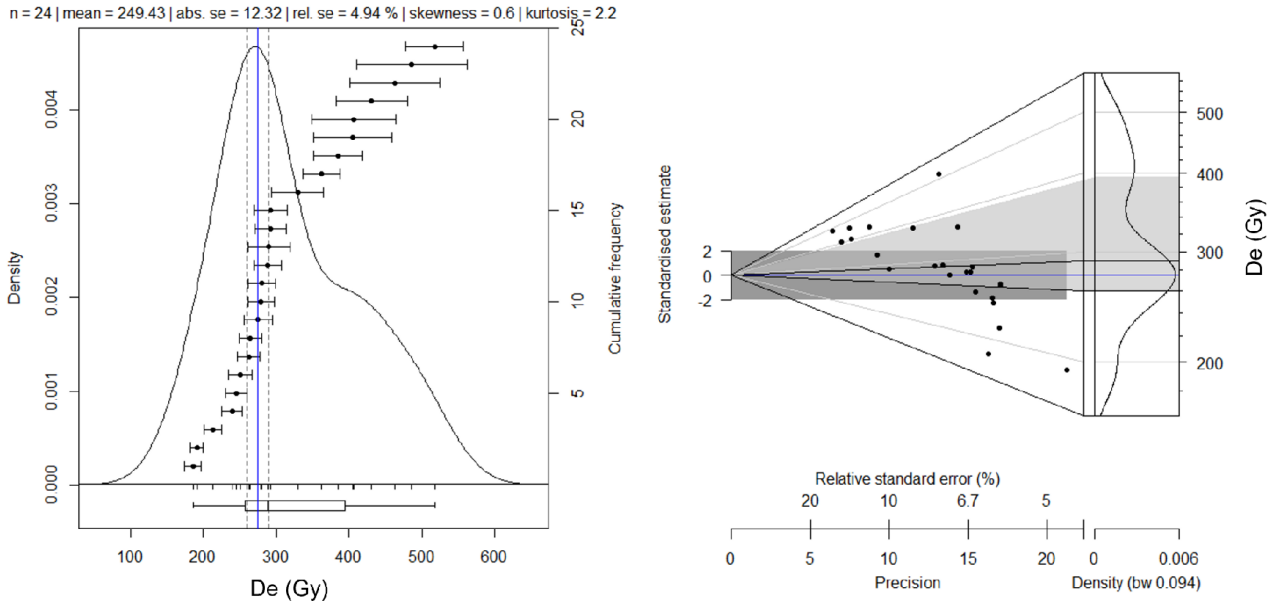

Figure 3. Continued...

FC005

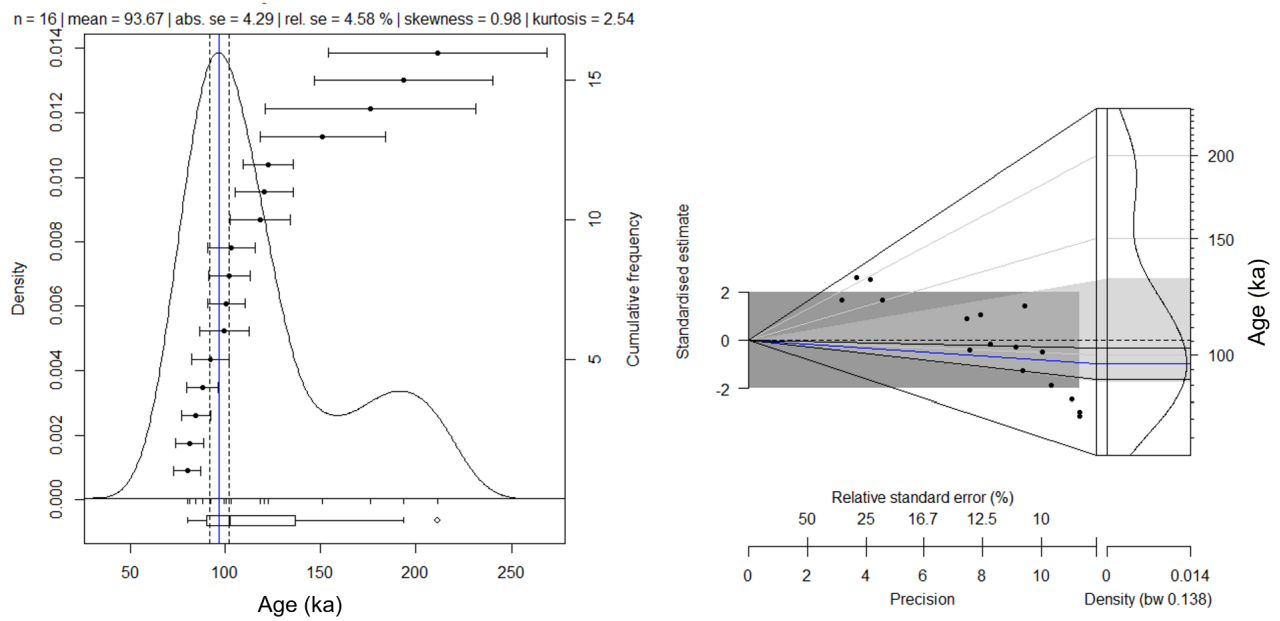

Figure 3. Continued…

FC006

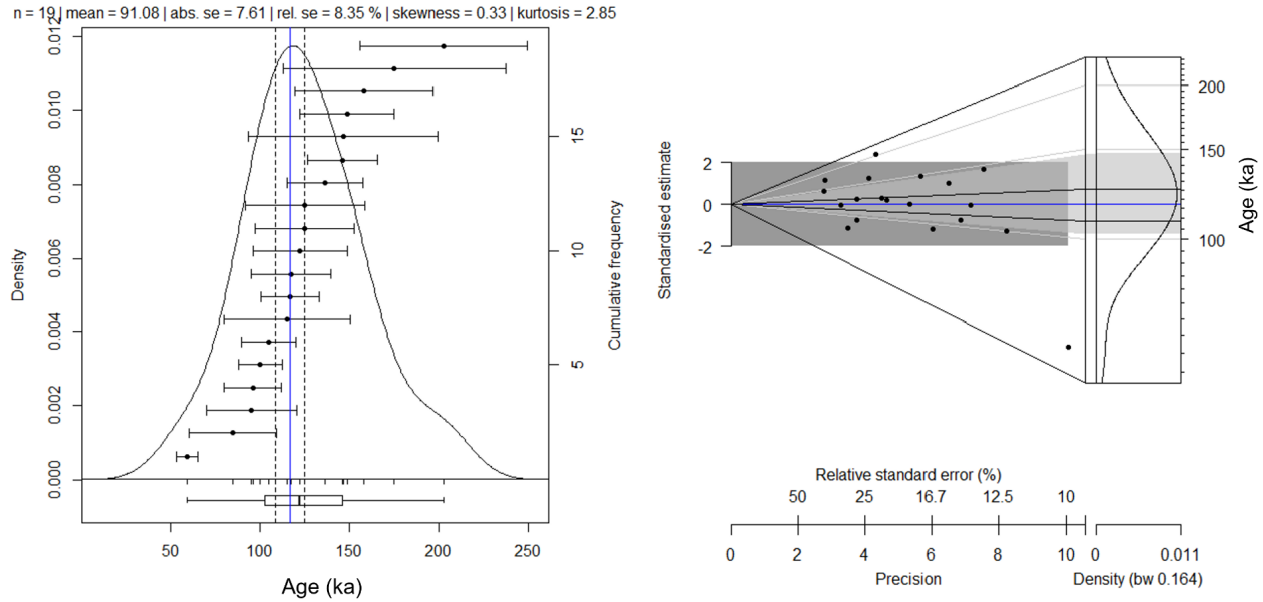

Figure 3. Continued…

FC007

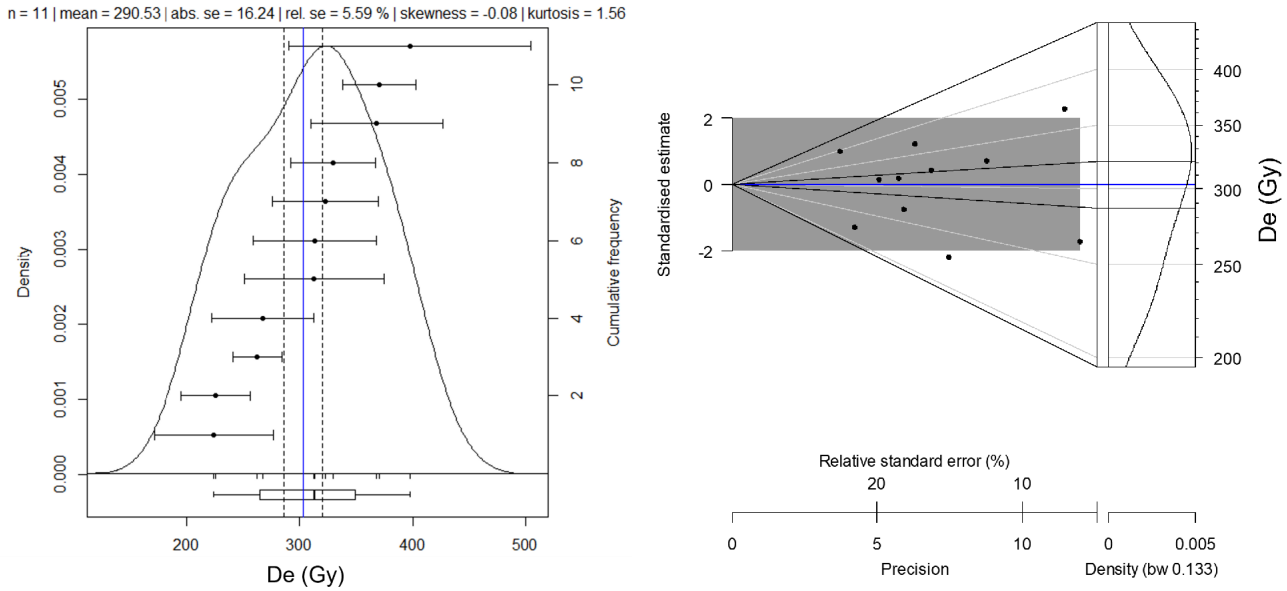

Figure 3. Continued…

FC008

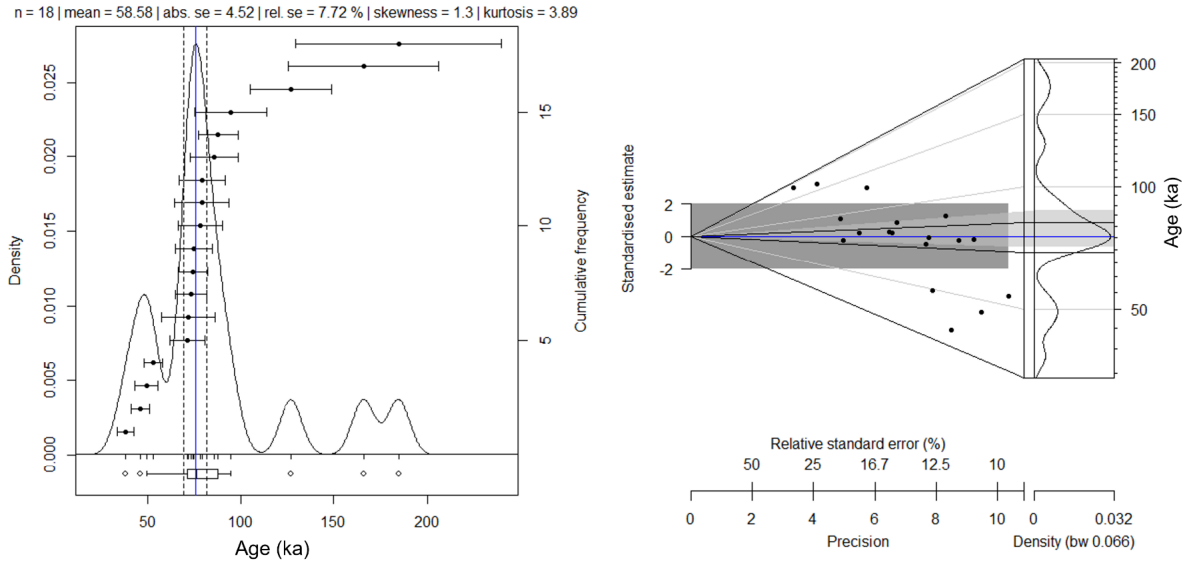

Figure 3. Continued…

References

Auclair, M., Lamothe, M., Huot, S., 2003. Measurement of anomalous fading for feldspar IRSL using SAR. Radiation Measurements, 37, 487–492.

Buylaert, J.P., Murray A.S., Thomsen, K.J., Jain, M., 2009. Testing the potential of an elevated temperature IRSL signal from K-feldspar. Radiation Measurements 44, 560–565.

Durcan, J.A., King, G.E., and Duller, G.A.T., 2015. DRAC: Dose rate and age calculator for trapped charge dating. Quaternary Geochronology, 28, 54-61.

Galbraith, R.F., Roberts, R.G., Laslett, G.M., Yosida, H., Olley, J.M., 1999. Optical dating of single and multiple grains of quartz from Jinmium rock shelter, northern Australia: Part 1 Experimental design and statistical models. Archaeometry, 41, 339–364.

Huntley, D.J., Lamothe, M., 2001. Ubiquity of anomalous fading in K-feldspars and the measurement and correction for it in optical dating. Canadian Journal of Earth Science, 38, 1093–1106.

Huntley, D.J., Lian, O.B., 2006. Some observations on tunneling of trapped electrons in feldspars and their implications for optical dating. Quaternary Science Reviews 25, 2503–2512.

Kreutzer, S., Burow, C., Dietze, M., Fuchs, M.C., Schmidt, C., Fischer, M., Friedrich, J., 2020. Luminescence: Comprehensive Luminescence Dating Data Analysis. R package version 0.9.7. https://CRAN.R-project.org/package=Luminescence

Kreutzer, S., Mercier, N., 2020. calc_Lamothe2003(): Apply fading correction after Lamothe et al., 2003. Function version 0.1.0. In: Kreutzer, S., Burow, C., Dietze, M., Fuchs, M.C., Schmidt, C., Fischer, M., Friedrich, J., Riedesel, S., Autzen, M., Mittelstrass, D., 2020. Luminescence: Comprehensive Luminescence Dating Data Analysis. R package version 0.9.10. https://CRAN.R-project.org/package=Luminescence

Lamothe, M., Auclair, M., Hamzaoui, C., Huot, S., 2003. Towards a prediction of long-term anomalous fading of feldspar IRSL. Radiation Measurements 47, 682–687.

Liritzis, I., Singhvi, A. K., Feathers, J.K., Wagner, G.A., Kadereit, A., Zacharias, N., Li, S-H., 2013. Luminescence Dating in Archaeology, Anthropology, and Geoarchaeology – An Overview. Springer Briefs in Earth System Sciences. 70 pp.

Murray, A.S., Wintle, A.G., 2000. Luminescence dating of quartz using an improved single-aliquot regenerative-dose protocol. Radiation Measurements, 32, 57–73.

Prescott, J.R., Hutton, J.T., 1994. Cosmic ray contributions to dose rates for luminescence and ESR dating: large depths and long-term time variations. Radiation Measurements, 23, 497–500.

Thiel, C., Buylaert, J.P., Murray, A., Terhorst, B., Hofer, I., Tsukamoto, S., Frechen, M., 2011. Luminescence dating of the Stratzing loess profile (Austria) – Testing the potential of an elevated temperature post-IR IRSL protocol. Quaternary International 234, 23–31.

APPENDIX A--BASICS OF LUMINESCENCE DATING

Luminescence refers to a suite of radiative chronological dating techniques whereby the time elapsed since the last exposure of some minerals (primarily quartz) to light or heat in excess of 300°C can be measured. Luminescence dating techniques include optically stimulated luminescence (OSL), thermoluminescence (TL), and infrared stimulated luminescence (IRSL) and have utility for a broad range of geological and archaeological applications. The following summary is adapted largely from Murray and Olley (2002), Duller (2008), Wintle (2008), and Rhodes (2011). When naturally occurring minerals are exposed to emissions released by radioactive decay, electrons may become stored and collected within defects in crystal lattices referred to as 'trapping centers' or 'traps'. Thus, naturally occurring minerals act as dosimeters that record the amount of radiation to which they have been exposed. The burial age of a sample is estimated as the ratio of the energy accumulated during burial and the energy per year delivered by radioactive decay:

$$Age\ (yr) = Equivalent\ dose\ (Gy)/Dose\ rate\ (Gy/year) \qquad Eqn.\ 1$$

When dosed minerals are then re-exposed to light or heat, they release the stored electrons, emitting a photon of light that is referred to as luminescence. This 'bleaching' process empties the electrons stored in the traps and resets or 'zeroes' the signal. Through controlled experiments using special analytical equipment such as a Risø TL/OSL Reader, the emission of luminescence can be controlled and measured. This set of measurements is used to estimate the equivalent dose (D_e). The dose rate is the amount of energy absorbed per year from radiation in the environment surrounding the sample material. It can be estimated by measuring the amount of radioactivity directly or by chemically analyzing the surrounding material and calculating the concentration of radioisotopes.

The age limit of luminescence generally ranges from years to hundreds of thousand years. The lower age limit is restricted by the efficacy of signal resetting, signal sensitivity, and thermal transfer components (signals generated by heating during analysis). The upper age limit is controlled by the capacity of the crystal lattice to store electrons (the number and nature of traps) and the dose rate of the environment. Dose saturation refers to the complete filling of traps such that continued exposure to emissions from radiation decay results in no more accumulation of electrons and thus no increase in luminescence signal. The properties of minerals that control signal sensitivity and dose saturation (as well as other luminescence characteristics) vary even within minerals of a single composition and the dose rate varies in different environments.

Luminescence typically has a high level of accuracy and precision. Age comparisons to samples of known age and to ages derived from independent methods are in excellent agreement indicating a high level of accuracy (*e.g.* Barnett, 2000; Bailiff, 2007; Murray and Olley, 2002; Rhodes et al., 2003; Rittenour, 2008). The combined uncertainty in the measurement of D_e and the measurement of the dose rate typically ranges from 5-10% including random and systematic error. Age estimates are typically reported as a central value with one standard deviation (68% confidence interval) uncertainty in years before the measurement.

Measurement of equivalent dose (D_e): Because there is no systematic relationship between luminescence brightness and radiation dose, the luminescence response of each sample is calibrated through a set of laboratory measurements that are used to derive a measure of D_e. Sediment samples are prepared for measurement by removing carbonates and organic material and isolating a target mineral (typically quartz and/or feldspar) and grain size. Additionally for coarse grains, hydrofluoric acid is used to etch the outer layer of the grains that is affected by alpha radiation. Although there are many approaches to D_e determination (see summaries by Duller (2004) and Lian and Roberts 2006)), the single aliquot

regenerative dose (SAR) procedure (Murray and Wintle, 2000) is now the most widely used owing to its accuracy and broad applicability to quartz, feldspar, and polymineral fine grain OSL, and IRSL. The technique has also been adapted to TL applications. The SAR protocol uses a regeneration approach to sample calibration whereby the natural signal (L_n) is measured and reset, then given a known laboratory dose by exposure to an artificial source of radioactivity regenerating the luminescence signal; the regenerated signal is then measured ($L_{1, 2, 3,...}$)(Fig 1). This procedure is repeated through a series of cycles of heating, light exposure and signal measurement, and irradiation at different regeneration doses. Because the sensitivity of an aliquot (the amount of light emitted per unit of radiation exposure) can change over the course of the measurement, it is monitored by including a small fixed radiation dose or 'test dose' and measuring the OSL signal ($T_{1, 2, 3...}$) during the second half of each SAR cycle. The sensitivity corrected measurements of luminescence signals can be used to construct a dose response curve from which to estimate D_e (Fig 1). Replicate measurements of D_e are made for each sample and then a variety of statistical models (e.g. Galbraith and Green, 1990; Galbraith et al, 1999; Galbraith 2005) are applied to the population of D_e to estimate the total D_e (sometimes 'D_b') used in age calculation. Owing to incomplete zeroing of the luminescence signal during transport and/or mixing after deposition, large amounts of scatter often occur in the population of D_e values measured from a single sample. For samples in these types of environments, single-grain OSL measurements are preferred. This approach replaces the LEDs used for optical stimulation in conventional measurements with a focused laser that can be directed so that each single grain is measured using the SAR protocol.

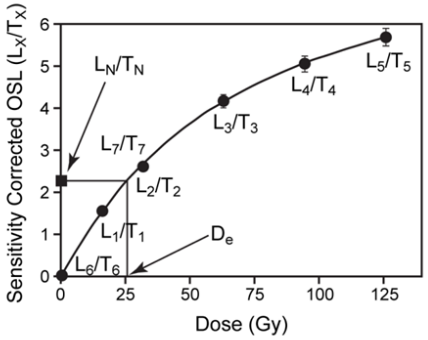

Fig 1. A SAR dose response curve for an aliquot of quartz. The natural signal (Ln) is measured and reset; a known laboratory dose is given by exposure to an artificial source of radioactivity regenerating the luminescence signal; the regenerated signal is then measured (L1, 2, 3,...). The procedure is repeated at varied regeneration doses. The sensitivity is monitored by including a small fixed test dose and measuring the OSL signal (T1, 2, 3...) during the second half of each SAR cycle. Adapted from Duller (2008).

The most commonly used minerals in luminescence are quartz and K feldspar. Luminescence dating is now well established for quartz except where sediment is recently eroded from its source resulting in low sensitivity. K feldspars typically have high sensitivity but are subject to loss of signal from unstable traps referred to as anomalous fading that can lead to age underestimation (Wintle, 1973). To overcome this problem, the rate of anomalous fading can be characterized and a correction applied (*e.g.* Huntly and Lamothe 2001; Aucliar et al, 2003) or a different luminescence signal that does not exhibit anomalous fading may be sought (*e.g.* Degering and Krbetschek, 2007; Novothny et al, Lauer et al., 2011). The property of anamolous fading in feldspars is particularly important in polymineral samples—either quartz that has feldspar inclusions or fine grained samples that contain both quartz and feldspar. Approaches to differentiate quartz and feldspar signals include combined IR and blue stimulation of samples (*e.g.* Wallinga et al., 2002) and pulsed stimulation or 'POSL' (Denby et al., 2006; Thomsen et al, 2008; Feathers et al., 2012).

Measurement of dose rate: Luminescence age calculation requires accurate assessment of both the equivalent dose and the dose rate (the radiation dose received per year by a sample) (Eqn 1). The annual radiation dose can be partitioned into the cosmogenic dose rate and the sediment dose rate. The contribution to the total dose rate from cosmogenic radiation is small and is typically estimated following equations of Prescott and Stephan (1982) and Prescott and Hutton (1994) which use latitude and sample depth in the calculations. The sediment dose rate comes from low level, ambient, ionizing radiation associated with ^{40}K, ^{87}Rb (to a very small degree), and the radioactive isotopes in the decay series of ^{238}U,

^{235}U, and ^{232}Th both in the sample and in the material surrounding it. Decay of these long lived radionuclides results in the emission of alpha particles (α), beta particles (β), and gamma rays (γ) (Fig 2). Alpha particles are relatively large and travel only 0.03 mm or less from their emitting nucleus. Beta particles and gamma rays travel a few millimeters to up to 0.3 m respectively. Because of these varied ranges of influence, the homogeneity of a sample is an important consideration in dose rate assessment. For coarse grains, hydrofluoric acid is used to etch the outer layer of the grains that is affected by alpha radiation and the evaluation of beta and gamma contributions to dose rate are most important. However, for fine grains, etching is not possible and the alpha dose rate should be assessed. Measuring the dose rate from a small sub-sample will determine the gamma dose accurately only if the material within 0.3 m of the sample is homogeneous. In many natural settings this is not the case, for example, the unit of interest could be very small or poorly sorted and made up of mixed sized sediments. In these situations, in situ measurements of gamma dose are important in determining the dose rate.

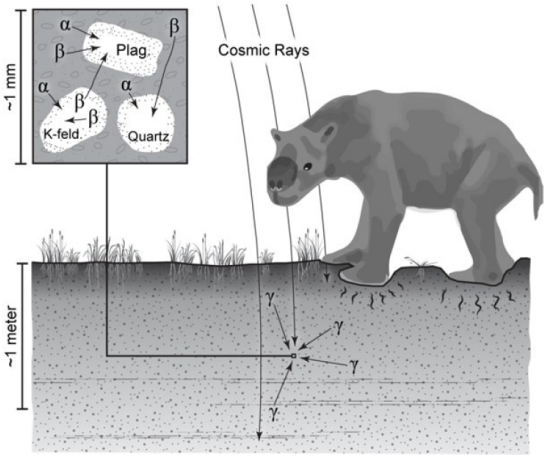

Fig 2. Environmental sources of radiation showing the travel distances of alpha and beta particles and gamma rays. Adapted from Duller 2008.

Another important consideration in the assessment of dose rate is whether the system is in secular equilibrium. Secular equilibrium in the decay series of U and Th is often assumed but is not a valid assumption in all environments especially where the parent material is unweathered (Olley et al., 1996). For example, water moving through sediment can selectively remove U but leave more immobile daughter isotopes such as Th behind. For porous samples, disequilibrium can arise from escape of gaseous Rn. For a system in disequilibrium, the dose rate changes throughout the burial period making accurate assessment less straightforward. As such, it is important to assess disequilibrium in the sample site.

There are two main groups of approaches to measuring dose rate: chemical methods in which the concentrations of U, Th, and K are used to calculate the radiation dose received by the sample and directly counting radiation emissions. For measuring K, chemical methods include atomic absorption spectrophotometry, flame photometry, X-ray fluorescence, and ICP-MS. For U and Th, which occur in lower concentrations, methods include ICP-MS and neutron activation analysis. Some problems with geochemical methods include i). concentrations being close to detection limits of many facilities, ii). underestimated concentrations owing to incomplete dissolving of resistant materials, iii). measurements made on small subsamples that may not be representative of the whole sample, and iv). equilibrium must be assumed.

Emission counting methods include thick source alpha counting (TSAC), alpha spectroscopy, thick source beta counting (TSBC), and gamma ray spectrometry. TSAC makes use of ZnS screens and a photomultiplier to count alpha emissions directly. The procedure is lengthy, requiring 7 days or more in some cases. To assess Rn escape, the sample must be counted a second time after it has been sealed for a month or more. Of course, this only assesses Rn loss at the time of measurement and not over the time

period of burial. With TSAC, the total combined counts of U and Th are measured (K cannot be measured) and owing to very low resolution, different energies of alpha emissions cannot be distinguished. Additionally, efficiencies can vary greatly among batches of ZnS screens resulting in varied accuracy of results (Sjostrand and Prescott, 2002). Alpha spectrometry is another way to directly observe alpha emissions, but like geochemical techniques, requires the sample to be dissolved which is difficult to fully achieve and is unlikely to be representative of the whole sample. Assessing the alpha dose is most important for fine grain applications in which the alpha dose must be taken into account, but is less relevant to dose rate in coarse grain applications in which beta and gamma contributions are more important. Beta particles are emitted at a range of energies so that spectroscopy is irrelevant (Duller, 2008), but counting can be done with TSBC using wafers of NE102A developed by Sanderson (1998) or with a Geiger-Muller system. Like alpha counting, the reliability of the results is bound to equilibrium in the U and Th decay series (Hossain, 2003).

Gamma-ray counting is used to assess dose rate for luminescence typically through either sodium iodide (NaI) or Germanium (Ge) gamma-ray spectrometers. NaI detectors are efficient but have low energy resolution. These are best suited to measuring in-situ environmental gamma dose rate (for example in heterogeneous sample sites) because they are more thermally stable than other types of detectors. Despite the low resolution, NaI detectors can be used to identify K and some of the radioisotopes of the U and Th decay series and as such are the preferred field instrument to make in-situ dose rate measurements for luminescence. Owing to excellent energy resolution, Ge gamma-ray spectrometry can both identify and quantify the elemental concentrations of a variety of individual radionuclides simultaneously including ^{40}K and those in the U and Th decay chains (Hossain, 2003).

References

Aitken, M.J., 1985. Thermoluminescence Dating. London: Academic Press.

Aitken, M.J., 1998. An Introduction to Optical Dating. Oxford: Oxford University Press.

Bailiff, I.K., 2007. Methodological developments in the luminescence dating of brick from English late-medieval and post-medieval buildings. *Archaeometry* 49, 827–851.

Barnett, S.M., 2000. Luminescence dating of pottery from later prehistoric Britain. *Archaeometry* 42, 431-457.

Duller, G.A.T., 2004. Luminescence dating of Quaternary sediments: recent advances. *Journal of Quaternary Science* 19, 183–192.

Duller GAT., 2008. *Luminescence Dating: Guidelines in Using Luminescence Dating in Archaeology*. Swindon: English Heritage

Galbraith, R.F., 2005. Statistics for Fission Track Analysis. Interdisciplinary Statistics, Chapman and Hall/CRC.

Galbraith, R.F., Green, P.F., 1990. Estimating the component ages in a finite mixture. *Nuclear Tracks and Radiation Measurements* 17, 197–206.

Galbraith, R.F., Roberts, R.G., Laslett, G.M., Yoshida, H. and Olley, J.M., 1999. Optical dating of single and multiple grains of quartz from Jinmium Rock Shelter, Northern Australia: Part I, Experimental design and statistical models, *Archaeometry* 41: 339–364.

Hossain, S.M., De Corte, F., Vandenberghe, D., Van den haute, P., 2002. A comparison of methods for the annual radiation dose determination in the luminescence dating of loess sediment. *Nuclear Instruments and Methods in Physics Research* A: 598–613

Hossain, S.M., 2003. A critical comparison and evaluation of methods for the annual radiation dose determination in the luminescence dating of sediments. PhD Thesis. Institute for Nuclear Sciences Laboratory of Analytical Chemistry, University of Ghent, Belgium.

Lian, O.B., Roberts, R.G., 2006. Dating the Quaternary: progress in luminescence dating of sediments. *Quaternary Science Reviews* 25, 2449–2468.

Murray AS, Olley JM., 2002. Precision and accuracy in the optically stimulated luminescence dating of sedimentary quartz: a status review. *Geochronometria* 21:1–16

Murray, A.S., Wintle, A.G., 2000. Luminescence dating of quartz using an improved single aliquot regenerative dose protocol. *Radiation Measurements* 32: 57–73.

Olley, J.M., Murray, A.S., Roberts, R.G., 1996. The effects of disequilibria in the uranium and thorium decay chains on burial dose rates in fluvial sediments. *Quaternary Science Reviews* 15: 751–60.

Prescott JR, Stephan LG., 1982. The contribution of cosmic radiation to the environmental dose for thermoluminescent dating. Latitude, altitude and depth dependences. *PACT J.* (*Council of Europe*) 6:17–25

Prescott, J.R., Hutton, J.T., 1994. Cosmic ray contributions to dose rates for luminescence and ESR dating: large depths and long-term variations. *Radiation Measurements* 23, 497–500.

Rhodes E.J., Bronk-Ramsey C., Outram Z., Batt C., Willis L., 2003. Bayesian methods applied to the interpretation of multiple OSL dates: high precision sediment age estimates from Old Scatness Broch excavations, Shetland Isles. *Quat. Sci. Rev.* 22:1231–44.

Rhodes, E.J., 2011. Optically Stimulated Luminescence Dating of Sediments over the Past 200,000 Years, *Annual Review of Earth and Planetary Sciences* 39, 461–488.

Sanderson, D.C.W., 1998. Thick source beta counting (TSBC): a rapid method for measuring beta dose-rates, *Nuclear Tracks and Radiation Measurements* 14: 203–207.

Sjostrand, H., Prescott, J.R., 2002. Thick source α counting: the measurement of thorium. *Ancient TL* 20: 7–10.

Wintle A.G., 2008. Luminescence dating: where it has been and where it is going. *Boreas* 37: 471–482.

APPENDIX B--READING ABANICO PLOTS

The abanico plot allows visualization of individual D_e values, relative errors and precision, as well as the D_e distribution shape and modality (Dietze et al., 2016). It is a modification of the more traditional "radial plot" commonly used to represent D_e distributions of luminescence samples (Vermeesch, 2009) by merging it with a kernel density estimate plot (or other univariate plot types of choice).

The abanico plot consists of two parts (Fig. 1): a bivariate part (showing standardized estimates in relation to the precisions) and a univariate part (showing the age or D_e frequency distribution) (Fig. 1).

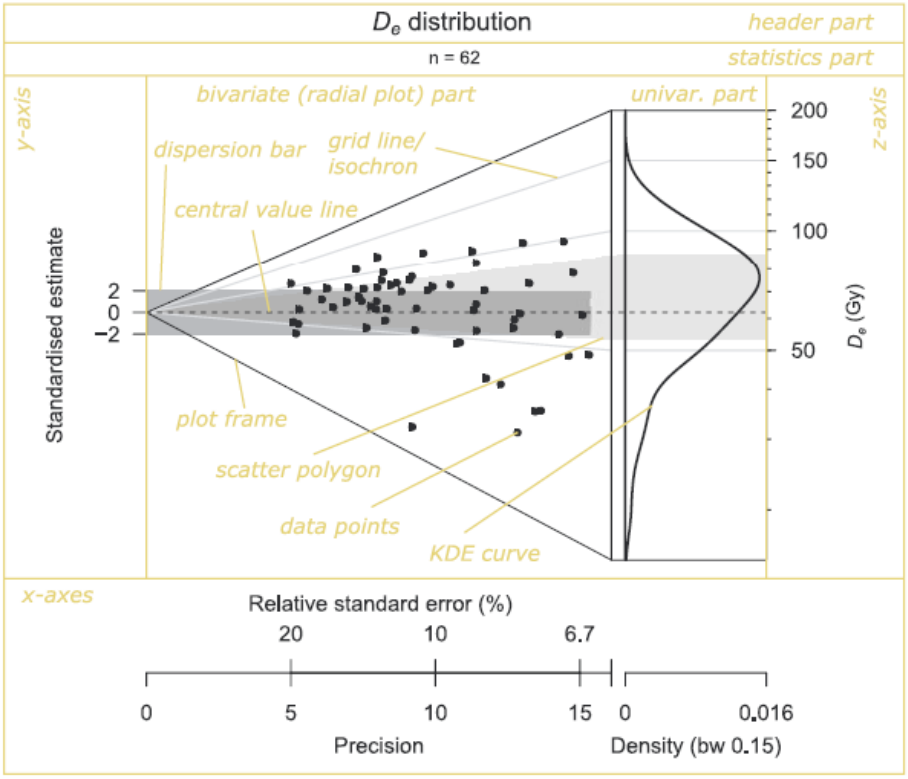

Figure 1. The abanico plot with example data provided by the R package "Lumiescence" (ExampleData.DeValues$CA1) reproduced from Dietze et al. (2016). De values are from single-grain (200-250 µm) quartz measurements performed on a Risoe TL/OSL DA-20 reader at the University of Cologne. The plot consists of two parts: a bivariate plot (a radial plot) on the left side and a univariate plot (such as a kernel density estimate) on the right side. De values are shown on a log-scale. For further details on plot construction, see Deitze et al. (2016).

The two parts are linked by a z-axis (with gridlines or isochrons radiating out from the standardized estimate of 0) giving an age scale that is common to both. In the traditional radial plot, the z-axis is usually drawn as an arc of a circle on the right side, but here it is drawn as a straight line so that it can be

integrated into an age (or D_e) frequency distribution such as a kernel density estimate. In general, a data set consists of n measured values z_i, i = [1; ::., n], each with an associated standard error σ_i (i.e., a measure of deviation, not scatter). When no log transformation is used, z_i denotes the estimated D_e for the ith individual aliquot or grain and σ_i is its standard error. When the log scale is used, z_i is the natural log of the D_e estimate and σ_i is the standard error of the log of the D_e estimate.

A 'scatter polygon' (e.g., the light grey polygon in Fig. 1) highlights the area between the lower and upper quartiles in the univariate plot and the corresponding isochrons on the radial plot (by default). As in Fig. 1, the scatter polygon may overlap with the dispersion bar. It is the dispersion bar, not the scatter polygon, that indicates agreement or otherwise of estimates with a specified value – i.e., all points within the dispersion bar are statistically equivalent within error. In contrast, the scatter polygon characterizes the age frequency distribution. Hence, by definition the two elements have different meanings and usually do not cover the same range.

A kernel density estimate (KDE) is a curve that depicts the empirical estimate of the probability density function of the distribution that the measured D_e values were drawn from (Galbraith and Roberts, 2012). A KDE with a Gaussian kernel is constructed by replacing each D_e value with a Gaussian density function with standard deviation centred at the D_e value, and then averaging these curves pointwise. This is simply a data-smoothing method that provides a reasonable picture of the underlying distribution for a sufficiently large number of D_e values. For more details see Galbraith and Roberts (2012).

References

Dietze, M., Kreutzer, S., Burow, C., Fuchs, M.C., Fischer, M., Schmidt, C., 2016. The abanico plot: visualizing chronometric data with individual standard errors. *Quaternary Geochronology* 31: 12–18.

Galbraith, R.F., Roberts, R.G., 2012. Statistical aspects of equivalent dose and error calculation and display in OSL dating: An overview and some recommendations. *Quaternary Geochronology* 11: 1–27.

Vermeesch, P., 2009. RadialPlotter: a Java application for fission track, luminescence and other radial plots, Radiation Measurements 44 (4): 409–410.

APPENDIX F—MINING DISTRICTS IN THE SOCORRO 30 X 60-MINUTE QUADRANGLE

USGS Earth Mapping Resources Initiative

District Data Form

NMBGMR Contact	Virginia T. McLemore New Mexico Bureau of Geology and Mineral Resources 801 Leroy Place Socorro, NM 87801 575 835 5521 virginia.mclemore@nmt.edu
USGS Contact	Nick Karl Denver Federal Center Box 25046, Mail Stop 973 Denver, CO 80225 303.236.1222 nkarl@usgs.gov

USGS Data Requirements

Information must be publicly available (no written or oral communications allowed).

Districts must have a verified latitude-longitude location.

Districts have polygon GIS files that are provided as a shapefile.

NOTE: The available data for this database is from a variety of published and unpublished reports (including theses and dissertations) and miscellaneous unpublished files in the NMBGMR mining archive. Listed in McLemore (2017).
New information is continuously becoming available and is incorporated into the database regularly.

Worksheet Tab Name	**Tab Description**
District	Data are entered into this worksheet for individual mineral region publications.
MetalsProduction	Metals production data are entered cumulative by district.
Field Definitions	Field definitions with examples.
USGS Terminology	Terminology definitions for districts.

Workbook Version Date: June 23, 2024

Federal Register—2022 Final List of Critical Minerals

mineral	symbol
aluminum (bauxite)	Al
antimony	Sb
arsenic	As
barite	Ba
beryllium	Be
bismuth	Bi
cesium	Cs
chromium	Cr
cobalt	Co
fluorspar	F
gallium	Ga
germanium	Ge
graphite (natural)	C
hafnium	Hf
helium (removed in 2022)	He
indium	In
lithium	Li
magnesium	Mn
manganese	Mg
nickel (added in 2022)	Ni
niobium	Nb
platinum group metals	PGM or PGE
potash (removed in 2022)	K
rare earth elements group	REE
rhenium (removed in 2022)	Rh
rubidium	Rb
scandium	Sc
strontium (removed in 2022)	Sr
tantalum	Ta
tellurium	Te
tin	Sn
titanium	Ti
tungsten	W
uranium (removed in 2022)	U
vanadium	V
zinc (added in 2022)	Zn
zirconium	Zr

Mining districts in the Socorro 30 x 60-minute quadrangle, Socorro, Torrance, and Valencia Counties, New Mexico (updated and modified from Lindgren et al., 1910; File and Northrop, 1966; Howard, 1967; North and McLemore, 1986; McLemore and Chenoweth, 1989; McLemore, 2001, 2017). Districts are in alphabetical order by district name. Estimated production is in dollars at the time of production. Commodity symbols are explained earlier in this appendix. Types of deposits are summarized in McLemore (2017) and described by McLemore and Lueth (2017) and McLemore and Austin (2017). REE=rare earth elements, PGE=platinum group elements, VMS=volcanic massive sulfide, MVT=Mississippi Valley type, RGR=Rio Grande rift, GPM=Great Plains Margin. Commodities in red are critical minerals. All coordinates are in NAD27.

District Id (NM)	County	District or Prospect Area (highlighted)	Major commodity category	Aliases (Synonyms, other names)	Year of Discovery	Year of Initial Production-Year of Last Production	Estimated Cumulative Production (all commodities)	Commodities Produced	Other commodities	Types of Deposits	Description	Comments	Source for district name	Selected References	Latitude	Longitude
DIS211	Socorro	Chupadero	metals	Minas de Chupadero, Chupadera, De La Parida, Del La Parida, La Parida, Escondida, Presilla	1800s	1959-1960	$2,000	Cu, Ag, fire clay, Ba, F	U, Pb, Th, REE, limestone, gypsum, clay	Rio Grande Rift copper-silver (uranium) vein, RGR, sedimentary-copper, disseminated uranium-REE deposits in Proterozoic rocks, fire clay, limestone, gypsum	Sedimentary-copper deposits in Pennsylvanian Moya sandstone. RGR deposits in Precambrian granite and limestone.		File and Northrop (1966), Mardirosian (1971)	Jaworski (1973), McLemore (1983a)	34.098	-106.796
DIS217	Socorro	Joyita Hills	metals	Canacito, Canyoncito, Dewey, La Joya, La Joyita, Los Canoncitos, Los Canyoncitos, Los Canyoncitos, Canacito	1880	1915	$1,000	Ag, Pb, F	Cu, Ba	Rio Grande Rift copper-silver (uranium) vein, RGR, sandstone uranium	Veins in fissures in Proterozoic gneiss and along the contact of Proterozoic rocks with Oligocene volcanic rocks and Pennsylvanian and Permian sedimentary rocks.		File and Northrop (1966), Mardirosian (1971)	Lasky (1932), Arendt (1971)	34.277	-106.82
DIS219	Socorro	Lemitar Mountains	metals	Box Canyon, Lemitar, Polvadera, Polvadero, Limitar, Sierra Lemitar	1880	?	$1,000	Cu, Pb, Ba, Ag, Mn, U	F, Zn, Ti, Nb, REE, Th	carbonatite, episyenites (metasomatites), REE-Th-U veins, RGR, Vein and replacement deposits in Proterozoic rocks	Veins with minor replacement along the unconformable contact of Proterozoic rocks and overlying Paleozoic sedimentary rocks, along the contact of Proterozoic mafic dikes intruding granite, associated with Ordovician carbonatite dikes, and in fissures in Paleozoic limestone.		File and Northrop (1966), Mardirosian (1971)	McLemore (1982a, 1983a, 1983b, 2015)	34.183	-106.993

District Id (NM)	County	District or Prospect Area (highlighted)	Major commodity category	Aliases (Synonyms, other names)	Year of Discovery	Year of Initial Production-Year of Last Production	Estimated Cumulative Production (all commodities)	Commodities Produced	Other commodities	Types of Deposits	Description	Comments	Source for district name	Selected References	Latitude	Longitude
DIS220	Socorro	Luis Lopez	metals	Genaros, Iron Horse, Luis Lopez Manganese, Red Hills, San Antoniom Socorro Manganese	1910s	1942-1958	$276,000	Mn, Fe	Au, Ag, Zn, Pb, W, Ni, Co, Ba, Be	epithermal manganese, volcanogenic uranium	Miocene to Pliocene manganese veins in Tertiary volcanic rocks.		File and Northrop (1966), Mardirosian (1971)	Miesch (1956), Hewitt (1964), Willard (1973), Norman et al. (1983), Eggleston et al. (1983), North and McLemore (1987)	33.966	-106.964
DIS224	Socorro	Rayo	metals	Joyita Mountains, La Joya, Manzanares	1900s	1900s	$1,000	Ag, Cu	U, V	sedimentary-copper	Stratabound sedimentary-copper deposits in sandstones of the Permian Yeso Formation.		File and Northrop (1966), Mardirosian (1971)	Soulé (1956), LaPoint (1976, 1979)	34.312	-106.526
DIS227	Socorro	San Lorenzo	metals	Jerome, San Acacia	1901	1901	$1,000	Cu, Ag	Au, U, Li	sandstone uranium, volcanic-epithermal vein, volcanogenic uranium	Veins filling faults in middle Tertiary andesite.		File and Northrop (1966), Mardirosian (1971)	Lasky (1932), North (1983), McLemore (1994, 1996a), Eveleth et al. (2009)	34.274	-107.003
DIS228	Socorro	Socorro	metals	Agua Torres, Carthage, Little Davie, Lucky Don, Marie	1950s	1955-1963	$70,000	U, V	Cu, gypsum	Rio Grande Rift copper-silver (uranium) vein, sandstone uranium, gypsum, RGR, sedimentary-copper	Uranium veins along faults.		McLemore and Chenoweth (1989), includes the Carthage district of File and Northrop (1966)	Lasky (1932), McLemore (1983a), McLemore and Chenoweth (1989)	34.169	-106.692

District Id (NM)	County	District or Prospect Area (highlighted)	Major commodity category	Aliases (Synonyms, other names)	Year of Discovery	Year of Initial Production-Year of Last Production	Estimated Cumulative Production (all commodities)	Commodities Produced	Other commodities	Types of Deposits	Description	Comments	Source for district name	Selected References	Latitude	Longitude
DIS219	Socorro	Socorro Peak	industrial minerals	Encarnacion, Encarnacion La, La Encarnacion, Socorro, Socorro Mountain	1867	1867-present	$11,000,000 (also $18,000,000 from smelter)	Ag, perlite, Pb, kaolin	Ba, F, W, V, Au, As, Br, Mn, Mo	volcanic-epithermal vein, perlite, smelter	Miocene veins filling faults in Miocene Socorro Peak Rhyolite and underlying Popotosa Formation. Some veins also cut Pennsylvanian Sandia and Madera Formations. Perlite only active mine in 2015.	Silver produced 1867-1900. Perlite produced 1949-2015. Possible pre-1867 Spanish workings. Billings smelter produced $18 million worth of Pb, Ag, Au. Socorro perlite mine was one of the first perlite mines in the US when it opened in 1949.	File and Northrop (1966), Mardirosian (1971)	Lasky (1932), Chapin et al. (1978), Chamberlin (1980), Moats and Queen (1981), North (1983), Eveleth (1983), McLemore (1994c, 1996a), Harben et al. (2008), McLemore and Austin (2017)	34.054	-106.943
DIS241	Torrance	Chupadera Mesa	metals	Blackington and Harris, Chupadera, Chupadera Iron, Chupadero Iron, Mud Springs	1900	1964-1975	$1,000	Fe	Cu, Ag	GPM (Fe skarn)	Iron deposits, either skarn or hydrothermal, adjacent to monzonite dikes and sills.		File and Northrop (1966), should be separate district, different from Jones district, McLemore (1984), North and McLemore (1986) called Chupadera Iron	Harrer and Kelly (1963), McLemore (1984)	34.28	-106.348

District Id (NM)	County	District or Prospect Area (highlighted)	Major commodity category	Aliases (Synonyms, other names)	Year of Discovery	Year of Initial Production-Year of Last Production	Estimated Cumulative Production (all commodities)	Commodities Produced	Other commodities	Types of Deposits	Description	Comments	Source for district name	Selected References	Latitude	Longitude
DIS246	Valencia, Socorro, Torrance	Scholle	metals	Abo, Carocito	1902, Spanish likely mined after 1629	1915-1961	$300,000	Cu, Ag, Au, Pb, Ra, limestone	U, V	sandstone uranium, sedimentary-copper, Vein and replacement deposits in Proterozoic rocks	Stratabound sedimentary-copper deposits in the Permian Bursum, Abo, and Yeso Formations. High Ca limestone near Abo Pass.		File and Northrop (1966), Mardirosian (1971)	Soulé (1956), Phillips (1960), Hilpert (1969), LaPoint (1979), McLemore (1984), McLemore et al. (1986)	34.44	-106.436
DIS264	Socorro	Jornada del Muerto coal field	coal		1910	1927		coal		coal			Tabet (1979)	Tabet (1979)	34.023	-106.633

Metals Production

Reported and estimated base and precious metals production by district (non-confidential data).
— = no reported production. W = withheld or not available. * = estimated data. ** = GOLD (oz) includes placer and lode gold production.

District Id (NM)	County	District	Period of Production	Ore (short tons)	Copper (pounds)	Gold (troy ounces)	Silver (troy ounces)	Lead (pounds)	Zinc (pounds)	Estimated Metals Value	References
DIS211	Socorro	Chupadero	1959-1960*	2,000	80,000	—	W	—	—	<$1,000	North and McLemore (1986)
DIS217	Socorro	Joyita Hills	1915	—	—	—	50	W	—	<$1,000	North and McLemore (1986)
DIS219	Socorro	Lemitar Mountains	?	—	W	—	W	W	—	<$1,000	North and McLemore (1986)
DIS220	Socorro	Luis Lopez	none								
DIS224	Socorro	Rayo	1900s	—	W	—	W	—	—	<$1,000	North and McLemore (1986)
DIS227	Socorro	San Lorenzo	1901	—	W	—	W	—	—	<$1,000	North and McLemore (1986)
DIS228	Socorro	Socorro	none								
DIS219	Socorro	Socorro Peak	1867-1900	—	—	—	750,000*	W	—	$1,000,000	North (1983)
DIS241	Torrance	Chupadera Mesa	none								
DIS246	Valencia, Socorro, Torrance	Scholle	1915-1961	15,037	1,122,468	10	8,147	426	—	$252,398	USGS (1902-1927), USBM (1927-1990), McLemore (1984)
DIS264	Socorro	Jornada del Muerto coal field	?								

Other Production

District Id (NM)	County	District	Period of Production	Commodity	Quantity	Units	Comments	References
DIS219	Socorro	Lemitar Mountains	1955	U3O8	6	pounds	grade 0.02% U3O8	McLemore and Chenoweth (1989)
DIS220	Socorro	Luis Lopez	1942-1958	Mn	118,000	long tons	grade of concentrate 35-48% Mn	Farnum (1961), Dorr, 1965)
DIS220	Socorro	Luis Lopez	1942-1958	Mn	97,000	short tons	grade of concentrate 41% Mn	Farnum (1961), Dorr, 1965)
DIS228	Socorro	Socorro	1955	U3O8	4,679	pounds	grade 0.20% U3O8	McLemore and Chenoweth (1989)
DIS246	Valencia, Socorro, Torrance	Scholle	1916	Ra	700	dollars		McLemore (1984)

Field Definitions

Field Name	Definition	Example
State	State in which the site resides (2-letter abbreviation)	NM
DistrictID (USGS)	The unique district identifier with the syntax state abbreviation followed by a 4-digit number. This number is created by the compiler to link the data table to the shapefile.	NM0001
DistrictID (NM)	Unique district identifer from McLemore (2017)	DIS229
DistrictNm	The common name for the district.	Socorro Peak
Other_Name	Other known names for the district.	Socorro
County	U.S. county where the feature is located. If the feature occurs in multiple counties, all county names are listed separated by semicolons.	Socorro
Primary_Comm	The primary commodity that was mined within the district. If there are production data provided in the fields Prod_Amnt, Prod_Unit unique records (rows) are to be entered for each commodity.	Ag, perlite, Pb, kaolin
Other_Comm	Other commodities that are in the district that may not have been mined, but are know to occur.	Ba, F, W, V, Au, As, Br, Mn, Mo
Latitude	Latitude as decimal degree value (WGS84) representing the location of the district. Coordinate values are required for districts represented by a point location only (e.g the distirct has no polygonal boundary).	
Longitude	Longitude as decimal degree value (WGS84) representing the location of the district. Coordinate values are required for districts represented by a point location only (e.g the distirct has no polygonal boundary).	
Discovery	The known year of the district discovery.	1867
Prod_Years	The known years of production in the district.	1867-present
Prod_Amnt	The known quantitative amount of material produced.	$11,000,000 (also $18,000,000 from smelter)
Prod_Unit	The units associated to the Prod_Amnt field.	dollars
Dep_Type	The deposit types known in the district. Multiple deposit types are separated with semicolons.	volcanic-epithermal vein, perlite, smelter
District_Link	DOI or URL link to the documentation used to compile the general district information.	
Prod_Link	DOI or URL link to the documentation used to compile the production information.	
District_Cite	Citation information for the district documents.	
Prod_Cite	Citation information for the production documents.	
Notes	Any additional notes that compiler feels are necessary to state.	

USGS Terminology

Term	Definition	Example
Mineral Region	An area defined by a grouping of mines and/or mineral deposits or a geological environment permissive for mineral deposits.	Mining District; Mineral District; Area
Mining District	A section of country usually designated by name, having described or understood boundaries within which minerals are found and worked under rules and regulations prescribed by the miners therein. There is no limit to its territorial extent and its boundaries may be changed if vested rights are not thereby interfered with.	Socorro Peak
Mineral District	An area, usually designated by name, defined by a group of deposits of similar type, origin, or commodity.	Socorro Peak
Prospect Area	Area of similar geology and deposit types, generally no known production	Chupadera Mountains

REFERENCES

Abbey, A.L., and Niemi, N.A., 2019, Perspectives on continental rifting processes from spatiotemporal patterns of faulting and magmatism in the Rio Grande rift: Tectonics, v. 39, no. 1, p. 1–31. https://doi.org/10.1029/2019TC005635

Aby, S.B., and Jochems, A.P., 2022, Geologic map of the Rayo Hills 7.5-minute quadrangle, Socorro County, New Mexico: New Mexico Bureau of Geology and Mineral Resources Open-File Geologic Map 300, scale 1:24,000. https://doi.org/10.58799/OF-GM-300

Aldrich, M.J., Jr., Chapin, C.E, and Laughlin, A.W., 1986, Stress history and tectonic development of the Rio Grande rift, New Mexico: Journal of Geophysical Research, Solid Earth, v. 91, issue B6, p. 6199–6211. https://doi.org/10.1029/JB091iB06p06199

Allen, B.D., Love, D.W., McCraw, D.J., and Rinehart, A.J., 2013, Geologic map of the Becker SW quadrangle, Socorro County, New Mexico: New Mexico Bureau of Geology and Mineral Resources Open-File Geologic Map 233, scale 1:24,000. https://doi.org/10.58799/OF-GM-233

Allen, B.D., Timmons, J.M., Luther, A.L., Miller, P.L., and Love, D.W., 2014, Geologic map of the Cerro Montoso 7.5-minute quadrangle, Socorro County, New Mexico: New Mexico Bureau of Geology and Mineral Resources Open-File Geologic Map 238, scale 1:24,000. https://doi.org/10.58799/OF-GM-238

Altares, T., III, 1990, Stratigraphic description and paleoenvironments of the Bursum Formation, Socorro County, New Mexico [M.S. thesis]: Socorro, New Mexico Institute of Mining and Technology, 184 p.

Arendt, W.W., 1971, The geology of La Joyita Hills, Socorro, County, New Mexico [M.S. thesis]: Albuquerque, University of New Mexico, 88 p.

Armstrong, A.K., and Mamet, B.L., 1988, Mississippian (Lower Carboniferous) biostratigraphy, facies, and microfossils, Pedrogegosa basin, southeastern Arizona and southwestern New Mexico: U.S. Geological Survey Bulletin 1826, 40 p. https://doi.org/10.3133/b1826

Armstrong, A.K., Mamet, B.L., and Repetski, J.E., 2004, Mississippian system of New Mexico and adjacent areas, *in* Mack, G.H., and Giles, K.A., eds., The Geology of New Mexico—A Geologic History: New Mexico Geological Society Special Publication 11, p. 77–93. https://doi.org/10.56577/SP-11

Armstrong, R.L., 1968, Sevier orogenic belt in Nevada and Utah: Geological Society of America Bulletin, v. 79, no. 4, p. 429–458. https://doi.org/10.1130/0016-7606(1968)79[429:SOBINA]2.0.CO;2

Baer, S., Karlstrom, K.E., Bauer, P., and Connell, S.D., 2004, Geologic map of the Manzano Peak 7.5-minute quadrangle, Valencia and Torrance Counties, New Mexico: New Mexico Bureau of Geology and Mineral Resources Open-File Geologic Map 61, scale 1:24,000. https://doi.org/10.58799/OF-GM-61

Barker, J.M., Hall, T.L., and Chamberlin, R.M., 1994, Geology and mining of the Socorro perlite deposit, *in* Chamberlin, R.M., Kues, B.S., Cather, S.M., Barker, J.M., and McIntosh, W.C., Mogollon Slope, West-Central New Mexico: New Mexico Geological Society Fall Field Conference Guidebook 45, p. 2–3. https://doi.org/10.56577/FFC-45

Bates, R.L., Wilpolt, R.H., MacAlpin, A.J., and Vorbe, G., 1947, Geology of the Gran Quivira quadrangle, New Mexico: New Mexico Bureau of Mines and Mineral Resources Bulletin 26, 52 p., 9 plates. https://doi.org/10.58799/B-26

Bauer, P.W., Karlstrom, K.E., Bowring, S.A., Smith, A., and Goodwin, L., 1993, Proterozoic plutonism and regional deformation—New constraints from the southern Manzano Mountains, central New Mexico: New Mexico Geology, v. 15, no. 3, p. 49–55. https://doi.org/10.58799/NMG-v15n3.49

Beaumont, C., 1981, Foreland basins: Geophysical Journal International, v. 65, no. 2, p. 291–329. https://doi.org/10.1111/j.1365-246X.1981.tb02715.x

Beck, W.C., 1993, Structural evolution of the Joyita Hills, Socorro County, New Mexico [Ph.D. dissertation]: Socorro, New Mexico Institute of Mining and Technology, 187 p.

Beck, W.C., and Johnson, D.B., 1992, New fusulinid data and multiple episodes of ancestral Rocky Mountain deformation in the Joyita Hills, Socorro County, New Mexico: New Mexico Geology, v. 14, no. 3, p. 53–59. https://doi.org/10.58799/NMG-v14n3.53

Behr, R.A., 1999, Structure and thermochronologic constraints on the movement history of the Montosa fault, central New Mexico [M.S. thesis]: Socorro, New Mexico Institute of Mining and Technology, 129 p.

Birkeland, P.W., 1984, Soils and geomorphology: New York, Oxford University Press, 372 p.

Birkeland, P.W., Machette, M.N., and Haller, K.M., 1991, Soils as a tool for applied Quaternary geology: Utah Geological and Mineral Survey (a division of Utah Department of Natural Resources), Miscellaneous Publication 91-3, 71 p.

Bobrow, D.J., 1984, Geochemistry and petrology of Miocene silicic lavas in the Socorro-Magdalena area, New Mexico [M.S. thesis]: Socorro, New Mexico Institute of Mining and Technology.

Bobrow, D.J., Kyle, P.R., and Osburn, G.R., 1983, Miocene rhyolitic volcanism in the Socorro area of New Mexico: New Mexico Geological Society Guidebook 34, p. 211-217.

Bowring, S.A., Kent, S.C., and Sumner, W., 1983, Geology and U-Pb geochronology of Proterozoic rocks in the vicinity of Socorro, New Mexico, *in* Chapin, C.E., and Callender, J.F., eds., Socorro Region II: New Mexico Geological Society Fall Field Conference Guidebook 34, p. 137–142. https://doi.org/10.56577/FFC-34.137

Broadhead, R.F., and Jones, G., 2004, Oil, natural gas, and helium potential of the Chupadera Mesa area, Lincoln and Socorro counties, New Mexico: New Mexico Bureau of Geology and Mineral Resources Open-File Report 478, 95 p. https://doi.org/10.58799/OFR-478

Brooks, J., Cornford, C., and Archer, R., 1987, The role of hydrocarbon source rocks in petroleum exploration, *in* Brooks, J., and Fleet, A.J., eds., Marine Petroleum Source Rocks: Geological Society of London Special Publication 26, pp. 17–46. https://doi.org/10.1144/GSL.SP.1987.026.01.02

Brown, K.B., 1987, Geology of the southern Cañoncita de la Uva area, Socorro County, New Mexico [M.S. thesis]: Socorro, New Mexico Institute of Mining and Technology, 89 p.

Bruning, J.E., 1973, Origin of the Popotsa Formation, north-central Socorro County, New Mexico [Ph.D. dissertation]: Socorro, New Mexico Institute of Mining and Technology, 132 p.

Cabezas, P., 1991, The southern Rocky Mountains in west-central New Mexico—Laramide structures and their impact on Rio Grande rift extension: New Mexico Geology, v. 13, no. 2, p. 25–37. https://doi.org/10.58799/NMG-v13n2.25

Cappa, J.A., 1975, The depositional environment, paleocurrents, provenance, and dispersal patterns of the Abo Formation in part of the Cerros de Amado area,

Socorro County, New Mexico [M.S. thesis]: Socorro, New Mexico Institute of Mining and Technology, 153 p.

Cappa, J.A., and McMillan, J.R., 1983, Paleocurrent analysis of the Abo Formation, Cerros de Amado area, *in* Chapin, C.E., and Callender, J.F., eds., Socorro Region II: New Mexico Geological Society Fall Field Conference Guidebook 34, p. 15–16. https://doi.org/10.56577/FFC-34

Cather, S.M., 1983, Laramide Sierra uplift—Evidence for major pre-rift uplift in central and southern New Mexico, *in* Chapin, C.E., and Callender, J.F., eds., Socorro Region II: New Mexico Geological Society Fall Field Conference Guidebook 34, p. 96–101. https://doi.org/10.56577/FFC-34.99

Cather, S.M., 1990, Stress and volcanism in the northern Mogollon-Datil volcanic field, New Mexico—Effects of the post-Laramide tectonic transition: Geological Society of America Bulletin, v. 102, no. 11, p. 1447–1458. https://doi.org/10.1130/0016-7606(1990)102<1447:SAVITN>2.3.CO;2

Cather, S.M., 2004, The Laramide orogeny in central and northern New Mexico and southern Colorado, *in* Mack, G.H., and Giles, K.A., eds., The Geology of New Mexico—A Geologic History: New Mexico Geological Society Special Publication 11, p. 203–248. https://doi.org/10.56577/SP-11

Cather, S.M., 2009a, Tectonics of the Chupadera Mesa region, central New Mexico, *in* Lueth, V., Lucas, S.G., and Chamberlin, R.M., eds., Geology of the Chupadera Mesa: New Mexico Geological Society Fall Field Conference Guidebook 60, p. 127–137. https://doi.org/10.56577/FFC-60.127

Cather, S.M., 2009b, Stratigraphy and structure of the Laramide Carthage–La Joya Basin, central New Mexico, *in* Lueth, V., Lucas, S.G., and Chamberlin, R.M., eds., Geology of the Chupadera Mesa: New Mexico Geological Society Fall Field Conference Guidebook 60, p. 227–234. https://doi.org/10.56577/FFC-60.227

Cather, S.M., 2009c, The Montosa fault, *in* Lueth, V., Lucas, S.G., and Chamberlin, R.M., eds., Geology of the Chupadera Mesa: New Mexico Geological Society Fall Field Conference Guidebook 60, p. 73–74. https://doi.org/10.56577/FFC-60

Cather, S.M., 2018, Revised basin geometry for the Bursum Formation (upper Virgilian-lower Wolfcampian), central New Mexico: New Mexico Geology, v. 40, no. 1, p. 6–16. https://doi.org/10.58799/NMG-v40n1.6

Cather, S.M., and Colpitts, R.M., Jr., 2005 (revised 2016), Geologic map of the Loma de las Cañas 7.5-minute quadrangle, Socorro County, New Mexico: New Mexico Bureau of Geology and Mineral Resources Open-File Geologic Map 110, scale 1:24,000. https://doi.org/10.58799/OF-GM-110

Cather, S.M., and Koning, D.J., eds., 2024, Geology of the Quebradas Region, Socorro County, Central New Mexico: New Mexico Bureau of Geology and Mineral Resources Memoir 51, 206 p. https://doi.org/10.58799/M-51

Cather, S.M., and Read, A.S., 2003, Geologic map of the Silver Creek 7.5-minute quadrangle, Socorro County, New Mexico: New Mexico Bureau of Geology and Mineral Resources Open-File Geologic Map 75, scale 1:24,000. https://doi.org/10.58799/OF-GM-75

Cather, S.M., Chamberlin, R.M., Chapin, C.E., and McIntosh, W.C., 1994a, Stratigraphic consequences of episodic extension in the Lemitar Mountains, central Rio Grande rift, *in* Keller, G.R., and Cather, S.M., eds., Basins of the Rio Grande Rift—Structure, Stratigraphy, and Tectonic Setting, p. 157–170. https://doi.org/10.1130/SPE291-p157

Cather, S.M., Chamberlin, R.M., and Ratté, J.C., 1994b, Tertiary stratigraphy and nomenclature for western New Mexico and eastern Arizona, *in* Chamberlin, R.M., Kues, B.S., Cather, S.M., Barker, J.M., and McIntosh, W.C., Mogollon Slope, West-Central New Mexico: New Mexico Geological Society Fall Field Conference Guidebook 45, p. 259–266. https://doi.org/10.56577/FFC-45.269

Cather, S.M., Colpitts, R.M., Jr., Hook, S.C., and Heizler, M.T., 2004 (revised 2016), Geologic map of the Mesa del Yeso 7.5-minute quadrangle, Socorro County, New Mexico: New Mexico Bureau of Geology and Mineral Resources Open-File Geologic Map 92, scale 1:24,000. https://doi.org/10.58799/OF-GM-92

Cather, S.M., Karlstrom, K.E., Timmons, J.M., and Heizler, M.T., 2006, Palinspastic reconstruction of Proterozoic basement-related aeromagnetic features in north-central New Mexico—Implications for Mesoporoterozoic to late Cenozoic tectonism: Geosphere, v. 2, no. 6, p. 299–323. https://doi.org/10.1130/GES00045.1

Cather, S.M., Zeigler, K.E., Mack, G.H., and Kelley, S.A., 2013, Toward standardization of Phanerozoic stratigraphic nomenclature in New Mexico: Rocky Mountain Geology, v. 48, no. 2, p. 101–124. https://doi.org/10.2113/gsrocky.48.2.101

Cather, S.M., Osburn, G.R., McIntosh, W.C., Heizler, M.T., Hook, S.C., Axen, G.J., Flores, S., and Green, M., 2014 (revised 2016), Geologic map of the Bustos Well 7.5-

minute quadrangle, Socorro County, New Mexico: New Mexico Bureau of Geology and Mineral Resources Open-File Geologic Map 237, scale 1:24,000. https://doi.org/10.58799/OF-GM-237

Chamberlin, R.M., 1980, Cenozoic stratigraphy and structure of the Socorro Peak volcanic center, central New Mexico: New Mexico Bureau of Mines and Mineral Resources Open-File Report 118, 395 p. https://doi.org/10.58799/OFR-118

Chamberlin, R.M., 1983, Cenozoic domino-style crustal extension in the Lemitar Mountains, New Mexico—A summary, *in* Chapin, C.E., and Callender, J.F., eds., Socorro Region II: New Mexico Geological Society Fall Field Conference Guidebook 34, p. 111-118. https://doi.org/10.56577/FFC-34.111

Chamberlin, R.M., 1999, Geologic map of the Socorro 7.5-minute quadrangle, Socorro County, New Mexico: New Mexico Bureau of Mines and Mineral Resources Open-File Geologic Map 34, scale 1:24,000. https://doi.org/10.58799/OF-GM-34

Chamberlin, R.M., and Eggleston, T.L., 1996, Geologic map of the Luis Lopez 7.5-minute quadrangle, Socorro County, New Mexico, New Mexico Bureau of Mines and Mineral Resources, Open-File Report 421, 152 p. https://doi.org/10.58799/OFR-421

Chamberlin, R.M., and Osburn, G.R., 2006, Geologic map of the Water Canyon quadrangle, Socorro County, New Mexico: New Mexico Bureau of Geology and Mineral Resources Open-File Geologic Map 118, scale 1:24,000. https://doi.org/10.58799/OF-GM-118

Chamberlin, R.M., Cather, S.M., Nyman, M.W., and McLemore, V.T., 2001, Geologic map of the Lemitar 7.5-minute quadrangle, Socorro County, New Mexico: New Mexico Bureau of Geology and Mineral Resources Open-File Geologic Map 38, scale 1:24,000. https://doi.org/10.58799/OF-GM-38

Chamberlin, R.M., Eggleston, T., and McIntosh, W.C., 2002, Geologic map of the Luis Lopez quadrangle, Socorro County, New Mexico: New Mexico Bureau of Geology and Mineral Resources Open-File Geologic Map 53, scale 1:24,000. https://doi.org/10.58799/OF-GM-53

Chamberlin, R.M., McIntosh, W.C., and Eggleston, T.L., 2004, $^{40}Ar/^{39}Ar$ geochronology and eruptive history of the eastern sector of the Oligocene Socorro caldera, central Rio Grande rift, New Mexico, *in* Cather, S.M., McIntosh, W.C., and Kelley, S.A., eds., Tectonics, Geochronology, and Volcanism in the Southern Rocky Mountains and Rio

Grande Rift: New Mexico Bureau of Geology and Mineral Resources Bulletin 160, p. 251–279. https://doi.org/10.58799/B-160

Chamberlin, R.M., Love, D.W., Harrison, J.B., Lueth, V.W., Frey, B.A., Williams, S., and Connell, S.D., 2016, Sevilleta West pre-meeting road log from Sevilleta National Wildlife Refuge Visitor Center to San Acacia, Cerritos de las Minas, West Mesa, and San Lorenzo Spring, *in* Frey, B.A., Karlstrom, K.E., Lucas, S.G., Williams, S., Zeigler, K., McLemore, V., and Ulmer-Scholle, D.S., eds., The Geology of the Belen Area: New Mexico Geological Society Field Conference Guidebook 67, p. 37–61. https://doi.org/10.56577/FFC-67.37

Chamberlin, R.M., McIntosh, W.C., Heizler, M.T., and Koning, D.J., 2022a, A new constraint on the onset of Cenozoic crustal extension in the central Rio Grande rift near Socorro, New Mexico, *in* Koning, D.J., Hobbs, K.M., Phillips, F.M., Nelson, W.J., Cather, S.M., Jakle, A.C., and Van Der Werff, B., eds., Socorro Region III: New Mexico Geological Society Field Conference Guidebook 72, p. 60–62. https://doi.org/10.56577/FFC-72

Chamberlin, R.M., Koning, D.J., and Jochems, A., 2022b, Lemitar Mountains and San Lorenzo Canyon, third day road log, from Socorro to northern Lemitar Mountains, Unconformity Butte, and San Lorenzo Canyon, *in* Koning, D.J., Hobbs, K.M., Phillips, F.M., Nelson, W.J., Cather, S.M., Jakle, A.C., and Van Der Werff, B., eds., Socorro Region III: New Mexico Geological Society Field Conference Guidebook 72, p. 122–142. https://doi.org/10.56577/FFC-72.122

Chang, C., and Liu, L., 2021, Investigating the formation of the Cretaceous Western Interior Seaway using landscape evolution simulations: Geological Society of America Bulletin, v. 133, no. 1–2, p. 347–361. https://doi.org/10.1130/B35653.1

Chapin, C.E., and Cather, S.M., 1994, Tectonic setting of axial basins of the northern and central Rio Grande rift, *in* Keller, G.R., Cather, S.M., eds., Basins of the Rio Grande Rift—Structure, Stratigraphy, and Tectonic Setting: Geological Society of America Special Paper 291, p. 5–25. https://doi.org/10.1130/SPE291

Chapin, C.E., Chamberlin, R.M., Osburn, G.R., White, D.W., and Sanford, A.R., 1978, Exploration framework of the Socorro geothermal area, New Mexico; *in* Chapin, C.E., and others, eds., Field guide to selected cauldrons and mining districts of the Datil-Mogollon volcanic field, New Mexico: New Mexico Geological Society, Special Publication 7, p. 114-129.

Cikoski, C.T., 2010, Geology of the Neogene basin fill on the Indian Well Wilderness 7.5-minute quadrangle, central Rio Grande rift, New Mexico [M.S. thesis]: Socorro, New Mexico Institute of Mining and Technology, 160 p.

Colpitts, R.M., Jr., 1986, Geology of the Sierra de la Cruz area, Socorro County, New Mexico [M.S. thesis]: Socorro, New Mexico Institute of Mining and Technology, 166 p.

Connell, S.D., and McCraw, D.J., 2007, Geologic map of the La Joya NW quadrangle, Socorro County, New Mexico: New Mexico Bureau of Geology and Mineral Resources Open-File Geologic Map 140, scale 1:24,000. https://doi.org/10.58799/OF-GM-140

Connell, S.D., Cather, S.M., Dunbar, N.W., McIntosh, W.C., and Peters, L., 2002, Stratigraphy of the Tanos and Blackshare Formations (lower Santa Fe Group), Hagan embayment, Rio Grande rift, New Mexico: New Mexico Geology, v. 24, no. 4, p. 107–120. https://doi.org/10.58799/NMG-v24n4.107

Connell, S.D., Hawley, J.W., and Love, D.W., 2005, Late Cenozoic drainage development in the southeastern Basin and Range of New Mexico, southeasternmost Arizona, and Western Texas, 2005, *in* Lucas, S.G., Morgan, G.S., and Zeigler, K.E., eds., New Mexico's Ice Ages: New Mexico Museum of Natural History and Science Bulletin No. 28, p. 125-150.

Cordell, L., 1978, Regional geophysical setting of the Rio Grande rift: Geological Society of America Bulletin, v. 89, no. 7, p. 1073–1090, https://doi.org/10.1130/0016-7606(1978)89<1073:RGSOTR>2.0.CO;2

Davydov, V.I., Glenister, B.F., Sinosa, C., Ritter, S.M., Chernykh, V.V., Wardlaw, B.R., and Snyder, W.S., 1998, Proposal of Aidaralash as global stratotype section and point (GSSP) for base of the Permian System: Episodes, v. 21, no. 1, p. 11–17. https://doi.org/10.18814/epiiugs/1998/v21i1/003

de Moor, M., Zinsser, A., Karlstrom, K., Chamberlin, R., Connell, S. and Read, A., 2005, Preliminary geologic map of the La Joya 7.5-minute quadrangle, Socorro County, New Mexico: New Mexico Bureau of Geology and Mineral Resources Open-File Geologic Map 102, scale 1:24,000. https://doi.org/10.58799/OF-GM-102

DeCelles, P.G., 1994, Late Cretaceous-Paleocene synorogenic sedimentation and kinematic history of the Sevier thrust belt, northeast Utah and southwest Wyoming:

Geological Society of America Bulletin, v. 106, no. 1, p. 32–56. https://doi.org/10.1130/0016-7606(1994)106%3C0032:LCPSSA%3E2.3.CO;2

Denny, C.S., 1940, Tertiary geology of the San Acacia area, New Mexico: Journal of Geology, v. 48, p. 73–106. https://doi.org/10.1086/624862

Dickinson, W.R., 1976, Sedimentary basins developed during evolution of the Mesozoic-Cenozoic arc-trench system in western North American: Canadian Journal of Earth Sciences, v. 13, no. 9, p. 1268–1287. https://doi.org/10.1139/e76-129

Dickinson, W.R., 2018, Tectonosedimentary relations of Pennsylvanian to Jurassic strata on the Colorado Plateau: Geological Society of America Special Paper 533, 184 p.

Dietz, H.M. and McLemore, V.T., 2022, Geochemistry of the Tajo granite, Socorro County, New Mexico, *in* Koning, D.J., Hobbs, K.M., Phillips, F.M., Nelson, W.J., Cather, S.M., Jakle, A.C., and Van Der Werff, B., eds., Socorro Region III: New Mexico Geological Society Field Conference Guidebook 72, p. 357–363. https://doi.org/10.56577/FFC-72.357

DiMichele, W.A., Chaney, D.S., Lucas, S.G., Nelson, J.W., Elrick, S.D., Falcon-Lang, H.J., and Kerp, H., 2017, Middle to Late Pennsylvanian fossil floras from Socorro County, New Mexico, U.S.A.: New Mexico Museum of Natural History and Science Bulletin 77, p. 25–99.

Dorr, J.V.N., II, 1965, Manganese: New Mexico Bureau of Mines and Mineral Resources Bulletin 87, p. 183–195. https://doi.org/10.58799/B-87

Dunbar, N.W. and Miggins, D., 1996, Chronology and thermal history of potassium metasomatism in the Socorro, NM, area—Evidence from $^{40}Ar/^{39}Ar$ dating and fission track analysis [abstract]: New Mexico Geological Society Annual Spring Meeting, April 12, 1996, pp. 23, Online ISSN: 2834-5800. https://nmgs.nmt.edu/meeting/abstracts/view.cfm?aid=1700

Dunbar, N.W., Chapin, C.E., Ennis, D.J., and Campbell, A.R., 1994, Trace element and mineralogical alteration associated with moderate and advanced degrees of K-metasomatism in a rift basin at Socorro, New Mexico, *in* Chamberlin, R.M., Kues, B.S., Cather, S.M., Barker, J.M., and McIntosh, W.C., Mogollon Slope, West-Central New Mexico: New Mexico Geological Society Fall Field Conference Guidebook 45, p. 225–231. https://doi.org/10.56577/FFC-45.225

Eaton, G.P., 1987, Topography and origin of the southern Rocky Mountains and Alvarado Ridge: Geological Society London Special Publications, v. 28, p. 355–369. https://doi.org/10.1144/GSL.SP.1987.028.01.22

Eggleston, T.L., Norman, D.I., Chapin, C.E., and Savin, S., 1983, Geology, alteration, and genesis of the Luis Lopez manganese district, New Mexico, in Chapin, C.E., and Callender, J.F., eds., Socorro Region II: New Mexico Geological Society Fall Field Conference Guidebook 34, p. 241–246. https://doi.org/10.56577/FFC-34.241

Eveleth, R.W., 1983, Gustav Billing, the Kelly mine, and the great smelter at Park City, Socorro County, New Mexico, *in* Chapin, C.E. and Callender, J.F., eds., Socorro Region II: New Mexico Geological Society Fall Field Conference Guidebook 34, p. 89–95. https://nmgs.nmt.edu/publications/guidebooks/details.cfml?ID=21931

Eveleth, R.W., 2009, Jerome copper prospects, San Lorenzo Canyon, Socorro County, New Mexico: New Mexico Geological Society Guidebook 60, p. 92-95.

Falcon-Lang, H.J., Jud, N.A., Nelson, W.J., DiMichele, W.A., Chaney, D.S., and Lucas, S.G., 2011, Pennsylvanian coniferopsid forests in sabkha facies reveal the nature of seasonal tropical biome: Geology, v. 39, p. 371–374. https://doi.org/10.1130/G31764.1

Farnham, L.L., 1961, Manganese deposits of New Mexico: U.S. Bureau of Mines Information Circular 8030, 176 p.

Ferguson, C.A, 1991, Stratigraphic and structural studies in the Mount Withington caldera, Grassy Lookout quadrangle, Socorro County, New Mexico: New Mexico Geology, v. 13, no. 3, p. 50–54, 59. https://doi.org/10.58799/NMG-v13n3.50

Ferguson, C.A., Osburn, G.R., and McIntosh, W.C., 2012, Oligocene calderas in the San Mateo Mountains, Mogollon-Datil volcanic field, New Mexico, *in* Lucas, S.G., McLemore, V.T., Lueth, V.W., Spielmann, J.A., and Krainer, K., eds., Geology of the Warm Springs Region: New Mexico Geological Society Fall Field Conference Guidebook 63, p. 74–77. https://doi.org/10.56577/FFC-63

File, L., and Northrop, S.A., 1966, County, township, and range locations of New Mexico's Mining Districts: New Mexico Bureau of Mines and Mineral Resources Circular 84, 66 p. https://doi.org/10.58799/C-84

Gale, A.S., Voigt, S., Sageman, B.B., and Kennedy, W.J., 2008, Eustatic sea-level record for the Cenomanian (Late Cretaceous)—Extension to the Western Interior Basin, USA: Geology, v. 36, no. 11, p. 859-862. https://doi.org/10.1130/G24838A.1

Gardner, J.H., 1910, The Carthage coal field, New Mexico: U.S. Geological Survey Bulletin 381, p. 452–460.

Gawne, C., 1981, Sedimentology and stratigraphy of the Miocene Zia Sand of New Mexico, summary: Geological Society of America, Bulletin, Part I, v. 92, no. 12, pp. 999–1007. https://doi.org/10.1130/0016-7606(1981)92<999:SASOTM>2.0.CO;2

Gile, L.H., Peterson, F.F., and Grossman, R.B., 1966, Morphological and genetic sequences of carbonate accumulation in desert soils: Soil Science, v. 101, p. 347-360. https://doi.org/10.1097/00010694-196605000-00001

Gile, L.H., Hawley, J.W., and Grossman, R.B., 1981, Soils and geomorphology in the Basin and Range area of Southern New Mexico—Guidebook to the Desert Project: New Mexico Bureau of Mines and Mienral Resources Memoir 39, 222 p. https://doi.org/10.58799/M-39

Grauch, V.J.S., and Connell, S.D., 2013, New perspectives on the geometry of the Albuquerque Basin, Rio Grande rift, New Mexico—Insights from geophysical models of rift-fill thickness, in Hudson, M.R., and Grauch, V.J.S., eds., New Perspectives on Rio Grande Rift Basins—From Tectonics to Groundwater: Geological Society of America Special Paper 494, p. 427-462. https://doi.org/10.1130/2013.2494(16)

Hamilton, W., 1981, Plate-tectonic mechanism of Laramide deformation, in Boyd, D.W., and Lillegraven, J.A. eds., Rocky Mountain Foreland Basement Tectonics: University of Wyoming Contributions to Geology, v. 19, p. 87–92.

Happ, S.C., 1948, Sedimentation in the middle Rio Grande Valley, New Mexico: GSA Bulletin, v. 59, no. 12, p. 1191-1216. https://doi.org/10.1130/0016-7606(1948)59[1191:SITMRG]2.0.CO;2

Haq, B.U., 2014, Cretaceous eustasy revisited: Global and Planetary Change, v. 113, p. 44-58, https://doi.org/10.1016/j.gloplacha.2013.12.007

Harben, P., Austin, G., Hoffman, G., McLemore, V., Caledon, M., and Barker, J., 2008, Industrial Minerals, a Staple in the Economy of New Mexico: Colorado Geological Survey, Resource Series 46, p. 11-156.

Harrer, C.M., and Kelly, F.J., 1963, Reconnaissance of iron resources of New Mexico: U.S. Bureau of Mines Information Circular 8190, 112 p.

Harrison, R.W., and Cather, S.M., 2004, The Hot Springs fault system of southern New Mexico—Evidence for the northward translation of the Colorado Plateau during the Laramide orogeny, *in* Cather, S.M., Kelley, S.A., and McIntosh, W.C., eds., Tectonics, Geochronology, and Volcanism in the Southern Rocky Mountains and the Rio Grande Rift: New Mexico Bureau of Geology and Mineral Resources Bulletin 160, p. 161-179. https://doi.org/10.58799/B-160

Hawley, J.W., and Kottlowski, F.E., 1969, Quaternary geology of the south-central New Mexico border region: New Mexico Bureau of Mines and Mineral Resources Circular 104, p. 89–115. https://doi.org/10.58799/C-104

Hay, W.W., 2008, Evolving ideas about the Cretaceous climate and ocean circulation: Cretaceous Research, v. 29, no. 5-6, p. 725-753, https://doi.org/10.1016/j.cretres.2008.05.025

Hayden, S.N., 1991, Dextral oblique-slip deformation along the Montosa fault zone at Abo Pass, Valencia and Socorro counties, New Mexico [abstract]: 1991 New Mexico Geological Society Annual Spring Meeting, April 5, 1991, Macey Center, Online ISSN: 2834-5800. https://nmgs.nmt.edu/meeting/abstracts/view.cfm?aid=2003

Hewitt, D.F., 1964, Veins of hypogene manganese oxide minerals in the southwestern United States: Economic Geology, v. 59, p. 1429-1472. https://doi.org/10.2113/gsecongeo.59.8.1429

Hilpert, L.S., 1969, Uranium resources of northwestern New Mexico: U.S. Geological Survey, Professional Paper 603, 166 p.

Holland, M.E., Grambling, T.A., Karlstrom, K.E., Jones, J.V. III, Nagotko, K.N., and Daniel, C.G., 2020, Geochronologic and Hf-isotope framework of Proterozoic rocks from central New Mexico, USA: Formation of the Mazatzal crustal province in an extended continental margin arc: Precambrian Research, v. 347. https://doi.org/10.1016/j.precamres.2020.105820\

Hook, S.C., 1983, Stratigraphy, paleontology, depositional framework, and nomenclature of marine Upper Cretaceous rocks, Socorro County, New Mexico, *in* Chapin, C.E., and Callender, J.F., eds., Socorro Region II: New Mexico Geological Society Fall Field Conference Guidebook 34, p. 165–172. https://doi.org/10.56577/FFC-34.165

Hook, S.C., 1984, Evolution of stratigraphic nomenclature of the Upper Cretaceous of Socorro County, New Mexico: New Mexico Geology, v. 6, p. 28–33. https://doi.org/10.58799/NMG-v6n2.28

Hook, S.C., 2010, Flemingostrea elegans, n. sp.: Guide fossil to marine, lower Coniacian (Upper Cretaceous) strata of central New Mexico: New Mexico Geology, v. 32, p. 35–55. https://doi.org/10.58799/NMG-v32n2.35

Hook, S.C., and Cobban, W.A., 2007, A condensed middle Cenomanian succession in the Dakota Sandstone (Upper Cretaceous), Sevilletta National Wildlife Refuge, Socorro County, New Mexico: New Mexico Geology, v. 29, p. 75–96. https://doi.org/10.58799/NMG-v29n3.75

Hook, S.C., and Cobban, W.A., 2011, The Late Cretaceous oyster Cameleolopha bellaplicata (Shumard 1860), guide fossil to middle Turonian strata in New Mexico: New Mexico Geology, v. 33, p. 67–89. https://doi.org/10.58799/NMG-v33n3.67

Hook, S.C., and Cobban, W.A., 2013, The Upper Cretaceous (Turonian) Juana Lopez Beds of the D-Cross Tongue of the Mancos Shale in central New Mexico and their relationship to the Juana Lopez Member of the Mancos Shale in the San Juan Basin: New Mexico Geology, v. 35, p. 59–81. https://doi.org/10.58799/NMG-v35n3.59

Hook, S.C., and Cobban, W.A., 2015, The type section of the Upper Cretaceous Tokay Tongue of the Mancos Shale (new name), Carthage coal field, Socorro County, New Mexico: New Mexico Geology, v. 37, p. 27–46. https://doi.org/10.58799/NMG-v37n2.27

Hook, S.C., Molenaar, C.M., and Cobban, W.A., 1983, Stratigraphy and revision of nomenclature of upper Cenomanian to Turonian (Upper Cretaceous) rocks of west-central New Mexico: New Mexico Bureau of Mines and Mineral Resources Circular 185, p. 7–28. https://doi.org/10.58799/C-185

Hook, S.C., Mack, G. H., and Cobban, W.A., 2012, Upper Cretaceous stratigraphy and biostratigraphy of south-central New Mexico, *in* Lucas, S.G., McLemore, V.T., Lueth, V.W., Spielmann, J.A., and Krainer, K., eds., Geology of the Warm Springs Region: New Mexico Geological Society Fall Field Conference Guidebook 63, p. 121–137. https://doi.org/10.56577/FFC-63

Howard, E.V., 1967, Metalliferous occurrences in New Mexico: Phase 1, state resources development plan: State Planning Office, Santa Fe, 270 p.

Hunt, J.M., 1996, Petroleum Geology and Geochemistry, second edition: New York, W.H. Freeman and Company, 743 pp.

Ingersoll, R. V., 2001, Structural and stratigraphic evolution of the Rio Grande rift, northern New Mexico and southern Colorado: International Geology Review, v. *43, no.* 10, p. 867-891.

Ingram, R.L., 1954, Terminology for the thickness of stratification and parting units in sedimentary rocks: Bulletin of the Geological Society of America, v. 65, no. 9, p. 937–938. https://doi.org/10.1130/0016-7606(1954)65[937:TFTTOS]2.0.CO;2

Ivanov, A.O., Lucas, S.G., and Krainer, K., 2009, Pennsylvanian fishes from the Sandia Formation, Socorro County, New Mexico: New Mexico Geological Society Guidebook 60, p. 243–248.

Jaworski, M.J., 1973, Copper mineralization of the upper Moya Sandstone, Chupadero mines area, Socorro County, New Mexico [M.S. thesis]: Socorro, New Mexico Institute of Mining and Technology, 102 p.

Jochems, A.P., and Aby, S.B., 2024, Geologic map of the Chupadera 7.5-minute quadrangle, Torrance and Socorro Counties, New Mexico: New Mexico Bureau of Geology and Mineral Resources, Open-File Geologic Map 306, scale 1:24,000.

Jordan, T.E, 1981, Thrust loads and foreland basin evolution, Cretaceous, western United States: AAPG Bulletin, v. 65, no. 12, p. 2506–2520. https://doi.org/10.1306/03B599F4-16D1-11D7-8645000102C1865D

Karlstrom, K.E., Amato, J.M., Williams, M.L., Heizler, M.T., Shaw, C.A., Read, A.S., and Bauer, P.W., 2004, Proterozoic tectonic evolution of the New Mexico region, *in* Mack, GH., and Giles, K.A., eds., The Geology of New Mexico—A Geologic History: New Mexico Geological Society Special Publication 11, p. 1-34. https://doi.org/10.56577/SP-11

Kelley, S.A., Chapin, C.E., and Corrigan, J., 1992, Late Mesozoic to Cenozoic cooling histories of the flanks of the northern and central Rio Grande rift, Colorado and New Mexico: New Mexico Bureau of Mines and Mineral Resources Bulletin 145, 39 p. https://doi.org/10.58799/B-145

Kelley, S.A., Chapin, C.E., Cather, S.M., and Person, M., 2009, Thermal history of the eastern Socorro Basin, Socorro County, New Mexico, based on apatite fission-track thermochronology: New Mexico Geological Society Guidebook 60, p. 347–358.

Koning, D.J., Rawling, G.C., Kelley, S., Goff, F., McIntosh, W., and Peters, L., 2014, Structure and tectonic evolution of the Sierra Blanca basin: New Mexico Geological Society Fall Field Conference Guidebook 65, p. 209-226. https://doi.org/10.56577/FFC-65.209

Koning, D.J., Hobbs, K.M., Jochems, A.P., and Chamberlin, R.M., 2022a, Sedimentologic evidence for a major paleogeographic change at 8.5-6.5 Ma near San Antonio, south-central New Mexico: New Mexico Geological Society Fall Field Conference Guidebook 72, p. 221-238. https://doi.org/10.56577/FFC-72.221

Koning, D.J., Chamberlin, R., and Love, D., 2022b, Chupadera Mountains, second-day road log—From Socorro to Box Canyon, northern Chupadera Mountains, Nogal Canyon, and San Antonio: New Mexico Geological Society Fall Field Conference Guidebook 72, p. 64-108. https://doi.org/10.56577/FFC-72

Koning, D.J., Heizler, M.T., and Chamberlin, R.M., 2024, Lake Socorro and the 7.5-7.0 Ma fluvial integration of the ancestral Rio Grande through the Socorro basin, south-central New Mexico: New Mexico Geological Society Annual Spring Meeting, p. 47-48. https://doi.org/10.56577/SM-2024.3007

Kottlowski, F.E., and Stewart, W.J., 1970, The Wolfcampian Joyita Uplift of central New Mexico: New Mexico Bureau of Mines and Mineral Resources Memoir 23, p. 3–31. https://doi.org/10.58799/M-23

Krainer, K., and Lucas, S.G., 2009, Cyclic sedimentation of the Upper Pennsylvanian (Lower Wolfcampian) Bursum Formation, central New Mexico—Tectonics versus glacioeustacy: New Mexico Geological Society Field Conference Guidebook 60, p. 167-182. https://doi.org/10.56577/FFC-60.167

Krainer, K., and Lucas, S.G., 2013, The Pennsylvanian Sandia Formation in northern and central New Mexico: New Mexico Museum of Natural History and Science Bulletin 59, p. 77–100.

Kues, B.S., 2001, The Pennsylvanian System in New Mexico—overview with suggestions for revision of stratigraphic nomenclature: New Mexico Geology, v. 23, no. 4, p. 103–122. https://doi.org/10.58799/NMG-v23n4.103

Kues, B.S., and Giles, K.A., 2004, The late Paleozoic Ancestral Rocky Mountains system in New Mexico, *in* Mack, G.H., and Giles, K.A., eds., The Geology of New Mexico—A Geologic History: New Mexico Geological Society Special Publication 11, p. 95-136. https://doi.org/10.56577/SP-11

Kuiper, K.F., Deino, F.J., Hilfen, W., Krijgsman, W., Renne, P.R, and Wijbrans, J.R., 2008, Synchronizing rock clocks of Earth history: Science, v. 320, no. 5875, p. 500-504. https://doi.org/10.1126/science.1154339

Landman, R.L., and Flowers, R.M., 2013, (U-Th)/He thermochronologic constraints on the evolution of the northern Rio Grande Rift, Gore Range, Colorado, and implications for rift propagation models: Geosphere, v. 9, no. 1, p. 170–187. https://doi.org/10.1130/GES00826.1

LaPoint, D.J., 1976, A comparison of selected sandstone copper deposits in New Mexico: Oklahoma Geological Survey Circular 77, p. 80-96.

LaPoint, D.J., 1979, Geology, geochemistry, and petrology of sandstone copper deposits in New Mexico [Ph.D. dissertation]: Boulder, University of Colorado, 333 p.

Lasky, S.G., 1932, The ore deposits of Socorro County, New Mexico: New Mexico Bureau of Mines and Mineral Resources Bulletin 8, 139 p. https://doi.org/10.58799/B-8

Lawton, T.F., 1994, Tectonic setting of Mesozoic sedimentary basins, *in* Caputo, M.V., Peterson, J.A., and Franczyk, K.J., eds., Mesozoic Systems of the Rocky Mountain Region, USA: Denver, Colorado, Rocky Mountain Section, Society for Sedimentary Geology (SEPM), p. 1–25.

Lerner, A.J, Lucas, S.G., Spielmann, J.A., Krainer, K., Dimichele, W.A., Chaney, D.S., Schneider, J.W., Nelson, W.J., and Ivanov, A., 2009, The biota and paleoecology of the upper Pennsylvanian (Missourian) Tinajas locality, Socorro County, New Mexico: New Mexico Geological Society Fall Field Conference Guidebook 60, p. 267–280. https://doi.org/10.56577/FFC-60.267

Lin, W., Bhattacharya, J.P., and Stockford, A., 2019, High-resolution sequence stratigraphy and implications for Cretaceous glacioeustacy of the Late Cretaceous Gallup System, New Mexico, U.S.A.: Journal of Sedimentary Research, v. 89, no. 6, p. 552-575. https://doi.org/10.2110/jsr.2019.32

Lindgren, W., Graton, L.C., and Gordon, C.H., 1910, The ore deposits of New Mexico: U.S. Geological Survey Professional Paper 68, 361 p. https://doi.org/10.3133/pp68

Lisiecki, L.E., and Raymo, M.E., 2005, A Pliocene-Pleistocene stack of 57 globally distributed benthic 18O records: Paleoceanography and Paleoclimatology: v. 20, issue 1. https://doi.org/10.1029/2004PA001071

Liu, S., and Nummedal, D., 2004, Late Cretaceous subsidence in Wyoming—Quantifying the dynamic component: Geology, v. 325, p. 397–400. https://doi.org/10.1130/G20318.1

Liu, S., Nummdeal, D., and Liu, L., 2011, Migration of dynamic subsidence across the Late Cretaceous United States Western Interior Basin in response to Farrllon plate subduction: Geology, v. 39, p. 555-558. https://doi.org/10.1130/G31692.1

Lucas, S.G., 1991, Triassic stratigraphy, paleontology and correlation, south-central New Mexico: New Mexico Geological Society Fall Field Conference Guidebook 42, p. 243–259. https://doi.org/10.56577/FFC-42.243

Lucas, S.G., 2004, The Triassic and Jurassic systems in New Mexico, in Mack, G.H., and Giles, K.A., eds., The Geology of New Mexico—A Geologic History: New Mexico Geological Society Special Publication 11, p. 137–152. https://doi.org/10.56577/SP-11

Lucas, S.G., and Estep, J.W., 2000, Pennsylvanian selachians from the Cerros de Amado, central New Mexico: New Mexico Museum of Natural History and Science, Bulletin 16, p. 21–27.

Lucas, S.G., and Krainer, K., 2017, The Permian System east of Socorro, central New Mexico (USA): New Mexico Museum of Natural History and Science Bulletin, v. 77, p. 231–261.

Lucas, S.G., and Williamson, T.E., 1993, Eocene vertebrates and late Laramide stratigraphy of New Mexico: New Mexico Museum of Natural History and Science Bulletin 2, p. 145–158.

Lucas, S.G., Krainer, K., and Colpitts, R.M., Jr., 2005, Abo-Yeso (lower Permian) stratigraphy in central New Mexico: New Mexico Museum of Natural History and Science, Bulletin 31, p. 101–117.

Lucas, S.G., Krainer, K., and Barrick, J.E., 2009, Pennsylvanian stratigraphy and conodont biotstratigraphy in the Cerros de Amado, Socorro County, New Mexico, *in* Lueth, V.W., Lucas, S.G., and Chamberlin, R.M., eds., Geology of Chupadera Mesa: New Mexico Geological Society Annual Field Conference Guidebook 60, p. 183–211. https://doi.org/10.56577/FFC-60.183

Lucas, S.G., Krainer, K., and Brose, R.J., 2013, The lower Permian Glorieta Sandstone in central New Mexico, *in* Lucas, S.G., Nelson, W.J., DiMichele, W.A., Speilmann, J.A., Krainer, K., Barrick, J.E., Elrick, S., and Voigt, S., The Carboniferous-Permian

transition in central New Mexico: New Mexico Museum of Natural History Bulletin 59, p. 201-211.

Lucas, S.G., Krainer, K., Barrick, J.E., Allen, B.D., and Nelson, W.J., 2022a, Pennsylvanian stratigraphy and biostratigraphy in the Cerros de Amado, Socorro County, New Mexico: New Mexico Geological Society Fall Field Conference Guidebook 72, p. 147-164. https://doi.org/10.56577/FFC-72.147

Lucas, S.G., Krainer, K., and Nelson, W.J., 2022b, Permian stratigraphy east of Socorro, central New Mexico: New Mexico Geological Society Fall Field Conference Guidebook 72, p. 187-201. https://doi.org/10.56577/FFC-72.187

Lueth, V.W., 2009, A summary of age dating in the Hansonberg district, Socorro County, New Mexico, *in* Lueth, V.W., Lucas, S.G., and Chamberlin, R.M., eds., Geology of Chupadera Mesa: New Mexico Geological Society Annual Field Conference Guidebook 60, p. 28–29. https://doi.org/10.56577/FFC-60

Luther, A.L., Karlstrom, K.E., Scott, L.A., Elrick, M., and Connell, S.D., 2005, Geologic map of the Becker 7.5-minute quadrangle, Valencia and Socorro Counties, New Mexico: New Mexico Bureau of Geology and Mineral Resources Open-File Geologic Map 100, scale 1:24,000. https://doi.org/10.58799/OF-GM-100

Machette, M.N., 1978, Geologic map of the San Acacia quadrangle, Socorro County, New Mexico: U.S. Geological Survey Geologic Quadrangle Map GQ-1415, scale 1:24,000.

Mack, G.H., 2003, Lower Permian terrestrial paleoclimatic indicators in New Mexico and their comparison to paleoclimate models: New Mexico Geological Society Fall Field Conference Guidebook 54, p. 231-240. https://doi.org/10.56577/FFC-54.231

Mack, G.H., and Dinterman, P.A., 2002, Depositional environments and paleogeography of the lower Permian (Leonardian) Yeso and correlative formations in New Mexico: Rocky Mountain Association of Geologists, v. 59, no. 4, p. 75-88.

Mack, G.H., Salyards, S.L., McIntosh, W.C., and Leeder, M.R., 1998, Reversal magnetostratigraphy and radioisotopic geochronology of the Plio-Pleistocene Camp Rice and Palomas Formations, southern Rio Grande rift: New Mexico Geological Society Fall Field Conference Guidebook 49, p. 229-236, https://doi.org/10.56577/FFC-49.229

Mack, G.H., Seager, W.R., and Leeder, M.R., 2003, Synclinal-horst basins—Examples from the southern Rio grande rift and southern transition zone of southwestern New

Mexico, USA: Basin Research, v. 15, no. 3, p. 365-377. https://doi.org/10.1046/j.1365-2117.2003.00212.x

Mack, G.H., Hook, S., Giles, K.A. and Cobban, W.A., 2016, Sequence stratigraphy of the Mancos Shale, lower Tres Hermanos Formation, and coeval middle Cenomanian to middle Turonian strata, southern New Mexico, USA. Sedimentology, v. 63: 781-808. https://doi.org/10.1111/sed.12238

Mardirosian, C.A., 1971, Mining districts and mineral deposits of New Mexico (exclusive of oil and gas): Charles A. Mardirosian, Salt Lake City, scale 1:1,000,000.

McCraw, D.J., Love, D.W., and Connell, S.D., 2006, Geologic map of the Abeytas quadrangle, Socorro County, New Mexico: New Mexico Bureau of Geology and Mineral Resources Open-File Geologic Map 121, scale 1:24,000. https://doi.org/10.58799/OF-GM-121

McIntosh, W. C., Chapin, C. E., Ratte, J. C. and Sutter, J. F., 1992, Time-stratigraphic framework for the Eocene-Oligocene Mogollon-Datil volcanic field, southwest New Mexico: Geological Society of America Bulletin, v. 104, p. 851-871. https://doi.org/10.1130/0016-7606(1992)104<0851:TSFFTE>2.3.CO;2

McLemore, V.T., 1982, Geology and geochemistry of Ordovician carbonatite dikes in the Lemitar Mountains, Socorro County, New Mexico: New Mexico Bureau of Mines and Mineral Resources Open-File Report 158, 104 p. https://doi.org/10.58799/OFR-158

McLemore, V.T., 1983a, Uranium and thorium occurrences in New Mexico—Distribution, geology, production, and resources, with selected bibliography: New Mexico Bureau of Mines and Mineral Resources Open-File Report 183, 950 p. https://doi.org/10.58799/OFR-183

McLemore, V.T., 1983b, Uranium in the Socorro area, New Mexico, *in* Chapin, C. E., and Callender, J. F., eds., Socorro Region II: New Mexico Geological Society Fall Field Conference Guidebook 34, p. 227-233. https://doi.org/10.56577/FFC-34.227

McLemore, V.T., 1983c, Carbonatites in the Lemitar and Chupadera Mountains, Socorro County, New Mexico; *in* Chapin, C.E., and Callender, J.F., eds., Socorro Region II: New Mexico Geological Society Fall Field Conference Guidebook 34, p. 235-240. https://doi.org/10.56577/FFC-34.235

McLemore, V.T., 1984, Preliminary report on the geology and mineral resource potential of Torrance County, New Mexico: New Mexico Bureau of Mines and Mineral Resources Open-File Report 192, 202 p. https://doi.org/10.58799/OFR-192

McLemore, V. T., 1994, Volcanic-epithermal deposits in the Mogollon-Datil volcanic field, New Mexico: New Mexico Geological Society, Guidebook 45, p. 299-309.

McLemore, V.T., 1996, Copper in New Mexico: New Mexico Geology, v. 18, no. 2, p. 25-36. https://doi.org/10.58799/NMG-v18n2.25

McLemore, V.T., 2001, Silver and gold resources in New Mexico: New Mexico Bureau of Mines and Mineral Resources Resource Map 21, 60 p. https://doi.org/10.58799/RM-21

McLemore, V.T., 2015, Rare Earth Elements (REE) Deposits in New Mexico: Update: New Mexico Geology, v. 37, p. 59-69, http://geoinfo.nmt.edu/publications/periodicals/nmg/current/home.cfml

McLemore, V.T., 2016, Geology and mineral deposits of the sedimentary-copper deposits in the Scholle Mining District, Socorro, Torrance and Valencia Counties, New Mexico, *in*, Frey, B.A., Karlstrom, K.E., Lucas, S.G., Williams, S., Zeigler, K., McLemore, V., and Ulmer-Scholle, D.S., eds., The Geology of the Belen Area: New Mexico Geological Society Fall Field Conference Guidebook 67, p. 249-254. https://doi.org/10.56577/FFC-67.249

McLemore, V.T., 2017, Mining districts and prospect areas of New Mexico: New Mexico Bureau of Geology and Mineral Resources, Resource Map 24, 65 p., scale 1:1,000,000.

McLemore, V.T., and Austin, G.S., 2017, Industrial minerals and rocks, *in* McLemore, V.T., Timmons, S., and Wilks, M., eds., Energy and Mineral Resources of New Mexico: New Mexico Bureau of Geology and Mineral Resources Memoir 50E, 128 p. https://doi.org/10.58799/M-50E

McLemore, V.T., and Chenoweth, W.C., 1989, Uranium resources in New Mexico: New Mexico Bureau of Mines and Mineral Resources Resource Map 18, 37 p. https://doi.org/10.58799/RM-18

McLemore, V.T., and Chenoweth, W.C., 2017, Uranium resources, *in* McLemore, V.T., Timmons, S., and Wilks, M., eds., Energy and Mineral Deposits in New Mexico: New Mexico Bureau of Geology and Mineral Resources Memoir 50C, 80 p. https://doi.org/10.58799/M-50C

McLemore, V.T., and Lueth, V., 2017, Metallic mineral deposits, *in* McLemore, V.T., Timmons, S., and Wilks, M., eds., Energy and Mineral Deposits in New Mexico: New Mexico Bureau of Geology and Mineral Resources Memoir 50D, 92 p. https://doi.org/10.58799/M-50D

McLemore, V. T., Broadhead, R. F., Barker, J. M., Austin, G. A., Klein, K., Brown K. B., Murray, D., Bowie, M. R., and Hingtgen, J. S., 1986, A preliminary mineral-resource potential of Valencia County, northwestern New Mexico: New Mexico Bureau of Mines and Mineral Resources, Open-File Report 229, 197 pp.

McLemore, V.T., Owen, E.J., and Newcomer, J., 2024, Critical minerals in sediment-hosted stratbound copper deposits in the Nacimiento and Zuni Mountains, Northwestern New Mexico: Preliminary results: New Mexico Geological Society Guidebook 74, p. 307-317.

Miall, A.D., Octavian, C., Vakarelov, B.K., and Post, R., 2008, The Western Interior Basin: Sedimentary basins of the world, v. 5, p. 329-362. https://doi.org/10.1016/S1874-5997(08)00009-9

Miesch, A.T., 1956, Geology of the Luis Lopez manganese district, Socorro County, New Mexico: New Mexico Bureau of Mines and Minerals Resources Circular 38, 31 p. https://doi.org/10.58799/C-38

Moats, W.P., and Queen, L.C., 1981, Minerals of the Socorro Peak district (abs.): New Mexico Geology, v. 3, p. 16.

Molenaar, C.M., 1983, Major depositional cycles and regional correlations of Upper Cretaceous rocks, southern Colorado Plateau and adjacent areas: Rocky Mountain Section, Society of Economic Paleontologists and Mineralogists, p. 201–224.

Moucha, R., Forte, A.M., Rowley, D.B., Mitrovica, J.X., Simmons, N.A., and Grand, S.P., 2008, Mantle convection and the recent evolution of the Colorado Plateau and the Rio Grande Rift valley: Geology, v. 36, no. 6, p. 439–442. https://doi.org/10.1130/G24577A.1

Murray, A.S., and Wintle, A.G., 2000, Luminescence dating of quartz using an improved single aliquot regenerative dose protocol: Radiation Measurements, v. 32, p. 57–73. https://doi.org/10.1016/S1350-4487(99)00253-X

NACSN [North American Commission on Stratigraphic Nomenclature], 2021, Stratigraphy, v. 18, no. 3, p. 153-204. https://doi.org/10.29041/strat.18.3.01

Newton, B.T., Cikoski, C., and Allen, B., 2020, Hydrogeologic framework of the Estancia Basin, New Mexico: New Mexico Bureau of Geology and Mineral Resources Open-File Report 609, 31 p. https://doi.org/10.58799/OFR-609

Norman, D.I., Bazrfshan, K., and Eggleston, T.L., 1983, Mineralization of the Luis Lopez epithermal manganese deposits in light of fluid inclusion and geologic studies, *in* Chapin, C.E., and Callender, J.F., eds., Socorro Region II: New Mexico Geological Society Fall Field Conference Guidebook 34, p. 247-251. https://doi.org/10.56577/FFC-34.247

North, R.M., 1983, History and geology of the precious metal occurrences in Socorro County, New Mexico, *in* Chapin, C.E., and Callender, J.F., eds., Socorro Region II: New Mexico Geological Society Fall Field Conference Guidebook 34, p. 261-268. https://doi.org/10.56577/FFC-34.261

North, R.M., and McLemore, V.T., 1986, Silver and gold occurrences in New Mexico: New Mexico Bureau of Mines and Mineral Resources Resource Map 15, 32 p., scale 1:1,000,000. https://doi.org/10.58799/RM-15

North, R.M., and McLemore, V.T., 1987, Mineralization in the Luis Lopez mining district, Socorro County, New Mexico—A summary, *in* Guidebook for the 1987 conference, 24th annual meeting of the Clay Minerals Society and 36th annual Clay Minerals Conference: New Mexico Bureau of Mines and Mineral Resources, p. 68-73.

Nummedal, D., 2004, Tectonic and eustatic controls on Upper Cretaceous stratigraphy of northern New Mexico, *in* Mack, G.H., and Giles, K.A., The Geology of New Mexico—A Geologic History: New Mexico Geological Society Special Publication 11, p. 169-182. https://doi.org/10.56577/SP-11

Osburn, G.R., and Chapin, C.E., 1983, Nomenclature for Cenozoic rocks of northeastern Mogollon–Datil volcanic field, New Mexico: New Mexico Bureau of Mines and Mineral Resources Stratigraphic Chart 1. https://doi.org/10.58799/SC-1

Oviatt, C.G., 2010, Geologic map of the Abo quadrangle, Torrance County, New Mexico: New Mexico Bureau of Geology and Mineral Resources Open-File Geologic Map 199, scale 1:24,000. https://doi.org/10.58799/OF-GM-199

Oviatt, C.G., 2013, Geologic map of the Gran Quivera quadrangle, Socorro County, New Mexico: New Mexico Bureau of Geology and Mineral Resources Open-File Geologic Map 248, scale 1:24,000. https://doi.org/10.58799/OF-GM-248

Pang, M., and Nummedal, D., 1995, Flexural subsidence and basement tectonics of the Cretaceous Western Interior basin, United States: Geology, v. 23, p. 173–176. https://doi.org/10.1130/0091-7613(1995)023<0173:FSABTO>2.3.CO;2

Personius, S.F., and Jochems, A.P., compilers, 2016a, Fault number 2112, Loma Blanca fault, *in* Quaternary fault and fold database of the United States: U.S. Geological Survey website, https://earthquakes.usgs.gov/hazards/qfaults, accessed (accessed June 22, 2024).

Personius, S.F., and Jochems, A.P., compilers, 2016b, Fault number 2113, Loma Peleda fault, *in* Quaternary fault and fold database of the United States: U.S. Geological Survey website, https://earthquakes.usgs.gov/hazards/qfaults (accessed June 22, 2024).

Phillips, F.M., and Sion, B.D., 2022, Geomorphic surfaces of the Rio Grande valley in the vicinity of Socorro, New Mexico: New Mexico Geological SocietyFall Field Conference Guidebook 72, p. 281-293. https://doi.org/10.56577/FFC-72.281

Phillips, J.S., 1960, Sandstone-type copper deposits of the western United States [Ph.D. dissertation]: Cambridge, Harvard University, 320 p.

Price, R.A., 1973, Large scale gravitational flow of the supracrustal rocks, southern Canadian Rockies, *in* De Jong, K.A., and Scholten, R., eds., Gravity and Tectonics: New York, John Wiley and Sons, p. 491–502.

Reiche, P., 1949, Geology of the Manzanita and north Manzano Mountains, New Mexico: Geological Society of America Bulletin, v. 60, no. 7, p. 1183-1212. https://doi.org/10.1130/0016-7606(1949)60[1183:GOTMAN]2.0.CO;2

Rejas, A., 1965, Geology of the Cerros de Amado area, Socorro County, New Mexico [M.S. thesis]: Socorro, New Mexico Institute of Mining and Technology, 128 p.

Ricketts, J.W., Karlstrom, K.E., and Kelley, S.A., 2015, Embryonic core complexes in narrow continental rifts—The importance of low-angle normal faults in the Rio Grande rift of central New Mexico: Geosphere, v. 11, no. 2, p. 425-444. https://doi.org/10.1130/GES01109.1

Ricketts, J.W., Kelley, S.A, Karlstrom, K.E., Schmandt, B., Donahue, M.S., and van Wijk, J., 2016, Synchronous opening of the Rio Grande rift along its entire length at 25-10 Ma supported by apatite (U-Th)/He and fission-track thermochronology, and evaluation of possible driving mechanisms: GSA Bulletin, v. 128, no. 3-4, p. 397-424. https://doi.org/10.1130/B31223.1

Rinehart, A.J., Love, D.W., and Miller, P.L., 2014, Geologic map of the Black Butte 7.5-minute quadrangle, Socorro and Valencia Counties, New Mexico: New Mexico Bureau of Geology and Mineral Resources Open-File Geologic Map 235, scale 1:24,000. https://doi.org/10.58799/OF-GM-235

Sanford, A.R., 1968, Gravity survey in central Socorro County, New Mexico: New Mexico Bureau of Mines and Mineral Resources Circular 91, 14 p. https://doi.org/10.58799/C-91

Scott, L.A., Elrick, M., Connell, S., and Karlstrom, K., 2005, Geologic map of the Scholle 7.5-minute quadrangle, Valencia, Torrance, and Socorro Counties, New Mexico: New Mexico Bureau of Geology and Mineral Resources Open-File Geologic Map 99, scale 1:24,000. https://doi.org/10.58799/OF-GM-99

Shastri, L.L., 1993, Proterozoic geology of the Los Pinos Mountains, central new Mexico—Timing of plutonism, deformation, and metamorphism [M.S. thesis]: Albuquerque, University of New Mexico, 82 p.

Sion, B.D., Phillips, F.M., Axen, G.J., and Harrison, J.B.J., Love, D.W., and Zimmerer, M.J., 2020, Chronology of terraces in the Rio Grande rift, Socorro basin, New Mexico—Implications for terrace formation: Geosphere, v. 16. https://doi.org/10.1130/GEOS.S.12858032.v1

Sion, B.D., Harrison, J.B.J., McDonald, E.V., Phillips, F.M., and Axen, G.J., 2021, Chronofunctions for New Mexico, USA, soils show relationships among climate, dust input, and soil development: Quaternary International, v. 618, p. 35-51. https://doi.org/10.1016/j.quaint.2021.06.024

Soulé, J.H., 1956, Reconnaissance of the "red bed" copper deposits in southeastern Colorado and New Mexico: U.S. Bureau of Mines Information Circular 7740, 74 p.

Spielmann, J.A., and Lucas, S.G., 2009, Triassic stratigraphy and biostratigraphy in Socorro County, New Mexico: New Mexico Geological Society Fall Field Conference Guidebook 60, p. 213–226. https://doi.org/10.56577/FFC-60.213

Staplin, F.L., 1969, Sedimentary organic matter, organic metamorphism, and oil and gas occurrence: Bulletin of Canadian Petroleum Geology, v. 17, no. 1, p. 47-66.

Stark, J.T., and Dapples, E.C., 1946, Geology of the Los Pinos Mountains, New Mexico: Geological Society of America Bulletin, v. 57, no. 12, p. 1121-1172. https://doi.org/10.1130/0016-7606(1946)57[1121:GOTLPM]2.0.CO;2

Tabet, D.E., 1979, Geology of the Jornada del Muerto coal field, Socorro County, New Mexico: New Mexico Bureau of Mines and Mineral Resources Circular 168, 19 p. https://doi.org/10.58799/C-168

Tedford, R.H., and Barghoorn, S., 1997, Miocene mammals of the Española and Albuquerque basins, north-central New Mexico, *in* Lucas, S.G., Estep, J.W., Williamson, T.E., and Morgan, G.S., eds., New Mexico's fossil record 1: New Mexico Museum of Natural History and Science, Bulletin 11, p. 77–95.

Tedford, R.H., and Barghoorn, S., 1999, Santa Fe Group (Neogene), Ceja del Rio Puerco, northwestern Albuquerque Basin, Sandoval County, New Mexico, *in* Pazzaglia, F.J., and Lucas, S.G., eds., Albuquerque Geology: New Mexico Geological Society Fall Field Conference Guidebook 50, p. 327–335. https://doi.org/10.56577/FFC-50.327

Tedford, R.H., Albright, L.B., III, Barnosky, A.D., Ferrusquia-Villafranca, I., Hunt, R.M., Jr., Storer, J.E., Swisher, C.C., III, Voorhies, M.R., Webb, S.D., and Whistler, D.P., 2004, Mammalian biochronology of the Arikareean through Hemphillian interval (late Oligocene through early Pleistocene epochs), *in* Woodburne, M.O., ed., Late Cretaceous and Cenozoic Mammals of North America—Biostratigraphy and Geochronology: New York, Columbia University Press, ch 6. https://doi.org/10.7312/wood13040-008

Thacker, J.O., Karlstrom, K.E., Kelley, S.A., Crow, R.S., Kendall, J.J., 2023, Late Cretaceous time-transgressive onset of Laramide arch exhumation and basin subsidence across northern Arizona–New Mexico, USA, and the role of a dehydrating Farallon flat slab: Geological Society of America Bulletin, v. 135, no. 1-2, p. 389–406. https://doi.org/10.1130/B36245.1

Thiel, C., Buylaert, J.P., Murray, A., Terhorst, B., Hofer, I., Tsukamoto, S. and Frechen, M., 2011, Luminescence dating of the Stratzing loess profile (Austria)–Testing the potential of an elevated temperature post-IR IRSL protocol: Quaternary International, v. 234, no. 1-2, p. 23-31. https://doi.org/10.1016/j.quaint.2010.05.018

Thompson, A.G., and Barnes, C.G., 1999, 1.4-Ga peraluminous granites in central New Mexico—Petrology and geochemistry of the Priest Pluton: Rocky Mountain Geology, v. 34, no. 2, p. 223-243. https://doi.org/10.2113/34.2.223

Tonking, W.H., 1957, Geology of Puertecito quadrangle, Socorro County, New Mexico: New Mexico Institute of Mining and Technology, State Bureau of Mines and Mineral Resources Bulletin 42, 67 p. https://doi.org/10.58799/B-41

Turner, C.E., and Peterson, F., 2004, Reconstruction of the Upper Jurassic Morrison Formation extinct ecosystem—A synthesis: Sedimentary Geology, v. 167, p. 309–355. https://doi.org/10.1016/j.sedgeo.2004.01.009

Tyson, R.V., 1987, The genesis and palynofacies characteristics of marine petroleum source rocks, *in* Brooks, J., and Fleet, A.J., eds., Marine Petroleum Source Rocks: Geological Society of London Special Publication 26, pp. 47-67. https://doi.org/10.1144/GSL.SP.1987.026.01.03

Udden, J.A., 1914, The mechanical composition of clastic sediment: Geological Society of America Bulletin, v. 25, no. 1, p. 655–744. https://doi.org/10.1130/GSAB-25-655

USBM (U.S. Bureau of Mines), 1927-1990, Minerals Yearbook: Washington, D.C., U.S. Government Printing Office, variously paginated.

USGS (U.S. Geological Survey), 1902-1927, Mineral resources of the United States (1901-1923): Washington, D.C., U.S. Government Printing Office, variously paginated.

van Wijk, J., van Hunen, J., and Goes, S., 2008, Small-scale convection during continental rifting: Evidence from the Rio Grande rift: Geology, v. 36, no. 7, p. 575–578. https://doi.org/10.1130/G24691A.1

van Wijk, J., Koning, D., Axen, G., Coblentz, D., Graff, E., and Sion, B., 2018, Tectonic subsidence, geoid analysis, and the Miocene-Pliocene unconformity in the Rio Grande rift, southwestern United States—Implications for mantle upwelling as a driving force for rift opening: Geosphere, v. 14, no. 2, p. 684–709. https://doi.org/10.1130/GES01522.1

Wentworth, C.K., 1922, A scale of grade and class terms for clastic sediments: The Journal of Geology, v. 30, no. 5, p. 377–392. https://doi.org/10.1086/622910

Wilks, M., and Chapin, C.E., 1997, The New Mexico Geochronological Database: New Mexico Bureau of Mines and Mineral Resources Digital Database Series-Database DDS DB1. https://doi.org/10.58799/DDS-1

Willard, M.E., 1973, Geology of the Luis Lopez manganese district, New Mexico: New Mexico Bureau of Mines and Mineral Resources, Open-File Report 186, 81 p.

Williams, R.T., Goodwin, L.B., Sharp, W.D., and Mozley, P.S., 2017, Reading a 400,000-year record of earthquake frequency for an intraplate fault: Earth, Atmospheric, and Planetary Sciences, v. 114, no. 19, p. 4893-4898. https://doi.org/10.1073/pnas.1617945114

Wilpolt, R.H., and Wanek, A.A., 1951, Geology of the region from Socorro and San Antonio east to Chupadera Mesa, Socorro County: U.S. Geological Survey Oil and Gas Investigations Map 121, scale 1:62.500, 2 sheets.

Ye, H., Royden, L., Burchfiel, C., and Schuepbach, M., 1996, Late Paleozoic deformation of interior North America—The greater ancestral Rocky Mountains: American Association of Petroleum Geologists Bulletin, v. 80, p. 1397–1432.

BIBLIOGRAPHY

Anderson, E.G., 1955, The metal resources of New Mexico and their economic features through 1954: New Mexico Bureau of Mines and Mineral Resources Bulletin 39, 183 p. https://doi.org/10.58799/B-39

Bachman, G.O., and Stotelmeyer, R.B., 1967, Summary report on the geology and mineral resources of the Bosque del Apache National Wildlife Refuge, Socorro County, New Mexico: U.S. Geological Survey Bulletin 1260-B, 9 p. https://doi.org/10.3133/b1260B

Bobrow, D.J., 1984, Geochemistry and petrology of Miocene silicic lavas in the Socorro-Magdalena area, New Mexico [M.S. thesis]: Socorro, New Mexico Institute of Mining and Technology.

Bobrow, D.J., Kyle, P.R., and Osburn, G.R., 1983, Miocene rhyolitic volcanism in the Socorro area of New Mexico, in Chapin, C.E., and Callender, J.F., eds., Socorro Region II: New Mexico Geological Society Annual Field Conference Guidebook 34, p. 211-217. https://doi.org/10.56577/FFC-34.211

Cather, S.M., 1992, Suggested revisions to the Tertiary tectonic history of north-central New Mexico, *in* Lucas, S.G., Kues, B.S., Williamson, T.E., and Hunt, A.P., eds., San Juan Basin IV: New Mexico Geological Society Fall Field Conference Guidebook 43, p. 109–122. https://nmgs.nmt.edu/publications/guidebooks/downloads/43/43_p0145_p0150.pdf

Cather, S.M., Colpitts, R.M., Jr., Green, M., Axen, G.J., and Flores, S., 2012 (revised 2016), Geologic map of the Sierra de la Cruz 7.5-minute quadrangle, Socorro County, New Mexico: New Mexico Bureau of Geology and Mineral Resources Open-File Geologic Map 227, scale 1:24,000. https://doi.org/10.58799/OF-GM-227

Connell, S.D., Koning, D.J., Kelley, S.A., and Brandes, N.N., 2007, Oligocene and early Miocene sedimentation in the southwestern Jemez Mountains and northwestern Albuquerque Basin, New Mexico, *in* Kues, B.S., Kelley, S.A., and Lueth, V.W., eds., Geology of the Jemez Region II: New Mexico Geological Society Fall Field Conference Guidebook 58. pp. 195–208. https://doi.org/10.56577/FFC-58.195

Dale, V.B., and McKinney, W.A., 1959, Tungsten deposits of New Mexico: U.S. Bureau of Mines, Report of Investigations 5517, 72 p.

Ellis, R.W., 1929, New Mexico mineral deposits except fuels: University of New Mexico, Bulletin 167, 148 p.

Force, E.R., 2000, Titanium mineral resources of the western U.S—An update: U.S. Geological Survey Open-File Report 00-442, 43 p.

Gott, G.B., and Erickson, R.L., 1952, Reconnaissance of uranium and copper deposits in parts of New Mexico, Colorado, Utah, Idaho, and Wyoming: U.S. Geological Survey Circular 219, 16 p. https://doi.org/10.3133/cir219

Green, M.W., Axen, G., and Cather, S.M., 2013, Low-angle normal faults within evaporite-rich Permian strata, Sierra Larga, New Mexico [abstract]: New Mexico Geological Society Spring Meeting, April 12, 2013, Macey Center, p. 21. https://doi.org/10.56577/SM-2013.62

Hall, R.G., 1978, World nonbauxite aluminum resources-alunite: U.S. Geological Survey Professional Paper 1076-A, 35 p. https://doi.org/10.3133/pp1076A

Harrer, C.M., 1965, Iron, *in* Mineral and Water Resources of New Mexico: New Mexico Bureau of Mines and Mineral Resources Bulletin 87, p. 176–183. https://doi.org/10.58799/B-87

Hill, G.T., 1994, Geochemistry of southwestern New Mexico fluorite deposits with possible base and precious metals exploration significance [M.S. thesis]: Socorro, New Mexico Institute of Mining and Technology, 44 p.

Hill, J.M., 1912, The mining districts of the western United States: U.S. Geological Survey Bulletin 507, 309 p.

Hoffman, G.K., 1996, Coal resources of New Mexico: New Mexico Bureau of Mines and Mineral Resources Resource Map 20, scale 1:1,000,000. https://doi.org/10.58799/RM-20

Hoffman, G.K., 2017, Coal resources in New Mexico, *in* McLemore, V.T., Timmons, S., and Wilks, M., eds., Energy and Mineral Deposits in New Mexico: New Mexico Bureau of Geology and Mineral Resources Memoir 50B. https://doi.org/10.58799/M-50B

Jones, F.A., 1904, New Mexico Mines and Minerals: Santa Fe, New Mexican Printing Company, 349 p.

Jones, F.A., 1908, Epitome of the economic geology of New Mexico: New Mexico Bureau Immigration, 47 p.

Jones, F.A., 1915, The Mineral Resources of New Mexico: New Mexico Bureau of Mines and Mineral Resources Bulletin 1, 77 p. https://doi.org/10.58799/B-1

Jones, W.R., 1965, Copper, *in* Mineral and water resources of New Mexico: New Mexico Bureau of Mines and Mineral Resources Bulletin 87, p. 160-176. https://doi.org/10.58799/B-87

Kelley, V.C., 1949, Geology and economics of New Mexico iron ore deposits: University of New Mexico Publications in Geology, no. 2, 246 p.

Lasky, S.G., and Wootton, T.P., 1933, The metal resources of New Mexico and their economic features: New Mexico Bureau of Mines and Mineral Resources Bulletin 12, 178 p. https://doi.org/10.58799/B-12

Long, K.R., DeYoung, J.H., Jr., and Ludington, S.D., 1998, Database of significant deposits of gold, silver, copper, lead, and zinc in the United States, Part B—Digital database: U.S. Geological Survey Open-File Report 98-206B.

Mack, G.H., Hook, S., Giles, K.A., and Cobban, W.A., 2016, Sequence stratigraphy of the Mancos Shale, lower Tres Hermanos Formation, and coeval middle Cenomanian to middle Turonian strata, southern New Mexico, USA: Sedimentology, v. 63, p. 781-808. https://doi.org/10.1111/sed.12238

Mardirosian, C.A., 1979, Principal mining districts of New Mexico: New Mexico Geology, v. 1, no. 3, p. 37-38, 48. https://doi.org/10.58799/NMG-v1n3.37

McAnulty, W.N., 1978, Fluorspar in New Mexico: New Mexico Bureau of Mines and Mineral Resources Memoir 34, 64 p. https://doi.org/10.58799/M-34

McIntosh, W. C., Kedzie, L. L. and Sutter, J. F., 1991, Paleomagnetism and 40Ar/39 Ar ages of ignimbrites, Mogollon-Datil field, southwestern New Mexico: New Mexico Bureau of Mines and Mineral Resources, Bulletin 135, 79 p. https://doi.org/10.58799/B-135

McLemore, V.T., and Barker, J.M., 1985, Barite in north-central New Mexico: New Mexico Geology, v. 7, no. 2, p. 21-25. https://doi.org/10.58799/NMG-v7n2.21

McLemore, V.T., Hoffman, G., Smith, M, Mansell, M., and Wilks, M., 2005, Mining districts of New Mexico: New Mexico Bureau of Geology and Mineral Resources Open-File Report 494. https://doi.org/10.58799/OFR-494

Myers, D.A., 1977, Geologic map of the Scholle quadrangle, Socorro, Valencia, and Torrance Counties, New Mexico: U.S. Geological Survey Geologic Quadrangle Map GQ-1412, scale 1:24,000.

Myers, D.A., McKay, E.J., and Sharps, J.A., 1981, Geologic map of the Becker quadrangle, Valencia and Socorro Counties, New Mexico: U.S. Geological Survey Geologic Quadrangle Map GQ-1556, scale 1:24,000.

Myers, D.A., Sharps, J.A., and McKay, E.J., 1986, Geologic map of the Becker SW and Cerro Montoso quadrangles, Socorro County, New Mexico: U.S. Geological Survey Miscellaneous Investigations Series Map I-1567, scale 1:24,000.

North, R.M., and McLemore, V.T., 1988, A classification of the precious metal deposits of New Mexico, *in* Bulk mineable precious metal deposits of the western United States Symposium Volume: Geological Society of Nevada, Reno, Symposium held April 6-8, 1987, p. 625-660.

Northrop, S.A., 1996, Minerals of New Mexico: Albuquerque, University of New Mexico Press, 356 p.

Osburn, G.R., 1984, Socorro County Geologic Map: New Mexico Bureau of Mines and Mineral Resources Open-File Report 238, 13 p., 1 figure, and 1 plate. https://doi.org/10.58799/OFR-238

Rothrock, H.E., Johnson, C.H., and Hahn, A.D., 1946, Fluorspar Resources in New Mexico: New Mexico Bureau of Mines and Mineral Resources Bulletin 21, 245 p. https://doi.org/10.58799/B-21

Talmage, S.B., and Wootton, T.P., 1937, The non-metallic mineral resources of New Mexico and their economic features (exclusive of fuels): New Mexico Bureau of Mines and Mineral Resources Bulletin 12, 159 p. https://doi.org/10.58799/B-12

Thompson, A.J., 1965a, Lead, in Mineral and Water Resources of New Mexico: New Mexico Bureau of Mines and Mineral Resources Bulletin 87, p. 149-154. https://doi.org/10.58799/B-87

Thompson, A.J., 1965b, Zinc, in Mineral and Water Resources of New Mexico: New Mexico Bureau of Mines and Mineral Resources Bulletin 87, p. 154-159. https://doi.org/10.58799/B-87

USGS (U.S. Geological Survey), 1965, Mineral and Water Resources of New Mexico: New Mexico Bureau of Mines and Mineral Resources Bulletin 87, 437 p. https://doi.org/10.58799/B-87

Van Allen, B.R., Emmons, D.L., and Paster, T.P., 1986, Carbonatite dikes of the Chupadera Mountains, Socorro, County, New Mexico: New Mexico Geology, v. 8, no. 2, p. 25-29, 40. https://doi.org/10.58799/NMG-v8n2.25

Wells, E.H., and Wootton, T.P., 1940, Gold mining and gold deposits in New Mexico: New Mexico Bureau of Mines and Mineral Resources Circular 5, 25 p. https://doi.org/10.58799/C-5

Williams, F.E., 1966, Fluorspar deposits of New Mexico: U.S. Bureau of Mines Information Circular 8307, 143 p.